
I A B E M 2 0 1 3
SYMPOSIUM OF THE
INTERNATIONAL ASSOCIATION FOR
BOUNDARY ELEMENT METHODS

Pontificia Universidad Católica de Chile
Santiago, Chile, January 9 – 11, 2013

PROCEEDINGS

ISBN 978-956-351-579-4 (CD)

Editors: Norbert Heuer, Carlos Jerez-Hanckes

INTRODUCTION

The International Association for Boundary Element Methods (IABEM) provides a forum for researchers and engineers around the world to discuss recent developments in the Boundary Element Method (BEM) and new challenges ahead. It fosters and facilitates scientific interaction, discussion and cooperation among mathematicians, computer scientists and engineers with background in the field of BEM. The Association has been organizing international symposia for more than 20 years. The last six symposia were held in Paris (1998), Brescia (2000), Austin (2002), Minneapolis (2004), Graz (2006) and Brescia (2011).

The 2013 IABEM Symposium takes place at the Pontificia Universidad Católica de Chile (PUC) in Santiago, Chile on January 9-11, 2013. It is being organized jointly by the Faculties of Engineering and Mathematics of the PUC.

We sincerely thank our sponsors who provided the necessary financial support to keep the registration fee low and to assign 15 studentships:

- Comisión Nacional de Investigación Científica y Tecnológica (CONICYT) through Project Anillo ACT1118,
- Nimbic,
- Vicerrectoría de Investigación, Pontificia Universidad Católica de Chile,
- Facultad de Ingeniería, Pontificia Universidad Católica de Chile, and
- Facultad de Matemáticas, Pontificia Universidad Católica de Chile.

Finally, we also thank all the participants for attending **IABEM 2013** and, in many cases, for traveling far to do so.

Norbert Heuer, Carlos Jerez-Hanckes
Organizers IABEM 2013

Santiago, Chile, January 2013

Symposium IABEM 2013

Table of Contents

A. I. Abreu (joint with A. Canelas, W. J. Mansur) <i>A Boundary Integral Formulation Based On The Convolution Quadrature Method For Transient Heat Conduction In Functionally Graded Materials</i>	5
Markus Bantle (joint with Stefan Funken) <i>Data Compression Techniques for the p-Version of the Boundary Element Method for the Laplace Equation in two dimensions</i>	11
M. Bebendorf (joint with R. Venn) <i>Frequency-independent approximation of integral formulations of Helmholtz boundary value problems</i>	17
S. Chaillat (joint with M. Bonnet) <i>Comparison of two Fast Multipole Accelerated BEMs for 3D elastodynamic problems in semi-infinite media</i>	18
Christopher Cooper (joint with Lorena A. Barba) <i>Using fast tree methods and GPU hardware for protein electrostatics</i> ...	20
Pieter Coulier (joint with Stijn François, Geert Lombaert, Geert Degrande) <i>A coupled finite element – hierarchical boundary element method based on Green’s functions for a horizontally layered halfspace</i>	21
Steven L. Crouch (joint with John A. L. Napier) <i>On the Displacement Discontinuity Method</i>	29
Róbert Čunderlík (joint with Róbert Špir, Karol Mikula) <i>Direct BEM for high-resolution gravity field modelling of the Earth</i>	30
Catalina Domínguez (joint with Norbert Heuer) <i>A posteriori error estimation for a hypersingular integral equation and non-conforming domain decomposition</i>	32
Ney A. Dumont (joint with Daniel Huamán) <i>On a consistent, mixed variational boundary element formulation for strain gradient elasticity</i>	33
CuiYing Fan (joint with Minghao Zhao, Ernian Pan, Guoning Liu) <i>Extended Boundary Integral Equation Method For Fracture Analysis In Magnetoelastic Media</i>	41
Michael Feischl (joint with Thomas Führer, Michael Karkulik, Dirk Praetorius) <i>Quasi-optimal adaptive BEM</i>	42

T. Führer (joint with M. Feischl, M. Karkulik, J.M. Melenk, D. Praetorius)	
<i>FEM-BEM couplings without stabilization</i>	48
R. Gallego (joint with M.A. Riveiro)	
<i>BEM-AEM for 3D multi-region non-homogeneous/homogeneous elastic bodies</i>	54
M. Ganesh (joint with J. S. Hesthaven, B. Stamm)	
<i>A model reduction boundary element algorithm for computational electromagnetism</i>	55
Heiko Gimperlein (joint with Matthias Maischak, Ernst P. Stephan)	
<i>FE/BE coupling for strongly nonlinear transmission problems with friction</i>	61
Joachim Gwinner	
<i>Approximation of Higher Order for Parabolic Unilateral Problems using hp- BEM</i>	62
Helmut Harbrecht (joint with Michael Peters)	
<i>Comparison of fast boundary element methods on parametric surfaces</i> ..	63
Fernando J. Henríquez (joint with Carlos F. Jerez–Hanckes)	
<i>Boundary Integral Formulation for the Electrical Response of a Nerve to an Extracellular Stimulation</i>	64
Ralf Hiptmair (joint with Carlos Jerez-Hanckes, Xavier Claeys)	
<i>Multiple Traces Boundary Integral Formulation for Helmholtz Transmission Problems</i>	66
Vikram Jandhyala (joint with Arun Sathanur)	
<i>Enabling High-Dimensional Electromagnetic Design on Computing Clouds</i>	72
Bernhard Kager (joint with Martin Schanz)	
<i>Sparse and \mathcal{H}-Matrix Representation Techniques applied to indirect Time-Domain BEM in Elastodynamics</i>	73
M. Karkulik (joint with M. Feischl, T. Führer, J.M. Melenk, D. Praetorius)	
<i>Novel inverse estimates for non-local operators</i>	79
Lars Kielhorn	
<i>Rapid prototyping of Boundary Element Methods with BETL</i>	85
A. Kimeswenger (joint with O. Steinbach)	
<i>Some FE and BE based approaches for boundary control problems</i>	86
Josue Labaki (joint with Euclides Mesquita, R. K. N. D. Rajapakse)	
<i>Influence of depth of embedment and material configuration on the coupled rocking-transverse vibration of rigid plates</i>	87
Yijun Liu (joint with Shuo Huang)	
<i>Fast Multipole BEM For Thin Plate Bending Problems</i>	89

Matthias Maischak	
<i>p</i> -BEM and <i>hp</i> -BEM – efficient methods for achieving high accuracy ...	90
Vladislav Mantič (joint with Christos G. Panagiotopoulos, Tomáš Roubíček)	
<i>BEM Analysis of Quasistatic Delamination of Viscoelastic Bodies with Very Small Viscosity</i>	91
Benjamin Marussig (joint with Christian Duenser, Gernot Beer)	
<i>Iso-geometric Boundary Element Methods for Tunneling</i>	98
Sofia G. Mogilevskaya (joint with Steven L. Crouch, Henryk K. Stolarski)	
<i>Generalized Maxwell's Methodology for Evaluating the Effective Properties of Orthotropic Composites</i>	105
Günther Of (joint with Dominic Amann, Andreas Blaszczyk, Olaf Steinbach)	
<i>Boundary Element Methods for Electrostatic Field Problems with Floating Potentials</i>	106
Ernian Pan (joint with Yanfei Zhao)	
<i>Fast boundary element analysis for 3D magneto-electro-elastic bimaterial</i>	107
Felipe Pinochet (joint with Norbert Heuer)	
<i>DPG method with optimal test functions for hypersingular operators in two dimensions</i>	109
Dirk Praetorius (joint with Markus Faustmann, Jens Markus Melenk)	
<i>Black-Box Preconditioning of BEM matrices by \mathcal{H}-matrix techniques</i> ...	110
Sergio Rojas (joint with Carlos Jerez-Hanckes, Ralf Hiptmair)	
<i>Multiple Traces Boundary Integral Formulation for Helmholtz Transmission Problems with screens</i>	112
A. Salvadori (joint with A. Temponi, F. Valvona)	
<i>Recent advances in modeling time dependent problems via boundary elements</i>	113
Francisco-Javier Sayas (joint with Constantin Bacuta, George C Hsiao)	
<i>News from the Single Layer Potential for the Transient Stokes Problem</i> .	114
Martin Schanz (joint with Peng Li)	
<i>Time Domain BE Formulation for Partially Saturated Poroelasticity</i> ...	115
E. Spindler (joint with R. Hiptmair, X. Claeys)	
<i>Second-kind Single Trace BEM for Acoustic Scattering</i>	122
Benjamin Stamm (joint with Jan S. Hesthaven, Shun Zhang)	
<i>Certified Reduced Basis Method for the Electric Field Integral Equation</i> .	129
E.P. Stephan	
<i>High order BEM for contact problems</i>	130
Wojciech Sulisz	
<i>Application Of Boundary Element Method To The Modelling Of A Wave Powered Plant</i>	131

Johannes Tausch	
<i>BEM for Parabolic Moving Boundary Problems</i>	137
M. Tezer-Sezgin (joint with B. Pekmen)	
<i>Unsteady mixed convection in a porous lid-driven enclosure under a magnetic field</i>	138
Thomas Traub (joint with Martin Schanz)	
<i>A Directional Fast Multipole Method for Elastodynamics</i>	144
Carolina A. Urzúa (joint with Carlos Jerez-Hanckes)	
<i>Operator preconditioning for two-dimensional screen and fracture problems using boundary elements</i>	150
W. Ye (joint with J. Xiao)	
<i>On the relationship between the frequency-domain BEM and the convolution quadrature BEM</i>	157
Minghao Zhao (joint with Ernian Pan, Cuiying Fan, Guoning Liu)	
<i>Hybrid Extended Displacement Discontinuity-Fundamental Solution Method For Two- And Three-Dimensional Smart Media</i>	159

Extended Abstracts

A Boundary Integral Formulation Based On The Convolution Quadrature Method For Transient Heat Conduction In Functionally Graded Materials

A. I. ABREU

(joint work with A. Canelas, W. J. Mansur)

A Boundary Element Method based on the Convolution Quadrature Method for transient heat conduction analysis is presented. Heat conduction problems inside homogeneous and non-homogeneous media are considered. In the case of the non-homogeneous media, the conductor is assumed to be a functionally graded material, i.e., the material properties vary spatially according to known smooth functions. The Convolution Quadrature Method is adopted to obtain a numerical approximation of the integral equation of the time-domain boundary element method. A numerical example of transient heat conduction problems is presented to show the versatility and accuracy of the method.

1. INTRODUCTION

For transient heat conduction problems, the classical time-domain (TD) formulation of the Boundary Element Method (BEM) presents convolution integrals with respect to the time variable. One of the recognized disadvantages of the classical TD-BEM approach lies in the high computational cost of the numerical evaluation of these convolution integrals. Moreover, the analysis of problems with complex-shaped domains becomes more computational intensive when numerical responses at a large number of interior points are required and, especially, when non-homogeneous problems are analyzed. In recent years, the Convolution Quadrature Method (CQM) [3] has been found suitable for application to TD-BEM approaches. The CQM-based BEM evaluates the convolution integrals of the TD-BEM formulation by means of a quadrature formula that uses the fundamental solution in the Laplace-transformed domain. One of the advantages of using the CQM is that it makes the BEM able for problems where the analytical TD fundamental solution is not available or is difficult to compute. Applications of the CQM-based BEM to elastodynamics, viscoelasticity and poroelasticity problems [4, 5], acoustics [1] and more recently to thermoelasticity problems [2] have shown that it is an appropriate time discretization method.

Functionally Graded Materials (FGM) are non-homogeneous materials for which some material properties vary according to a smooth function on the spatial coordinates. An increasing number of papers concerning applications of FGMs are being published, and the technique proposed in [6] reduces the heat conduction problem inside a FGM to a standard problem inside a homogeneous material. In the present work a clear characterization of the material variations that can be addressed through this technique is achieved by means of a simple differential

equation expressed in terms of the square root of the thermal conductivity function. In addition, numerical examples of transient heat conduction problems are presented to show the versatility and accuracy of the method.

2. GOVERNING EQUATION AND FUNDAMENTAL SOLUTIONS

The heat equation describing the evolution of the temperature T inside a general non-homogeneous isotropic conductor Ω , in the case of zero heat sources is:

$$(1) \quad \rho(x)c_e(x)\frac{\partial T}{\partial t}(x,t) - \nabla \cdot [K(x)\nabla T(x,t)] = 0 \quad \text{in } \Omega,$$

where $K(x) > 0$ is the thermal conductivity of the material, $c_e(x) > 0$ is the specific heat, and $\rho(x) > 0$ is the mass density. The material properties are known, as well as the initial condition $T(x, t_0) = T_0(x)$ at time t_0 and the following boundary conditions for $t > t_0$: $T(x, t) = \bar{T}(x, t)$ in Γ_T and $q(x, t) = \bar{q}(x, t)$ in Γ_q , where $q(x, t) = -K(x)\frac{\partial T}{\partial n}(x, t)$ is the normal heat flux on the boundary Γ of Ω ($\Gamma_T \cup \Gamma_q = \Gamma$). \bar{T} and \bar{q} are known functions and n is the outward-pointing unit normal vector on Γ .

For the analysis of FGMs, the approach proposed in [6] is followed, but it is presented here in a slightly different way, providing also a complete characterization of the spatial variations of the material properties that can be treated by this technique. The material properties are considered constant over time, the density ρ is also considered constant over space, and the material properties K and c_e must have a spatial variation in such a way that the thermal diffusivity $\kappa = \frac{K(x)}{\rho c_e(x)}$ of the material is constant. In this case, the substitutions $K(x) = \varphi^2(x)$ and $T(x, t) = \varphi^{-1}(x)v(x, t)$ in Eq. (1) lead to the following equation:

$$(2) \quad \frac{\partial v}{\partial t}(x, t) - \kappa \nabla^2 v(x, t) + \frac{\kappa \nabla^2 \varphi(x)}{\varphi(x)} v(x, t) = 0.$$

The particular case that can be addressed by the present approach is when the function K is such that its square root φ satisfies:

$$(3) \quad \kappa \nabla^2 \varphi(x) = -\alpha \varphi(x) \quad \text{for a constant value } \alpha.$$

The additional substitution $v(x, t) = \exp(\alpha t)u(x, t)$ leads to the standard heat equation for homogeneous materials in terms of the variable u :

$$(4) \quad \frac{\partial u}{\partial t}(x, t) - \kappa \nabla^2 u(x, t) = 0.$$

If Eq. (3) is satisfied, then the original heat equation (1) can be reduced to the standard heat equation for homogeneous materials (4).

The fundamental solution T^* of the original problem of Eq. (1) is a free-space Green's function describing the temperature field generated by a unit heat source applied at point ξ at time t_0 . It satisfies:

$$(5) \quad \rho c_e(x) \frac{\partial T^*}{\partial t}(x, t; \xi, t_0) - \nabla_x \cdot [K(x) \nabla_x T^*](x, t; \xi, t_0) = \delta(\xi - x) \delta(t_0 - t).$$

Assuming $\kappa \nabla^2 \varphi(x) = -\alpha \varphi(x)$, the substitutions $K(x) = \varphi^2(x)$, $T^*(x, t; \xi, t_0) = \varphi^{-1}(x) v^*(x, t; \xi, t_0)$ and $v^*(x, t; \xi, t_0) = \exp(\alpha t) w^*(x, t; \xi, t_0)$ in Eq. (5) give:

$$(6) \quad \frac{\partial w^*}{\partial t}(x, t; \xi, t_0) - \kappa \nabla_x^2 w^*(x, t; \xi, t_0) = \frac{\kappa \delta(\xi - x) \delta(t_0 - t)}{\varphi(\xi) \exp(\alpha t_0)}.$$

Then, w^* is given by:

$$(7) \quad w^*(x, t; \xi, t_0) = \frac{\kappa}{\varphi(\xi) \exp(\alpha t_0)} u^*(x, t; \xi, t_0),$$

where u^* is the fundamental solution of the standard heat equation. Returning back to the original variables, the TD fundamental solution T^* is:

$$(8) \quad T^*(x, t; \xi, t_0) = \frac{1}{4\pi \sqrt{K(\xi)K(x)} \tau} \exp\left(-\frac{r^2}{4\kappa\tau} + \alpha\tau\right) H(\tau),$$

where $r = \|\xi - x\|$, $\tau = t - t_0$, and the Heaviside function H enforces the causality condition $T^* \equiv 0$ for $t < t_0$. Note that setting $\alpha = 0$ in Eq. (8) and considering constant properties K , c_e and ρ , the TD fundamental solution for homogeneous materials is achieved.

3. CQM-BASED BEM FORMULATION FOR FGMS

Assuming a homogeneous initial condition, the following boundary integral equation in terms of T is achieved:

$$(9) \quad c(\xi)T(\xi, \tilde{t}) = \int_{\Gamma} \int_{t_0}^{t_f} [T^*(x, \tilde{t}; \xi, t) p(x, t) - p^*(x, \tilde{t}; \xi, t) T(x, t)] dt d\Gamma,$$

where T^* is the TD fundamental solution given by Eq. (8), $p^*(x, \tilde{t}; \xi, t) = K(x) \frac{\partial T^*}{\partial n}(x, \tilde{t}; \xi, t)$ and $p(x, t) = K(x) \frac{\partial T}{\partial n}(x, t)$ (note that $p^* = -q^*$ and $p = -q$). The time $\tilde{t} \in [t_0, t_f]$, where t_f is the final time of analysis, and the coefficient $c(\xi)$ is the same as that of the static problem. To solve the TD boundary integral equation (9) the boundary is divided into n_e elements Γ_j ($j = 1, 2, \dots, n_e$) and the time span $[t_0, t_f]$ is divided into N time-steps of equal size Δt . The discrete version of Eq. (9) using the CQM for a point source ξ_i and the time $t_n = t_0 + n\Delta t$ ($n = 0, 1, \dots, N$) is given by:

$$(10) \quad c(\xi_i)T(\xi_i, t_n) = \sum_{j=1}^{n_e} \sum_{m=0}^n \mathbf{g}_{n-m}^j(\xi_i, \Delta t) \mathbf{p}_m^j - \sum_{j=1}^{n_e} \sum_{m=0}^n \mathbf{h}_{n-m}^j(\xi_i, \Delta t) \mathbf{T}_m^j.$$

The quadrature weights \mathbf{g}_n^j and \mathbf{h}_n^j of Eq. (10) are given by:

$$(11) \quad \mathbf{g}_n^j(\xi_i, \Delta t) = \frac{\sigma^{-n}}{L} \sum_{\ell=0}^{L-1} \int_{\Gamma_j} \hat{T}^*(x, \xi, s_\ell) \mathbf{N}^j(x) d\Gamma e^{-\theta n \ell},$$

$$(12) \quad \mathbf{h}_n^j(\xi_i, \Delta t) = \frac{\sigma^{-n}}{L} \sum_{\ell=0}^{L-1} \int_{\Gamma_j} \hat{p}^*(x, \xi, s_\ell) \mathbf{N}^j(x) d\Gamma e^{-\theta n \ell},$$

where $\theta = 2\pi i/L$ ($i = \sqrt{-1}$), $\mathbf{N}^j(x)$ represents the matrix of interpolation functions of the spatial discretization, the discrete parameter $s_\ell = \gamma(\sigma e^{\theta \ell})/\Delta t$, and the

function γ is the quotient of the characteristic polynomial generated by a linear multi-step method that is usually a backward differentiation formula of order N_γ . $\hat{T}^*(r, \cdot)$ and $\hat{p}^*(r, \cdot)$ are the Laplace transforms of $T^*(r, \cdot)$ and $p^*(r, \cdot)$, respectively. The expression of the TD fundamental solution T^* for FGMs due to a heat point source was given in Eq. (8) and the corresponding fundamental solution \hat{T}^* in the Laplace-transformed domain is:

$$(13) \quad \hat{T}^*(x, \xi, s) = \frac{1}{2\pi\sqrt{K(\xi)K(x)}} K_0 \left(r \sqrt{\frac{s-\alpha}{\kappa}} \right),$$

where K_0 is the modified Bessel function of the second kind and order zero. For homogeneous materials, the corresponding fundamental solution \hat{T}_h^* in the Laplace-transformed domain is given by:

$$(14) \quad \hat{T}_h^*(x, \xi, s) = \frac{1}{2\pi K} K_0 \left(\sqrt{\frac{s}{k}} r \right).$$

The vectors \mathbf{T}_m^j and \mathbf{p}_m^j of Eq. (10) represent, respectively, the prescribed or unknown nodal values of T and p defined at each element j of the boundary. They are given by $\mathbf{T}_m^j = \mathbf{T}^j(t_m)$ and $\mathbf{p}_m^j = \mathbf{p}^j(t_m)$ ($m = 0, 1, \dots, N$ in the time). Equation (10) can be rewritten in matrix form as follows:

$$(15) \quad \mathbf{c}\mathbf{T}_n = \sum_{m=0}^n \mathbf{G}_{n-m}\mathbf{p}_m - \sum_{m=0}^n \mathbf{H}_{n-m}\mathbf{T}_m.$$

The responses on the boundary and at interior points are calculated from Eq. (15), where \mathbf{G} and \mathbf{H} are the BEM influence matrices and \mathbf{c} is the diagonal matrix containing the coefficients $c(\xi)$. The indices n and m correspond to the discrete times $t_n = t_0 + n\Delta t$ and $t_m = t_0 + m\Delta t$, respectively. By imposing the boundary conditions into Eq. (15), the following expression is obtained:

$$(16) \quad \mathbf{A}_0\mathbf{y}_n = \mathbf{f}_n + \sum_{m=0}^{n-1} (\mathbf{G}_{n-m}\mathbf{p}_m - \mathbf{H}_{n-m}\mathbf{T}_m),$$

where \mathbf{A}_0 stores the columns of $\mathbf{c} + \mathbf{H}_0$ corresponding to the unknown values of \mathbf{T} and the columns of \mathbf{G} corresponding to the unknown values of \mathbf{p} . The unknown values of \mathbf{T} and \mathbf{p} at time t_n are stored in the vector \mathbf{y}_n . The known values of \mathbf{T} and \mathbf{p} are multiplied by their respective columns of \mathbf{H} and \mathbf{G} to assemble the vector \mathbf{f}_n . The CQM-based BEM solves Eq. (16) consecutively to obtain the solutions \mathbf{y}_n with $n = 0, 1, \dots, N$.

4. NUMERICAL EXAMPLE

A transient heat conduction problem in a rotor subject to mixed boundary conditions is analyzed for two cases: A homogeneous and a FGM rotor with a radial spatial variation of the material properties. The rotor has eight mounting holes like the considered in [6]. To solve the homogeneous rotor, the fundamental solution \hat{T}_h^* given by Eq. (14) is used. For the other one the fundamental solution \hat{T}^* given by Eq. (13) is used. The CQM parameters are $L = N$ and $\sigma^N = \sqrt{\varepsilon}$

with $\varepsilon = 10^{-4}$, and $\gamma(z)$ corresponds to a backward differentiation formula of order $N_\gamma = 2$ [3]. The spatial discretization uses linear elements, and the initial condition is $T_0(X) = 0$ at $t_0 = 0$.

Homogeneous rotor: The results of the CQM-based BEM for a homogeneous rotor are compared against the results obtained using the Finite Element Method (FEM). In this case the material properties are given in Table 1. In the case of the FEM, a mesh of 292 nodes, and 504 triangular elements was used. For the CQM-based BEM, a boundary mesh of $n_e = 80$ elements was used (the nodes coincide with the 80 boundary nodes of the FEM mesh). The time discretization used for both methods consists of 128 time-steps $\Delta t = 0.001$ from $t_0 = 0$ to $t_f = 0.128$.

FGM rotor: In this case the results of the CQM-based BEM for a FGM rotor are compared against the results corresponding to the homogeneous rotor. The material properties of the FGM rotor are also given in Table 1. In this case the results for the FGM rotor are different from the results obtained for the homogeneous rotor, despite the fact that the diffusivity κ is the same in both cases. Contour plots of the temperature at times $t = 0.005$ and $t = 0.1$ for both rotors are shown in Fig. 1.

TABLE 1. Material properties of the FGM rotor problem

<i>Variation</i>	α	κ	K	c_1	c_2	β	$K(r)$
Homogeneous	0	0.001	0.001	1	0	0	0.001
FGM	0	0.001	0.001	4	1	0	$0.001(4 + \log(r))^2$

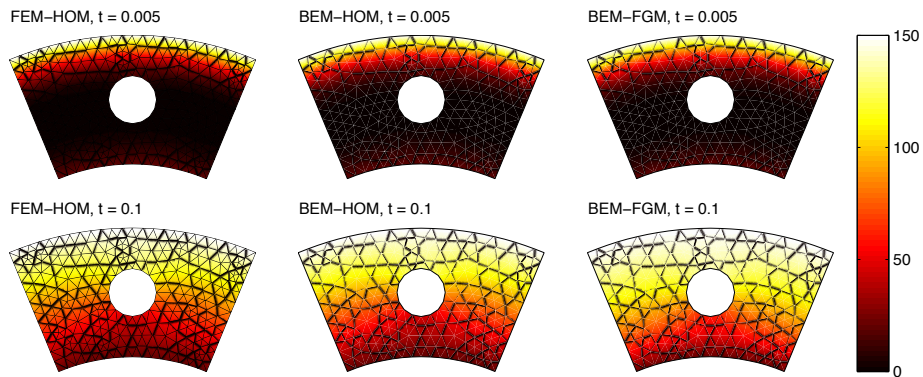


FIGURE 1. Contour plots of the temperature in the homogeneous and FGM rotors at different times.

5. CONCLUSIONS

A CQM-based BEM formulation was proposed with the purpose of analyzing two-dimensional problems governed by the heat equation in homogeneous materials and FGMs. The formulation proposed can accurately obtain the solutions to the example studied, which considers different spatial variations of the material properties of the FGM, mixed boundary conditions, and a complex shaped domain.

A. I. Abreu, W. J. Mansur

Department of Civil Engineering, COPPE/Federal University of Rio de Janeiro, CP 68506, CEP 21945-970, Rio de Janeiro, RJ, Brazil
anai@coc.ufrj.br

A. Canelas

Instituto de Estructuras y Transporte, Facultad de Ingeniería, Universidad de la República. J. Herrera y Reissig 565 - 11300, Montevideo, Uruguay
acanelas@fing.edu.uy

REFERENCES

- [1] A. I. Abreu, J. A. M. Carrer, and W. J. Mansur. Scalar wave propagation in 2D: A BEM formulation based on the operational quadrature method. *Eng. Anal. Bound. Elem.*, 27(2): 101–105, 2003.
- [2] A. I. Abreu, A. Canelas, B. Sensale, and W. J. Mansur. CQM-based BEM formulation for uncoupled transient quasistatic thermoelasticity analysis. *Eng. Anal. Bound. Elem.*, 36(4): 568–578, 2011.
- [3] C. Lubich. Convolution quadrature and discretized operational calculus I and II. *Numer. Math.*, 52:129–145 (and 413–425), 1988.
- [4] M. Schanz. *Wave propagation in viscoelastic and poroelastic continua: A boundary element approach*, volume II of *Lecture Notes in Applied Mechanics*. Springer-Verlag, Berlin, Heidelberg, New York, 2001.
- [5] M. Schanz. On a reformulated convolution quadrature based boundary element method. *CMES Comput. Model. Eng. Sci.*, 58(2010), pp. 109-129.
- [6] A. Sutradhar and G. H. Paulino. The simple boundary element method for transient heat conduction in functionally graded materials. *Comput. Methods Appl. Mech. Eng.*, 193(42-44):4511–4539, 2004.

Data Compression Techniques for the p -Version of the Boundary Element Method for the Laplace Equation in two dimensions

MARKUS BANTLE

(joint work with Stefan Funken)

We consider Symm's integral equation

$$(1) \quad V\phi = f, \quad \text{on } \Gamma = \partial\Omega,$$

where Ω is a bounded Lipschitz domain in \mathbb{R}^2 with polygonal boundary Γ and V denotes the single layer operator for the Laplace equation in two dimensions. Using the Boundary Element Method (BEM) to solve (1) generally results in a linear system with densely populated Galerkin matrix \mathbf{V} . For the h -version of BEM and Wavelet Galerkin methods there are various data compression schemes. Using \mathcal{H} - and \mathcal{H}^2 -Matrices one can reduce the computational cost for assembly and matrix vector multiplication to $\mathcal{O}(N \log(N))$ and $\mathcal{O}(N)$, respectively, where N is the number of degrees of freedom (e.g. [8], [4]). In Wavelet-BEM data compression techniques result in sparse matrices that yield $\mathcal{O}(N)$ for the complexities for assembly and matrix vector multiplication. In [9], a data compression scheme for the p -BEM is presented that builds upon the idea that small matrix entries can be neglected. However, no complexity estimates are provided.

In this paper we present a data compression scheme for the single layer Galerkin Matrix that arises in the p -version of the BEM. Combining different techniques that are used for \mathcal{H} -Matrices and the approach of [9] and using different techniques for different sub-blocks of the Galerkin matrix, we obtain a compression scheme that allows for the assembly of the Galerkin matrix and the matrix vector multiplication with $\mathcal{O}(N \log(N)^2)$ operations.

1. GALERKIN DISCRETIZATION AND COMPUTATION OF GALERKIN ENTRIES

Consider a quasi-uniform triangulation $\mathcal{T} = \{T_i, i = 1, \dots, M\}$ with mesh-widths $h_i := |T_i| > 0$ and polynomial degrees $p_i \in \mathbb{N}_0$. Let $\underline{h} := \min_{i=1, \dots, M} h_i$ and $\bar{p} := \min\{1, \max_{i=1, \dots, M} p_i\}$. We define the ansatz space

$$S^0 := \left\{ \phi : \phi|_{T_i} \in \text{span}\{P_\ell^{(i)}, \ell = 0, \dots, p_i\} \forall T_i \in \mathcal{T} \right\}.$$

Here $P_\ell^{(i)}$ is the ℓ -th Legendre polynomial mapped to the element T_i by an affine mapping. Using S^0 for the Galerkin discretization we obtain a block Galerkin matrix $\mathbf{V} = (\mathbf{V}^{(i,j)})_{i,j=1, \dots, M}$ with blocks $\mathbf{V}^{(i,j)} \in \mathbb{R}^{p_i \times p_j}$ and

$$V_{k,\ell}^{(i,j)} = -\frac{1}{2\pi} \int_{T_i} P_k^{(i)}(x) \int_{T_j} P_\ell^{(j)}(y) \log|x-y| ds_y ds_x.$$

For the case of identical elements, i.e. $T_i = T_j$, there holds

$$(2) \quad V_{k,\ell}^{(i,i)} = -\frac{h_i^2}{4\pi} \begin{cases} \log h_i^2 - 3 & , \text{ if } k = m = 0, \\ \frac{2}{(k + \ell + 2)(\ell + k)((\ell - k)^2 - 1)} & , \text{ if } k + \ell > 0, k - \ell \text{ even,} \\ 0 & , \text{ otherwise.} \end{cases}$$

This allows for the direct computation of Galerkin entries. For non-identical elements, we define m_i as the midpoint of T_i , u_i as the tangent vector of T_i with length $h_i/2$, and $w := m_j - m_i$ and get

$$V_{k,\ell}^{(i,j)} = -\frac{h_i h_j}{8\pi} \left(2\delta_{k0}\delta_{\ell0} \log(u_j^T u_j) + \operatorname{Re} \int_{-1}^1 P_k(s) \int_{-1}^1 P_\ell(t) \log(z(s) - t) dt ds \right)$$

with $z(s) = a(u_j, w) + b(u_j, u_i)s$, where $a(u_j, w), b(u_j, u_i) \in \mathbb{C}$. Thus, the computation of Galerkin entries can be reduced to the evaluation of the function

$$I_{k,\ell}^{-1}(a, b) := \int_{-1}^1 P_k(s) \int_{-1}^1 P_\ell(t) \log(z(s) - t) dt ds.$$

There exist recurrence relations for $I_{k,\ell}^{-1}(a, b)$ with respect to k, ℓ (see [2]). However, these recurrence relations are unstable for general $a, b \in C$. Therefore, we use the multiple-precision libraries `mpfr` and `mpc` ([6], [5]) for the evaluation of these recurrence relations.

2. FAR FIELD BLOCKS

For the matrix blocks that correspond the boundary elements $T_i, T_j \in \mathcal{T}$ with $T_i \cap T_j = \emptyset$, we use the idea that small matrix entries can be neglected. In order to derive an upper bound for the magnitude of the matrix entries that can be neglected, we follow an approach presented in [7] that analyzes the influence of perturbations in the Galerkin entries on the consistency error for h -BEM. Adapting the notation of [7] we introduce an abstract index set $\mathcal{F} = \{1, \dots, N\}$ for all basis functions of S^0 . Furthermore, $\mathbf{V} = (V_{f,f'})_{f,f' \in \mathcal{F}}$ is the Galerkin matrix for the bilinear form $a(u, v) = (Vu, v)_{L^2(\Gamma)}$ and $\tilde{\mathbf{V}} = (\tilde{V}_{f,f'})_{f,f' \in \mathcal{F}}$ denotes the Galerkin matrix for the perturbed bilinear form a_h . We obtain the following estimate, which can be proven using the Cauchy Schwarz inequality and an inverse estimate from [11].

Theorem 2.1. *If $|V_{f,f'} - \tilde{V}_{f,f'}| < \varepsilon$ for all $f, f' \in \mathcal{F}$, then*

$$\frac{|a(v, w) - a_h(v, w)|}{\|v\|_{H^{-1/2}(\Gamma)} \|w\|_{H^{-1/2}(\Gamma)}} \leq \varepsilon \left(\frac{\bar{p}}{\underline{h}} \right)^3$$

for all $v, w \in S_0$.

Thus, if the Galerkin error behaves like $\|\phi - \phi_h^p\|_{H^{-1/2}(\Gamma)} \lesssim \underline{h}^s \bar{p}^{2s}$ with $s > 0$, we have to request

$$(3) \quad \varepsilon \lesssim \varepsilon_0 := \frac{\underline{h}^{3+s}}{\bar{p}^{3+2s}}$$

in order to keep the consistency error below the Galerkin error. This means that all matrix entries with $|V_{k,\ell}^{(i,j)}| < \varepsilon_0$ can be neglected.

In [9] the estimate

$$(VP_k^{(i)}, P_\ell^{(j)})_{L^2(\Gamma)} \leq \frac{C}{\pi} \left(\frac{\max\{|T_i|, |T_j|\}}{2\text{dist}(T_i, T_j)} \right)^{k+\ell}$$

with C only depending on Γ is derived. Combining this estimate with (3) shows that we can neglect all entries $V_{k,\ell}^{i,j}$ with

$$(4) \quad k + \ell \gtrsim F(\log(\underline{h}), \log(\bar{p}), \text{dist}(T_i, T_j)) = \mathcal{O}(\log(\bar{p})).$$

Hence, for one far field block only $\mathcal{O}(\log(\bar{p})^2)$ entries need to be computed.

We are now ready to formulate an algorithm for the computation of the far field blocks:

- (i) (First row) Calculate ℓ_0 such that $\ell \lesssim F(\log(\underline{h}), \log(\bar{p}), \text{dist}(T_i, T_j))$, $\ell = 1, \dots, \ell_0$.
- (ii) (A priori compression) Calculate the matrix block $V_{k,\ell}^{(i,j)}$, $k, \ell = 1, \dots, \ell_0 + 1$.
- (iii) (A posteriori compression) Remove all entries which are smaller than ε_0 (see (3)).
- (iv) Store the remaining entries in a sparse matrix.

Numerical experiments (see Table 1) show that the estimate (4) is too coarse. Therefore, we derive another estimate for the Galerkin entries. For this purpose we define the function

$$\tilde{Q}_n^{-1}(z) := \int_{-1}^1 P_n(t) \log(z-t) dt, \quad z \in \mathbb{C},$$

which is closely related to the associated Legendre function of the second kind, $Q_n^{-1}(z)$. Using this relation and an asymptotic expansion of $Q_n^{-1}(z)$ (see [10]), we obtain

$$\tilde{Q}_n^{-1}(z) \sim 2\sqrt{\pi} n^{-3/2} \xi^{-n} (1 - \mathcal{O}(\xi^{-2}))$$

with $\xi = z + \sqrt{z^2 - 1}$ as $n \rightarrow \infty$ ([2]). Defining $\hat{Q}_n^{-1}(z) := 2\sqrt{\pi} n^{-3/2} \xi^{-n}$ and using the Cauchy Schwarz inequality, we can derive an estimate for the values of $I_{k,\ell}^{-1}(a, b)$ by

$$(5) \quad \begin{aligned} |I_{k,\ell}^{-1}(a, b)|^2 &= \left| \int_{-1}^1 P_k(s) \tilde{Q}_\ell^{-1}(z(s)) ds \right|^2 \lesssim \int_{-1}^1 (P_k(s))^2 ds \cdot \int_{-1}^1 \left(\hat{Q}_\ell^{-1}(z(s)) \right)^2 ds \\ &= \frac{2}{2k+1} \int_{-1}^1 \left(\hat{Q}_\ell^{-1}(z(s)) \right)^2 ds. \end{aligned}$$

This estimate can be used to determine ℓ_0 in step (i) of the algorithm. Table 1 shows that the estimate (5) performs better than (4), especially if the two boundary pieces are close together.

TABLE 2. Number of non-zero entries in a far field block after the a-priori compression with (4) and (5), respectively, and the a-posteriori compression. Here we choose $T_i = [-1, 1] \times \{0\}$, $T_j = \text{conv}\{A_j, B_j\}$, and $\varepsilon_0 = 4.3e - 08$.

A_j	B_j	nnz (a priori (4))	nnz (a priori (5))	nnz (a posteriori)
(3.0, 0.0)	(5.0, 0.0)	529	100	37
(2.0, 2.0)	(4.0, 4.0)	1225	121	39
(-1.0, 2.0)	(1.0, 2.0)	529	144	31
(-5.0, -1.0)	(-3.0, 0.0)	784	121	37

3. DIAGONAL BLOCKS

For the diagonal blocks $\mathbf{V}^{(i,i)}$ we use a hierarchical matrix format. This format is based on the idea that the matrix entries which are separated from the diagonal behave smoothly with respect to their indices and can thus be interpolated (see [1]). Our goal is to divide $\mathbf{V}^{(i,i)}$ hierarchically into sub-blocks and to create low-rank approximations on sub blocks that are separated from the diagonal. Adopting the \mathcal{H} -Matrix terminology, we say that a d -by- d sub-block $\mathbf{V}_S = (\mathbf{V}_{k,\ell}^{(i,i)})_{(k,\ell) \in S}$ with $S = \{k_0, \dots, k_0 + d\} \times \{\ell_0, \dots, \ell_0 + d\} =: \sigma \times \tau$ is separated from the diagonal if $d < \eta \text{dist}(\sigma, \tau)$ with $\eta \in (0, 2)$ and $\text{dist}(\sigma, \tau) := \min\{0, k_0 - \ell_0 - 1\}$. Equation (2) indicates that on admissible sub blocks the matrix entries $V_{k,\ell}^{(i,i)}$ can be expressed by $V_{\ell,k}^{(i,i)} = V_{k,\ell}^{(i,i)} = -\frac{h^2}{4\pi} f(k, \ell)$ with a smooth function f . To obtain a low rank approximation on an admissible sub-block, we use Lagrange interpolation with Chebyshev nodes $t_r \in [0, 1]$, $r = 1, \dots, \nu$ and obtain

$$V_{k_0+k, \ell_0+\ell}^{(i,i)} = f(k_0 + k, \ell_0 + \ell) \approx \sum_{r=1}^{\nu} f(k_0 + t_r d, \ell_0 + \ell) \cdot L_r\left(\frac{k}{d}\right).$$

Here $L_r(x)$ is the r -th Lagrange basis polynomial with respect to the Chebyshev nodes. In order to determine the interpolation order ν , which is also the rank of the low rank approximation of \mathbf{V}_S , we analyze the interpolation error $E(F_y, \nu, S)$ for the function $F_y := f(\cdot, y)$ on the square $S := [x_0, x_0 + d] \times [y_0, y_0 + d]$. Using Cauchy's integral formula to get an upper bound for the derivatives of F_y , the error formula for Lagrange interpolation, and the admissibility condition, we obtain

$$E(F_y, \nu, S) \lesssim \left(\frac{\eta}{2}\right)^{\nu} \left(\frac{\eta}{d}\right)^2 \frac{1}{(x_0 + y_0)^2},$$

i.e. the interpolation error converges exponentially with respect to the interpolation order ν . Theorem 2.1 yields that choosing $\nu = \mathcal{O}(\log \bar{p})$ suffices to keep the order of convergence. Furthermore, the complexity estimates for \mathcal{H} -Matrices (see [8]) show that the storage amount and the complexity for one matrix vector multiplication is $\mathcal{O}(\bar{p} \log(\bar{p}))$.

4. OFF-DIAGONAL BLOCKS

For the blocks $\mathbf{V}^{(i,j)}$ that correspond to neighboring elements $T_i, T_j \in \mathcal{T}$ we use a generalized cross approximation scheme to obtain a rank k approximation. Unlike in the cross approximation scheme introduced in [3], we have to search the pivot elements in the full residual matrix in general. Numerical experiments indicate that the choice $r = \mathcal{O}(\log(\bar{p})^2)$ is sufficient to retain the order of convergence of the underlying Galerkin scheme. Thus, for the general case, the complexity for storage and matrix vector multiplication for one off-diagonal block is $\mathcal{O}(\bar{p} \log(\bar{p})^2)$.

5. NUMERICAL RESULTS

We consider the p -BEM for $V\phi = \frac{\log(2)}{2}$ on $\Gamma = \partial\Omega$, where Ω is the L-shaped domain $[-1, 1] \times [-1, 1] \setminus [-1, 0] \times [-1, 0]$ and the boundary is split into 8 elements. For the diagonal blocks we use $\eta = 1$ and a minimum block size of $d = 16$. Figure 1 shows the energy errors and the required storage for the full system and the compressed one. We see that the original rate of convergence is maintained. Furthermore, the size of the compressed matrix behaves asymptotically like $\mathcal{O}(\bar{p} \log(\bar{p})^2)$. Computation times can be seen in Figure 2. In order to search for pivot elements for the off-diagonal blocks, we have to assemble the full block first. Thus, the computational time for the assembly of the off-diagonal blocks is proportional to the assembly time for the full system. For the other matrix blocks and for the matrix vector multiplication with the compressed matrix, the computational times behave like $N \log(N)$.

Markus Bantle, Stefan Funken

University of Ulm

markus.bantle@uni - ulm.de, stefan.funken@uni - ulm.de

REFERENCES

- [1] B. Alpert and V. Rokhlin. A fast algorithm for the evaluation of legendre expansions. *Research Report Yale University*, 1991.

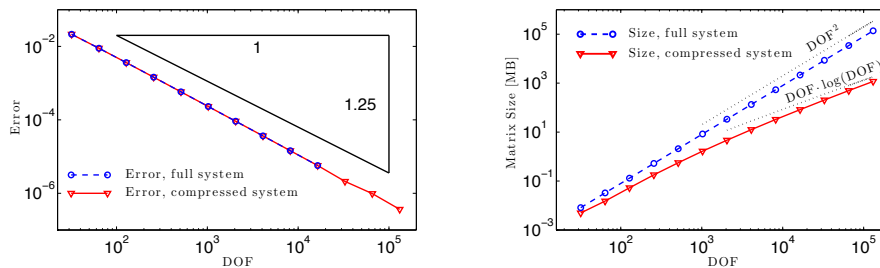


FIGURE 1. Energy error (left) and matrix size (right) for the full and the compressed system.

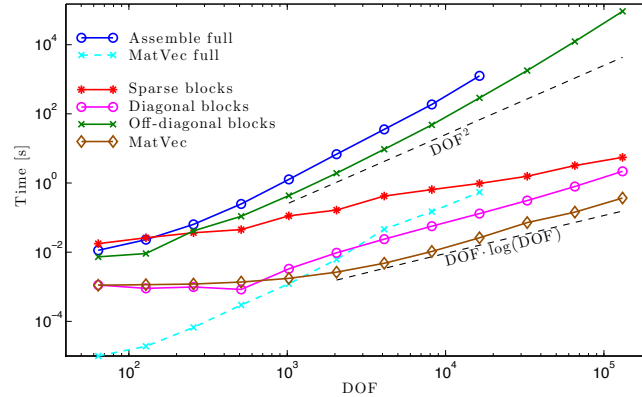


FIGURE 2. Computation times for the full system and the compressed system.

- [2] M. Bantle. *Dissertation (in preparation)*, 2013.
- [3] M. Bebendorf. Approximation of boundary element matrices *Numer. Math.*, 86:565-589, 2000
- [4] S. Boerm. \mathcal{H}^2 -Matrix arithmetics in linear complexity. *Computing*, 77(1):1-28, 2006.
- [5] A. Enge, M. Gastineau, P. Théveny, and P. Zimmermann. mpc — A library for multiprecision complex arithmetic with exact rounding. 2012.
- [6] L. Fousse, G. Hanrot, V. Lefèvre, P. Pélissier, and P. Zimmermann. Mpfr: A multiple-precision binary floating-point library with correct rounding. *ACM Transactions on Mathematical Software*, 33(2):13:1-13:15, 2007.
- [7] I. G. Graham, W. Hackbusch, and S. Sauter. Finite elements on degenerate meshes: Inverse-type inequalities and applications. *IMA J. Numer. Anal.*, 25(2):379-407, 2005.
- [8] W. Hackbusch. A sparse matrix arithmetic based on \mathcal{H} -matrixes. Part I: Introduction to \mathcal{H} -Matrixes. *Computing*, 62:89-108, 1999.
- [9] N. Heuer. Efficient algorithms for the p-version of the Boundary Element Method. *Journal of Integral Equations and Applications*, 8(3):1-24, 1996.
- [10] E.W. Hobson. The theory of spherical and ellipsoidal harmonics. *Chelsea Pub. Co.*, 1955.
- [11] M. Karkulik. Zur Konvergenz und Quasioptimalität adaptiver Randelementmethoden. *Dissertation*, 2012.

**Frequency-independent approximation of integral formulations of
Helmholtz boundary value problems**

M. BEBENDORF

(joint work with R. Venn)

We present recent numerical techniques for the treatment of integral formulations of Helmholtz boundary value problems in the case of high frequencies. The combination of \mathcal{H}^2 -matrices with recent developments of the adaptive cross approximation allows to solve such problems with logarithmic-linear complexity independent of the frequency. An advantage of this new approach over existing techniques such as fast multipole methods is its stability over the whole range of frequencies, whereas other methods are efficient either for low or high frequencies.

M. Bebendorf, R. Venn

Institute for Numerical Simulation, University of Bonn Wegelerstr. 6, 53115 Bonn, Germany

`bebendorf@ins.uni - bonn.de`, `venn@ins.uni - bonn.de`

Keywords: Integral equations, high-frequency scattering, adaptive cross approximation.

Comparison of two Fast Multipole Accelerated BEMs for 3D elastodynamic problems in semi-infinite media

S. CHAILLAT

(joint work with M. Bonnet)

This contribution is concerned with the development of the Fast Multipole accelerated Boundary Element Method (FM-BEM) to simulate the propagation of elastic waves in semi-infinite media. In [1], we previously developed a FM-BEM based on the elastic full-space fundamental solution. This method has been shown to be very efficient to simulate elastic wave in semi-infinite media, but nevertheless suffers from the drawback of requiring a discretization of the free surface. In practice, the free-surface was truncated at a chosen radius "large enough" for achieving a good accuracy in the target domain of study. A large number of BEM degrees of freedom (DOFs) was thus required on the free-surface for the sole purpose of enforcing the traction-free boundary condition.

To avoid the truncation issue, one can use fundamental solutions that intrinsically satisfies a traction-free boundary condition on the free-surface. This formulation thus reduces the overall size of the BE model since the free-surface no longer requires discretization. The derivation and implementation of the corresponding fundamental solution [3] are involved. In particular, unlike its full-space counterpart, the half-space fundamental solution cannot be expressed in terms of simpler kernels (e.g. Laplace or Helmholtz fundamental solutions) having already-known multipole expansions. Multipole expansions of the elastic half-space fundamental solution thus cannot be obtained in a simple way.

In [2], we have proposed an expansion of the elastic half-space fundamental solution in a form which achieves the separation of variables required by the FMM. The approach has been shown, by means of empirically-obtained complexity estimates and other numerical experiments, to possess the attributes required for a fast BEM, namely substantial acceleration and the ability to perform on large BE models. In this communication, we present a new FM-BEM based on this treatment of the half-space fundamental solution. The accuracy of this new FM-BEM (which does not require meshing the free surface) is compared to that of the FM-BEM based on the elastic full-space fundamental solutions (which does require meshing the free surface). Moreover, the numerical efficiency of both approaches is compared on seismology-oriented examples such as the scattering of plane waves by a cavity embedded in an elastic half-space, using the same mesh for the latter. Despite the additional computational effort required by the evaluation of the proposed FM-capable form of the half-space fundamental solution (relative to that of the diagonal-form expansion of the full-space fundamental solution), the new approach is shown to reduce several-fold the overall analysis time, thus establishing the overall benefit brought by removing the free-surface mesh.

Keywords: Fast Multipole Method, Elastodynamics, Half-space problems

Mathematics Subject Classifications (2000): 65Y20, 74S15, 31B10, 86-08

S. Chaillat, M. Bonnet

Laboratoire Poems (UMR CNRS-INRIA-ENSTA 7231), ENSTA, France

`stephanie.chaillat@ensta - paristech.fr`, `marc.bonnet@ensta - paristech.fr`

REFERENCES

- [1] S. Chaillat, M. Bonnet and J. F. Semblat, A multi-level fast multipole BEM for 3-D elastodynamics in the frequency domain. *Computer Methods in Applied Mechanics and Engineering* 197:4233-4249, 2008.
- [2] S. Chaillat and M. Bonnet, A new Fast Multipole Formulation for the Elastodynamic Half-space fundamental solutions. *Submitted*.
- [3] L. Pan, F. Rizzo and P.A. Martin, Some efficient boundary integral strategies for time-harmonic wave problems in an elastic halfspace. *Computer Methods in Applied Mechanics and Engineering* 164:207-221, 1998.

Using fast tree methods and GPU hardware for protein electrostatics

CHRISTOPHER COOPER

(joint work with Lorena A. Barba)

Biomolecular systems usually consist of proteins in ionic solutions. These can be modeled by continuum approximations that result in a coupled system of Poisson and Poisson-Boltzmann equations. A molecular surface is defined via solvent-accessible areas, and the system of equations expressed in the integral formulation can be solved with a boundary element method (BEM) [2]. We have developed a BEM application of this problem that uses a fast tree algorithm [1] and accelerator hardware (GPUs). The method scales as $O(N \log N)$, is memory-efficient and fast, and was validated with standard benchmarks [3]. It also maintains a Python interfaces with the user, for easy adoption. We now present an extension able to solve problems with multiple interfaces, making it applicable to realistic biological situations involving many proteins in a system.

Keywords: Integral equations, BEM, treecode, multipole methods, molecular electrostatics, GPU

Mathematics Subject Classifications (2000): 65N38, 31B10, 78M16, 92C40.

Christopher Cooper, Lorena A. Barba

Department of Mechanical Engineering, Boston University.

cdcooper@bu.edu, labarba@bu.edu

REFERENCES

- [1] P. Li, H. Johnston, and R. Krasny. *A Cartesian treecode for screened coulomb interactions*. *Journal of Computational Physics*, 228:3858–3868, 2009.
- [2] B J. Yoon and A. M. Lenhoff. *A boundary element method for molecular electrostatics with electrolyte effects*, *Journal of Computational Chemistry*, 11(9), 1990.
- [3] J. G. Kirkwood. *Theory of Solutions of Molecules Containing Widely Separated Charges with Special Application to Zwitterions*, *Journal of Chemical Physics*, 2, 1934.

A coupled finite element – hierarchical boundary element method based on Green’s functions for a horizontally layered halfspace

PIETER COULIER

(joint work with Stijn François, Geert Lombaert, Geert Degrande)

This paper discusses the coupling of finite elements and hierarchical boundary elements to solve problems of three-dimensional elastodynamic wave propagation involving dynamic soil–structure interaction. Green’s functions for a layered halfspace are incorporated in the hierarchical boundary element formulation, avoiding the necessity to mesh the free surface and the layer interfaces. Both direct and iterative coupling schemes are presented; special attention is paid to an optimized interface relaxation technique in the iterative solution procedure in order to ensure and/or speed up the convergence.

Keywords: boundary element method; elastodynamics; \mathcal{H} –matrices; halfspace Green’s functions; finite element – boundary element coupling; interface relaxation.

1. INTRODUCTION

The numerical prediction of three-dimensional (3D) elastodynamic wave propagation in a stratified halfspace arises in a variety of problems, such as the simulation of seismic site effects [?], the modelling of railway induced vibrations [?] and other applications involving dynamic soil–structure interaction (SSI) [?]. A subdomain approach is often introduced in computational models, where distinct numerical methods are used for different subdomains. A well-known methodology is the coupled finite element – boundary element (FE–BE) approach, which combines the flexibility offered by the FE method to model complex geometries with the possibility to take the radiation of waves towards infinity into account by means of the BE method.

The applicability of classical BE formulations to large scale problems is hindered, however, due to stringent memory and CPU requirement resulting from the dense, fully populated unsymmetric matrices arising in the formulation. This has led to the development of fast BE methods to improve the computational efficiency, including the fast multipole method (FMM) [2] and methods based on hierarchical matrices (\mathcal{H} –matrices) [3]. Recently, a \mathcal{H} –BE method for visco-elastodynamics based on Green’s functions for a horizontally layered halfspace has been presented [?]. These Green’s functions are computed by means of the direct stiffness method [4], as no closed form analytical expressions are available; their application avoids meshing of the free surface and the layer interfaces.

The coupling of FE and \mathcal{H} –BE models for the solution of dynamic SSI problems is more involved than in case of classical BE formulations. The aim of this paper is therefore to discuss different FE– \mathcal{H} –BE coupling procedures and to assess their computational performance; all models are formulated in the frequency domain. The text is organized as follows. Sections 2 and 3 briefly summarize the governing equations of the FE and \mathcal{H} –BE method, respectively. A direct and

iterative coupling strategy are introduced in section 4, while a numerical example is investigated in section 5.

2. FINITE ELEMENT FORMULATION

Finite element equilibrium equations of a domain Ω can be obtained by introducing a FE discretization in the weak variational formulation of the equilibrium of Ω , and by subsequently applying a Galerkin procedure. This provides the following set of equations [?]:

$$(1) \quad [\mathbf{K} + i\omega\mathbf{C} - \omega^2\mathbf{M}] \hat{\mathbf{u}}(\omega) = \hat{\mathbf{f}}(\omega) + \hat{\mathbf{f}}^s(\omega)$$

where a hat above a variable denotes its representation in the frequency domain. $\hat{\mathbf{u}}(\omega)$ collects the nodal degrees of freedom, while \mathbf{K} , \mathbf{C} and \mathbf{M} are the frequency independent stiffness, damping and mass matrices. The bracketed term on the left hand side of equation (1) is identified as the dynamic stiffness matrix $\hat{\mathbf{K}}(\omega)$. The force vectors $\hat{\mathbf{f}}(\omega)$ and $\hat{\mathbf{f}}^s(\omega)$ result from external forces and an incident wavefield on Ω , respectively. Adequate solvers which account for the sparsity and symmetry of the system can be employed to solve the system of equations (1).

3. HIERARCHICAL BOUNDARY ELEMENT FORMULATION

The BE method is based on the discretization of the boundary Σ of a domain Ω with an appropriate number of boundary elements in order to numerically solve a (regularized) boundary integral equation. The method leads to a reduction of the spatial problem dimension (i.e. surface instead of volume discretization), but the storage of the resulting BE collocation matrices requires a quadratic amount of memory with respect to the number of degrees of freedom N_{DOF} . The use of \mathcal{H} -matrices provides an elegant way to treat fully populated matrices with almost linear complexity [?], as they approximate the original matrices (with an arbitrary prescribed accuracy) by means of data-sparse, memory-efficient representations. The construction of \mathcal{H} -matrices is based on the identification of admissible and inadmissible hierarchical cluster pairs in the BE mesh; the reader is referred to references [3, ?, ?] for a detailed description of the methodology.

For an unbounded domain, the displacements $\hat{\mathbf{u}}(\omega)$ and tractions $\hat{\mathbf{t}}(\omega)$ at the collocation points are in the \mathcal{H} -BE method related as follows:

$$(2) \quad \left(\hat{\mathbf{T}}_{\mathcal{H}}(\omega) + \mathbf{I} \right) \hat{\mathbf{u}}(\omega) = \hat{\mathbf{U}}_{\mathcal{H}}(\omega) \hat{\mathbf{t}}(\omega)$$

where $\hat{\mathbf{T}}_{\mathcal{H}}(\omega)$ and $\hat{\mathbf{U}}_{\mathcal{H}}(\omega)$ are hierarchical representations of the BE collocation matrices. Throughout this paper, Green's functions for a horizontally layered halfspace are employed in the BE formulation [?]. Equation (2) can be rewritten as:

$$(3) \quad \hat{\mathbf{A}}_{\mathcal{H}}(\omega) \hat{\mathbf{x}}(\omega) = \hat{\mathbf{b}}(\omega)$$

where the vector of unknowns $\hat{\mathbf{x}}(\omega)$ contains displacements, tractions or both, depending on whether a Neumann, Dirichlet or mixed Neumann–Dirichlet problem is considered, respectively. In order to solve equation (3), iterative Krylov subspace methods such as the generalized minimal residual method (GMRES) [?] are well

suites. The matrix–vector multiplication forms the core of iterative solvers, and the complexity of this operation is only $\mathcal{O}(N_{\text{DOF}} \log N_{\text{DOF}})$ for \mathcal{H} –matrices [?].

As will become clear in section 4, equation (3) has to be solved multiple times with a varying right hand side $\hat{\mathbf{h}}(\omega)$ in FE–BE coupling algorithms, and the implementation of a suitable preconditioner is therefore desirable to reduce the computation time. A right preconditioner $\widehat{\mathbf{M}}(\omega)$ is used throughout this paper in order to lower the condition number of the coefficient matrix:

$$(4) \quad \widehat{\mathbf{A}}_{\mathcal{H}}(\omega) \widehat{\mathbf{M}}^{-1}(\omega) \hat{\mathbf{y}}(\omega) = \hat{\mathbf{h}}(\omega)$$

with $\widehat{\mathbf{M}}(\omega) \hat{\mathbf{x}}(\omega) = \hat{\mathbf{y}}(\omega)$. An example of an efficient preconditioner is the approximate \mathcal{H} –LU decomposition proposed in [?]; its computation requires, however, additional arithmetic operations. A much simpler strategy is applied in this paper, using a block diagonal preconditioner $\widehat{\mathbf{M}}(\omega) = \text{blkdiag}(\widehat{\mathbf{A}}_{\mathcal{H}}(\omega))$, where the size of the diagonal blocks is determined by the lowest hierarchical cluster level. An inner GMRES solver is applied to solve the preconditioning linear systems, resulting in a nested inner–outer iteration scheme. Furthermore, the flexible GMRES (FGMRES) algorithm [?] is employed for the outer iteration in order to avoid the explicit application of $\widehat{\mathbf{M}}^{-1}(\omega)$ to the Krylov vectors. As $\widehat{\mathbf{M}}(\omega)$ is already computed and stored, the proposed approach is very cheap in terms of computational resources. A similar preconditioning strategy has recently been adopted by Chaillat et al. for the acceleration of FMM calculations [?].

4. FE – \mathcal{H} -BE COUPLING PROCEDURES

Without loss of generality, it is assumed in the following that finite elements are used to model the structural domain, while boundary elements are employed to model wave propagation in the layered halfspace. The soil–structure interface is denoted as Σ . An appropriate coupling of both methods is required to solve the global problem.

4.1. Direct coupling. In a classical direct coupling strategy [6], the governing equations of the FE and BE subdomain are straightforwardly combined, accounting for continuity of displacements and equilibrium of tractions at the soil–structure interface Σ . This results in a global coupled system of equations:

$$(5) \quad \left(\begin{bmatrix} \hat{\mathbf{K}}_{11}(\omega) & \hat{\mathbf{K}}_{12}(\omega) \\ \hat{\mathbf{K}}_{21}(\omega) & \hat{\mathbf{K}}_{22}(\omega) \end{bmatrix} + \begin{bmatrix} \mathbf{0} & \mathbf{0} \\ \mathbf{0} & \hat{\mathbf{K}}_{22}^s(\omega) \end{bmatrix} \right) \begin{Bmatrix} \hat{\mathbf{u}}_1(\omega) \\ \hat{\mathbf{u}}_2(\omega) \end{Bmatrix} = \begin{Bmatrix} \hat{\mathbf{f}}_1(\omega) \\ \hat{\mathbf{f}}_2(\omega) \end{Bmatrix} + \begin{Bmatrix} \mathbf{0} \\ \hat{\mathbf{f}}_2^s(\omega) \end{Bmatrix}$$

where a subdivision into block matrices according to degrees of freedom $\hat{\mathbf{u}}_2(\omega)$ on the soil–structure interface Σ and degrees of freedom $\hat{\mathbf{u}}_1(\omega)$ internally in the structural domain is introduced. $\hat{\mathbf{K}}_{22}^s(\omega)$ represents the dynamic soil stiffness

matrix and is defined as:

$$(6) \quad \hat{\mathbf{K}}_{22}^s(\omega) = \int_{\Sigma} \mathbf{N}^T(\mathbf{x})\mathbf{N}(\mathbf{x})\hat{\mathbf{t}}(\mathbf{N}(\mathbf{x}))(\omega) \, dS$$

where $\mathbf{N}(\mathbf{x})$ indicates the FE shape functions on the soil–structure interface Σ , corresponding to the BE interpolation functions.

Although equation (5) provides a straightforward solution to the dynamic SSI problem, it suffers from some major drawbacks. Equation (6) requires the evaluation of tractions $\hat{\mathbf{t}}(\mathbf{N}(\mathbf{x}))(\omega)$ by means of the \mathcal{H} -BE method, which implies that equation (3) has to be solved for multiple right hand sides (i.e. for all shape functions $\mathbf{N}(\mathbf{x})$ on Σ); the implemented FGMRES algorithm is only able to handle one right hand side at a time. Furthermore, addition of the dense unsymmetric dynamic soil stiffness matrix $\hat{\mathbf{K}}_{22}^s(\omega)$ to $\hat{\mathbf{K}}(\omega)$ strongly reduces the sparsity of the system, reducing the efficiency of sparse finite element solvers applied to equation (5).

4.2. Iterative coupling. Iterative coupling procedures provide a valuable alternative to the direct strategy outlined in the previous subsection. The governing equations are solved separately for each subdomain in such an approach, while the boundary conditions at the soil–structure interface are updated until convergence is achieved. Although iterative schemes are often used for dynamic SSI problems in the time domain [7], their application in the frequency domain remains rather limited, mainly due to convergence difficulties [?].

In the present paper, a sequential Neumann–Dirichlet algorithm with interface relaxation is considered. At iteration step k of the procedure, the finite element subdomain is analyzed with Neumann boundary conditions at the soil–structure interface Σ :

$$(7) \quad \begin{bmatrix} \hat{\mathbf{K}}_{11}(\omega) & \hat{\mathbf{K}}_{12}(\omega) \\ \hat{\mathbf{K}}_{21}(\omega) & \hat{\mathbf{K}}_{22}(\omega) \end{bmatrix} \begin{Bmatrix} \hat{\mathbf{u}}_1^{(k)}(\omega) \\ \hat{\mathbf{u}}_2^{(k)}(\omega) \end{Bmatrix} = \begin{Bmatrix} \hat{\mathbf{f}}_1(\omega) \\ \hat{\mathbf{f}}_2(\omega) \end{Bmatrix} + \begin{Bmatrix} \mathbf{0} \\ \hat{\mathbf{f}}_2^s(\omega) \end{Bmatrix} + \begin{Bmatrix} \mathbf{0} \\ \hat{\mathbf{q}}^{(k)}(\omega) \end{Bmatrix}$$

where $\hat{\mathbf{q}}^{(k)}(\omega)$ denotes the soil–structure interaction forces. Solving equation (7) by means of a standard finite element solver provides the internal and interface displacements $\hat{\mathbf{u}}_1^{(k)}(\omega)$ and $\hat{\mathbf{u}}_2^{(k)}(\omega)$. The latter are subsequently imposed as Dirichlet boundary conditions on the boundary element subdomain, allowing to solve the preconditioned system of equations (4) for the interface tractions $\hat{\mathbf{t}}^{(k)}(\omega)$ using the FGMRES solver. These tractions are used to calculate equivalent nodal forces $\hat{\mathbf{q}}^{(k+\lambda)}(\omega)$:

$$(8) \quad \hat{\mathbf{q}}^{(k+\lambda)}(\omega) = \int_{\Sigma} \mathbf{N}^T(\mathbf{x})\mathbf{N}(\mathbf{x})\hat{\mathbf{t}}^{(k)}(\omega) \, dS$$

The interaction forces are finally relaxed using a relaxation parameter $\lambda^{(k)}$:

$$(9) \quad \hat{\mathbf{q}}^{(k+1)}(\omega) = \lambda^{(k)}\hat{\mathbf{q}}^{(k+\lambda)}(\omega) + (1 - \lambda^{(k)})\hat{\mathbf{q}}^{(k)}(\omega)$$

Once the relaxed interaction forces $\hat{\mathbf{q}}^{(k+1)}(\omega)$ are computed, a subsequent step in the iterative procedure is performed until convergence is obtained; a relative accuracy for both displacements and interaction forces is prescribed.

The choice of a suitable relaxation parameter $\lambda^{(k)}$ in equation (9) is of great importance in order to ensure and/or speed up the convergence of the iterative algorithm. In this paper, Aitken's Δ^2 -method [?] is employed for the determination of an optimized relaxation parameter $\lambda^{(k)}$ [7]:

$$(10) \quad \lambda^{(k)} = 1 - \mu^{(k)}$$

where the Aitken factor $\mu^{(k)}$ is defined as:

$$(11) \quad \mu^{(k)} = \mu^{(k-1)} + \left(\mu^{(k-1)} - 1 \right) \frac{\left(\Delta \hat{\mathbf{q}}^{(k-1)}(\omega) - \Delta \hat{\mathbf{q}}^{(k)}(\omega) \right)^T \Delta \hat{\mathbf{q}}^{(k)}(\omega)}{\| \Delta \hat{\mathbf{q}}^{(k-1)}(\omega) - \Delta \hat{\mathbf{q}}^{(k)}(\omega) \|^2}$$

with $\mu^{(0)} = 0$ and $\Delta \hat{\mathbf{q}}^{(k)}(\omega) = \hat{\mathbf{q}}^{(k-1)}(\omega) - \hat{\mathbf{q}}^{(k+\lambda)}(\omega)$.

In order to further accelerate the convergence, the relaxed interaction forces obtained in iteration k can, after conversion into tractions, be used as an initial guess in the FGMRES algorithm in iteration $k + 1$. Furthermore, if a loop with a sufficiently fine frequency sampling is considered, the converged solution at a particular frequency can be passed as an initial guess for the first FGMRES iteration at the subsequent frequency.

5. NUMERICAL EXAMPLE: FLEXIBLE SURFACE FOUNDATION ON A HORIZONTALLY LAYERED HALFSPACE

A flexible square surface foundation resting on a horizontally layered halfspace is considered in this section. The foundation has dimensions $5 \text{ m} \times 5 \text{ m} \times 0.25 \text{ m}$ and consists of concrete with a Young's modulus $E = 33 \text{ GPa}$, a Poisson's ratio $\nu = 0.20$, and a density $\rho = 2500 \text{ kg/m}^3$. Rayleigh damping is assumed, allowing to write the proportional damping matrix as $\mathbf{C} = \alpha \mathbf{M} + \beta \mathbf{K}$. A modal damping ratio $\xi = 0.03$ is attributed to the first two non rigid body modes.

The soil consists of two layers on a halfspace, each with a thickness of 2 m. The shear wave velocity C_s is equal to 150 m/s in the top layer, 250 m/s in the second layer, and 300 m/s in the underlying halfspace. The Poisson's ratio ν is 1/3 everywhere, resulting in dilatational wave velocities C_p of 300 m/s, 500 m/s, and 600 m/s, respectively. Material damping ratios $\beta_s = \beta_p = 0.025$ in both deviatoric and volumetric deformation are attributed to the layers and the halfspace, while a uniform density $\rho = 1800 \text{ kg/m}^3$ is considered throughout the medium.

The foundation is discretized by means of 30×30 equally sized shell elements based on Kirchhoff plate theory, which are coupled to a conforming BE mesh for the soil. A nodal collocation scheme is used for the latter to facilitate the FE-BE coupling. Up to nine elements per minimal shear wavelength $\lambda_s = C_s/f$ are provided at the maximum frequency of 100 Hz (determined by the shear wave velocity of the top layer).

The foundation is excited by a unit harmonic vertical point load applied at its center, within a frequency range between 0 Hz and 100 Hz. A frequency sampling of 1 Hz is used. Figure 1 shows the real and imaginary part of the vertical displacement $\hat{u}_z(\mathbf{x}, \omega)$ at the center of the foundation, calculated with the direct and iterative coupling procedure, respectively. A perfect agreement between the results of both methods can be observed, but the computation effort is significantly higher in the direct than in the iterative approach. The latter does not allow, however, to determine the static solution, as application of Neumann boundary conditions to the unconstrained structure results in a singularity of the FE equations. For this reason, the frequency sweep is performed from high to low frequencies.

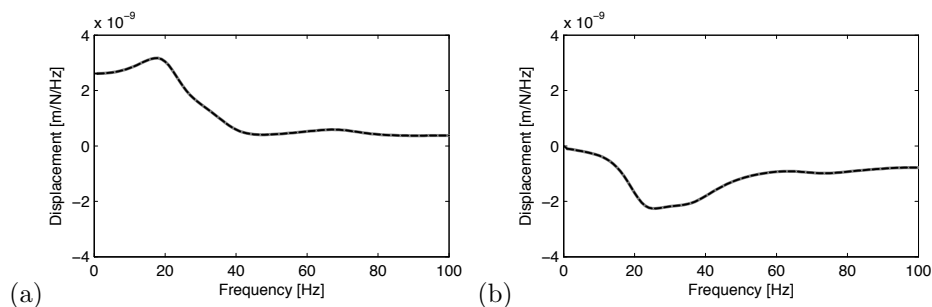


FIGURE 1. (a) Real and (b) imaginary part of the vertical displacement $\hat{u}_z(\mathbf{x}, \omega)$ at the center of the foundation excited by a unit harmonic vertical point load. The solution of the direct coupling strategy (black dashed line) is compared to the solution of the iterative coupling procedure (grey solid line).

The integral representation theorem subsequently allows for the computation of the radiated wavefield in the soil from the displacements and tractions on the boundary. Figures 2a and 2b show the vertical displacement of the foundation and the surrounding soil at 25 Hz and 100 Hz, respectively. It is clearly visible that the wave fronts at the surface of the soil are at 100 Hz no longer cylindrical due to the dynamic interaction between the foundation and the soil.

The benefit of using the result from a previous iteration as initial guess in the FGMRES solver is illustrated in figure 3, by showing the number of iterations required in the FGMRES solver in function of the frequency and the iteration step k in the iterative algorithm. Figure 3b demonstrates that applying the solution obtained in step k as initial guess in step $k + 1$ strongly decreases the number of iterations in the FGMRES solver required in subsequent iteration steps, while this number remains almost constant in case no initial guess is used as in figure 3a. Furthermore, passing the converged solution at a particular frequency as initial guess for the first FGMRES iteration at the subsequent frequency is also advantageous, resulting in a lower number of iteration steps in the iterative algorithm.

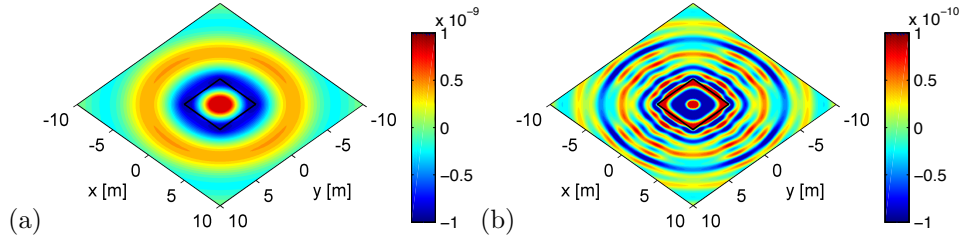


FIGURE 2. Real part of the vertical displacement $\hat{u}_z(\mathbf{x}, \omega)$ of the foundation and the soil at (a) 25 Hz and (b) 100 Hz.

Peaks in figures 3a and 3b at 40 Hz and 62 Hz correspond to natural frequencies of the foundation.

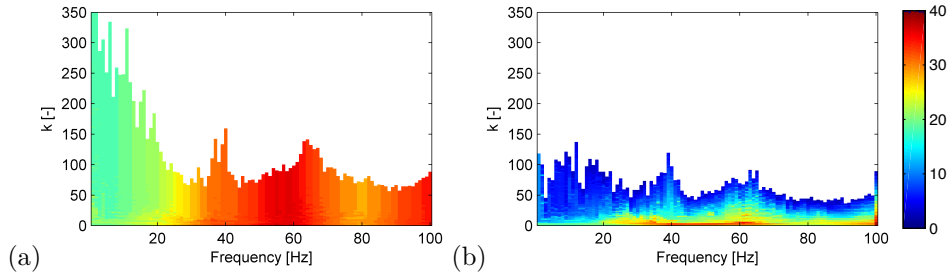


FIGURE 3. Number of iterations in the FGMRES solver in function of the frequency and the iteration step k in the iterative algorithm (a) in case no initial guess is used and (b) in case the result from a previous iteration is used as initial guess.

Numerical simulations have also demonstrated that application of the optimized interface relaxation presented in subsection 4.2 is crucial in order to ensure convergence in the iterative algorithm. No convergence could be obtained in case a fixed value was attributed to the relaxation parameter λ (where several values between 0 and 1 have been considered), in the whole frequency range under concern.

6. CONCLUSION

In this paper, the coupling of FE and \mathcal{H} -BE models to solve problems involving dynamic SSI has been discussed. Green's functions for a layered halfspace are incorporated in the \mathcal{H} -BE approach, avoiding the necessity to mesh the free surface and the layer interfaces. First, a direct coupling strategy has been considered, where a global coupled system of equations is assembled and solved. This requires the computation of the dynamic soil stiffness matrix, which is inefficient due to the fact that the \mathcal{H} -BE equations have to be solved many times. Second, an iterative sequential Neumann–Dirichlet procedure was introduced, where the governing

equations are solved separately for each subdomain, while the boundary conditions at the soil–structure interface are updated until convergence is achieved. A proper interface relaxation parameter is determined in each step by means of Aitken’s Δ^2 –method to ensure and speed up the convergence of this iterative procedure. Providing a thoughtful initial guess in the FGMRES algorithm results in further acceleration.

Pieter Coulier, Stijn François, Geert Lombaert, Geert Degrande

Department of Civil Engineering, KU Leuven, Belgium

`pieter.coulier@bwk.kuleuven.be`

REFERENCES

- [1] V. Rokhlin. Rapid solution of integral equations of classical potential theory. *Journal of Computational Physics*, 60:187–207, 1985.
- [2] S. Chaillat, M. Bonnet, and J.-F. Semblat. A multi-level fast multipole BEM for 3-D elastodynamics in the frequency domain. *Computer Methods in Applied Mechanics and Engineering*, 197(49–50):4233–4249, 2008.
- [3] W. Hackbusch. A sparse matrix arithmetic based on \mathcal{H} -matrices. Part I: Introduction to \mathcal{H} -matrices. *Computing*, 62(2):89–108, 1999.
- [4] E. Kausel and J.M. Roësset. Stiffness matrices for layered soils. *Bulletin of the Seismological Society of America*, 71(6):1743–1761, 1981.
- [5] M. Schevenels, S. François, and G. Degrande. EDT: An ElastoDynamics Toolbox for MATLAB. *Computers & Geosciences*, 35(8):1752–1754, 2009.
- [6] O. Von Estorff and E. Kausel. Coupling of boundary and finite elements for soil-structure interaction. *Earthquake Engineering and Structural Dynamics*, 18:1065–1075, 1989.
- [7] S. François, H.R. Masoumi, and G. Degrande. An iterative coupled boundary-finite element method for the dynamic response of structures. In P. Sas and M. De Munck, editors, *Proceedings of ISMA2006 International Conference on Noise and Vibration Engineering*, pages 1701–1716, Leuven, Belgium, September 2006.

On the Displacement Discontinuity Method

STEVEN L. CROUCH

(joint work with John A. L. Napier)

Since its introduction nearly 40 years ago, the displacement discontinuity method has been enhanced and refined by a number of researchers and used to tackle a variety of problems in applied mechanics. Several variants of the basic approach have been devised to deal with applications ranging from design of underground mine workings to simulation of crack propagation in brittle materials. This talk gives an updated summary of the basic method, shows the connection between its indirect and direct formulations, and presents a simplified treatment of the relatively new Galerkin formulation of the method. Finally, some thoughts are ventured on possible future developments and applications of the displacement discontinuity method

Steven L. Crouch

College of Science and Engineering, University of Minnesota, Minneapolis, Minnesota,
U.S.A

John A. L. Napier

Department of Mining Engineering, University of Pretoria, Pretoria, South Africa

Direct BEM for high-resolution gravity field modelling of the Earth

RÓBERT ČUNDERLÍK

(joint work with Róbert Špir, Karol Mikula)

We present a high-resolution gravity field modelling of the Earth using the boundary element method (BEM). A direct BEM formulation for the Laplace equation is applied to get a numerical solution to the geodetic boundary-value problem (GBVP) [2, 5]. GBVP represents an exterior oblique derivative problem for the Laplace equation. Our numerical scheme uses the collocation with linear basis functions. It involves a triangulated discretization of the Earth's surface as our computational domain considering its complicated topography. The oblique derivative problem is treated by a decomposition of the gradient of the unknown disturbing potential into its normal and tangential components [4].

With respect to a giant size of the Earth and in order to get accuracy as high as possible, a parallelization of the algorithm including the BiCGSTAB iterative solver is implemented by the MPI subroutines [1]. To eliminate the far zones' interactions we present an iterative procedure, where the matrix components corresponding to far zones are multiplied by a solution obtained from the previous iteration [3]. In the first iteration, solutions on coarse grids or from known satellite-only geopotential models can be incorporated. Such an iterative approach reduces large memory requirements similarly as the fast multipole method although the CPU time consumptions remain almost unchanged in each iteration.

Numerical experiments deal with global as well as local gravity field modelling. The final global quasigeoid model with the resolution 0.075 deg (5,760,002 nodes) is compared with the EGM-2008 geopotential model, which has been developed by spherical harmonics up to degree 2160 and released by NGA and NASA [6]. We also present local refinements in areas of Slovakia and New Zealand, where we have at disposal original terrestrial gravimetric measurements. The GPS/Levelling test of the obtained local quasigeoid models indicates their accuracy.

Keywords: Direct BEM formulation, collocation with linear basis functions, oblique derivative in 3D, iterative elimination of far zones' interactions, global and local gravity field modelling

Róbert Čunderlík, Róbert Špir, Karol Mikula

Slovak University of Technology, Bratislava, Slovakia

cunderli@svf.stuba.sk, spir@math.sk, mikula@math.sk

REFERENCES

- [1] Y. Aoyama, J. Nakano. RS/6000 SP: Practical MPI Programming. IBM, Poughkeepsie, New York, 1999.
- [2] R. Čunderlík, K. Mikula, and M. Mojzeš. Numerical solution of the linearized fixed gravimetric boundary-value problem. *Journal of Geodesy*, 82(1): 15-29, 2008.
- [3] R. Čunderlík, K. Mikula. Direct BEM for high-resolution global gravity field modelling. *Studia Geophysica et Geodaetica*, 54(2): 219-238, 2010.

-
- [4] R. Čunderlík, R. Špir, K. Mikula. An oblique derivative in the direct BEM formulation of the fixed gravimetric BVP. In: N. Sneeuw et al. (eds.), VII Hotine-Marussi Symposium on Mathematical Geodesy, *International Association of Geodesy Symposia*, 137: 227-231, 2012. DOI 10.1007/978-3-642-22078-4
 - [5] R. Klees, M. Van Gelderen, C. Lage, C. Schwab. Fast numerical solution of the linearized Molodensky problem. *Journal of Geodesy*, 75(7-8): 349-362, 2001.
 - [6] N.K. Pavlis, S.A. Holmes, S.C. Kenyon, J.K. Factor. An Earth gravitational model to degree 2160: EGM2008. Presented at the 2008 General Assembly of EGU, Vienna, Austria, April 13-18, 2008.

A posteriori error estimation for a hypersingular integral equation and non-conforming domain decomposition

CATALINA DOMÍNGUEZ

(joint work with Norbert Heuer)

In this work we establish a two-level a posteriori error estimate for the solution of the hypersingular boundary integral equation governing the Laplacian in three dimensions, discretized by a non-conforming domain decomposition based on the Nitsche technique [2]. Using the energy norm and a saturation assumption, reliability and efficiency can be established for the error estimator. The energy norm for boundary elements is non-local and not suitable for steering adaptive refinements. Using localization techniques, we therefore present an error estimator based on the L^2 -norm instead of the energy norm.

Theoretical techniques are similar to [3, 1], and are extended to the non-conforming case by taking ideas from [4].

Numerical experiments underline our theoretical results.

Support by FONDECYT project 1110324, CONICYT project Anillo ACT1118 (ANANUM) and DIDI, Universidad del Norte is gratefully acknowledged.

Keywords: a posteriori error estimate, integral equations, hypersingular operator, Nitsche method, non-conforming boundary elements, adaptive algorithm.

Mathematics Subject Classifications (2000): 65N38

Catalina Domínguez

Universidad del Norte, Barranquilla, Colombia
dcatalina@uninorte.edu.co

Norbert Heuer

Pontificia Universidad Católica de Chile, Santiago, Chile
nheuer@mat.puc.cl

REFERENCES

- [1] C. CARSTENSEN AND S. BARTELS, *Each averaging technique yields reliable a posteriori error control in FEM on unstructured grids. I. Low order conforming, nonconforming, and mixed FEM*, Math. Comp., 71 (2002), pp. 945–969.
- [2] F. CHOULY AND N. HEUER, *A Nitsche-based domain decomposition method for hypersingular integral equations*, Numerische Mathematik, 121 (2012), pp. 705–729.
- [3] S. FERRAZ-LEITE AND D. PRAETORIUS, *Simple a posteriori error estimators for the h-version of the boundary element method*, Computing, 83 (2008), pp. 135–162.
- [4] S. MEDDAHI AND N. HEUER, *Discontinuous Galerkin hp-BEM with quasi-uniform meshes*, Numerische Mathematik, to appear.

On a consistent, mixed variational boundary element formulation for strain gradient elasticity

NEY A. DUMONT

(joint work with Daniel Huamán)

1. INTRODUCTION

The mathematical modeling of microdevices, in which structure and microstructure have approximately the same scale of magnitude, as well as of macrostructures of markedly granular or crystal nature (microcomposites), demands a nonlocal approach for strains and stresses [11, 4, 7]. Mindlin's works in the 1960s may be accounted the basis of the strain gradient theory [9, 10]. It has recently become the subject of a large number of analytical and experimental investigations motivated by the development of new structural materials. Starting in the 1990s, Aifantis and coworkers [1] managed to develop a simplified strain gradient theory based on only one additional elasticity constant, which opened up a series of interesting practical applications [11]. Since Toupin and Mindlin's time, investigations have been under development to establish the variational basis of the theory and to formulate equilibrium and kinematic boundary conditions consistently [2, 6].

Although the conceptual developments have already been extended to the frequency-domain analysis of time-dependent problems [7], the present outline is restricted to the static analysis, which actually involves the most relevant concepts. A comprehensive manuscript is being prepared, in which Aifantis' proposition is numerically implemented in a variationally consistent framework, generalized patch tests are carried out and several spectral properties of the resulting matrices are assessed.

2. PROBLEM FORMULATION

Throughout this paper, repeated indices stand for summation and $(\cdot)_{,i}$ denotes a derivative with respect to the i -th direction. Following equations are given by Aifantis as a development of Mindlin's work:

$$(1) \quad \bar{\epsilon}_{ij} = \epsilon_{ij} + c_\epsilon \nabla^2 \epsilon_{ij}; \quad \bar{\sigma}_{ij} = \sigma_{ij} + c_\sigma \nabla^2 \sigma_{ij}; \quad \bar{\sigma}_{ij} = \lambda \bar{\epsilon}_{kk} \delta_{ij} + 2\mu \bar{\epsilon}_{ij}$$

where, quoting [1], “ $(\sigma_{ij}, \epsilon_{ij})$ denote the stress and strain tensors for elastic deformation. The quantities (λ, μ) are the usual Lamé constants. The gradient coefficients c 's are new phenomenological coefficients. ... (In fact, the simplest form of gradient elasticity theory corresponds to the case $c_\sigma = 0$).”

2.1. Approximate domain stress field. The stresses are approximated in the domain Ω of a generic three-dimensional elastic body by the Cauchy stress $\tau_{ij}^s = \tau_{ij}^* + \tau_{ij}^p$ and the double stress $\mu_{kij}^s = \mu_{kij}^* + \mu_{kij}^p$. The superscript $(\cdot)^s$ stands for *stress assumption*. $(\cdot)^*$ and $(\cdot)^p$ stand respectively for the homogeneous and a particular solution of the differential equilibrium equation

$$(2) \quad \sigma_{ji,j}^s + f_i = 0 \quad \text{in } \Omega$$

defined in terms of the tensor of total stresses $\sigma_{ij}^s = \tau_{ij}^s - \mu_{kij,k}^s$, where τ_{ij}^s is the Cauchy stress tensor and $\mu_{kij,k}^s$ is the “couple” stress tensor. σ_{ij}^s , τ_{ij}^s and μ_{kij}^s are symmetric with respect to i and j . This formulation corresponds to a “Type II” description of three equivalent forms of the strain energy density [10, 2]. The present notation is a simplified version of the notation proposed by Mindlin and Eshel, with the equivalences $\tau_{ij}^s \equiv \bar{\sigma}_{ij}^s$ and $\mu_{kij}^s \equiv \hat{\mu}_{kij}$. The strain field corresponding to τ_{ji}^s is $\epsilon_{ij}^s = \frac{1}{2}(u_{i,j}^s + u_{j,i}^s) \equiv \epsilon_{ij}$, and the strain gradient corresponding to μ_{kji}^s is $\frac{1}{2}(u_{i,jk}^s + u_{j,ik}^s) = \hat{\kappa}_{kij}$. As for the rest of the paper, Mindlin’s notation is followed as closely as possible, with just a few exceptions.

According to Aifantis’ proposition, $\mu_{kij}^s = g^2 \tau_{ij,k}^s$, where g^2 is the “material characteristic length”. The homogeneous part τ_{ij}^* of τ_{ij}^s is approximated in Ω , in the frame of the present variational formulation, by the sum of a sufficiently large number of “fundamental solutions” ,

$$(3) \quad \tau_{ij}^* = \tau_{ijm}^* p_m^* \Rightarrow \mu_{kij}^* = \mu_{kijm}^* p_m^* \quad \text{in } \Omega$$

such that (2) is satisfied. The set of n^* parameters p_m^* are, together with the nodal displacement parameters of the next Section, the problem’s primary unknowns. Fundamental solutions τ_{ijm}^* are known in the literature for truss, beam and boundary elements, in general, and for some specific finite elements [2]. General solutions for 2D and 3D finite elements have been developed by the authors [4, 7].

2.2. Approximate boundary displacement field. As proposed by Mindlin, the variation of the normal component $n_j u_{i,j}$ of the displacement gradient is independent from δu_i on the boundary, with double tractions T_{ij} performing (virtual) work on the normal gradient variation $n_j n_l \delta u_{i,l} \equiv \delta u_{i,j} - (\delta_{jl} - n_j n_l) \delta u_{i,l}$ along Γ . In this equation, n_i are the Cartesian projections of the outward unit normal to Γ and δ_{jl} is the Kronecker delta. A mechanical interpretation of the non-symmetric tensor T_{ij} , including its correlation with the Cosserat couple-stress vector, is given by Mindlin [9].

The displacements are approximated on Γ by a field u_i^d (where $()^d$ stands for *displacement assumption*) that satisfies the required boundary continuity conditions. A normal gradient field q_i^d must be postulated on Γ independently from $u_{i,j}^d n_j$, also satisfying interelement compatibility. Then,

$$(4) \quad u_i^d = u_{in} d_n; \quad q_i^d = q_{in} q_n \quad \text{on } \Gamma$$

for the 3D geometry of Γ described in terms of boundary parametric variables (ξ, η) , where u_{in} and q_{in} are interpolation functions of a total of n^d parameters d_n and q_n (not to be confounded with q_i). These parameters are – together with p_m^* of (14) – the primary unknowns of the variational problem.

3. THE HELLINGER-REISSNER POTENTIAL APPLIED TO GRADIENT ELASTICITY

The Hellinger-Reissner potential is split up into two virtual work principles in order to clarify the conceptual aspects affected by the gradient elasticity [4].

One starts by stating the two-field assumptions necessary to develop all matrix equations in terms of stress and displacement parameters.

3.1. Displacement virtual work for equilibrium checking. Except for the last term, the following statement is found in similar form in several displacement-based developments on gradient elasticity as $\delta W^{\text{int}} = \delta W^{\text{ext}}$ [10, 2]. However, in the present context, $\delta u_i^s \neq \delta u_i^d$ on Γ , according to the numerical approximations proposed above, besides the fact that u_i^d is not defined in Ω . Equilibrium of the stress field is weakly enforced by means of the displacement virtual work statement

$$(5) \quad \int_{\Omega} (\tau_{ji}^s \delta u_{i,j}^d + \mu_{kji}^s \delta u_{i,jk}^d) d\Omega = \int_{\Omega} f_i \delta u_i^d d\Omega + \int_{\Gamma} (P_i \delta u_i^d + R_i \delta q_i^d + Q_{is} \delta u_{i,s}^d) d\Gamma$$

where f_i and P_i are *classical* body forces and boundary tractions, respectively, which perform virtual work on displacements, as indicated, whereas R_i and Q_{is} are *normal* and *tangential* double tractions. The subscript s refers to the natural coordinates (ξ, η) that describe the boundary surface of a 3D problem. $R_i = T_{ji} n_j = \mu_{kji} n_k n_j$ performs virtual work on normal displacement gradients $\delta q_i \equiv n_l \delta u_{i,l}$. In (5), one resorts to the *tangential* double tractions Q_{is} , which perform virtual work on tangential displacement gradients $\delta u_{i,s}^d$, in a way that is apparently new in the technical literature¹. This term is also not shown in Reference [4] and has only turned out as a required force component after a sequence of patch and convergence tests. Its meaning may be inferred in the following equation. The boundary integrals are expressed as if plain Neumann conditions are applied. However, (5) is consistent and general, as $\delta u_i^d = 0$ and $\delta q_i^d = 0$ wherever u_i^d and q_i^d are prescribed in a numerical problem, with corresponding classical or double boundary forces interpreted as reaction forces.

Integrating by parts the terms at the left-hand side of (5) and applying the divergence theorem, it results after some manipulation

$$(6) \quad \int_{\Gamma} [(\sigma_{ji}^s n_j - P_i) \delta u_i^d + (\mu_{kji}^s n_k n_j - R_i) \delta q_i^d + (\mu_{kji}^s n_k |J|^{-2} \tilde{t}_{js} - Q_{is}) \delta u_{i,s}^d] d\Gamma = 0$$

The term $|J|^{-2} \tilde{t}_{js} \delta u_{i,s}^d \equiv (\delta_{jl} - n_j n_l) \delta u_{i,l}^d$ makes evident that u_i^d is a function of (ξ, η) on Γ [3]. To arrive at this equation, the boundary tangent vectors are defined in terms of $u_{in} \equiv u_{in}(\xi, \eta)$ in (4):

$$(7) \quad \mathbf{u} = [\partial x / \partial \xi \quad \partial y / \partial \xi \quad \partial z / \partial \xi]^T; \quad \mathbf{v} = [\partial x / \partial \eta \quad \partial y / \partial \eta \quad \partial z / \partial \eta]^T$$

¹There is some confusion in the literature on the denomination of T_{ij} and R_i , as both are usually referred to as *double tractions*. In this paper, the qualificative *normal* is used for the latter. The static action referred to by Mindlin as T_{ji} shall not be used in the subsequent developments. In general, the notation proposed by [9] is followed as closely as possible, with the only flagrant exception that lower case is used for the body forces f_i in order to be consistent with previous developments in the classical elasticity. Moreover, one resorts to the *tangential* double tractions Q_{is} proposed by Mindlin, which perform virtual work on tangential displacement gradients $\delta u_{i,s}^d$, although in a way that is apparently new in the technical literature.

For $|J|^2 = |\mathbf{u} \times \mathbf{v}|$ and introducing the matrices $\mathbf{t} = [\mathbf{u} \ \mathbf{v}]$ and $\mathbf{t}^\perp = [\mathbf{v} \ -\mathbf{u}]$, it results that

$$(8) \quad \delta_{jl} - n_j n_l = |J|^{-2} t_{jr} t_{mr}^\perp t_{ms}^\perp t_{ls}$$

The indices r and s vary from 1 to 2, as they refer to ξ and η . In (6), $\delta u_{i,s}^d$ comes from $t_{ls} \delta u_{i,l}^d \equiv \delta u_{i,s}^d$, where $(\cdot)_{,s}$ denotes derivatives with respect to ξ and η . According to (8), $\tilde{t}_{js} = t_{jr} t_{mr}^\perp t_{ms}^\perp$.² This development departs from the one precluded by Mindlin [9] and followed by other researchers, as they were reasoning in terms of a plain displacement formulation, which ends up requiring the computation of “jumping” terms (and boundary conditions that can be hardly grasped), for a non-smooth boundary of a 3D problem. Remarkably, several authors show numerical implementations that have become feasible only by artificially smoothing the boundary around corner points. Three-dimensional implementations seem to be extremely complicated in such a framework. The consistency and the advantages of the implementation given as in (6) are explored in the full manuscript.

3.2. Stress virtual work for displacement compatibility checking. The second statement that comes from the Hellinger-Reissner potential may be obtained by weakly enforcing compatibility of the displacements u_i^s and u_i^d in terms of the stress virtual work equation

$$(9) \quad \int_{\Omega} (u_{i,j}^s - u_{i,j}^d) \delta \tau_{ji}^* d\Omega + \int_{\Omega} (u_{i,jk}^s - u_{i,jk}^d) \delta \mu_{kji}^* d\Omega = 0$$

Some manipulation, as done in the preceding Section, leads to the expression

$$(10) \quad \int_{\Gamma} \delta \sigma_{ji}^* n_j (u_i^s - u_i^d) d\Gamma + \int_{\Gamma} \delta \mu_{kji}^* n_k (u_{i,j}^s - n_j q_i^d - |J|^{-2} \tilde{t}_{js} u_{i,s}^d) d\Gamma = 0$$

4. FUNDAMENTAL SOLUTION

4.1. Stress fundamental solution. The Cauchy stresses τ_{ij}^s , the double stresses μ_{kij}^s and the total stresses σ_{ij}^s are approximated in Ω , according to (3), by the sum of a sufficiently large number of “fundamental solutions” τ_{ijm}^* plus a particular solution:

$$(11) \quad \tau_{ij}^s = \tau_{ijm}^* P_m^* + \tau_{ij\ell}^R R_\ell^* + \tau_{ij}^p;$$

$$(12) \quad \mu_{kij}^s = \mu_{kijm}^* P_m^* + \mu_{kij\ell}^R R_\ell^* + \mu_{kij}^p;$$

$$(13) \quad \sigma_{ij}^s = \sigma_{ijm}^* P_m^* + \sigma_{ij\ell}^R R_\ell^* + \sigma_{ij}^p$$

The parameters P_m^* and R_ℓ^* are context-dependent in a general formulation, as developed by the authors in the frame of a finite element implementation [3, 4, 5]. In the present case of use of singular fundamental solutions, the set of n^*

²It is possible to arrive at simpler expressions of (6) by using normalized expressions of \mathbf{t} as well as by referring to the surface length in the definition of Q_{is} and $\delta u_{i,s}^d$, so that $|J|^{-2}$ drops out. However, the proposed expressions seem easier to grasp mechanically and more efficient in terms of code writing. In the three-dimensional model, $|J| \equiv |g|$, where $g_{\alpha\beta}$ is the surface metric tensor, according to the literature on differential geometry [8]. The product $|J|^{-1} t_{mr}^\perp t_{ms}^\perp$ is the inverse of $g_{\alpha\beta}$.

parameters P_m^* correspond to point forces applied along the boundary of the elastic body. Moreover, a set of n^R parameters R_ℓ^* is added in order to provide a sufficient number of equations to solve the boundary element problem. The parameters R_ℓ^* are point double tractions (couples) applied along the boundary, in such a way that $R_\ell^* \delta q_\ell$ – as well as $P_m^* \delta u_m$ – has the meaning of mechanical work. The points of application of P_m^* and R_ℓ^* correspond to singularities in the stress field and must be excluded from the domain of interest of the elasticity problem under analysis.

The relation between the fundamental solutions σ_{ijm}^* and $\sigma_{ij\ell}^R$ is elucidated in Section 4.3 and discussed in detail in the full paper. The matrix derivation of (20) is simplified if (11) is written in the compact notation of the classical elasticity, for τ_{ijm}^* , μ_{kijm}^* and σ_{ijm}^* standing for $\langle \tau_{ijm}^* \quad \tau_{ij\ell}^R \rangle$, $\langle \mu_{kijm}^* \quad \mu_{kij\ell}^R \rangle$ and $\langle \sigma_{ijm}^* \quad \sigma_{ij\ell}^R \rangle$, respectively, and p_m^* equivalent to $\langle P_m^* \quad R_\ell^* \rangle$:

$$(14) \quad \tau_{ij}^s = \tau_{ijm}^* p_m^* + \tau_{ij}^p; \quad \mu_{kij}^s = \mu_{kijm}^* p_m^* + \mu_{kij}^p; \quad \sigma_{ij}^s = \sigma_{ijm}^* p_m^* + \sigma_{ij}^p$$

P_m^* and R_ℓ^* are, together with the nodal displacement parameters of Section 2.2, the primary unknowns of the problem one is about to formulate. Non-singular fundamental solutions τ_{ijm}^* are known in the literature for truss, beam and boundary elements, in general, and for some specific finite elements [2]. General non-singular solutions for 2D and 3D finite elements have already been developed by [3, 4, 5].

4.2. Displacement fundamental solution. Displacement solutions u_i^s are obtained from τ_{ij}^s , μ_{kij}^s in terms of the fundamental solutions of (3) and of the particular solution τ_{ij}^p , μ_{kij}^p ,

$$(15) \quad u_i^s = u_{im}^* P_m^* + u_{i\ell}^R R_\ell^* + u_i^p + u_i^r \quad \text{in } \Omega$$

which include a set u_i^r of rigid-body displacements. This explicit expression of the rigid body displacements may be omitted in the above equation with no conceptual harm, as they are implicitly included as an arbitrary amount of the particular solution u_i^p .

According to eq (15), a portion of the elastic body whose outward unit normal is n_j has as displacement gradient ($u_{i,j}^r \neq 0$ in the case of rigid-body rotation):

$$(16) \quad q_i^s = n_j (u_{im}^* P_m^* + u_{i\ell}^R R_\ell^* + u_i^p + u_i^r)_{,j} \quad \text{in } \Omega$$

4.3. A displacement-reciprocity assessment. In (11-16), the arguments of the stress and displacement functions are omitted. In the case of displacements, for instance, $u_{im}^* \equiv u_i^*(\mathbf{y}, P_m^*(\mathbf{x}) = 1)$ is the displacement caused by a unit force P_m^* applied at the point of coordinates $\mathbf{x} \equiv (x_x, y_x, z_x)$ (the source point) and Cartesian orientation m , as measured at the point of coordinates $\mathbf{y} \equiv (x_y, y_y, z_y)$ (the field point) and Cartesian orientation i . Accordingly, one adopts the convention that $u_{i\ell}^R \equiv u_i^*(\mathbf{y}, R_\ell^*(\mathbf{z}) = 1)$ at $\mathbf{z} \equiv (x_z, y_z, z_z)$. This is illustrated in Figure 1. Since the director co-sine n_j refers to an orientation at the field point, one way of avoiding inconsistency in the following developments is to write (16) as

$$(17) \quad q_i^* = n_{j(y)} u_{im,j(y)}^* P_m^* + n_{j(y)} u_{i\ell,j(y)}^R R_\ell^*$$

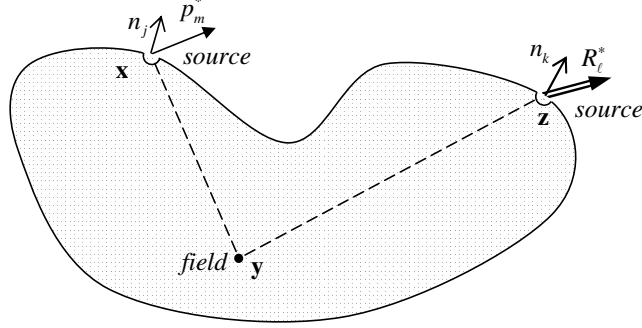


FIGURE 1. Scheme for the displacement-reciprocity assessment.

The reciprocity of actions for $P_m^*(\mathbf{x}) = 1$ and $R_\ell^*(\mathbf{z}) = 1$ can be stated as

$$(18) \quad q_\ell^*(\mathbf{z}, P_m^*(\mathbf{x}) = 1) \equiv n_{k(z)} u_{\ell m, k(z)}^* \stackrel{\text{(reciprocity)}}{=} u_m^*(\mathbf{x}, R_\ell^*(\mathbf{z}) = 1) \equiv u_{m\ell}^R$$

Then, $u_{m\ell}^R = n_{k(z)} u_{\ell m, k(z)}^*$ and (15) and (16) become, for the homogeneous part,

$$(19) \quad u_i^* = u_{im}^* P_m^* + n_{k(z)} u_{\ell i, k(z)}^* R_\ell^*; \quad q_i^* = n_{j(y)} u_{im, j(y)}^* P_m^* + n_{j(y)} n_{k(z)} u_{\ell i, k(z)j(y)}^* R_\ell^*$$

This fundamental solution is symmetric by definition. Observe the attempt to keep notation consistency, reserving the indices i, j for the field point \mathbf{y} , the index m for the source point \mathbf{x} at which the point force P_m^* is applied, and ℓ to the source point \mathbf{z} at which the (point) double force R_ℓ^* is applied. Later on, the index n will be used to characterize a measured nodal displacement whereas the index q will be applied to a measured nodal displacement gradient. One way of keeping both notation simplicity and consistency is to just use (19), where $u_{i\ell}^R = n_{k(z)} u_{\ell i, k(z)}^*$. Moreover, observe that, according to Figure 1, $\partial r(\mathbf{y} - \mathbf{z}) / \partial \mathbf{z} = -\partial r(\mathbf{y} - \mathbf{z}) / \partial \mathbf{y}$ and $u_{\ell m, k(z)}^* \equiv -u_{\ell m, k(y)}^*$.

5. RESULTANT MATRIX EQUATIONS

As outlined in the full manuscript, numerical discretization of (6) and (10) in terms of the assumed displacement and forces approximations (4), (11), (15) and (16) leads to the matrix system

$$(20) \quad \mathbf{H}^T \mathbf{p}^* = \mathbf{p} - \mathbf{p}^p; \quad \mathbf{F}^* \mathbf{p}^* = \mathbf{H} \mathbf{d} - \mathbf{b}$$

for arbitrary variations δd_n , δq_n , δP_m^* and δR_ℓ^* . In the first equation above, \mathbf{H}^T is an equilibrium matrix that relates the vectors of nodal forces \mathbf{p} and \mathbf{p}^p to the domain stress field parameters \mathbf{p}^* . In the second equation, a symmetric flexibility matrix \mathbf{F}^* transforms \mathbf{p}^* into equivalent nodal displacements that are compatible with the transformed displacement vector $\mathbf{H} \mathbf{d}$ plus a displacement term \mathbf{b} related to the particular solution. The transformation matrices \mathbf{F}^* and \mathbf{H} are explicitly

expressed as:

$$(21) \quad \mathbf{F}^* = \begin{bmatrix} \int_{\Gamma} \left(\sigma_{jim}^* n_j u_{in}^* + \mu_{kjim}^* n_k u_{in,j}^* \right) d\Gamma & \int_{\Gamma} \left(\sigma_{jim}^* n_j u_{il}^R + \mu_{kjim}^* n_k u_{il,j}^R \right) d\Gamma \\ \int_{\Gamma} \left(\sigma_{jiq}^R n_j u_{in}^* + \mu_{kjiq}^R n_k u_{in,j}^* \right) d\Gamma & \int_{\Gamma} \left(\sigma_{jiq}^R n_j u_{il}^R + \mu_{kjiq}^R n_k u_{il,j}^R \right) d\Gamma \end{bmatrix}$$

$$(22) \quad \mathbf{H} = \begin{bmatrix} \int_{\Gamma} \left(\sigma_{jim}^* n_j u_{in} + \mu_{kjim}^* n_k |J|^{-2} \tilde{t}_{js} u_{in,s} \right) d\Gamma & \int_{\Gamma} \mu_{kjim}^* n_k n_j q_{il} d\Gamma \\ \int_{\Gamma} \left(\sigma_{jiq}^R n_j u_{in} + \mu_{kjiq}^R n_k |J|^{-2} \tilde{t}_{js} u_{in,s} \right) d\Gamma & \int_{\Gamma} \mu_{kjiq}^R n_k n_j q_{il} d\Gamma \end{bmatrix}$$

Although the displacement fundamental solution u_{in}^* is non-singular in the strain gradient elasticity (for $g \neq 0$), there are several cases of singularity and hyper-singularity to be dealt with in the evaluation of \mathbf{F}^* and \mathbf{H} . On the other hand, the time-consuming evaluation of \mathbf{F}^* can be circumvented in the framework of a simplified formulation that lets go of the variational strictness of the method [7]. The simpler case of Neumann boundary conditions, in which only \mathbf{H} is needed, has been implemented for two-dimensional problems with linear, quadratic and cubic elements, and the spectral properties investigated, as a rigid-body rotation, for instance, contains displacement gradients that correspond to zero applied forces. Several patch tests have been also carried out in order to assess the consistency of the formulation.

6. CONCLUSIONS

This paper presents a concise hybrid boundary element formulation of gradient elasticity problems based on two virtual work principles that stem from the Hellinger-Reissner potential. The most important contribution seems to be the evidence that the proposed hybrid formulation naturally approximates normal displacement gradients along Γ independently from displacements, which would improve Mindlin's [10] pioneer proposition. As shown in the full manuscript under preparation, a series of simple patch tests is being developed to check consistency and the correlation between local and global physical quantities, so that meaningful non-classical boundary conditions can be established.

ACKNOWLEDGMENTS

This project was supported by the Brazilian agencies CAPES, CNPq and FAPERJ.

Ney A. Dumont, Daniel Huamán

Civil Engineering Department, PUC-Rio, Rio de Janeiro, Brazil

dumont@puc-rio.br, dhm@aluno.puc-rio.br

REFERENCES

- [1] E. C. Aifantis. Exploring the applicability of gradient elasticity to certain micro/nano reliability problems. *Microsystem Technologies*, 15:109–115, 2009.

-
- [2] E. Amanatidou and N. Aravas. Mixed finite element formulations of strain-gradient elasticity problems. *Computer Methods in Applied Mechanics and Engineering*, 191:1723–1751, 2002.
 - [3] N. A. Dumont and D. Huamán. Hybrid finite/boundary element formulation for strain gradient elasticity problems. In E. J. Sapountzakis and M. H. Aliabadi, editors, *BETeq 2009 - International Conference on Boundary Element Techniques*, pages 295–300, Athens, Greece, July 2009.
 - [4] N. A. Dumont and D. Huamán. A family of 2d and 3d hybrid finite elements for strain gradient elasticity. In C. Zhang, M. H. Aliabadi, and M. Schanz, editors, *Advances in Boundary Element Techniques XI, Proceedings of the 11th International Conference*, pages 144–153, Berlin, Germany, July 2010.
 - [5] N. A. Dumont and D. Huamán. A hybrid finite element implementation of gradient elasticity. In *11th Pan-American Congress of Applied Mechanics - PACAM XI*, page 6 pp, Foz do Iguaçu, Brazil, January 2010.
 - [6] A. E. Giannakopoulos, E. Amanatidou, and N. Aravas. A reciprocity theorem in linear gradient elasticity and the corresponding Saint-Venant principle. *International Journal of Solids and Structures*, 43:3875–3894, 2006.
 - [7] D. Huamán. *Hybrid Finite/Boundary Element Methods Applied to Gradient Elasticity*. Ph.d. thesis, PUC-Rio, Rio de Janeiro, Brazil, 2012.
 - [8] E. Kreyszig. *Differential Geometry*. Dover, New York, 1991.
 - [9] R. D. Mindlin. Micro-structure in linear elasticity. *Archive for Rational Mechanics and Analysis*, 16:51–78, 1964.
 - [10] R. D. Mindlin and N. N. Eshel. On first strain gradient theories in linear elasticity. *International Journal of Solids and Structures*, 4:109–124, 1968.
 - [11] D. Polyzos, K. G. Tsepoura, S. V. Tsinopoulos, and D. E. Beskos. A boundary element method for solving 2-d and 3-d static gradient elastic problems part I: Integral formulation. *Computer Methods in Applied Mechanics and Engineering*, 192:2845–2873, 2003.

Extended Boundary Integral Equation Method For Fracture Analysis In Magnetoelastoelectroelastic Media

CUIYING FAN

(joint work with Minghao Zhao, Ernian Pan, Guoning Liu)

Using the hyper-singular boundary integral equation in 3D transversely isotropic magnetoelastoelectroelastic (MEE) media, the near crack tip fields and the intensity factors in terms of the extended displacement discontinuities are derived by boundary integral equation approach. The influence of different electric and magnetic boundary conditions, i.e., electrically and magnetically impermeable and permeable conditions, electrically impermeable and magnetically permeable condition, and electrically permeable and magnetically impermeable condition, on the solutions is studied. Considering both the electric and magnetic yielding near the crack tip in MEE media, the nonlinear models of planar electricmagnetic polarization saturation (PEMPS) model and planar electricmagnetic breakdown (PEMB) model are both studied by using the extended boundary integral equation method.

Keywords: MEE medium, PEMPS model, PEMB model, extended displacement discontinuity, boundary integral equation, extended stress intensity factor

CuiYing Fan, MingHao Zhao, Ernian Pan, GuoNing Liu

The School of Mechanical Engineering, Zhengzhou University, Zhengzhou, 450001, China
fancy@zzu.edu.cn, memhzhao@zzu.edu.cn, panernian@zzu.edu.cn, l11egn@yahoo.com

REFERENCES

- [1] Crouch SL. Solution of plane elasticity problems by the displacement discontinuity method. *Int. J. Meth. Eng.*, 10: 301-343, 1976.
- [2] Zhao MingHao, Fan CuiYing, Yang Feng, Liu Tong. Analysis method of planar cracks of arbitrary shape in the isotropic plane of a three-dimensional transversely isotropic magnetoelastoelectroelastic medium *International Journal of Solids and Structures*, 56: 34413458, 2008.
- [3] Zhao Ming Hao, Fan Cui Ying. Strip electric-magnetic breakdown model in magnetoelastoelectroelastic medium. *Journal of the Mechanics and Physics of Solids*, 27:101-106, 2003.
- [4] Fan Cui Ying, Zhao Ming Hao. Nonlinear fracture of 2D magnetoelastoelectroelastic media: Analytical and numerical solutions. *International Journal of Solids and Structures*, 48(16-17): 2373-2382, 2011.

Quasi-optimal adaptive BEM

MICHAEL FEISCHL

(joint work with Thomas Führer, Michael Karkulik, Dirk Praetorius)

There are two main reasons to use a posteriori error estimation in finite and boundary element methods: First, to check whether a computed solution is accurate enough. Second, if it is not, to find out where to refine the mesh to obtain the optimal improvement in accuracy. The latter leads immediately to the idea of the following adaptive feedback loop

$$(1) \quad \boxed{\text{solve}} \longrightarrow \boxed{\text{estimate}} \longrightarrow \boxed{\text{mark}} \longrightarrow \boxed{\text{refine}}$$

where the computed solution is checked for accuracy and then improved by marking elements with big error contributions and by refining at least these elements to obtain an improved mesh. Hereafter, the index ℓ indicates the iteration index in the adaptive loop of (1).

The usual observation is that the improvement compared to uniform mesh-refinement is vast in terms of error versus degrees of freedom, see also Figure 1 below for some typical model problem of 2D BEM. This is due to singularities of the given data and/or the (unknown) solution which lead to suboptimal convergence rates if the meshes are refined uniformly. However, besides these empirical observations, two important questions arise from a mathematical point of view:

- (i) Convergence? Since the mesh-size does not necessarily tend to zero everywhere in Ω , it is far from obvious that the approximate solutions Φ_ℓ converge towards the exact solution ϕ as $\ell \rightarrow \infty$.
- (ii) Speed of convergence? Empirically, adaptive schemes recover the optimal convergence rate even in the presence of singularities. For adaptive FEM, mathematical explanations for this observation are available, see e.g. [4]. Unfortunately, the contemporary FEM proofs cannot be directly transferred to adaptive BEM, as the non-locality of the involved operators and norms leads to severe technicalities.

The following sections state the model problem, clarify the adaptive algorithm (1), and give positive answers to both (i) and (ii). Moreover, we shall give a short overview on the current state of research.

1. MODEL PROBLEM & STATE OF THE ART

With V and K being the simple-layer and double-layer potential of the 2D or 3D Laplacian, we consider the weakly singular integral equation

$$(2) \quad V\phi = (1/2 + K)g \quad \text{on } \Gamma$$

for some given Dirichlet data $g \in H^{1/2}(\Gamma)$. Here, $\Gamma = \partial\Omega$ is the boundary of a polygonal Lipschitz domain $\Omega \subset \mathbb{R}^d$ for $d = 2, 3$. For $d = 2$, we ensure $\text{diam}(\Omega) < 1$ and hence ellipticity of V by scaling. The equation (2) is thus the prototype of an elliptic integral equation of the first-kind.

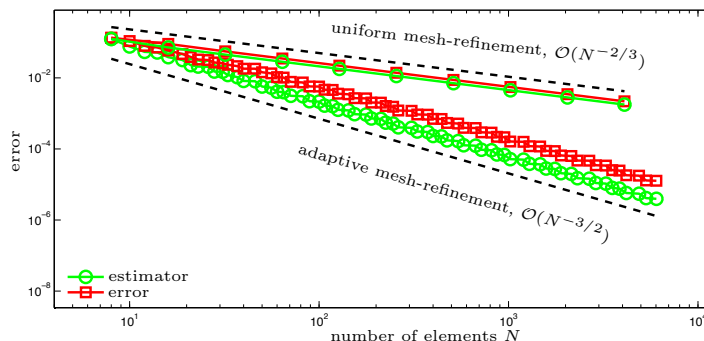


FIGURE 1. Adaptive mesh-refinement yields an improved convergence rate compared to uniform mesh-refinement.

Convergence of the adaptive algorithm (1) with quasi-optimal algebraic rates has independently first been proved in [7, 5]. Therein, the discretization is restricted to lowest-order elements, and the right-hand side is assumed to be computed exactly. While the wavelet based analysis of [5] covers general integral kernels, but requires the boundary to be smooth, the work [7] restricts to the Laplace kernel, but also covers piecewise polygonal resp. polyhedral boundaries. The work [7] extends the analysis to arbitrary but fixed-order polynomials and includes the adaptive resolution of the right-hand side. For an overview, we refer to the recent PhD thesis [8], where also the hypersingular integral equation is analyzed. Finally, we also refer to [1], where the present analysis is used to show convergence of an adaptive FEM-BEM coupling method by means of the estimator reduction principle.

For the ease of presentation, we restrict to the weakly singular integral equation (2) with lowest-order elements as in [7], but also include the approximation of the given Dirichlet data [7].

2. THE ADAPTIVE ALGORITHM

We now specify the four modules of algorithm (1). For `solve`, we use a Galerkin BEM to approximate the solution ϕ of (2) by a piecewise constant function $\Phi_\ell \in \mathcal{P}^0(\mathcal{T}_\ell)$ which is given as the solution of the linear system

$$(3) \quad \langle V\Phi_\ell, \Psi_\ell \rangle = \langle (1/2 + K)P_\ell g, \Psi_\ell \rangle \quad \text{for all } \Psi_\ell \in \mathcal{P}^0(\mathcal{T}_\ell).$$

Here, we use an arbitrary $H^{1/2}$ -stable projection P_ℓ onto piecewise affine, globally continuous functions on a mesh \mathcal{T}_ℓ , e.g. the L^2 -projection [11] or the Scott-Zhang projection [12], and approximate $g \approx G_\ell := P_\ell g$. For 2D and continuous g , one may also use nodal interpolation. Then, the linear system (3) relies only on operator matrices of V and K which can be assembled fast and, in certain cases, even exactly.

For `estimate`, we build on the weighted residual estimator from [4, 6]

$$\eta_\ell^2 = \sum_{T \in \mathcal{T}_\ell} \eta_\ell(T)^2 \text{ with } \eta_\ell(T)^2 := \text{diam}(T) \|\nabla(V\Phi_\ell - (1/2+K)G_\ell)\|_{L^2(T)}^2.$$

Here, ∇ denotes the surface gradient on the $(d-1)$ -dimensional manifold Γ . In 2D, ∇ is simply the arclength derivative. To take account of the additional data approximation error, we assume $g \in H^1(\Gamma)$ and define

$$\text{osc}_\ell^2 = \sum_{T \in \mathcal{T}_\ell} \text{osc}_\ell(T)^2 \text{ with } \text{osc}_\ell(T)^2 := \text{diam}(T) \|(1 - \Pi_\ell^0)\nabla g\|_{L^2(T)}^2,$$

where $\Pi_\ell^0 : L^2(\Gamma) \rightarrow \mathcal{P}^0(\mathcal{T}_\ell)$ denotes the \mathcal{T}_ℓ -elementwise integral mean. The advantage of this oscillation term is that it incorporates only a fairly easy-to-compute projection Π_ℓ^0 . Moreover, it is independent of the exact choice of P_ℓ for data approximation. The combined error estimator

$$\rho_\ell^2 = \sum_{T \in \mathcal{T}_\ell} \rho_\ell(T)^2 \text{ with } \rho_\ell(T)^2 = \eta_\ell(T)^2 + \text{osc}_\ell(T)^2$$

will then be provided by the module `estimate`. We stress the upper bound

$$(4) \quad \|\phi - \Phi_\ell\| \leq C_{\text{rel}} \rho_\ell$$

where $\|\cdot\| := \langle V \cdot, \cdot \rangle^{1/2} \simeq \|\cdot\|_{H^{-1/2}(\Gamma)}$ denotes the energy norm induced by V . Moreover, in 2D and under certain regularity assumptions on the Dirichlet data g , we also obtain a lower bound [2]

$$(5) \quad C_{\text{eff}}^{-1} \rho_\ell \leq \|\phi - \Phi_\ell\| + \text{osc}_\ell + \text{hot}_\ell,$$

where hot_ℓ is a term of higher order, compared to the generic rate of convergence $\mathcal{O}(h^{3/2})$ of lowest-order BEM for uniform meshes and smooth solutions. Exactly speaking, there holds for $g \in H^{2+\varepsilon}(\Gamma)$

$$\text{hot}_\ell = \mathcal{O}(h^{3/2+\varepsilon}) = o(\|\phi - \Phi_\ell\|)$$

for uniform meshes \mathcal{T}_ℓ with mesh-size $h > 0$.

In the module `mark`, we use a separate Dörfler marking strategy also employed in [3]: For given parameters $0 < \theta, \vartheta < 1$, we determine the set of marked elements $\mathcal{M}_\ell \subseteq \mathcal{T}_\ell$ as a set of minimal cardinality which satisfies

$$(6a) \quad \theta \eta_\ell^2 \leq \sum_{T \in \mathcal{M}_\ell} \eta_\ell(T)^2 \text{ for } \text{osc}_\ell^2 \leq \vartheta \eta_\ell^2$$

resp.

$$(6b) \quad \theta \text{osc}_\ell^2 \leq \sum_{T \in \mathcal{M}_\ell} \text{osc}_\ell(T)^2 \text{ for } \text{osc}_\ell^2 > \vartheta \eta_\ell^2.$$

For the special case when P_ℓ is the Scott-Zhang projection (or for $d = 2$ the nodal interpolant), we may also use the standard Dörfler marking

$$(7) \quad \theta \rho_\ell^2 \leq \sum_{T \in \mathcal{M}_\ell} \rho_\ell(T)^2,$$

and all results below hold accordingly.

Finally, the module `refine` consists of a fixed refinement rule. For 3D, we use the so-called *newest vertex bisection*, see e.g. [4, 11], whereas we use the bisection algorithm of [2] for 2D.

3. CONVERGENCE

By proving certain (local) inverse-type estimates [1], we are able to conclude that ρ_ℓ satisfies the estimator reduction estimate

$$(8) \quad \rho_{\ell+1}^2 \leq \tilde{\kappa} \rho_\ell^2 + C_{\text{inv}} \left(\|\Phi_{\ell+1} - \Phi_\ell\|^2 + \|G_{\ell+1} - G_\ell\|_{H^{1/2}(\Gamma)}^2 \right)$$

with ℓ -independent constants $0 < \tilde{\kappa} < 1$ and $C_{\text{inv}} > 0$. Abstract functional analysis provides that the discrete solutions Φ_ℓ and discretized data G_ℓ converge in $H^{-1/2}(\Gamma)$ resp. $H^{1/2}(\Gamma)$ to certain (yet unknown) limits. In particular, ρ_ℓ is thus contractive up to a perturbation which tends to zero as $\ell \rightarrow \infty$. In particular, we thus obtain the following convergence result.

Theorem 3.1. *For arbitrary marking parameters $0 < \theta, \vartheta < 1$, there holds*

$$(9) \quad C_{\text{rel}}^{-1} \|\phi - \Phi_\ell\| \leq \rho_\ell \rightarrow 0 \quad \text{as } \ell \rightarrow \infty,$$

i.e. algorithm (1) always yields convergence. □

The observation in Figure 1 is that the adaptive algorithm converges even with the best possible rate for lowest-order BEM for this problem type. A first step towards a mathematical justification for this observation is to prove linear convergence of the estimator ρ_ℓ in the sense of

$$(10) \quad \rho_\ell \leq C_{\text{conv}} q_{\text{conv}}^\ell$$

where $C_{\text{conv}} > 0$ and $0 < q_{\text{conv}} < 1$ are independent of $\ell \in \mathbb{N}$. However, due to the changing right-hand side $(1/2 + K)G_\ell$ in each step of the algorithm, we cannot rely on the usual Galerkin orthogonality as e.g. in [4], i.e.

$$\|\phi - \Phi_\ell\|^2 \neq \|\phi - \Phi_{\ell+1}\|^2 + \|\Phi_{\ell+1} - \Phi_\ell\|^2$$

in general. Nevertheless, one may prove the following contraction result [7].

Theorem 3.2. *For sufficiently small $0 < \vartheta < 1$, but arbitrary $0 < \theta < 1$, there exist constants $0 < \kappa < 1$ and $\alpha, \beta > 1$ such that the contraction quantity*

$$(11) \quad \Delta_\ell := \|\phi_\ell - \Phi_\ell\|^2 + \alpha \eta_\ell^2 + \beta \text{osc}_\ell^2$$

with $\phi_\ell := V^{-1}(1/2 + K)G_\ell$ satisfies the estimate

$$(12) \quad \Delta_{\ell+1} \leq \kappa \Delta_\ell \quad \text{for all } \ell \in \mathbb{N}.$$

Since $\min\{\alpha, \beta\} \rho_\ell^2 \leq \Delta_\ell \leq (C_{\text{rel}}^2 + \max\{\alpha, \beta\}) \rho_\ell^2$, this implies linear convergence (10). □

4. OPTIMAL CONVERGENCE RATES

Given the initial mesh \mathcal{T}_0 , let \mathbb{T} be the set of all triangulations which can be generated by means of the fixed mesh-refinement strategy. For arbitrary $s > 0$, we say that ϕ belongs to the *approximation class* \mathbb{A}_s provided that there exists a sequence $(\tilde{\mathcal{T}}_\ell)_{\ell \in \mathbb{N}_0}$ of meshes in \mathbb{T} such that

$$(13) \quad \tilde{\rho}_\ell \leq C (\#\tilde{\mathcal{T}}_\ell - \#\mathcal{T}_0)^{-s} \quad \text{for all } \ell \in \mathbb{N}.$$

Here, $\tilde{\rho}_\ell$ is the error estimator corresponding to the Galerkin approximations $\tilde{\Phi}_\ell$ on $\tilde{\mathcal{T}}_\ell$, and (13) states the decay $\tilde{\rho}_\ell = \mathcal{O}(N^{-s})$ for the estimator sequence.

We emphasize that in the definition of \mathbb{A}_s , the sequence of meshes can be chosen in an *optimal* way, i.e., to ensure (13) with $C > 0$ as small as possible. However, this sequence is chosen *a priori* and is hence not computable. The following theorem from [7] states that the approximation classes to which ϕ belongs, i.e. each possible decay $\rho_\ell = \mathcal{O}(N^{-s})$ of the error estimator, is in fact characterized and will be achieved by the adaptive algorithm (1).

Theorem 4.1. *Assume that the adaptivity parameters $0 < \theta, \vartheta < 1$ are sufficiently small. Then, for all $s > 0$, there holds equivalence*

$$(14) \quad \phi \in \mathbb{A}_s \iff \forall \ell \in \mathbb{N} : \rho_\ell \leq C_{\text{opt}} (\#\mathcal{T}_\ell - \#\mathcal{T}_0)^{-s},$$

i.e. algorithm (1) will lead to optimal algebraic convergence rates for the error estimator. \square

Finally, we restrict ourselves to the 2D case on a 1D manifold $\Gamma = \partial\Omega$. We use the efficiency result (5) from [2] to characterize the class of problems ϕ for which (13) is possible, by means of the best approximation error only. Recall that the optimal rate of convergence for lowest-order BEM is $\mathcal{O}(h^{3/2})$ which corresponds to $s = 3/2$ for $d = 2$.

Theorem 4.2. *Let $d = 2$ and $g \in H^{2+\varepsilon}(\Gamma)$. Assume that $0 < \theta, \vartheta < 1$ are sufficiently small. Then, for all $0 < s \leq 5/2$, there holds equivalence*

$$(15) \quad \phi \in \mathbb{A}_s \iff \forall \ell \in \mathbb{N} : \min_{\Psi_\ell \in \mathcal{P}^0(\mathcal{T}_\ell)} \|\phi - \Psi_\ell\| \leq C_{\text{opt}} (\#\mathcal{T}_\ell - \#\mathcal{T}_0)^{-s},$$

i.e. algorithm (1) will also lead to the optimal algebraic convergence rate for the Galerkin error. \square

In particular, we see that the weighted-residual error estimator η_ℓ from [4, 6] performs (in terms of convergence rate) at least as good as any other error estimator and especially better than uniform mesh refinement.

5. SUMMARY AND EXTENSIONS

We have empirically observed that the use of adaptivity for the model problem (2) is advantageous in terms of error versus degrees of freedom. This empirical observation can now be explained and guaranteed mathematically. In experiments, we even observe that adaptivity is superior in terms of computational time and memory consumption. The used techniques are also applicable to the Neumann

problem for the Laplacian. Moreover, other elliptic equations as the Lamé system might be analysed in the same fashion.

Michael Feischl, Thomas Führer, Michael Karkulik, Dirk Praetorius

Vienna University of Technology, Institute for Analysis and Scientific Computing, Wiedner Hauptstrasse 8-10, 1040 Vienna

michael.feischl@tuwien.ac.at, thomas.fuehrer@tuwien.ac.at,

michael.karkulik@tuwien.ac.at, dirk.praetorius@tuwien.ac.at

REFERENCES

- [1] M. AURADA, M. FEISCHL, T. FÜHRER, M. KARKULIK, J.M. MELENK, AND D. PRAETORIUS, *Inverse estimates for elliptic boundary integral operators and their application to the adaptive coupling of FEM and BEM*, ASC Report, 07/2012, TU Wien, 2012.
- [2] M. AURADA, M. FEISCHL, T. FÜHRER, M. KARKULIK, AND D. PRAETORIUS, *Efficiency and optimality of some weighted-residual error estimator for adaptive 2D boundary element method*, ASC Report, 15/2012, TU Wien, 2012.
- [3] M. AURADA, M. FEISCHL, J. KEMETMÜLLER, M. PAGE, AND D. PRAETORIUS, *Adaptive FEM with inhomogeneous Dirichlet data: convergence and quasi-optimality in \mathbb{R}^d* , M2AN Math. Model. Numer. Anal., accepted for publication (2012).
- [4] J. CASCON, C. KREUZER, R. NOCHETTO, AND K. SIEBERT, *Quasi-optimal convergence rate for an adaptive finite element method*, SIAM J. Numer. Anal., 46 (2008), pp. 2524–2550.
- [5] C. CARSTENSEN, M. MAISCHAK, AND E. STEPHAN, *A posteriori error estimate and h-adaptive algorithm on surfaces for Symm’s integral equation*, Numer. Math., 90 (2001), pp. 197–213
- [6] C. CARSTENSEN AND E. STEPHAN, *A posteriori error estimates for boundary element methods*, Math. Comp., 64 (1995), pp. 483–500.
- [7] M. FEISCHL, T. FÜHRER, M. KARKULIK, J.M. MELENK, AND D. PRAETORIUS, *Quasi-optimal convergence rates for adaptive boundary element methods with data approximation*, work in progress (2012).
- [8] M. FEISCHL, M. KARKULIK, J.M. MELENK, AND D. PRAETORIUS, *Quasi-optimal convergence rate for an adaptive boundary element method*, SIAM J. Numer. Anal., under review (2012).
- [9] T. GANTUMUR, *Adaptive boundary element methods with convergence rates*, Numer. Math., accepted for publication (2012).
- [10] M. KARKULIK, *Zur Konvergenz und Quasioptimalität adaptiver Randelementmethoden*, PhD thesis (in German), Institute for Analysis and Scientific Computing, Vienna University of Technology, Wien, 2012.
- [11] M. KARKULIK, D. PAVLICEK, AND D. PRAETORIUS, *On 2D newest vertex bisection: Optimality of mesh-closure and H^1 -stability of L_2 -projection*, Constr. Approx., under review (2012).
- [12] L. R. SCOTT AND S. ZHANG, *Finite element interpolation of nonsmooth functions satisfying boundary conditions*, Math. Comp., 54 (1990), pp. 483–493.

FEM-BEM couplings without stabilization

T. FÜHRER

(joint work with M. Feischl, M. Karkulik, J.M. Melenk, D. Praetorius)

We consider a nonlinear interface problem with the Laplacian, which can equivalently be stated via various FEM-BEM coupling methods. We treat the symmetric coupling [4, 8], the Johnson-Nédélec coupling [9, 16] as well as the one-equation Bielak-MacCamy coupling [2]. Due to constant functions in the kernel of these equations, these formulations are not elliptic and unique solvability cannot be shown directly. Available results concerning solvability of these methods include the following:

- For the symmetric coupling and certain nonlinear problems with additional Dirichlet boundary, Gatica & Hsiao [6] proved unique solvability.
- For the symmetric coupling and certain nonlinear problems, Carstensen & Stephan [3] proved unique solvability for sufficiently fine meshes, but without an additional interior Dirichlet boundary.
- For the Johnson-Nédélec coupling and the linear Laplace and Yukawa transmission problem, Sayas [11] proved unique solvability on polyhedral boundaries, whereas the original work [9] relied on the Fredholm alternative and hence smooth coupling boundaries.
- For the Johnson-Nédélec coupling and a general class of linear problems, Steinbach [13] introduced a stabilization to prove ellipticity of the stabilized coupling equations, cf. also [10]. His approach, however, requires pre- and postprocessing steps which involve the numerical solution of an additional integral equation with the simple-layer potential.

We present a framework based on *implicit stabilization* to prove well-posedness of nonlinear FEM-BEM coupling formulations [1]. We build on the works of Sayas [11] and Steinbach [13] and introduce stabilized coupling equations which are uniquely solvable and have the same solution as the (original) continuous resp. discrete coupling equations. With this *theoretic auxiliary problem*, we obtain unique solvability of the original (non-stabilized) coupling equations. In particular, we have to implement and solve the original coupling equations only, and we avoid the solution of any additional equation and corresponding pre- and postprocessing steps as well as any assumption on the mesh-size. Our approach also applies to nonlinear elasticity [5].

1. MODEL PROBLEM

Let $\Omega \subseteq \mathbb{R}^d$ for $d = 2, 3$ be a connected, bounded Lipschitz domain with polyhedral boundary $\Gamma := \partial\Omega$. We refer to Ω as interior domain and to the unbounded domain $\Omega^{\text{ext}} := \mathbb{R}^d \setminus \overline{\Omega}$ as exterior domain. For given data $f \in H^1(\Omega)$, $u_0 \in$

$H^{1/2}(\Gamma)$, $\phi_0 \in H^{-1/2}(\Gamma)$, our model problem then reads:

$$\begin{aligned}
(1a) \quad & -\operatorname{div}(\mathcal{A}\nabla u) = f \quad \text{in } \Omega, \\
(1b) \quad & -\Delta u^{\text{ext}} = 0 \quad \text{in } \Omega^{\text{ext}}, \\
(1c) \quad & u - u^{\text{ext}} = u_0 \quad \text{on } \Gamma, \\
(1d) \quad & (\mathcal{A}\nabla u - \nabla u^{\text{ext}}) \cdot \mathbf{n} = \phi_0 \quad \text{on } \Gamma, \\
(1e) \quad & u^{\text{ext}}(x) = \mathcal{O}(1/|x|) \quad \text{for } |x| \rightarrow \infty.
\end{aligned}$$

Here, \mathbf{n} is the outer normal vector on Γ . Let $\langle \cdot, \cdot \rangle_\Omega$ denote the $L^2(\Omega)$ scalar product and let $\langle \cdot, \cdot \rangle_\Gamma$ denote the $L^2(\Gamma)$ scalar product which is continuously extended to the duality bracket between $H^{-1/2}(\Gamma)$ and $H^{1/2}(\Gamma)$. We assume $\mathcal{A} : \mathbb{R}^d \rightarrow \mathbb{R}^d$ to be strongly monotone (2a) as well as Lipschitz continuous (2b) with constants $c_{\text{mon}}, c_{\text{lip}} > 0$, i.e.

$$(2a) \quad \langle \mathcal{A}\nabla u - \mathcal{A}\nabla v, \nabla u - \nabla v \rangle_\Omega \geq c_{\text{mon}} \|\nabla u - \nabla v\|_{L^2(\Omega)}^2$$

as well as

$$(2b) \quad \|\mathcal{A}\nabla u - \mathcal{A}\nabla v\|_{L^2(\Omega)}^2 \leq c_{\text{lip}} \|\nabla u - \nabla v\|_{L^2(\Omega)}^2 \quad \text{for all } u, v \in H^1(\Omega).$$

In 2D, the compatibility condition

$$(3) \quad \langle f, 1 \rangle_\Omega + \langle \phi_0, 1 \rangle_\Gamma = 0$$

has to be imposed on the data to ensure the radiation condition (1e).

Throughout, K denotes the double-layer potential with adjoint K' , V denotes the simple-layer potential, and W the hypersingular integral operator. Moreover, we assume $\operatorname{diam}(\Omega) < 1$ to guarantee ellipticity $\langle \phi, V\phi \rangle_\Gamma \geq \|\phi\|_{H^{-1/2}(\Gamma)}$ of the simple-layer potential.

Under these assumptions, problem (1) allows for a unique solution $(u, u^{\text{ext}}) \in H^1(\Omega) \times H_{\text{loc}}^1(\Omega^{\text{ext}})$ with finite energy $\|\nabla u^{\text{ext}}\|_{L^2(\Omega^{\text{ext}})} < \infty$, see e.g. [3].

2. SYMMETRIC COUPLING

As shown in e.g. [3, 6], the nonlinear transmission problem (1) can equivalently be stated via the symmetric coupling [4, 8], which reads in variational formulation as follows: Find $\mathbf{u} = (u, \phi) \in \mathcal{H} := H^1(\Omega) \times H^{-1/2}(\Gamma)$ such that

$$(4) \quad b(\mathbf{u}, \mathbf{v}) = F(\mathbf{v}) \quad \text{holds for all } \mathbf{v} \in \mathcal{H},$$

where the mapping $b : \mathcal{H} \times \mathcal{H} \rightarrow \mathbb{R}$ and the linear functional $F : \mathcal{H} \rightarrow \mathbb{R}$ are defined for all $\mathbf{u} = (u, \phi), \mathbf{v} = (v, \psi) \in \mathcal{H}$ via

$$(5a) \quad \begin{aligned} b(\mathbf{u}, \mathbf{v}) := & \langle \mathcal{A}\nabla u, \nabla v \rangle_\Omega + \langle (K' - \tfrac{1}{2})\phi, v \rangle_\Gamma + \langle Wu, v \rangle_\Gamma \\ & + \langle \psi, (\tfrac{1}{2} - K)u \rangle_\Gamma + \langle \psi, V\phi \rangle_\Gamma, \end{aligned}$$

$$(5b) \quad F(\mathbf{v}) := \langle f, v \rangle_\Omega + \langle \phi_0 + Wu_0, v \rangle_\Gamma + \langle \psi, (\tfrac{1}{2} - K)u_0 \rangle_\Gamma$$

By taking $(u, \phi) = (1, 0) = (v, \psi)$ in (5a), we see that $b((1, 0), (1, 0)) = 0$ and thus constant functions are in the kernel of the mapping $\mathbf{u} \mapsto b(\mathbf{u}, \mathbf{u})$. Therefore,

$b(\cdot, \cdot)$ is not elliptic and solvability of (4) cannot be shown directly by applying well-known PDE theory, such as the Lax-Milgram lemma for linear problems.

We stress that clearly (4) is uniquely solvable up to a constant in the interior domain Ω . Early works, including [4, 8] as well as [6], use interior Dirichlet boundaries to tackle this constant in Ω . The very first work which circumvented this technical restriction was [3]. However, the latter work requires the mesh-size to be sufficiently fine.

In the following, we introduce the concept of *implicit stabilization* and show that the second equation of (4), i.e. $b((u, \phi), (0, \psi)) = F((0, \psi))$, already fixes the constant in the interior domain. Unfortunately, this information is lost when trying to prove ellipticity of $b(\cdot, \cdot)$, but can be reconstructed by adding appropriate stabilization terms to the mapping $b(\cdot, \cdot)$. This leads to a modified (or stabilized) formulation that admits a unique solution. Moreover, Lemma 2.3 states equivalence of this modified problem to (4) in the sense that both problems have the same solution even in the discrete formulation.

For the remainder, let $\mathcal{H}_h = \mathcal{X}_h \times \mathcal{Y}_h \subseteq \mathcal{H}$ be a closed subspace of \mathcal{H} . In particular, $\mathcal{H}_h = \mathcal{H}$ is a valid choice. We stress that \mathcal{H} , associated with the natural product norm

$$\|\mathbf{u}\|_{\mathcal{H}}^2 = \|u\|_{H^1(\Omega)}^2 + \|\phi\|_{H^{-1/2}(\Gamma)}^2 \quad \text{for all } \mathbf{u} = (u, \phi) \in \mathcal{H},$$

becomes a Hilbert space. The following theorem from [1] shows solvability of the continuous formulation (4) as well as of its Galerkin discretization.

Theorem 2.1. *The symmetric coupling (4) admits a unique solution $\mathbf{u} \in \mathcal{H}$. Moreover, assume that*

$$(6) \quad \exists \xi \in \mathcal{Y}_h \quad \langle \xi, 1 \rangle_{\Gamma} \neq 0.$$

Then, the discretized equations

$$(7) \quad b(\mathbf{u}_h, \mathbf{v}_h) = F(\mathbf{v}_h) \quad \text{for all } \mathbf{v}_h \in \mathcal{H}_h$$

also admit a unique solution $\mathbf{u}_h \in \mathcal{H}_h$. There holds the Céa-type estimate

$$(8) \quad \|\mathbf{u} - \mathbf{u}_h\|_{\mathcal{H}} \leq C \min_{\mathbf{v}_h \in \mathcal{H}_h} \|\mathbf{u} - \mathbf{v}_h\|_{\mathcal{H}},$$

where the constant $C > 0$ depends only on \mathcal{A}, Ω , and $\xi \in \mathcal{Y}_h$.

Remark 2.2. (i) For a sequence $(\mathcal{Y}_h)_{h>0}$ of closed subspaces of $H^{-1/2}(\Gamma)$ with

$$(9) \quad \exists \xi \in \bigcap_{h>0} \mathcal{Y}_h \quad \langle \xi, 1 \rangle_{\Gamma} \neq 0,$$

the constant in (8) is independent of $h > 0$.

(ii) For an arbitrary sequence $(\mathcal{E}_h)_{h>0}$ of regular triangulations and $\mathcal{Y}_h = \mathcal{P}^p(\mathcal{E}_h)$ being the space of \mathcal{E}_h -piecewise polynomials of degree $p \geq 0$, $\xi = 1 \in \mathcal{Y}_h$ satisfies (9).

Note that the following lemma from [1] holds for arbitrary $\xi \in \mathcal{Y}_h$. But to prove solvability in Theorem 2.1 we have to impose the assumption (6), which also appears in [11].

Lemma 2.3. For fixed $\xi \in \mathcal{Y}_h$, define

$$(10a) \quad \tilde{b}(\mathbf{u}_h, \mathbf{v}_h) := b(\mathbf{u}_h, \mathbf{v}_h) + \langle \xi, (\frac{1}{2} - K)u_h + V\phi_h \rangle_\Gamma \langle \xi, (\frac{1}{2} - K)v_h + V\psi_h \rangle_\Gamma$$

as well as

$$(10b) \quad \tilde{F}(\mathbf{v}_h) := F(\mathbf{v}_h) + \langle \xi, (\frac{1}{2} - K)u_0 \rangle \langle \xi, (\frac{1}{2} - K)v_h + V\psi_h \rangle_\Gamma$$

for all $\mathbf{u}_h = (u_h, \phi_h)$, $\mathbf{v}_h = (v_h, \psi_h) \in \mathcal{H}_h$. Then, a function $\mathbf{u}_h \in \mathcal{H}_h$ solves (7) if and only if \mathbf{u}_h solves

$$(11) \quad \tilde{b}(\mathbf{u}_h, \mathbf{v}_h) = \tilde{F}(\mathbf{v}_h) \quad \text{for all } \mathbf{v} \in \mathcal{H}_h.$$

□

The following lemma is used to prove Theorem 2.1 and essentially states that the stabilization terms added to $b(\cdot, \cdot)$ to obtain $\tilde{b}(\cdot, \cdot)$ can be used to define an equivalent norm on \mathcal{H} .

Lemma 2.4. Let the linear functional $L : \mathcal{H} \rightarrow \mathbb{R}$ fulfill

$$(12) \quad L((1, 0)) \neq 0.$$

Then, $\|\mathbf{u}\|^2 := \|\nabla u\|_{L^2(\Omega)}^2 + \langle \phi, V\phi \rangle_\Gamma + |L(\mathbf{u})|^2$ for $\mathbf{u} = (u, \phi) \in \mathcal{H}$ defines an equivalent norm $\|\cdot\| \simeq \|\cdot\|_{\mathcal{H}}$ on \mathcal{H} . Moreover, $L(\mathbf{v}) := \langle \xi, (\frac{1}{2} - K)v + V\psi \rangle_\Gamma$ for $\mathbf{v} = (v, \psi) \in \mathcal{H}$ satisfies (12) if $\xi \in \mathcal{Y}_h$ fulfills (6). □

Sketch of proof of Theorem 2.1. We consider the operator $\tilde{B} : \mathcal{H} \rightarrow \mathcal{H}^*$ associated to the mapping $\tilde{b}(\cdot, \cdot)$. With Lemma 2.4, one can show that \tilde{B} is strongly monotone and Lipschitz continuous. Therefore, standard arguments [15] prove the assertions of Theorem 2.1 for (7) replaced by (11). The equivalence of Lemma 2.3 then concludes the proof. □

3. JOHNSON-NÉDÉLEC COUPLING

The nonlinear transmission problem (1) can also be reformulated by means of the Johnson-Nédélec coupling [9, 16]. It reads as (4), where the mapping $b : \mathcal{H} \times \mathcal{H} \rightarrow \mathbb{R}$ and the linear functional $F : \mathcal{H} \rightarrow \mathbb{R}$ are now defined for all $\mathbf{u} = (u, \phi)$, $\mathbf{v} = (v, \psi) \in \mathcal{H}$ via

$$(13a) \quad b(\mathbf{u}, \mathbf{v}) := \langle \mathcal{A}\nabla u, \nabla v \rangle_\Omega - \langle \phi, v \rangle_\Gamma + \langle \psi, (\frac{1}{2} - K)u \rangle_\Gamma + \langle \psi, V\phi \rangle_\Gamma,$$

$$(13b) \quad F(\mathbf{v}) := \langle f, v \rangle_\Omega + \langle \phi_0, v \rangle_\Gamma + \langle \psi, (\frac{1}{2} - K)u_0 \rangle_\Gamma$$

As in Section 2, we infer that constant functions lie in the kernel of the mapping $\mathbf{u} \mapsto b(\mathbf{u}, \mathbf{u})$. Thus, solvability cannot be shown directly. Still, Theorem 2.3 holds essentially true for the Johnson-Nédélec coupling [1].

Theorem 3.1. Assume that $c_{\text{mon}} > c_K/4$, where $c_{\text{mon}} > 0$ denotes the monotonicity constant (2a) of \mathcal{A} and $0 < c_K < 1$ denotes the contraction constant of the double-layer potential [12]. Then, the assertions of Theorem 2.1 hold true for the Johnson-Nédélec coupling. □

Remark 3.2. (i) The very same results as for the Johnson-Nédélec coupling also hold for the non-symmetric Bielak-MacCamy one-equation coupling [1].

(ii) In [10], it is proven that the assumption $c_{\text{mon}} > c_K/4$ is not only sufficient but also necessary to prove ellipticity of the bilinear form associated to the stabilized formulation of Steinbach [13]. Nevertheless, numerical experiments in [1] indicate that the assumption $c_{\text{mon}} > c_K/4$ is not necessary for existence and uniqueness of discrete solutions of the Johnson-Nédélec coupling.

4. EXTENSIONS

The recent work [5] presents how to transfer the ideas of *implicit stabilization* developed for nonlinear Laplace transmission problems [1] to nonlinear elasticity transmission problems. As in [1], we treat the symmetric coupling as well as the non-symmetric one-equation couplings of Johnson-Nédélec and Bielak-MacCamy type. In contrast to Laplace problems, one faces the problem that the kernel of the Lamé operator contains the space of rigid body motions \mathcal{R} , with $\dim(\mathcal{R}) = 3$ in 2D and $\dim(\mathcal{R}) = 6$ in 3D. The stabilization process then becomes more complicated, since not only constant functions have to be fixed in the interior domain. However, under the assumption

$$(14) \quad \forall r \in \mathcal{R} \setminus \{0\} \exists \xi \in \mathcal{Y}_h \cap L^2(\Gamma) \quad \langle \xi, r \rangle_\Gamma \neq 0$$

on the discrete space \mathcal{Y}_h , which is the extension of (6) to elasticity problems, similar results as in Sections 2–3 hold true for nonlinear elasticity problems. It is shown in [5] that assumption (14) is satisfied for $\mathcal{P}^0(\mathcal{E}_h) \subseteq \mathcal{Y}_h$ and regular triangulations \mathcal{E}_h of the boundary into plane surface triangles

Unlike [7], we prove that interior Dirichlet boundaries can be avoided to fix the rigid body motions in the interior domain. Moreover, the explicit stabilization as recently proposed in [14] is avoided by our analysis [5], i.e. we have to implement and solve the original coupling equations only.

M. Feischl, T. Führer, M. Karkulik, J.M. Melenk, D. Praetorius

Institute for Analysis and Scientific Computing, Vienna University of Technology, Wiedner Hauptstrasse 8–10, A-1040 Vienna

Michael.Feischl@tuwien.ac.at, Thomas.Fuehrer@tuwien.ac.at

Michael.Karkulik@tuwien.ac.at, Melenk@tuwien.ac.at

Dirk.Praetorius@tuwien.ac.at

REFERENCES

- [1] M. AURADA, M. FEISCHL, T. FÜHRER, M. KARKULIK, J.M. MELENK, AND D. PRAETORIUS, *Classical FEM-BEM couplings: well-posedness, nonlinearities, and adaptivity*, Comput. Mech. (2012), published online Sep. 2012: DOI: 10.1007/s00466-012-0779-6.
- [2] J. BIELAK AND R.C. MACCAMY, *An exterior interface problem in two-dimensional elastodynamics*, Quart. Appl. Math., 41 (1983/84), pp. 143–159.
- [3] C. CARSTENSEN AND E.P. STEPHAN, *Adaptive coupling of boundary elements and finite elements*, Math. Model. Numer. Anal., 29 (1995), pp. 779–817.

-
- [4] M. COSTABEL, *A symmetric method for the coupling of finite elements and boundary elements*, in: The Mathematics of Finite Elements and Applications VI, MAFELAP 1987, (J. Whiteman ed.), Academic Press, London, 1988, pp. 281–288.
 - [5] M. FEISCHL, T. FÜHRER, M. KARKULIK, AND D. PRAETORIUS, *Stability of symmetric and non-symmetric FEM-BEM couplings for nonlinear elasticity problems*, in progress, (2012/13).
 - [6] G. GATICA AND G. HSIAO, *Boundary-field equation methods for a class of nonlinear problems*, Longman, Harlow, 1995.
 - [7] G. GATICA, G. HSIAO, AND F.J. SAYAS, *Relaxing the hypotheses of Bielak-MacCamy’s BEM-FEM coupling*, Numer. Math., 120 (2012), pp. 465–487.
 - [8] H. HAN, *A new class of variational formulations for the coupling of finite and boundary element methods*, J. Comput. Math., 8 (1990), pp. 223–242.
 - [9] C. JOHNSON AND J.C. NÉDÉLEC, *On the coupling of boundary integral and finite element methods*, Math. Comp., 35 (1980), pp. 1063–1079.
 - [10] G. OF AND O. STEINBACH, *Is the one-equation coupling of finite and boundary element methods always stable?*, Berichte aus dem Institut für Numerische Mathematik, 06 (2012), TU Graz.
 - [11] F.J. SAYAS, *The validity of Johnson-Nédélec’s BEM-FEM coupling on polygonal interfaces*, SIAM J. Numer. Anal., 47 (2009), pp. 3451–3463.
 - [12] O. STEINBACH, *Numerical approximation methods for elliptic boundary value problems: Finite and boundary elements*, Springer, New York, 2008.
 - [13] O. STEINBACH, *A note on the stable one-equation coupling of finite and boundary elements*, SIAM J. Numer. Anal., 49 (2011), pp. 1521–1531.
 - [14] O. STEINBACH, *On the stability of the non-symmetric BEM/FEM coupling in linear elasticity*, Comput. Mech. (2012), published online Aug. 2012, DOI: 10.1007/s00466-012-0782-y.
 - [15] E. ZEIDLER, *Nonlinear functional analysis and its applications, part II/B*, Springer, New York, 1990.
 - [16] O.C. ZIENKIEWICZ, D.W. KELLY, AND P. BETTESS, *Marriage la mode – the best of both worlds (finite elements and boundary integrals)*, Energy Methods in Finite Element Analysis, Wiley, Chichester, 1979.

BEM-AEM for 3D multi-region non-homogeneous/homogeneous elastic bodies

R. GALLEGO

(joint work with M.A. Riveiro)

A study of the application of Boundary Element Methods (BEM) to problems involving 3D multi-region bodies including homogeneous and non-homogeneous materials like Functionally Graded Materials (FGMs) is presented. In the non-homogeneous zones of the domain the Analogue Equation Method (AEM) is used to transform the original problem into a new problem with unknown forcing term but known fundamental solution. By means of this transformation a system of Boundary Integral Equations (BIEs) can be obtained combining standard boundary element discretization and a Radial Basis Functions (RBFs) approximation for the residual term. The application of the original differential operator to the displacement BIE provides the extra equations to compute the unknown forcing term. BEM-AEM or standard BEM can be used in the homogeneous zones of the domain and the coupling of the different systems of equations in the inter-phase is studied in every case. Numerical examples for three-dimensional problems in multi-region isotropic and linear elastic FGMs are presented and discussed to show the effects of the material gradation.

Keywords: Functionally Graded Materials, Elasticity, Boundary Element Method, Analog Equation Method, Radial basis functions, Multi-region, Three-dimensional domains

R. Gallego, M.A. Riveiro

Dept. Structural Mechanics, E.T.S. Ingeniería de Caminos, Canales y Puertos, University of Granada, 18071 Granada, Spain
gallego@ugr.es, mriveiro@ugr.es

REFERENCES

- [1] C.A. Brebbia and J. Dominguez, *Boundary elements, an introductory course*, Computational Mechanics Publication, Southampton, Boston, 1992.
- [2] J.T. Katsikadelis. The BEM for nonhomogeneous bodies. *Archive of Applied Mechanics*, 74(11-12):780-789,2005
- [3] A. Sutradhar and G.H. Paulino. A simple boundary element method for problems of potential in non-homogeneous media. *International Journal for Numerical Methods in Engineering*, 60(13):2203-2230,2004
- [4] J. Dominguez, M.P. Ariza and R. Gallego. Flux and traction boundary elements without hypersingular or strongly singular integrals. *International Journal for Numerical Methods in Engineering*, 48(1):111-135,2000.
- [5] B. Natalini and V. Popov. Tests of radial basis functions in the 3D DRM-MD. *Communications in numerical Methods in Engineering*, 22:13-22,2006.
- [6] X. Gao, L. Guo and Ch. Zhang. Three-step multi-domain BEM solver for nonhomogeneous material problems. *Engineering Analysis with Boundary Elements*, 31(12):965-973,2007.
- [7] M.S. Nerantzaki and C.B. Kandilas. A boundary element method solution for anisotropic nonhomogeneous elasticity. *Acta Mechanica*, 200(3-4):199-211,2008.

A model reduction boundary element algorithm for computational electromagnetism

M. GANESH

(joint work with J. S. Hesthaven, B. Stamm)

Simulation of scattered electromagnetic waves from three dimensional configurations comprising multiple perfectly conducting particles is fundamental for several applications. It is efficient to develop algorithms that facilitate various choices of parameters describing the multiple particle Maxwell problem. The parameter set may include the location, orientation, size, shape and number of scattering bodies as well as properties of the source field such as frequency, polarization and incident direction. The emphasis in this work is on fast simulation of the interactive scattered fields under parametric variation. The boundary element computer models of the Maxwell problem play an important role in computational electromagnetism. However, the standard boundary element method (BEM) is very expensive for the parameterized three dimensional Maxwell problem. In this article, following our recent work [1], we describe an efficient BEM based generalized iterative model reduction algorithm for parameterized multiple particle electromagnetic scattering.

1. INTRODUCTION

We consider an electromagnetic scattering configuration in three-dimensional space, consisting of a collection of disjoint perfect conductor obstacles Ω_j , $j = 1, \dots, J$ situated in a homogeneous medium with vanishing conductivity, the free space permittivity $\epsilon_0 = 10^7/(4\pi c^2)$ F/m and permeability $\mu_0 = 4\pi \times 10^{-7}$ H/m, where $c = 299,792,458$ m/s is the speed of light.

Time-harmonic interacting waves are generated by an incident electromagnetic wave $[\mathbf{E}^{\text{inc}}, \mathbf{H}^{\text{inc}}]$, impinging on the configuration $\Omega = \bigcup_{j=1}^J \Omega_j$. The incident field is parameterized by the wavenumber $k \in \mathbb{R}^+$, incident direction $\tilde{\mathbf{d}}_{\text{inc}} \in \mathbb{S}^2$ and polarization vector $\mathbf{p} \in \mathbb{R}^3$. Here, \mathbb{S}^2 is the unit sphere in \mathbb{R}^3 and $k = \omega\sqrt{\mu_0\epsilon_0}$, with $\omega > 0$ being the angular frequency.

The plane wave vector fields $\mathbf{E}^{\text{inc}}, \mathbf{H}^{\text{inc}} : (\mathbb{R}^3 \setminus \overline{\Omega}) \times \mathbb{R}^+ \times \mathbb{S}^2 \times \mathbb{R}^3 \rightarrow \mathbb{C}^3$ are respectively electric and magnetic fields with wavelength $\lambda = 2\pi/k$:

$$\mathbf{E}^{\text{inc}}(\mathbf{x}; \boldsymbol{\mu}) = \mathbf{p}_{\text{inc}} e^{ik\mathbf{x} \cdot \tilde{\mathbf{d}}_{\text{inc}}}, \quad \mathbf{H}^{\text{inc}}(\mathbf{x}; \boldsymbol{\mu}) = \left[\tilde{\mathbf{d}}_{\text{inc}} \times \mathbf{p}_{\text{inc}} \right] e^{ik\mathbf{x} \cdot \tilde{\mathbf{d}}_{\text{inc}}}, \quad \tilde{\mathbf{d}}_{\text{inc}} \perp \mathbf{p}_{\text{inc}},$$

where $\boldsymbol{\mu} = (k, \tilde{\mathbf{d}}_{\text{inc}}, \mathbf{p}_{\text{inc}}) \in \mathcal{D} := [k^-, k^+] \times \mathbb{S}^2 \times P \subset \mathbb{R}^5$, with $P \subset \mathbb{R}^2$ representing the coefficients of \mathbf{p}_{inc} in a two-dimensional local coordinate system that is perpendicular to $\tilde{\mathbf{d}}_{\text{inc}}$.

The bounded parameter domain $\mathcal{D} \subset \mathbb{R}^5$ is enriched by parameters that describe the location and geometry of the J obstacles in the configuration Ω . For many applications, the multiple scattering configuration is usually described through a few reference particles and some affine transformations.

For notational convenience, we assume a single reference Lipschitz domain \widehat{D} and that for $j = 1, \dots, J$, each obstacle Ω_j in the configuration is the image of a

rotation, an isotropic stretch/shrink and a translation of \widehat{D} . That is, there exists additional 3J parameters, $B_j \in \mathbb{R}^{3 \times 3}$, $\mathbf{b}_j \in \mathbb{R}^3$ and $\gamma_j \in \mathbb{R}^+$ such that $T_j : \widehat{D} \rightarrow \Omega_j$ defined as $T_j(\widehat{\mathbf{x}}) = \gamma_j B_j \widehat{\mathbf{x}} + \mathbf{b}_j$ satisfies $T_j(\widehat{D}) = \Omega_j$ with B_j being a rotation matrix.

It is often not practical using standard finite/boundary element methods to attempt to evaluate the impact of such variations in the above parameterized model. In this work, we propose a generalized version of the iterative reduced basis method in [1], based on a boundary element discretization of the reference scatterer to resolve the computationally challenging large scale problem. The approach includes (i) a computationally intensive offline procedure to create a selection of a set of snapshot parameters and the construction of an associated reduced basis for each reference scatterer and (ii) an inexpensive generalized version of the online algorithm in [1] to generate the surface current and scattered field of the parametrized configuration, for *any* choice of parameters within the parameter space used in the offline procedure. Comparison of our numerical results with that in [1] demonstrate the efficiency of the extension in this article. In [1] several simulated results comparing directly measured results for some benchmark configurations demonstrate the power of the method to rapidly simulate the interacting electromagnetic fields under parametric variations.

2. QUANTITY OF INTEREST AND ELECTRIC FIELD INTEGRAL EQUATION

An important quantity of interest in the electromagnetic scattering model, with intrinsic impedance $Z = \sqrt{\mu_0/\epsilon_0}$, is the simulation of the radar cross section (RCS) of the configuration Ω . This can be represented as [3]

$$(1) \quad \sigma(\widetilde{\mathbf{d}}_{\text{rcs}}, \boldsymbol{\mu}) = 10 \log_{10} \left(4\pi \left| \mathbf{E}_{\infty}(\widetilde{\mathbf{d}}_{\text{rcs}}; \boldsymbol{\mu}) \right|^2 / |\mathbf{p}_{\text{inc}}|^2 \right),$$

where \mathbf{E}_{∞} is the electric far field. The electric far field can be represented as a surface integral on the scattering ensemble [3]:

$$(2) \quad \mathbf{E}_{\infty}(\widetilde{\mathbf{d}}_{\text{rcs}}, \boldsymbol{\mu}) = \mathbf{E}_{\infty}(\mathbf{w}; \widetilde{\mathbf{d}}_{\text{rcs}}, \boldsymbol{\mu}) = \frac{ikZ}{4\pi} \int_{\partial\Omega} \widetilde{\mathbf{d}}_{\text{rcs}} \times [\mathbf{w}(\mathbf{x}; \boldsymbol{\mu}) \times \widetilde{\mathbf{d}}_{\text{rcs}}] e^{ik\mathbf{x} \cdot \widetilde{\mathbf{d}}_{\text{rcs}}} ds(\mathbf{x}),$$

where $\mathbf{w}(\boldsymbol{\mu}) = \mathbf{w}(\cdot; \boldsymbol{\mu}) \in \mathbf{H}^{-1/2}(\text{div}_{\partial\Omega}, \partial\Omega)$ satisfies electric field integral equation (EFIE)

$$(3) \quad ikZ(\pi_T \circ \mathbf{S}_e \mathbf{w})(\mathbf{x}; \boldsymbol{\mu}) = -(\pi_T \mathbf{E}^{\text{inc}})(\mathbf{x}; \boldsymbol{\mu}), \quad \mathbf{x} \in \partial\Omega, \quad \boldsymbol{\mu} \in \mathcal{D}.$$

Here, π_T is the tangential component trace operator defined for $\mathbf{x} \in \partial\Omega_j$, $j = 1, \dots, J$, by $(\pi_T \mathbf{v})(\mathbf{x}) = \mathbf{n}(\mathbf{x}) \times [\mathbf{v}(\mathbf{x}) \times \mathbf{n}(\mathbf{x})]$, and

$$(4) \quad (\mathbf{S}_e \mathbf{a})(\mathbf{x}; \boldsymbol{\mu}) = \int_{\partial\Omega} \left[\Phi_k(\mathbf{x}, \mathbf{y}) \mathbf{a}(\mathbf{y}) + \frac{1}{k^2} \mathbf{grad}_{\mathbf{x}} \Phi(\mathbf{x}, \mathbf{y}) \text{div}_{\mathbf{y}} \mathbf{a}(\mathbf{y}) \right] ds(\mathbf{y}).$$

In (4), Φ_k is the fundamental solution of the Helmholtz equation with wavenumber k .

The operator $\mathbf{T}_e = \pi_T \circ \mathbf{S}_e : \mathbf{H}^{-1/2}(\text{div}_{\partial\Omega}, \partial\Omega) \rightarrow \mathbf{H}^{-1/2}(\mathbf{curl}_{\partial\Omega}, \partial\Omega)$ governing the EFIE (3) is invertible if $\partial\Omega$ is an open surface. Otherwise, for unique solvability of the EFIE we replace \mathcal{D} in (3) with $\mathcal{D} \setminus \mathcal{K}(\Omega)$, where the set $\mathcal{K}(\Omega)$ contains all resonant wavenumbers of the configuration Ω . Henceforth we use \mathcal{D} to denote the parameter set in \mathbb{R}^5 that does not include $\mathcal{K}(\Omega)$, if $\partial\Omega$ is a closed surface.

For $\boldsymbol{\mu} \in \mathcal{D}$, let $\mathbf{w}_i(\boldsymbol{\mu}) = \mathbf{w}|_{\partial\Omega_i}(\boldsymbol{\mu})$, for $i = 1, \dots, J$, where $\mathbf{w}(\boldsymbol{\mu}) \in \mathbf{H}^{-1/2}(\text{div}_{\partial\Omega}, \partial\Omega)$ denotes the unique global solution of (3). Then the multiple particle parametrized electromagnetic scattering problem is: for each $\boldsymbol{\mu} \in \mathcal{D}$, find J surface currents $\mathbf{w}_j(\boldsymbol{\mu}) \in \mathbf{H}^{-1/2}(\text{div}_{\partial\Omega_j}, \partial\Omega_j)$, $j = 1, \dots, J$ by solving the coupled surface scattering system

$$(5) \quad \sum_{j=1}^J a^{ij}[\mathbf{w}_j(\boldsymbol{\mu}), \mathbf{v}_i; \boldsymbol{\mu}] = f^i[\mathbf{v}_i; \boldsymbol{\mu}], \quad \mathbf{v}_i \in \mathbf{H}^{-1/2}(\text{div}_{\partial\Omega_i}, \partial\Omega_i), \quad i = 1, \dots, J,$$

where $a^{ij}[\cdot, \cdot; \boldsymbol{\mu}]$ is the sesquilinear forms are obtained from the EFIE using integration by parts and the RHS depends on the incident wave [1].

3. AN ITERATIVE MODEL REDUCTION BOUNDARY ELEMENT ALGORITHM

For $i = 1, \dots, J$, corresponding to the i -th scatterer in the configuration Ω , let $\mathbb{V}_{h,i}$ be an \mathcal{N}_h -dimensional boundary element subspace of $\mathbf{H}^0(\text{div}_{\partial\Omega_i}, \partial\Omega_i) \subset \mathbf{H}^{-1/2}(\text{div}_{\partial\Omega_i}, \partial\Omega_i)$ based on the discretization mesh parameter h for the surface $\partial\Omega_i$. For $i = 1, \dots, J$, each of these spaces are constructed from the boundary element space $\widehat{\mathbb{V}}_h$ for the reference obstacle \widehat{D} and using the Piola transformations $\widehat{\mathcal{P}}_i : \mathbf{H}^{-1/2}(\text{div}_{\partial\Omega_i}, \partial\Omega_i) \rightarrow \mathbf{H}^{-1/2}(\text{div}_{\partial\widehat{D}}, \partial\widehat{D})$ from the physical surface $\partial\Omega_i$ to the reference surface $\partial\widehat{D}$.

Following details in [1], the boundary element approximation $\mathbf{w}_{h,i}(\boldsymbol{\mu}) = \widehat{\mathcal{P}}_i^{-1} \widehat{\mathbf{w}}_{h,i}(\boldsymbol{\mu})$ to $\mathbf{w}_i(\boldsymbol{\mu})$, for $i = 1, \dots, J$, can be obtained by solving the JN_h -dimensional boundary element system

$$(6) \quad \sum_{j=1}^J \widehat{a}^{ij}[\widehat{\mathbf{w}}_{h,j}(\boldsymbol{\mu}), \widehat{\mathbf{v}}_i; \boldsymbol{\mu}] = \widehat{f}^i[\widehat{\mathbf{v}}_i; \boldsymbol{\mu}], \quad \forall \widehat{\mathbf{v}}_i \in \widehat{\mathbb{V}}_h, \quad i = 1, \dots, J,$$

where for $\widehat{\boldsymbol{\psi}}, \widehat{\boldsymbol{\eta}} \in \mathbf{H}^{-1/2}(\text{div}_{\partial\widehat{D}}, \partial\widehat{D})$,

$$(7) \quad \begin{aligned} & \widehat{a}^{ij}[\widehat{\boldsymbol{\psi}}, \widehat{\boldsymbol{\eta}}; \boldsymbol{\mu}] \\ &= ikZ\gamma_i\gamma_j \int_{\partial\widehat{D}} \int_{\partial\widehat{D}} \widehat{\Phi}_k^{ij}(\widehat{\mathbf{x}}, \widehat{\mathbf{y}}) \left[(\mathbf{B}_j \widehat{\boldsymbol{\psi}}(\widehat{\mathbf{y}})) \cdot (\mathbf{B}_i \overline{\widehat{\boldsymbol{\eta}}(\widehat{\mathbf{x}})}) - \frac{1}{k^2\gamma_i\gamma_j} \text{div}_{\widehat{\mathbf{y}}} \widehat{\boldsymbol{\psi}}(\widehat{\mathbf{y}}) \text{div}_{\widehat{\mathbf{x}}} \overline{\widehat{\boldsymbol{\eta}}(\widehat{\mathbf{x}})} \right], \end{aligned}$$

with $\widehat{\Phi}_k^{ij}(\widehat{\mathbf{x}}, \widehat{\mathbf{y}}) = \Phi_k(T_i(\widehat{\mathbf{x}}), T_j(\widehat{\mathbf{y}}))$ and for $\widehat{\boldsymbol{\eta}} \in \mathbf{H}^{-1/2}(\text{div}_{\partial\widehat{D}}, \partial\widehat{D})$,

$$(8) \quad \widehat{f}^i[\widehat{\boldsymbol{\eta}}; \boldsymbol{\mu}] = -\gamma_i \int_{\partial\widehat{D}} \mathbf{B}_i^T \mathbf{E}^{\text{inc}}(T_i(\widehat{\mathbf{x}}); \boldsymbol{\mu}) \cdot \overline{\widehat{\boldsymbol{\eta}}(\widehat{\mathbf{x}})} ds(\widehat{\mathbf{x}}).$$

Solving the above system is prohibitive if J is large or if we need to solve the model for large number of parameters.

Our main aim is to efficiently simulate the three dimensional electromagnetic scattering model for *any* parameter $\boldsymbol{\mu} \in \mathcal{D}$, to facilitate Monte Carlo type approach to compute, for example, the average RCS with respect variations in the configuration, including large number of particles. We achieve this, as part of an offline procedure, by adaptively constructing, say, N snapshot parameters in \mathcal{D} and then rapidly simulate the model using an iterative online procedure only in an N -dimensional space with $N \ll \mathcal{N}_h$.

To this end, following [1], our first step is to develop decomposition approximations (to any desired accuracy) of the sesquilinear forms for the interactive and individual scatterers and also the input source term in (6), based on the Empirical Interpolation Method (EIM) [2]:

$$(9) \quad \hat{a}^{ij}[\hat{\boldsymbol{\psi}}, \hat{\boldsymbol{\eta}}; \boldsymbol{\mu}] \approx \sum_{m=1}^{M_G} \alpha_m^G(\boldsymbol{\mu}) \hat{a}_m^{ij}[\hat{\boldsymbol{\psi}}, \hat{\boldsymbol{\eta}}], \quad i \neq j,$$

$$(10) \quad \hat{a}^{ii}[\hat{\boldsymbol{\psi}}, \hat{\boldsymbol{\eta}}; \boldsymbol{\mu}] \approx \sum_{m=1}^{M_M} \alpha_m^M(\boldsymbol{\mu}) \hat{a}_m^{ii}[\hat{\boldsymbol{\psi}}, \hat{\boldsymbol{\eta}}], \quad \hat{f}^i[\hat{\boldsymbol{\eta}}; \boldsymbol{\mu}] \approx \sum_{m=1}^{M_F} \alpha_m^F(\boldsymbol{\mu}) \hat{f}_m^i[\hat{\boldsymbol{\eta}}],$$

for some parameter-dependent functionals $\alpha_m^M(\boldsymbol{\mu})$, $\alpha_m^G(\boldsymbol{\mu})$ and $\alpha_m^F(\boldsymbol{\mu})$ and parameter-independent forms $\hat{a}_m^{ij}[\cdot, \cdot]$, $\hat{a}_m^{ii}[\cdot, \cdot]$ and $\hat{f}_m^i[\cdot]$. Efficient construction of the snapshot parameters crucially depends on such decompositions.

We use N -adaptive iterative steps to construct the snapshot parameters and for each $n = 1, \dots, N$ iteration we construct an n dimensional space spanned by solutions of full BEM models for the reference geometry \hat{D} with snapshot parameters $\boldsymbol{\mu}^{(\ell)}$, $\ell = 1, \dots, n$. Following the offline procedure described in detail in [1], we assemble a reduced basis N -dimensional space \hat{V}_N for the reference geometry \hat{D} that is trained to respond accurately for all values in \mathcal{D} . As demonstrated in [1], $N \ll \mathcal{N}_h$, with dimension reduction even over 90% in several cases.

Now we are ready to solve the multiple scattering problem for *any* choice of parameter $\boldsymbol{\mu} \in \mathcal{D}$, with approximation sought in \hat{V}_N . Our iterative online procedure in this article differs from that described in [1]. We demonstrate efficiency of the current approach compared to that in [1]. For an online parameter $\boldsymbol{\mu} \in \mathcal{D}$, as in [1], the first step is to construct the coefficients in (10)-(10), by solving lower triangular systems.

For *any* $\boldsymbol{\mu} \in \mathcal{D}$, we recall the representation (2) that requires computable approximations to $\mathbf{w}_i(\boldsymbol{\mu}) = \mathbf{w}(\boldsymbol{\mu})|_{\Omega_i} \in \mathbf{H}^{-1/2}(\text{div}_{\partial\Omega_i}, \partial\Omega_i)$ for $i = 1, \dots, J$. We compute the approximations as $\mathbf{w}_{N,i}(\boldsymbol{\mu}) = \hat{\mathcal{P}}_i^{-1} \hat{\mathbf{w}}_{N,i}(\boldsymbol{\mu})$ for each $i = 1, \dots, J$, with $\hat{\mathbf{w}}_{N,i}(\boldsymbol{\mu}) \in \hat{V}_N$. Instead of solving a JN -dimensional system, we compute

$\widehat{\mathbf{w}}_{N,i}(\boldsymbol{\mu}) \in \widehat{\mathbb{V}}_N$ through uncoupled N -dimensional systems. To this end, we consider the series representation

$$(11) \quad \widehat{\mathbf{w}}_{N,i}(\boldsymbol{\mu}) = \sum_{\ell=1}^{\infty} \widehat{\mathbf{w}}_{N,i}^{(\ell)}(\boldsymbol{\mu}), \quad \mathbf{i} = 1, \dots, \mathbf{J},$$

where the sequence of $\widehat{\mathbf{w}}_{N,i}^{(\ell)}(\boldsymbol{\mu})$ satisfies uncoupled N -dimensional systems

$$(12) \quad \widehat{a}^{ii}[\widehat{\mathbf{w}}_{N,i}^{(1)}, \widehat{\mathbf{v}}_N; \boldsymbol{\mu}] = \widehat{f}^i[\widehat{\mathbf{v}}_N; \boldsymbol{\mu}], \quad \forall \widehat{\mathbf{v}}_N \in \widehat{\mathbb{V}}_N, \quad \mathbf{i} = 1, \dots, \mathbf{J},$$

and for $\ell = 1, 2, 3, \dots$ and $\forall \widehat{\mathbf{v}}_N \in \widehat{\mathbb{V}}_N$,

$$(13) \quad \widehat{a}^{ii}[\widehat{\mathbf{w}}_{N,i}^{(\ell+1)}, \widehat{\mathbf{v}}_N; \boldsymbol{\mu}] = - \sum_{j=1}^{i-1} \widehat{a}^{ij}[\widehat{\mathbf{w}}_{N,i}^{(\ell+1)}, \widehat{\mathbf{v}}_N; \boldsymbol{\mu}] - \sum_{j=i+1}^{\mathbf{J}} \widehat{a}^{ij}[\widehat{\mathbf{w}}_{N,i}^{(\ell)}, \widehat{\mathbf{v}}_N; \boldsymbol{\mu}].$$

The systems in (13) incorporate reflected waves from all particles in the configuration and this update procedure is different from that in [1]. We truncate the series with a finite number L of reflections since in practice, for well separated obstacles, the intensity of such reflections will reduce after some iterated reflections. Each reflection $\widehat{\mathbf{w}}_{N,i}^{(\ell)}$ can be expressed is a linear combination of the reduced basis $\{\boldsymbol{\xi}_n\}_{n=1}^N$ of $\widehat{\mathbb{V}}_N$ and hence

$$\widehat{\mathbf{w}}_{N,i}^{(\ell)}(\mathbf{x}; \boldsymbol{\mu}) = \sum_{n=1}^N w_{n,i}^{(\ell)}(\boldsymbol{\mu}) \boldsymbol{\xi}_n(\mathbf{x}).$$

We choose the series truncation parameter L such that for a prescribed tolerance level `tol`,

$$\text{Error} < \text{tol}, \quad \text{Error} = \max_{1 \leq i \leq \mathbf{J}} \max_{1 \leq n \leq N} |w_{n,i}^{(L)}(\boldsymbol{\mu}) - w_{n,i}^{(L-1)}(\boldsymbol{\mu})|$$

and define the iterative reduced basis approximation (on the reference surface) as

$$(14) \quad \widehat{\mathbf{w}}_{N,L}(\mathbf{x}; \boldsymbol{\mu}) = \sum_{j=1}^{\mathbf{J}} \sum_{l=1}^L \widehat{\mathbf{w}}_{N,i}^{(l)}(\mathbf{x}; \boldsymbol{\mu}), \quad \mathbf{x} \in \partial\Omega = \bigcup_{j=1}^{\mathbf{J}} \partial\Omega_j.$$

For our numerical experiments, we chose `tol` = 10^{-8} and observed excellent results, similar to that reported for various experiments. Compared to the online method (Method-1) in [1], the main advantage of the method (Method-2) in this article is that there are substantial reductions in the number of iterations L to achieve the `tol`. This is demonstrated in Figure 1.

Acknowledgment. The research of the first and second authors was supported, in part, respectively by the NSF grant DMS-1216889 and the AFOSR grant OSD/AFOSR FA9550-09-1-0613.

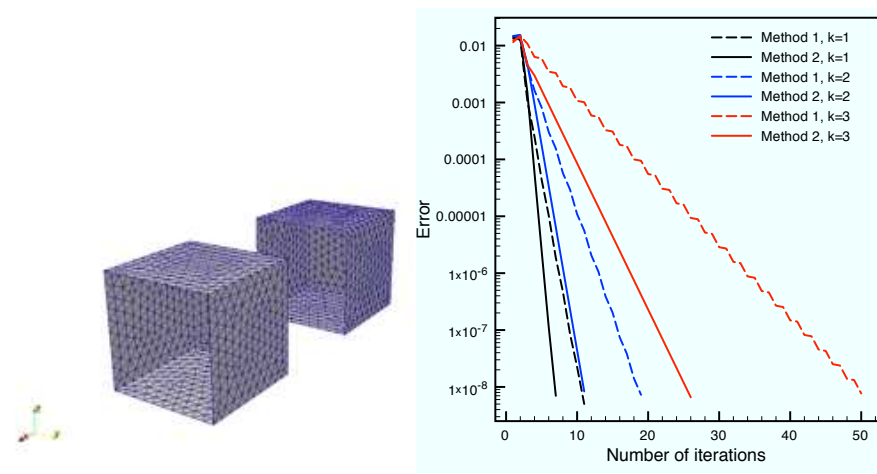


FIGURE 1. Scattering by two open metallic cavities of unit diameter: Convergence of online iterative schemes using Method-1 [1] and Method-2, for wavenumbers $k = 1, 2, 3$.

M. Ganesh

Department of Applied Mathematics and Statistics, Colorado School of Mines, Golden, CO 80401, USA

mganesh@mines.edu

J.S. Hesthaven

Division of Applied Mathematics, Brown University, Box F, Providence, RI 02912, USA

Jan.Hesthaven@brown.edu

B. Stamm

UPMC University of Paris 06 and CNRS, UMR 7598, Laboratoire Jacques-Louis Lions, F-75005, Paris, France

stamm@ann.jussieu.fr

REFERENCES

- [1] M. GANESH, J. HESTHAVEN, AND B. STAMM, *A reduced basis method for multiple electromagnetic scattering in three dimensions*, J. Comput. Phys., 231 (2012), pp 7756–7779.
- [2] Y. MADAY, N. C. NGUYEN, A. T. PATERA AND G. S. H. PAU, *A general multipurpose interpolation procedure: The magic points*, Commun. Pure Appl. Anal., 8 (2009), pp 383–404.
- [3] J.-C. NÉDÉLEC, *Acoustic and Electromagnetic Equations: Integral Representations for Harmonic Problems*, vol. 44 of Applied Mathematical Sciences, Springer-Verlag, Berlin, 2001.

FE/BE coupling for strongly nonlinear transmission problems with friction

HEIKO GIMPERLEIN

(joint work with Matthias Maischak, Ernst P. Stephan)

We analyze an adaptive finite element/boundary element formulation for nonlinear transmission and contact problems. In the model problem, the p -Laplacian or a double-well potential in a bounded domain Ω is coupled to the homogeneous Laplace equation in $\mathbb{R}^n \setminus \bar{\Omega}$. The exterior problem is reduced to an integral equation on $\partial\Omega$, and an equivalent coupled boundary/domain variational inequality is solved. We discuss the well-posedness in suitable L^2 - L^p Sobolev spaces, the appearance of microstructure in the nonconvex case and a priori/a posteriori error estimates for Galerkin approximations. Extensions to strongly anisotropic coupling problems will be considered.

Keywords: FE/BE coupling, transmission problem, p -Laplacian, microstructure

Mathematics Subject Classifications (2000): 65N30, 65N38, 74M10

Heiko Gimperlein

University of Copenhagen
gimperlein@math.ku.dk

Matthias Maischak

Brunel University
Matthias.Maischak@brunel.ac.uk

Ernst P. Stephan

Leibniz University Hannover
stephan@ifam.uni-hannover.de

REFERENCES

- [1] H. Gimperlein, M. Maischak, E. Schrohe, E. P. Stephan, *Adaptive FE-BE coupling for strongly nonlinear transmission problems with Coulomb friction*, Numer. Math. 117 (2011), 307–332.
- [2] H. Gimperlein, M. Maischak, E. P. Stephan, *FE-BE coupling for a transmission problems with microstructure*, preprint (2012).

**Approximation of Higher Order for Parabolic Unilateral Problems
using hp - BEM**

JOACHIM GWINNER

In this talk we treat the initial unilateral boundary value problem

$$\begin{cases} \partial_t u - \Delta u = 0; u(0) = u_0 \\ u \geq g, \frac{\partial u}{\partial n} \geq h, (u - g)(\frac{\partial u}{\partial n} - h) = 0 \text{ on } \Gamma_S \\ u = g \text{ on } \Gamma_D, \frac{\partial u}{\partial n} = h \text{ on } \Gamma_N \end{cases}$$

on some Lipschitz domain Ω with boundary $\partial\Omega = \overline{\Gamma_S} \cup \overline{\Gamma_D} \cup \overline{\Gamma_N}$ and on some time interval $[0, T]$.

This problem can be considered as a simple model problem for more general problems like quasi-stationary unilateral contact in linear elasticity and as building block that can be used in FEM-BEM coupling for nonlinear applications in electromagnetism and heat flow.

For time discretization we use a backward Euler scheme. This is combined with the BEM in its hp -version using Gauss-Lobatto quadrature after transforming the problem to the boundary using potential theory. The aim of this contribution are norm convergence results for the fully discrete nonconforming approximations.

In the analysis we use some arguments on nonconforming approximation of inequality constraints by Gauss-Lobatto quadrature within hp - BEM from [2] and abstract approximation results for evolution inequalities from [1].

Keywords: Singular integral equations/inequalities, boundary variational inequalities, nonconforming approximation

Mathematics Subject Classifications (2000): 35K05, 49J40, 65M06, 65N38

Joachim Gwinner

Institut für Mathematik, Fakultät für Luft- und Raumfahrttechnik, Universität der Bundeswehr München, 85577 Neubiberg/München, Germany

Joachim.Gwinner@unibw – muenchen.de

REFERENCES

- [1] C. Carstensen and J. Gwinner. A theory of discretization for nonlinear evolution inequalities applied to parabolic Signorini problems. *Annali di Matematica pura ed applicata*, 177(ser. 4):363-394, 1999.
- [2] M. Maischak and E.P. Stephan. Adaptive hp -versions of BEM for Signorini problems. *Appl. Numer. Math.*, 54:425-449, 2005.

Comparison of fast boundary element methods on parametric surfaces

HELMUT HARBRECHT

(joint work with Michael Peters)

We compare fast black-box boundary element methods on parametric surfaces in \mathbb{R}^3 . These are the adaptive cross approximation [1], the multipole method based on interpolation [3], and the wavelet Galerkin method [2]. The surface representation by a piecewise smooth parametrization is in contrast to the common approximation of surfaces by panels. Nonetheless, parametric surface representations are easily accessible from Computer Aided Design (CAD) and are recently topic of the studies in Isogeometric Analysis. Especially, we can apply two-dimensional interpolation in the multipole method. A main feature of this approach is that the cluster bases and the respective moment matrices are independent of the geometry. This results in a superior compression of the far field compared to other cluster methods.

Keywords: Integral equations, fast boundary element methods, parametric surface.

Mathematics Subject Classifications (2000): 65F50, 65N38, 65R20.

Helmut Harbrecht, Michael Peters

University of Basel

helmut.harbrecht@unibas.ch, michael.peters@unibas.ch

REFERENCES

- [1] M. Bebendorf. Approximation of boundary element matrices. *Numer. Math.*, 86:565–589, 2000.
- [2] W. Dahmen, H. Harbrecht, and R. Schneider. Compression techniques for boundary integral equations. Optimal complexity estimates. *SIAM J. Numer. Anal.*, 43:2251–2271, 2006.
- [3] W. Hackbusch and S. Börm. \mathcal{H}^2 -matrix approximation of integral operators by interpolation. *Appl. Numer. Math.*, 43(1-2):129–143, 2002.

Boundary Integral Formulation for the Electrical Response of a Nerve to an Extracellular Stimulation

FERNANDO J. HENRÍQUEZ

(joint work with Carlos F. Jerez–Hanckes)

We present a two-dimensional boundary integral formulation of a nerve propagation. A nerve impulse is a potential difference across the cellular membrane propagated along the nerve fiber. The traveling transmembrane potential is produced by the transfer of ionic species between the intra and extra cellular media [1, 3]. This current flux across the membrane –composed of conduction, diffusion and capacitive terms– is regulated by passive and active mechanisms that are highly complicated to describe mathematically from a microscopic point of view [2]. During the last century, several models have been developed, based on experimental considerations in the field of neuroscience; the first and most popular one proposed by Hodgkin and Huxley in 1952 [4, 8]. By means of ordinary differential equations, with parameters depending on the transmembrane voltage –the Dirichlet jump across the membrane–, their model is able to describe the dynamics of the nerve membrane in a suitable way[5]. We propose an integral formulation of this problem based on the Hodgkin–Huxley model and a quasi-static approximation for which Calderon’s Projectors and the Boundary Element Method apply [7]. Existence and uniqueness of the problem, and convergence estimations of the solution are shown [8].

Support by PUC VRI Interdisciplina 2011, FONDECYT project 11121166 and CONICYT project Anillo ACT1118 (ANANUM) is gratefully acknowledged.

Keywords: Integral equations, peripheral nerve stimulation, non-linear ordinary differential equation.

Mathematics Subject Classifications (2010): 35Q92, 46N60, 62P10, 92C50.

Fernando J. Henríquez, Carlos F. Jerez–Hanckes

Departamento de Ingeniería Eléctrica, Escuela de Ingeniería, Pontificia Universidad Católica de Chile. Santiago, Chile.

fjhenriq@uc.cl, cjerez@ing.puc.cl

REFERENCES

- [1] J. KEENER AND J. SNEYD, *Mathematical Physiology*, Springer–Verlag, New York, 1998.
- [2] A. SCOTT, *Neuroscience: A Mathematical Premier*, Springer–Verlag, New York, 2002.
- [3] R. PLONSEY AND R. BARR, *Bioelectricity: A Quantitative Approach*, Springer–Verlag, New York, 2007, Third Edition.
- [4] A.L. HODGKIN AND A.F. HUXLEY. A quantitative description of membrane current and its application to conduction and excitation in nerve. *The Journal of Physiology*. (London) 117 (1952) 500-544.

-
- [5] W. YING, C.S. HENRIQUEZ. Hybrid Finite Element Method for Describing the Electrical Response of Biological Cells to Applied Fields. *IEEE Transactions on Biomedical Engineering*, Vol 54, No. 4, April 2007.
 - [6] O. STEINBACH, *Numerical approximation methods for elliptic boundary value problems*, Springer-Verlag, New York, 2008.
 - [7] S. SAUTER AND C. SCHWAB, *Boundary Element Methods*, Springer-Verlag, Berlin Heidelberg, 2011.
 - [8] J. Bell and P. Cook, On the Solutions of a Nerve Conduction Equation. *SIAM Journal on Applied Mathematics*, Vol. 35, No. 4 (1978), pp. 678-688.

Multiple Traces Boundary Integral Formulation for Helmholtz Transmission Problems

RALF HIPTMAIR

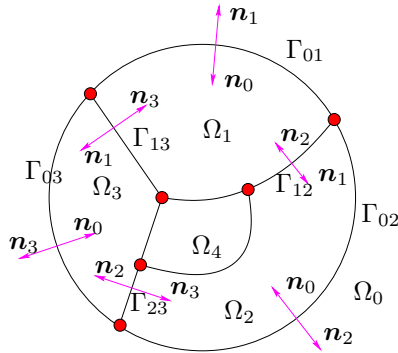
(joint work with Carlos Jerez-Hanckes, Xavier Claeys)

Summary. We consider second-order linear transmission problems with piecewise constant coefficients corresponding to different homogeneous materials. They can be converted into a so-called 1st-kind single trace boundary integral equation formulations (STF) featuring Cauchy data on the material interfaces. Their Ritz-Galerkin discretization by means of low-order piecewise polynomial boundary elements on fine interface triangulations leads to ill-conditioned linear systems of equations, which defy the operator preconditioning approach.

A remedy is offered by multi-trace formulations (MTF) that arise from a domain decomposition idea and owe their name to the use of at least two sets of Cauchy traces as unknowns on interfaces. The new approaches come in several flavors: (i) Global MTF arise from a gap idea applied to STF. (ii) Local MTF obtained through introducing transmission conditions into weak boundary integral equations arising from Calderón identities.

In contrast to STF, after Galerkin discretization both MTFs lend themselves to operator preconditioning based on discrete boundary integral operators on dual meshes.

1. TRANSMISSION PROBLEM



Let $\Omega_i \subset \mathbb{R}^3$, $i = 0, \dots, N$, be disjoint open connected Lipschitz “material sub-domains” that form a partition in the sense that $\mathbb{R}^3 = \overline{\Omega}_1 \cup \dots \cup \overline{\Omega}_N$. Among them only Ω_0 is unbounded. Two adjacent sub-domains Ω_i and Ω_j are separated by their common interface Γ_{ij} , whose union forms the skeleton Σ . For $N > 1$ the skeleton Σ will usually not be orientable, nor be a manifold.

Given diffusion coefficients $\mu_i > 0$, $i = 0, \dots, N$, we focus on the model transmission problem that seeks $U_i \in$

$H_{\text{loc}}^1(\Omega_i)$, $i = 0, \dots, N$, solving

$$(1) \quad \begin{aligned} & -\operatorname{div}(\mu_i \operatorname{grad} U_i) = 0 \quad \text{in } \Omega_i, \\ & U_i|_{\Gamma_{ij}} - U_j|_{\Gamma_{ij}} = g_{ij}, \quad \mu_i \frac{\partial U_i}{\partial \mathbf{n}_i}|_{\Gamma_{ij}} + \mu_j \frac{\partial U_j}{\partial \mathbf{n}_j}|_{\Gamma_{ij}} = h_{ij} \quad \text{on } \Gamma_{ij}, \end{aligned}$$

plus suitable decay conditions at ∞ . The jump data g_{ij} , h_{ij} have to comply with certain compatibility conditions that we gloss over in the sequel. The weak

formulation of (1) is posed on a weighted Sobolev space [9, Sect. 2.9.2.4] contained in $H_{\text{loc}}^1(\mathbb{R}^3)$.

Here, we discuss low-order boundary element methods for (1) based on multi-trace boundary integral equation formulations (MTF). In combination with matrix compression methods and iterative solvers they form the foundation of a scalable solution method for (1), that is, a method, whose effort increases almost linearly with the number of degrees of freedom of the discretized problem.

MTFs were first introduced for acoustic and electromagnetic scattering at composite objects: [2] proposed the global MTF for acoustic scattering, [1] its extension to electromagnetics, and [5] introduced the local MTF for acoustics. A comprehensive survey is given in [3]. The local MTF is closely related with domain decomposition algorithms pioneered by J.-F. Lee and collaborators in computational electromagnetics [7]. We also point out that domain decomposition ideas also pave the way for another class of scalable methods for (1) called ‘‘Boundary element tearing and interconnecting’’ (BETI) [6].

2. SKELETON TRACE SPACES [3, Sect. 3.1]

Traces on the skeleton Σ will figure as unknowns in the boundary integral equations. Thus, we introduce the *multi-trace space*

$$(2) \quad \mathcal{MT}(\Sigma) := \underbrace{(H^{\frac{1}{2}}(\partial\Omega_0) \times \cdots \times H^{\frac{1}{2}}(\partial\Omega_N))}_{:=\mathcal{MT}_D(\Sigma)} \times \underbrace{(H^{-\frac{1}{2}}(\partial\Omega_0) \times \cdots \times H^{-\frac{1}{2}}(\partial\Omega_N))}_{:=\mathcal{MT}_N(\Sigma)} .$$

It owes its name to the fact that a function $\vec{u} \in \mathcal{MT}(\Sigma)$ comprises four different functions on each interface, two belonging to the sub-domain on either side. No connection between both sides is implied in the definition of $\mathcal{MT}(\Sigma)$. Of course, the (homogeneous) transmission conditions in (1) enforce a connection, which is captured in the *single-trace space*

$$(3) \quad \mathcal{ST}(\Sigma) := \mathcal{ST}_D(\Sigma) \times \mathcal{ST}_N(\Sigma) \subset \mathcal{MT}(\Sigma) ,$$

$$(4) \quad \begin{aligned} \mathcal{ST}_D(\Sigma) &:= \{(u_0, \dots, u_N) \in \mathcal{MT}_D(\Sigma) : \exists \mathbf{u} \in H_{\text{loc}}^1(\mathbb{R}^d), u_i = \mathbb{T}_{D,i} \mathbf{u}\} , \\ \mathcal{ST}_N(\Sigma) &:= \{(\nu_0, \dots, \nu_N) \in \mathcal{MT}_N(\Sigma) : \exists \phi \in \mathbf{H}_{\text{loc}}(\text{div}, \mathbb{R}^d), \nu_i = \mathbb{T}_{N,i} \phi\} , \end{aligned}$$

where $\mathbb{T}_{D,i}$, $\mathbb{T}_{N,i}$ are the Dirichlet and Neumann trace operators for Ω_i . Note that $\mathbb{T}_{N,i}$'s definition involves the diffusion coefficient μ_i . To isolate the contribution of a single sub-domain we rely on trivial localization operators

$$\mathbb{L}_i : \mathcal{MT}(\Sigma) \rightarrow H^{\frac{1}{2}}(\partial\Omega_i) \times H^{-\frac{1}{2}}(\partial\Omega_i), \quad \mathbb{L}_i \vec{u} := \begin{pmatrix} u_i \\ \nu_i \end{pmatrix}, \quad \vec{u} = (u_0, \dots, u_N, \nu_0, \dots, \nu_N), \quad u_i \in H^{\frac{1}{2}}(\partial\Omega_i), \quad \nu_i \in H^{-\frac{1}{2}}(\partial\Omega_i) .$$

3. SINGLE TRACE BOUNDARY INTEGRAL FORMULATIONS (STF)

Using the notations for boundary integral operators from [9, Sect. 3.1], we write

$$(5) \quad \mathbb{P}_i := \mathbb{A}_i + \frac{1}{2}\text{Id} = \begin{pmatrix} \mathbb{K}_i & \mathbb{V}_i \\ \mathbb{W}_i & \mathbb{K}'_i \end{pmatrix} : H^{\frac{1}{2}}(\partial\Omega_i) \times H^{-\frac{1}{2}}(\partial\Omega_i) \rightarrow H^{\frac{1}{2}}(\partial\Omega_i) \times H^{-\frac{1}{2}}(\partial\Omega_i),$$

for the *Calderón projector* associated with Ω_i [9, Sect. 3.6]. Local traces of solutions of (1) belong to the kernel of \mathbb{P}_i . Hence, if U solves (1), then $\vec{u} := (\mathbb{T}_{D,0} U, \dots, \mathbb{T}_{D,N} U, \mathbb{T}_{N,0} U, \dots, \mathbb{T}_{N,i} U)$ satisfies the linear boundary integral equation $\sum_{i=0}^N \mathbb{P}_i \mathbb{L}_i \vec{u} = \dots$, where the jump data spawn the right hand side. Denoting by $[\![\cdot, \cdot]\!]_i$ the bilinear pairing with $L^2(\partial\Omega_i)$ pivot space inducing the self-duality of $H^{\frac{1}{2}}(\partial\Omega_i) \times H^{-\frac{1}{2}}(\partial\Omega_i)$, we can recast (5) in weak form [3, Sect. 3.1]: seek $\vec{u} \in \mathcal{ST}(\Sigma)$ such that

$$(6) \quad \sum_{j=0}^N [\![\mathbb{A}_j \mathbb{L}_j \vec{u}, \mathbb{L}_j \vec{v}]\!]_j = \dots \quad \forall \vec{v} \in \mathcal{ST}(\Sigma),$$

which is the classical first-kind single-trace boundary integral formulation (STF), see [6], in electromagnetics known as PMCHWT [8]. Existence and uniqueness of solutions can be concluded from the fact that *the bilinear form of (6) is $\mathcal{ST}(\Sigma)$ -elliptic*.

However, low order Galerkin boundary element discretization of the first-kind boundary integral equation (6) will lead to ill-conditioned linear systems on fine meshes. Thus, efficient iterative solution methods require preconditioning.

4. OPERATOR PRECONDITIONING [3, Sect. 4]

The abstract theory of [4, Sect. 2] considers an isomorphism $\mathbf{A} : V \rightarrow V'$ on a Hilbert space V , which is self-dual with respect to the bilinear form $d : V \times V \rightarrow \mathbb{R}$. Using a trial/test space $V_h \subset V$ that guarantees “uniform” stability of the Galerkin discretization of both \mathbf{A} and $d(\cdot, \cdot)$, we find

$$(7) \quad \text{cond}(\mathbf{D}^{-\top} \mathbf{A} \mathbf{D}^{-1} \mathbf{A}) \quad \text{uniformly bounded},$$

where \mathbf{A} and \mathbf{D} are the Galerkin matrices associated with \mathbf{A} and $d(\cdot, \cdot)$, respectively. Hence, $\mathbf{D}^{-\top} \mathbf{A} \mathbf{D}^{-1}$ qualifies as a preconditioner for \mathbf{A} . Note that its evaluation involves solving linear systems for \mathbf{D} and \mathbf{D}^\top .

However, applying such preconditioner to \mathbf{A} from (6) is generally thwarted by the lack of a suitable stable self-duality pairing $d(\cdot, \cdot)$ for $\mathcal{ST}(\Sigma)$. There is one exception, and this is the situation of well separated subdomains $\Sigma = \partial\Omega_0$, because in this case a self-duality of $\mathcal{ST}(\Sigma)$ is induced by

$$(8) \quad d(\vec{u}, \vec{v}) := \sum_{j=1}^N [\![\mathbb{L}_j \vec{u}, \mathbb{L}_j \vec{v}]\!]_j, \quad \vec{u}, \vec{v} \in \mathcal{ST}(\Sigma).$$

A stable boundary element discretization of this pairing, which also leads to *sparse* matrices \mathbf{D} , can be accomplished by means of boundary element spaces on dual meshes.

5. GLOBAL MULTI-TRACE FORMULATION [2, 1]

The general geometric arrangement introduced in Section 1 can be regarded as the limit case of sub-domains separated by small gaps of width $\delta > 0$ when letting δ tend to zero, see Figure 1. It turns out that all boundary integral operators in (6) remain well defined for $\delta \rightarrow 0$; we obtain the global multi-trace formulation (MTF).

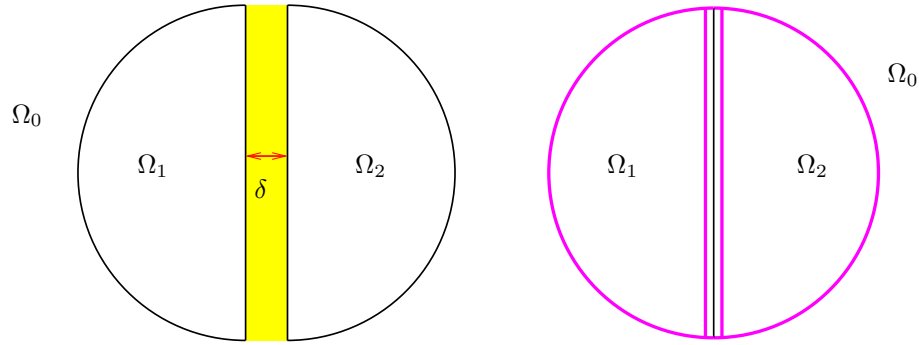


FIGURE 1. Illustration of the “gap idea” for $N = 2$. Left: sub-domains separated by gap of width $\delta > 0$. Right: closed gap

The right function space for the global MTF will be $\mathcal{ST}(\Sigma)$ “in the gap limit”, which comprises four traces on each interior interface (“multi-trace”), and two on interfaces belonging to $\partial\Omega_0$:

$$(9) \quad \widehat{\mathcal{MT}}(\Sigma) := (H^{\frac{1}{2}}(\partial\Omega_1) \times \cdots \times H^{\frac{1}{2}}(\partial\Omega_N)) \times (H^{-\frac{1}{2}}(\partial\Omega_1) \times \cdots \times H^{-\frac{1}{2}}(\partial\Omega_N)).$$

The weak form of the global multi-trace formulation inherits all good properties of the STF, in particular $\widehat{\mathcal{MT}}(\Sigma)$ -ellipticity. Moreover, $\widehat{\mathcal{MT}}(\Sigma)$ is clearly self-dual with an L^2 -type duality pairing. Thus, *operator preconditioning is possible for the global MTF*.

6. LOCAL MULTI-TRACE FORMULATION [5]

Consider *local transmission operators* $\mathbb{X}_{i \rightarrow j}$ which carry traces across interfaces Γ_{ij} ; they take a pair of functions on $\partial\Omega_i$, restrict both functions to Γ_{ij} , flip the sign of the second (in order to account for the different orientations of the normal vectors), and, finally, extend both functions by zero to functions on $\partial\Omega_j$:

$$\mathbb{X}_{i \rightarrow j} : \begin{cases} L^2(\partial\Omega_i) \times L^2(\partial\Omega_i) & \rightarrow L^2(\partial\Omega_j) \times L^2(\partial\Omega_j) \\ \mathbf{u} := \begin{pmatrix} u \\ \varphi \end{pmatrix} & \mapsto (\mathbb{X}_{i \rightarrow j} \mathbf{u})(\mathbf{x}) := \begin{cases} \begin{pmatrix} u(\mathbf{x}) \\ -\varphi(\mathbf{x}) \end{pmatrix} & \text{for } \mathbf{x} \in \Gamma_{ij}, \\ 0 & \text{elsewhere on } \partial\Omega_j. \end{cases} \end{cases}$$

Again, write $\vec{\mathbf{u}} := (\mathbb{T}_{D,0} U, \dots, \mathbb{T}_{D,N} U, \mathbb{T}_{N,0} U, \dots, \mathbb{T}_{N,i} U) \in \mathcal{MT}(\Sigma)$, U the solution of (1), and note that $\mathbb{P}_i \mathbb{L}_i \vec{\mathbf{u}} = (\frac{1}{2} \text{Id} - \mathbb{A}_i) \mathbb{L}_i \vec{\mathbf{u}} = \dots$, with a right hand side

depending only on the data. Due to the transmission conditions from (1) we can locally replace the traces by those “from the other side of the interface” and arrive at

$$(10) \quad \mathbb{A}_i \mathbb{L}_i \vec{\mathbf{u}} - \frac{1}{2} \sum_{\substack{j=0 \\ j \neq i}}^N \mathbb{X}_{j \rightarrow i} \mathbb{L}_j \vec{\mathbf{u}} = \dots, \quad i = 0, \dots, N.$$

For fixed i this can be regarded as an equation in $H^{\frac{1}{2}}(\partial\Omega_i) \times H^{-\frac{1}{2}}(\partial\Omega_i)$ and duality pairing readily yields a formal variational formulation: see $\vec{\mathbf{u}} \in \mathcal{MT}(\Sigma)$ (?) such that

$$(11) \quad \llbracket \mathbb{A}_i \mathbb{L}_i \vec{\mathbf{u}}, \mathbb{L}_i \vec{\mathbf{v}} \rrbracket_{\partial\Omega_i} - \frac{1}{2} \sum_{\substack{j=0 \\ j \neq i}}^N \llbracket \mathbb{X}_{j \rightarrow i} \mathbb{L}_j \vec{\mathbf{u}}, \mathbb{L}_i \vec{\mathbf{v}} \rrbracket_{\partial\Omega_i} = \dots \quad \forall \vec{\mathbf{v}} \in \mathcal{MT}(\Sigma). \quad (?)$$

The interesting identity

$$\llbracket \mathbb{X}_{i \rightarrow j} \mathbb{L}_i \vec{\mathbf{u}}, \mathbb{L}_j \vec{\mathbf{u}} \rrbracket_j = -\llbracket \mathbb{X}_{j \rightarrow i} \mathbb{L}_j \vec{\mathbf{u}}, \mathbb{L}_i \vec{\mathbf{u}} \rrbracket_i, \quad \vec{\mathbf{u}} \in \mathcal{MT}(\Sigma),$$

shows “formal” $\mathcal{MT}(\Sigma)$ -ellipticity of the bilinear form (11). Then why the question marks and quotation marks above? Because $\mathbb{X}_{j \rightarrow i}$ fails to be defined on $H^{\frac{1}{2}}(\partial\Omega_j) \times H^{-\frac{1}{2}}(\partial\Omega_j)$, since restriction and extension by zero are unbounded operators on trace spaces! To remedy this, the variational formulation has to be considered on

$$\widetilde{\mathcal{MT}}(\Sigma) := (H^{\frac{1}{2}}(\partial\Omega_0) \times \dots \times H^{\frac{1}{2}}(\partial\Omega_N)) \times (\widetilde{H}^{-\frac{1}{2}}(\partial\Omega_0) \times \dots \times \widetilde{H}^{-\frac{1}{2}}(\partial\Omega_N)),$$

where $\widetilde{H}^{-\frac{1}{2}}(\partial\Omega_i)$ is a subspace of $H^{-\frac{1}{2}}(\partial\Omega_i)$ of functions that allow zero extension from the interfaces Γ_{ij} . Fortunately, also this space offers self-duality through an L^2 -type pairing, which paves the way for operator preconditioning as discussed in Section 4.

Xavier Claeys

X. Claeys is with Laboratoire J.-L. Lions, Université Pierre et Marie Curie, Paris, France
claeys@ann.jussieu.fr

Ralf Hiptmair

R. Hiptmair is with SAM, ETH Zürich, Switzerland
hiptmair@sam.math.ethz.ch

Carlos Jerez-Hanckes

C. Jerez-Hanckes is with Escuela de Ingeniería, Pontificia Universidad Católica de Chile, Santiago
cjerez@ing.puc.cl

REFERENCES

- [1] X. CLAEYS AND R. HIPTMAIR, *Electromagnetic scattering at composite objects: A novel multi-trace boundary integral formulation*, Report 2011-58, SAM, ETH Zürich, Zürich, Switzerland, 2011. To appear in M2AN.

-
- [2] ———, *Boundary integral formulation of the first kind for acoustic scattering by composite structures*, Comm. Pure Applied Math., (2012). To appear.
 - [3] X. CLAEYS, R. HIPTMAIR, AND C. JEREZ-HANCKES, *Multi-trace boundary integral equations*, Report 2012-20, SAM, ETH Zürich, Zürich, Switzerland, 2012.
 - [4] R. HIPTMAIR, *Operator preconditioning*, Computers and Mathematics with Applications, 52 (2006), pp. 699–706.
 - [5] R. HIPTMAIR AND C. JEREZ-HANCKES, *Multiple traces boundary integral formulation for Helmholtz transmission problems*, Adv. Appl. Math., 37 (2012), pp. 39–91.
 - [6] U. LANGER AND O. STEINBACH, *Boundary element tearing and interconnecting methods*, Computing, 71 (2003), pp. 205–228.
 - [7] Z. PENG, K.-H. LIM, AND J.-F. LEE, *Nonconformal domain decomposition methods for solving large multiscale electromagnetic scattering problems*, Proceedings of the IEEE, electronic (2012), pp. 1–22.
 - [8] A. POGGIO AND E. MILLER, *Integral equation solution of three-dimensional scattering problems*, in Computer Techniques for Electromagnetics, R. Mittra, ed., Pergamon, New York, 1973, ch. 4, pp. 159–263.
 - [9] S. SAUTER AND C. SCHWAB, *Boundary Element Methods*, vol. 39 of Springer Series in Computational Mathematics, Springer, Heidelberg, 2010.
 - [10] T. VON PETERSDORFF, *Boundary integral equations for mixed Dirichlet, Neumann and transmission problems*, Math. Meth. Appl. Sci., 11 (1989), pp. 185–213.

Enabling High-Dimensional Electromagnetic Design on Computing Clouds

VIKRAM JANDHYALA
(joint work with Arun Sathanur)

Dual advances in computational electromagnetics solvers and scalable computing hardware have enabled significant speed and scale benefits. An example of this is Nimbics nWave and nCloud product line. The availability of scalable computing nodes on platforms such as Amazon Web Services EC2 also creates the opportunity to make significant progress on the frontier of electromagnetic design. This talk discusses challenges and opportunities in cloud-based design of electromagnetic systems including large degrees of freedom, connection to parametric simulation, variability and Monte-Carlo simulation, and elements of machine learning and sparse sampling of large design spaces.

Vikram Jandhyala

Chief Technologist, Nimbic Inc, and Department Chair, Department of Electrical Engineering, University of Washington, Seattle
vikram@nimbic.com

Arun Sathanur

Co-Director, Applied Computational Engineering Lab, Department of Electrical Engineering, University of Washington

Sparse and \mathcal{H} -Matrix Representation Techniques applied to indirect Time-Domain BEM in Elastodynamics

BERNHARD KAGER

(joint work with Martin Schanz)

The computation of wave propagation phenomena may be done by using the boundary element method, since this approach allows for computations of infinite and semi-infinite domains. In general, storage and computational complexity are of order $O(N^2M)$, where M is the number of time steps and N corresponds to the number of degrees of freedom. We present a data efficient algorithm for the computation of the indirect approach with analytical convolution. Storage and computational efficiency is based on special time dependent single layer operator properties. Most of the arising matrices are sparsely populated in an unstructured way. Introducing a geometrical clustering within each time step allows to identify larger blocks with non-zero entries and those who must be zero due to causality reasons. The latter reduce storage and computing time. Further enhancement is obtained by a low rank approximation of the non-zero blocks in the hierarchical structure. A numerical test shows the reduction of storage obtained by the proposed algorithm.

1. BOUNDARY INTEGRAL EQUATIONS

When dealing with time dependent, linear elastic problems the underlying partial differential equation is the Lamé-Navier equation. For $\Omega \in \mathbb{R}^3$, $t \in (0, T)$ and $\mathbf{u}(\mathbf{x}, t)$ there holds

$$(c_1^2 - c_2^2) \nabla (\nabla \cdot \mathbf{u}) + c_2^2 \nabla^2 \mathbf{u} + \frac{\mathbf{f}}{\rho} = \frac{\partial^2 \mathbf{u}}{\partial t^2}$$

with the density ρ , the body forces \mathbf{f} , the compression and shear wave velocities c_1 and c_2 . In the following, the body forces, as well as initial conditions are assumed to vanish. For the definition of the indirect approach with the single layer potential we introduce a density function $\mathbf{v}(\mathbf{x}, t)$ such that

$$\mathbf{u}(\mathbf{x}, t) = \int_{\Gamma} \mathbf{U}(\mathbf{x}, \mathbf{y}, t) * \mathbf{v}(\mathbf{y}, t) d\Gamma \text{ with } \mathbf{x} \in \Gamma .$$

The star denotes convolution in time and $\mathbf{U}(\mathbf{x}, \mathbf{y}, t)$ is the displacement fundamental solution for the elastodynamic problem (see, e.g., [1]).

2. BOUNDARY ELEMENT FORMULATION

2.1. Temporal Discretization. As defined in section 1, the integral equation contains a convolution in time which is treated analytically in the following. The time interval $(0, T)$ is divided into M equidistant subintervals Δt , i.e., $t_m = m\Delta t$,

with $m = 0, \dots, M$. The density is approximated by constant ansatz functions $\psi^m(t)$ in time. Thus, the convolution integral is

$$\mathbf{U}(\mathbf{x}, \mathbf{y}, t) * \mathbf{v}(\mathbf{y}, t) \approx \sum_{m=1}^M \mathbf{v}^m(\mathbf{y}) \underbrace{\int_{t_{m-1}}^{t_m} \mathbf{U}(\mathbf{x}, \mathbf{y}, t_n - \tau) \psi^m(\tau) d\tau}_{=\mathbf{U}_i^{n,m}(\mathbf{x}, \mathbf{y})} .$$

Due to the structure of the fundamental solution the integrals per time step can be computed analytically

$$\mathbf{U}_i^{n,m}(\mathbf{x}, \mathbf{y}) = \begin{cases} \mathbf{U}_1^{n,m}(\mathbf{x}, \mathbf{y}) = \mathbf{0} & \text{for } t_n - \frac{r}{c_2} < t_n - \frac{r}{c_1} < t_{m-1} < t_m \\ \mathbf{U}_2^{n,m}(\mathbf{x}, \mathbf{y}) & \text{for } t_n - \frac{r}{c_2} < t_{m-1} < t_n - \frac{r}{c_1} < t_m \\ \mathbf{U}_3^{n,m}(\mathbf{x}, \mathbf{y}) & \text{for } t_n - \frac{r}{c_2} < t_{m-1} < t_m < t_n - \frac{r}{c_1} \\ \mathbf{U}_4^{n,m}(\mathbf{x}, \mathbf{y}) & \text{for } t_{m-1} < t_n - \frac{r}{c_2} < t_n - \frac{r}{c_1} < t_m \\ \mathbf{U}_5^{n,m}(\mathbf{x}, \mathbf{y}) & \text{for } t_{m-1} < t_n - \frac{r}{c_2} < t_m < t_n - \frac{r}{c_1} \\ \mathbf{U}_6^{n,m}(\mathbf{x}, \mathbf{y}) = \mathbf{0} & \text{for } t_{m-1} < t_m < t_n - \frac{r}{c_2} < t_n - \frac{r}{c_1} \end{cases} ,$$

with $i = 1, \dots, 6$ being an index for the case distinction.

2.2. Storage Efficiency. A closer look at the cases $i = 1$ and $i = 6$ of subsection 2.1 allows the statement

$$\mathbf{U}_i^{n,m} = \mathbf{0} \text{ if } \begin{cases} r < r_{min} = c_2 \Delta t (n - m) \\ \text{or} \\ r > r_{max} = c_1 \Delta t (n - m + 1) \end{cases} .$$

For a certain spatial point \mathbf{x} and a time interval $\Delta t (n - m)$, radii deceeding the upper inequality or exceeding the lower inequality do not contribute to the computation. Both inequalities are related to the travelling wave fronts as illustrated in Fig. 1.

Considering case $i = 1$, it becomes obvious that for a distinct time step \tilde{n} , r_{min} is larger than the largest extent of the domain. Henceforth, the system matrices are zero. This is well known as the cut off property.

For time steps $n < \tilde{n}$, all elements which are cut by one of the wavefronts, as well as those elements lying in between the fronts (Γ_c in Fig. 1), contribute to the system matrices. The disjoint part $\Gamma_0 = \Gamma / \Gamma_c$ is zero and does not contribute to the calculation.

Since the strategy is based on the avoidance of zero evaluations, the storage efficiency and speedup is evident. The data efficient storage might be seen as a kind of sparse representation since the main part of the relevant matrices is sparsely populated. Furthermore, for implementation reasons we have to provide data sparse structures and arithmetics (see, e.g., [2]).

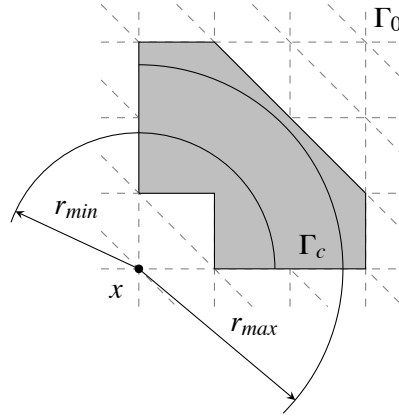


FIGURE 1. Relevant (Γ_c) and negligible part (Γ_0) of the domain.

2.3. Spatial Discretization. The field approximation is chosen to be constant for the density $\mathbf{v}(\mathbf{x}, t)$ in the single layer potential. Moreover, the geometry is approximated via linear triangles. For the regular integration standard Gaussian quadrature is used, whereas the weakly singular integration is done via the Duffy transformation.

3. LOW RANK APPROXIMATION

3.1. Geometrical Clustering Process. Examining the structure of the system matrices after a geometrical clustering process gives evidence for some important facts. The matrices are sparsely populated if n is small or reaches \tilde{n} . For intermediate time steps more or less larger densely populated blocks can be identified. While both waves are present in the domain, these blocks are growing in time. If the compression wave has left the domain, the blocks are shrinking until they vanish as $n = \tilde{n}$ (the shear wave has left the domain). Within the larger blocks, case $i = 3$ of section 2.1 is dominant

$$\mathbf{U}_3^{n,m} \text{ if } \begin{cases} r > r_{3,min} = c_2 \Delta t (n - m) \\ \text{and} \\ r < r_{3,max} = c_1 \Delta t (n - m + 1) \end{cases},$$

thus we can state another radius criterion similar to section 2.2. While setting up block cluster trees for all relevant time steps, it is possible to compute the minimum and maximum distance (d_{min} , d_{max}) of two clusters (Cl_x , Cl_y) as illustrated in Fig. 2. Moreover, we can identify pairs of clusters that fulfill the inequalities $d_{min} > r_{3,min}$ and $d_{max} < r_{3,max}$. For these combinations of clusters it is ensured that solely case $i = 3$ is used for computation (i.e., the kernel function is smooth for $r > 0$). If the clusters are furthermore admissible, a low rank approximation becomes applicable (see, e.g., [3]).

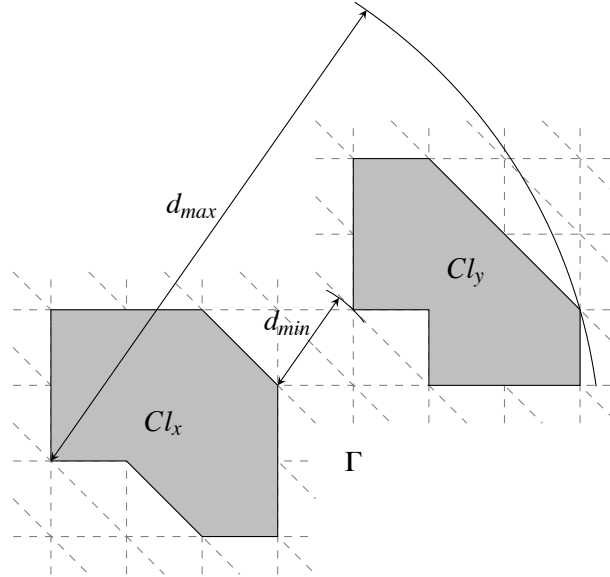


FIGURE 2. Maximal and minimal distances of clusters Cl_x and Cl_y .

3.2. Low Rank Approximation and Implementation. The presented algorithm uses the adaptive cross approximation (ACA) for the computation of low rank blocks in the hierarchical system matrices. As a hierarchical concept, the \mathcal{H} -matrix library AHMED written by Mario Bebendorf is used, which allows for a data efficient representation of the system matrices and contains a large variety of hierarchical matrix arithmetics. Due to the radius criterion of section 3.1 the library had to be modified slightly.

4. NUMERICAL RESULTS

4.1. Compression rates. The numerical test focuses on the storage efficiency of the proposed algorithm. To analyse the storage savings due to the data efficient representation and the low rank approximation, we define two measures

$$c_{1,j} = \frac{\text{Mem}(e)}{\text{Mem}(f)}, \quad c_{2,j} = \frac{\text{Mem}(e, \text{ACA})}{\text{Mem}(f)}$$

usually denoted as compression. $\text{Mem}(f)$ denotes the memory consumption of the full matrix. Hence, a full matrix has a compression of $c_f = 1$. $\text{Mem}(e)$ refers to the memory consumption of the data efficient system matrix (see section 2.2), whereas $\text{Mem}(e, \text{ACA})$ denotes the memory consumption of the data efficient system matrix including a further compression with the ACA algorithm (see section 3.2). The subscript j at both measures will refer to the mesh number.

4.2. **Examples.** For two triangulated spheres as illustrated in Fig. 3 (exterior domain problem) the compression rates are computed. The radius $R = 1m$ and

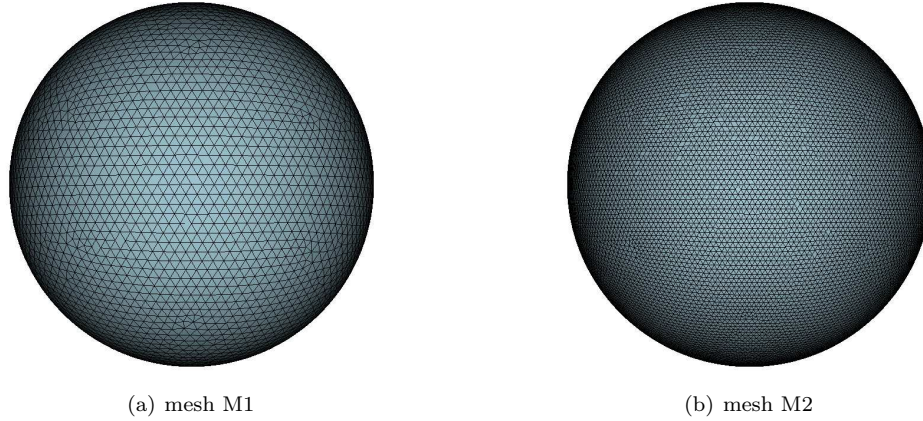


FIGURE 3. Sphere with radius $R = 1m$: used meshes.

the computational and material data are listed in table 3. h_e is the mean value

mesh	h_e [m]	β	# elements	c_1 [m/s]	c_2 [m/s]
M1	≈ 0.06250	≈ 1	7746	1.054	0.645
M2	≈ 0.03125	≈ 1	31470	1.054	0.645

TABLE 3. Computational and material data.

of the largest edge of each triangle and $\beta = \frac{c_1 \Delta t}{h_e}$, which was set to ≈ 1 for stability reasons. Concerning the low rank approximation, the accuracy of the ACA algorithm was set to $\epsilon_{ACA} = 10^{-6}$. Fig. 4 shows the matrix compression for the relevant time steps.

4.3. **Conclusions.** For both meshes the efficient representation yields a significant compression $c_{1,1}$ and $c_{1,2}$ as can be seen in Fig. 4. The further low rank approximation of admissible, densely populated blocks improves the compression rate. As expected, the compression due to the application of ACA is only significant for the larger mesh M_2 (see $c_{2,2}$ in Fig. 4). Tests have shown that choosing a lower accuracy ϵ_{ACA} results in better compression rates and may be used in practical applications.

Bernhard Kager, Martin Schanz

Institute of Applied Mechanics

Graz University of Technology, Technikerstr. 4, 8010 Graz, Austria

bernhard.kager@tugraz.at, m.schanz@tugraz.at

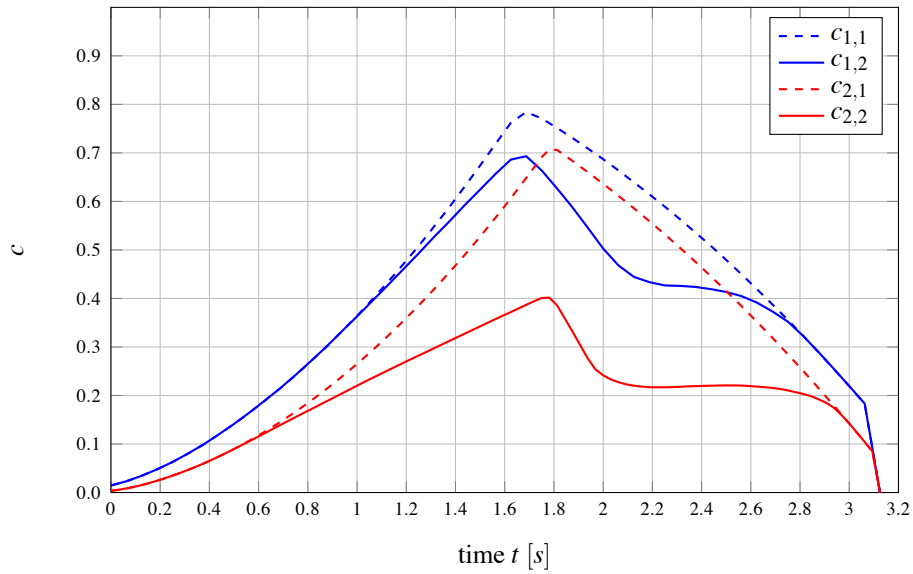


FIGURE 4. Compression rates versus time.

REFERENCES

- [1] J.D. Achenbach wave propagation in elastic solids. *North-Holland/American Elsevier*, 1973.
- [2] H. Yoshikawa and N. Nishimura. An improved implementation of time domain elastodynamic BIEM in 3D for large scale problems and its application to ultrasonic NDE. *Electronic Journal of Boundary Elements*, 1(2):201-217, 2003.
- [3] M. Messner and M. Schanz. An accelerated symmetric time-domain boundary element formulation for elasticity. *Engineering Analysis with Boundary Elements*, 34(11):944-955, 2010.

Novel inverse estimates for non-local operators

M. KARKULIK

(joint work with M. Feischl, T. Führer, J.M. Melenk, D. Praetorius)

1. INVERSE ESTIMATES

Inverse estimates are a means to bound expressions in stronger norms than in the generic situation by exploiting additional structure. Two examples of such structures are the following:

- (a) In FEM, strong norms of piecewise polynomials can be bounded in terms of weak norms. The key point is the ability to use norm equivalence on finite dimensional spaces on a reference configuration. Scaling arguments provide the correct powers of the local mesh size.
- (b) In regularity theory for elliptic PDE, “interior regularity” of solutions can be seen as an inverse estimate. By using the underlying equation directly, strong norms of solutions can be controlled by weaker norms at the expense of slightly enlarging the domain.

In the following, \mathcal{T} denotes a (even locally refined) mesh on a subset $\Gamma \subseteq \partial\Omega$ of the boundary $\partial\Omega$ of a polyhedral domain $\Omega \subset \mathbb{R}^d$. The local mesh size is denoted by $h \in \mathcal{P}^0(\mathcal{T})$ where $\mathcal{P}^p(\mathcal{T})$ is the space of piecewise polynomials of degree at most p . An example for (a) is given, e.g., in [6, Theorem 3.6]:

Theorem 1.1 (Inverse estimate for piecewise constants). *There exists a constant $C > 0$, which depends only on an upper bound for the shape-regularity constant of \mathcal{T} and the polynomial degree $p \geq 0$, such that*

$$\|h^{1/2}\Psi\|_{L_2(\Gamma)} \leq C\|\Psi\|_{H^{-1/2}(\Gamma)} \quad \text{for all } \Psi \in \mathcal{P}^p(\mathcal{T}).$$

As an example for (b) serves [9, Lemma 5.7.1]:

Theorem 1.2 (Interior regularity/Caccioppoli inequality). *There is $C > 0$ such that the following holds: If B_r, B_{r+h} are balls with radii $r, r+h > 0$ around a joint midpoint, and if $u \in H^1(B_{r+h})$ satisfies $\Delta u = 0 \in L_2(B_{r+h})$ for some $r, h > 0$, then $u \in H^2(B_r)$ with*

$$\|D^2u\|_{L_2(B_r)} \leq Ch^{-1}\|\nabla u\|_{L_2(B_{r+h})}.$$

In the following, we present a possibility how to obtain inverse estimates involving boundary layer potentials by combining the two inverse estimates above. As a prototype for such a layer potential serves the simple-layer potential of the 3D-Laplacian, which is given by

$$(1) \quad V\psi(x) := \frac{1}{4\pi} \int_{\Gamma} \frac{\psi(y)}{|x-y|} ds_y.$$

Hereafter, K and K' denote the double layer potential and its adjoint, and W denotes the hypersingular integral operator. Our main result, which is taken from [1, 8], is the following.

Theorem 1.3 (Inverse estimates for boundary integral operators). *There is $C > 0$ which depends only on Γ and an upper bound for the shape-regularity constant of \mathcal{T} , such that*

$$(2) \quad \|h^{1/2}\nabla_{\Gamma}V\psi\|_{L_2(\Gamma)} \leq C \left[\|\psi\|_{H^{-1/2}(\Gamma)} + \|h^{1/2}\psi\|_{L_2(\Gamma)} \right],$$

$$(3) \quad \|h^{1/2}K'\psi\|_{L_2(\Gamma)} \leq C \left[\|\psi\|_{H^{-1/2}(\Gamma)} + \|h^{1/2}\psi\|_{L_2(\Gamma)} \right],$$

$$(4) \quad \|h^{1/2}\nabla_{\Gamma}Kv\|_{L_2(\Gamma)} \leq C \left[\|v\|_{H^{1/2}(\Gamma)} + \|h^{1/2}\nabla_{\Gamma}v\|_{L_2(\Gamma)} \right],$$

$$(5) \quad \|h^{1/2}Wv\|_{L_2(\Gamma)} \leq C \left[\|v\|_{H^{1/2}(\Gamma)} + \|h^{1/2}\nabla_{\Gamma}v\|_{L_2(\Gamma)} \right],$$

holds for all $\psi \in L_2(\Gamma)$ and $v \in H^1(\Gamma)$. Here, ∇_{Γ} denotes the surface gradient for $d \geq 3$, and the arclength derivative for $d = 2$.

Some observations regarding this result are the following.

- We stress that a difficulty in proving Theorem 1.3 lies in the consideration of *locally refined* meshes. If we consider a *globally uniform* mesh \mathcal{T} , we can use stability $V : L_2(\Gamma) \rightarrow H^1(\Gamma)$ to estimate, e.g.,

$$\begin{aligned} \|h^{1/2}\nabla_{\Gamma}V\psi\|_{L_2(\Gamma)} &= h^{1/2}\|\nabla_{\Gamma}V\psi\|_{L_2(\Gamma)} \lesssim h^{1/2}\|\psi\|_{L_2(\Gamma)} \\ &= \|h^{1/2}\psi\|_{L_2(\Gamma)}. \end{aligned}$$

- As already mentioned, inverse estimates typically require a space with some structure. Theorem 1.3 holds for $\psi \in L_2(\Gamma)$, which might not be regarded as a space with a rich structure. However, if $\psi = \Psi \in \mathcal{P}^p(\mathcal{T})$, we can use Theorem 1.1 to estimate, e.g.,

$$(6) \quad \|h^{1/2}\nabla_{\Gamma}V\Psi\|_{L_2(\Gamma)} \lesssim \|\Psi\|_{H^{-1/2}(\Gamma)}.$$

By stability of V and its inverse, the last estimate is equivalent to

$$(7) \quad \|h^{1/2}\nabla_{\Gamma}V\Psi\|_{L_2(\Gamma)} \lesssim \|V\Psi\|_{H^{1/2}(\Gamma)},$$

which is indeed an inverse estimate.

An analogous result to Theorem 1.3 was proven independently in [5] for lowest-order discretizations and $C^{1,1}$ surfaces. In the next section, we present the ideas for proving the bound for the simple layer potential V in Theorem 1.3, and in the last section we comment on several applications.

2. INVERSE ESTIMATE FOR V

The main difficulty in proving (2) is the fact that V is a non-local operator. We restrict our considerations to local configurations, i.e. elements, via

$$\|h^{1/2}\nabla_{\Gamma}V\psi\|_{L_2(\Gamma)}^2 = \sum_{T \in \mathcal{T}} \|h^{1/2}\nabla_{\Gamma}V\psi\|_{L_2(T)}^2.$$

Even if we would restrict to $\psi = \Psi \in \mathcal{P}^0(\mathcal{T})$, it would be impossible to bound the contributions of $V\Psi$ on T , as the local dimension of this space is dominated by the

whole mesh \mathcal{T} – actually, V is non-local. On T , we therefore split the potential $u = V\psi$ in a part u_T^{near} with a bounded and small dimension, and a rest u_T^{far} via

$$V\psi = V(\psi_T) + V(\psi_{\Gamma \setminus T}) = u_T^{\text{near}} + u_T^{\text{far}}.$$

Here, $\psi_\omega := \psi\chi_\omega$, where χ_ω is the characteristic function of the set ω . We stress that the actual splitting that is used in the proofs of [1, 8] extends a little to the neighborhood of T , but we stick to this simplification for ease of presentation. We call u_T^{near} the *nearfield* and u_T^{far} the *farfield* and write

$$(8) \quad \|h^{1/2}\nabla_\Gamma V\psi\|_{L_2(\Gamma)}^2 \lesssim \sum_{T \in \mathcal{T}} \|h^{1/2}\nabla_\Gamma u_T^{\text{near}}\|_{L_2(T)}^2 + \sum_{T \in \mathcal{T}} \|h^{1/2}\nabla_\Gamma u_T^{\text{far}}\|_{L_2(T)}^2.$$

Due to the locality of the nearfield and stability $V : L_2(\Gamma) \rightarrow H^1(\Gamma)$,

$$(9) \quad \|\nabla_\Gamma u_T^{\text{near}}\|_{L_2(T)}^2 \leq \|\nabla_\Gamma u_T^{\text{near}}\|_{L_2(\Gamma)}^2 \lesssim \|\psi_T\|_{L_2(\Gamma)}^2 = \|\psi\|_{L_2(T)}^2,$$

and a multiplication with the local mesh width h and a sum over all elements bounds the nearfield terms in (8). It remains to bound the farfield terms in (8), which is done by exploiting Theorem 1.2. We may do so, because

1. V is a potential in \mathbb{R}^d , i.e., $\Delta V(\psi_{\Gamma \setminus T}) = 0$ in Ω and in $\mathbb{R}^d \setminus \Omega$, and it is smooth in both parts,
2. and the farfield term is smooth in a d -dimensional neighborhood of T , as the density $\psi_{\Gamma \setminus T}$ vanishes on T .

Put differently, u_T^{far} is a potential that is induced by a density on $\Gamma \setminus T$. A standard trace inequality applied to $\nabla_\Gamma u_T^{\text{far}}$ involves the second derivative of u_T^{far} in a volume U_T around T ,

$$\|\nabla_\Gamma u_T^{\text{far}}\|_{L_2(T)}^2 \lesssim h_T^{-1} \|\nabla u_T^{\text{far}}\|_{L_2(U_T)}^2 + \|\nabla u_T^{\text{far}}\|_{L_2(U_T)} \|D^2 u_T^{\text{far}}\|_{L_2(U_T)}.$$

Due to reasons 1. and 2., we can bound the second derivative by Theorem 1.2 and obtain

$$\|\nabla_\Gamma u_T^{\text{far}}\|_{L_2(T)}^2 \lesssim h_T^{-1} \|\nabla u_T^{\text{far}}\|_{L_2(\tilde{U}_T)}^2$$

with a slightly enlarged volume \tilde{U}_T . A sum over T bounds the farfield terms in (8), which is then splitted into the difference $u_T^{\text{far}} = V\psi - u_T^{\text{near}}$ of the whole potential and the nearfield,

$$\sum_{T \in \mathcal{T}} \|h^{1/2}\nabla_\Gamma u_T^{\text{far}}\|_{L_2(T)}^2 \lesssim \sum_{T \in \mathcal{T}} \|\nabla V\psi\|_{L_2(\tilde{U}_T)}^2 + \sum_{T \in \mathcal{T}} \|\nabla u_T^{\text{near}}\|_{L_2(\tilde{U}_T)}^2$$

We ensure that only a bounded number of \tilde{U}_T overlap, such that the terms on the right hand side can be estimated by stability of the potential $V\psi$ and the locality of the nearfield analogous to (9).

3. APPLICATIONS

3.1. Convergence of adaptive BEM. For given data f , the (unknown) solution ϕ of the weakly-singular integral equation

$$(10) \quad V\phi = f$$

can be approximated adaptively by a Galerkin method. To that end, we employ the following adaptive algorithm.

Algorithm 3.1. Input: coarse mesh \mathcal{T}_0 , approximation order $p \in \mathbb{N}_0$, parameter $\theta \in (0, 1)$, counter $\ell := 0$.

- (i) compute Galerkin solution $\Phi_\ell \in \mathcal{P}^p(\mathcal{T}_\ell)$ of (10).
- (ii) for every $T \in \mathcal{T}_\ell$, compute error indicator

$$\rho_\ell(T) := \|h_\ell^{1/2} \nabla_\Gamma (V\Phi_\ell - f)\|_{L_2(T)}.$$

- (iii) choose a set $\mathcal{M}_\ell \subseteq \mathcal{T}_\ell$ of minimal cardinality such that

$$\theta \sum_{T \in \mathcal{T}} \rho_\ell(T)^2 \leq \sum_{T \in \mathcal{M}_\ell} \rho_\ell(T)^2.$$

- (iv) refine at least the elements \mathcal{M}_ℓ in \mathcal{T}_ℓ and obtain $\mathcal{T}_{\ell+1}$.
- (v) increase counter $\ell := \ell + 1$ and goto (i).

Output: sequence of solutions $(\Phi_\ell)_{\ell \in \mathbb{N}_0}$, sequence of estimators, $(\rho_\ell)_{\ell \in \mathbb{N}_0}$.

We can employ the inverse estimate for V to show that the adaptive Algorithm 3.1 converges, cf. [7]:

Theorem 3.2. *The sequence of Galerkin solutions $(\Phi_\ell)_{\ell \in \mathbb{N}_0}$ computed by Algorithm 3.1 converges to ϕ , i.e.,*

$$\|\phi - \Phi_\ell\|_{H^{-1/2}(\Gamma)} \rightarrow 0.$$

Two important observations regarding algorithm 3.1 are the following:

- In [4], it is shown that the estimator ρ_ℓ , employed in Algorithm 3.1, is reliable, i.e.,

$$(11) \quad \|\phi - \Phi_\ell\|_{H^{-1/2}(\Gamma)} \lesssim \rho_\ell := \left(\sum_{T \in \mathcal{T}} \rho_\ell(T)^2 \right)^{1/2}.$$

- Arguments from [3] show that Algorithm 3.1 converges *a priori*, i.e.,

$$(12) \quad \|\Phi_{\ell+1} - \Phi_\ell\|_{H^{-1/2}(\Gamma)} \rightarrow 0.$$

Using the contraction of the mesh size on refined elements, it is possible to show that Algorithm 3.1 yields the so-called *estimator reduction*

$$(13) \quad \rho_{\ell+1} \leq \kappa \rho_\ell + C_{\text{red}} \|h_{\ell+1}^{1/2} \nabla_\Gamma V(\Phi_{\ell+1} - \Phi_\ell)\|_{L_2(\Gamma)}$$

with some $\kappa \in (0, 1)$ and $C_{\text{red}} > 0$. This means that ρ_ℓ is a contraction up to a perturbation term, which consists of the difference of two successive Galerkin solutions, measured in a stronger norm compared to (12). We use the inverse

estimate (6) to bound the perturbation term by the weaker $H^{-1/2}$ norm and use the a priori convergence (12),

$$(14) \quad \|h_{\ell+1}^{1/2} \nabla_{\Gamma} V(\Phi_{\ell+1} - \Phi_{\ell})\|_{L_2(\Gamma)} \lesssim \|\Phi_{\ell+1} - \Phi_{\ell}\|_{H^{-1/2}(\Gamma)} \rightarrow 0.$$

Hence, we conclude from (13) and (14) that ρ_{ℓ} is a contraction up to a zero sequence. From basic calculus, we infer that $\rho_{\ell} \rightarrow 0$. Due to reliability (11), we conclude the statement of Theorem 3.2.

3.2. Convergence of adaptive FEM-BEM coupling. We adaptively solve a Laplace transmission problem with given Dirichlet and Neumann jumps u_0 and ϕ_0 . We use the symmetric FEM-BEM coupling formulation and seek $u \in H^1(\Omega)$ and $\phi \in H^{-1/2}(\Gamma)$ s.t.

$$\begin{aligned} \langle \nabla u, \nabla v \rangle_{\Omega} + \langle Wu + (K' - 1/2)\phi, v \rangle_{\Gamma} &= \langle f, v \rangle_{\Omega} + \langle \phi_0 + Wu_0, v \rangle_{\Gamma} \\ \langle \psi, V\phi - (K - 1/2)u \rangle_{\Gamma} &= -\langle \psi, (K - 1/2)u_0 \rangle_{\Gamma}, \end{aligned}$$

hold true for all $v \in H^1(\Omega)$ and $\psi \in H^{-1/2}(\Gamma)$. We stress that the following arguments also apply to other couplings, e.g. the Johnson-Nédélec or Bielak-McCamy coupling. For a posteriori error estimation, we use a combination η_{ℓ} of the residual FEM error estimator and the weighted residual BEM estimator ρ_{ℓ} from Subsection 3.1, cf. [1]. Again, an adaptive algorithm of the form of Algorithm 3.1 exhibits the estimator reduction for η_{ℓ} , where strong norms involving all 4 boundary integral operators appear in the perturbation terms. These strong norms can be estimated by the inverse estimates from Theorem 1.3, such that we obtain $\eta_{\ell} \rightarrow 0$, cf. Subsection 3.1, which results in convergence of the adaptive coupling due to the reliability of η_{ℓ} , cf. [1].

3.3. Efficiency of weighted residual estimates in BEM. The inverse estimate for V can be used to show the efficiency of the residual error estimate ρ_{ℓ} from Subsection 3.1 for $d = 2$. We recall that ϕ is the exact solution of the weakly singular integral equation (10), and $\Phi_{\ell} \in \mathcal{P}^0(\mathcal{T}_{\ell})$ denotes a lowest-order Galerkin solution. The estimate for V in Theorem 1.3 states that

$$\rho_{\ell} = \|h_{\ell}^{1/2} \nabla_{\Gamma} V(\phi - \Phi_{\ell})\|_{L_2(\Gamma)} \lesssim \|\phi - \Phi_{\ell}\|_{H^{-1/2}(\Gamma)} + \|h_{\ell}^{1/2}(\phi - \Phi_{\ell})\|_{L_2(\Gamma)}.$$

By an explicit use of the singular behaviour of ϕ on polygonal boundaries, we can bound the last term in the preceding estimate and obtain the following, cf. [2].

Theorem 3.3 (Efficiency of ρ_{ℓ} in 2D). *If $f \in H^s(\Gamma)$ for $s > 2$, then*

$$\rho_{\ell} \lesssim \|\phi - \Phi_{\ell}\|_{H^{-1/2}(\Gamma)} + \text{hot}_{\ell},$$

where, for all $\varepsilon > 0$,

$$\text{hot}_{\ell}^2 = \sum_{T \in \mathcal{T}} \text{hot}_{\ell}(T)^2 \quad \text{and} \quad \text{hot}_{\ell}(T) \leq C_{\text{hot}} h_{\ell}(T)^{\min(s, 5/2) - 1/2 - \varepsilon}.$$

The constant C_{hot} depends only on Γ , an upper bound of the shape regularity constant of \mathcal{T}_{ℓ} , s , and ε .

If we again restrict to globally uniform meshes, we see that the preceding Theorem yields, for some $\varepsilon > 0$,

$$\rho_\ell \lesssim \|\phi - \Phi_\ell\|_{H^{-1/2}(\Gamma)} + \mathcal{O}(h_\ell^{3/2+\varepsilon}).$$

As the optimal rate of convergence for lowest order BEM is $\mathcal{O}(h^{3/2})$, we obtain efficiency of ρ_ℓ up to terms of higher order.

Michael Karkulik

Pontificia Universidad Católica de Chile, Facultad De Matemáticas, Avenida Vicuña Mackenna 4860, Santiago, Chile

michael.karkulik@tuwien.ac.at

M. Feischl, T. Führer, J.M. Melenk, D. Praetorius

Institute for Analysis and Scientific Computing, Vienna University of Technology, Wiedner Hauptstraße 8-10, A-1040 Wien, Austria

michael.feischl@tuwien.ac.at, thomas.fuehrer@tuwien.ac.at

melenk@tuwien.ac.at, dirk.praetorius@tuwien.ac.at

REFERENCES

- [1] M. AURADA, M. FEISCHL, T. FÜHRER, M. KARKULIK, J. M. MELENK, AND D. PRAETORIUS, *Inverse estimates for elliptic boundary integral operators and their application to the adaptive coupling of FEM and BEM*, ASC Report 07/2012, Institute for Analysis and Scientific Computing, Vienna University of Technology, Wien, 2012.
- [2] M. AURADA, M. FEISCHL, T. FÜHRER, M. KARKULIK, AND D. PRAETORIUS, *Efficiency and optimality of some weighted-residual error estimator for adaptive 2D boundary element method*, ASC Report 15/2012, Institute for Analysis and Scientific Computing, Vienna University of Technology, Wien, 2012.
- [3] I. BABUSKA AND M. VOGELIUS, *Feedback and adaptive finite element solution of one-dimensional boundary value problems*, Numer. Math., 44 (1984), 75–102.
- [4] C. CARSTENSEN, M. MAISCHAK, AND E. STEPHAN, *A posteriori error estimate and h-adaptive algorithm on surfaces for Symm’s integral equation*, Numer. Math., 90 (2001), 197–213.
- [5] T. GANTUMUR, *Adaptive boundary element methods with convergence rates*, to appear in Numer. Math., cf. arXiv:1107.0524.
- [6] I. GRAHAM, W. HACKBUSCH, AND S. SAUTER, *Finite elements on degenerate meshes: Inverse-type inequalities and applications*, IMA J. Numer. Anal. 25 (2005), 379–407.
- [7] M. FEISCHL, M. KARKULIK, J. MELENK, AND D. PRAETORIUS, *Quasi-optimal convergence rate for an adaptive boundary element method*, submitted to SIAM J. Numer. Anal.
- [8] M. KARKULIK, *Zur Konvergenz und Quasioptimalität adaptiver Randelementmethoden*, PhD thesis (in German), Institute for Analysis and Scientific Computing, Vienna University of Technology, Wien, 2012.
- [9] J. C. B. MORREY, *Multiple integrals in the calculus of variations*, Classics in Mathematics. Springer, Berlin, 2008. Reprint of the 1966 edition.

Rapid prototyping of Boundary Element Methods with BETL

LARS KIELHORN

The *Boundary Element Template Library* (BETL) [2] implements building blocks for the 3D Galerkin discretization of quite arbitrary boundary integral operators. It equally aims for rapid prototyping of new Boundary Element Methods as well as for the development of industrial-strength BEM solvers.

BETL's implementation is based on generic software paradigms. Entirely written in C++, its core functionality is implemented as a header-only library, which makes it highly portable and attractive for being used with existing C++ codes.

The present work gives a short overview on BETL and its features. Beside this, we present example problems such as the transmission problem for composite scatterers [1], which easily can be tackled by making use of BETL. In particular, we focus on how BETL mimics the mathematical notion of the involved boundary integral operators and their respective discrete trace spaces.

Keywords: Integral equations, Boundary element software library, software design

Lars Kielhorn

ETH Zurich

`lars.kielhorn@sam.math.ethz.ch`

REFERENCES

- [1] R. Hiptmair and C. Jerez-Hanckes. Multiple traces boundary integral formulation for Helmholtz transmission problems. *Advances in Computational Mathematics*, 37:39–91, 2012.
- [2] R. Hiptmair and L. Kielhorn. BETL — A boundary element template library. Technical Report 2012-36, Seminar for Applied Mathematics, ETH Zürich, 2012. (*submitted to ACM TOMS*).

Some FE and BE based approaches for boundary control problems

A. KIMESWENGER

(joint work with O. Steinbach)

In this talk some approaches will be presented to handle boundary control problems. As the Dirichlet datum is typically considered in $H^{\frac{1}{2}}(\Gamma)$ when dealing with partial differential equations, the same will be done for the control variable. The Steklov-Poincaré operator is used to realize the $H^{\frac{1}{2}}(\Gamma)$ regularization. When dealing with boundary control problems, one has to treat an optimality system containing a primal problem, a dual problem and an optimality condition. In the case of bounded domains a FE, a BE and a FE/BE approach will be presented to handle the optimality system. For unbounded domains the coupled FE/BE approach will turn out to be suitable and practicable. A standard FE and/or BE discretization will be used and some 2d simulations will be discussed. To handle box constraints a semi-smooth Newton method will be used.

Keywords: Boundary control problems, FE/BE approach

Mathematics Subject Classifications (2000): 49M25, 65N38

A. Kimeswenger, O. Steinbach

Graz University of Technology, Austria

arno.kimeswenger@tugraz.at, o.steinbach@tugraz.at

REFERENCES

- [1] G. Of, T. X. Phan, O. Steinbach. Boundary element methods for Dirichlet boundary control problems. *Math. Methods Appl. Sci.* 33 2187-2205 (2010).
- [2] G. Of, T. X. Phan, O. Steinbach. An energy space finite element approach for elliptic Dirichlet boundary control problems. *Berichte aus dem Institut für Numerische Mathematik, Bericht 2012/5 Graz University of Technology* (2012).
- [3] T. X. Phan. Boundary element methods for boundary control problems. *PhD thesis Graz University of Technology* (2011).

Influence of depth of embedment and material configuration on the coupled rocking-transverse vibration of rigid plates

JOSUE LABAKI

(joint work with Euclides Mesquita, R. K. N. D. Rajapakse)

This paper examines the steady-state rocking and horizontal vibratory response of a rigid circular plate at different embedment configurations within viscoelastic, transversely isotropic, three-dimensional layered media. A Green's function for the aforementioned media has been derived by Rajapakse and Wang [1]. The Cauchy-Navier equations were solved by using Hankel integral transforms. The viscoelastic behavior of the medium is introduced by the elastic-viscoelastic correspondence principle. Boundary-value problems corresponding to the cases of distributed horizontal and rocking ring loads are considered.

The case of rigid a plate embedded at the interface of three dimensional transverse isotropic layers is formulated in terms of a discretized integral equation, which couples the rigid body displacements of the plate with the tractions acting over its contact surface through a set of displacement influence functions. The disc is discretized into a number of annular discs, and over each of these elements the tractions are considered to be constant. The system of resulting discretized integral equations is solved numerically, which gives the tractions over each disc element. The case of bimaterial interfaces is characterized by a coupling of the rocking and horizontal response of the plate, which depends on the properties of the interfacing media. Horizontal excitations result not only in horizontal displacement of the plate, but also in its *nutaton* (rocking rotation). Rocking excitations result in nutation and horizontal displacement of the plate. This paper focuses on the cross response of the plates, i.e., their horizontal displacements due to rocking moments (C_{XM}) and their rotations due to horizontal loads (C_{MX}). In the case of embedment of the plate within a homogeneous full-space, and because the traction distributions on both surfaces of the plate are balanced, both C_{XM} and C_{MX} are zero. It has been observed that embedment configurations which differs from this case results in non-zero C_{XM} and C_{MX} [2]. The most extreme case is when the plate rests on the surface of an unbounded half-space. This paper investigates three representative embedment configurations within these two limits. The first case considers that the plate rests on the surface of an unbounded half-space. The second case considers that the plate is embedded at a finite depth within a layered medium, each layer of which can be made of a different transversely isotropic material. In the third case, the plate is embedded at the interface of two unbounded half-spaces of different materials. The understanding of the cross response of embedded plates is fundamental to the proper design of buried foundations and anchors in non-homogeneous anisotropic soils.

Keywords: Embedded foundations, Soil-foundation interaction, Transverse isotropy.

Josue Labaki, Euclides Mesquita

Dept. of Computational Mechanics, University of Campinas
labaki@fem.unicamp.br, euclides@fem.unicamp.br

R. K. N. D. Rajapakse
Faculty of Applied Sciences, Simon Fraser University
rajapakse@sfu.ca

REFERENCES

- [1] R. K. N. D. Rajapakse and Y. Wang. Green's Functions for Transversely Isotropic Elastic Half Space. *Journal of Engineering Mechanics*, 119(9):1724-1746, 1993.
- [2] J. Labaki. Vibration of Flexible and Rigid Plates on Transversely Isotropic Media. *University of Campinas*, Ph.D. Thesis, Campinas, 2012.

Fast Multipole BEM For Thin Plate Bending Problems

YIJUN LIU

(joint work with Shuo Huang)

A new fast multipole boundary element method (BEM) for analyzing large-scale thin plate bending problems will be presented in this talk. Thin plate bending problems are governed by bi-harmonic equation under given boundary conditions. This PDE can be transformed into two direct boundary integral equations (BIEs) that are sufficient to solve the unknown boundary variables deflection, rotation, shear force, or bending moment two at each boundary point [1, 2, 3]. New fast multipole formulations are developed for the two direct BIEs based on the results for 2D potential problems [4]. Large-scale BEM models of thin plates with numerous holes (perforated plates) are solved using the new fast multipole BEM to characterize their mechanical responses (such as the effective bending stiffness of perforated plates). The BEM results are compared with analytical solutions or finite element solutions, and good agreements are observed.

Yijun Liu, Shuo Huang

Mechanical Engineering, University of Cincinnati, Cincinnati, Ohio, USA

Yijun.Liu@uc.edu, shuohg@mail.uc.edu

REFERENCES

- [1] D. E. Beskos, ed. *Boundary Element Analysis of Plates and Shells*. Springer-Verlag, Berlin, 1991.
- [2] T. Q. Ye and Y. J. Liu. Finite deflection analysis of elastic plate by the boundary element method. *Applied Mathematical Modelling*, , 9, 183-188, 1985.
- [3] Y. J. Liu. Elastic stability analysis of thin plate by the boundary element method a new formulation. *Engineering Analysis with Boundary Elements*, 4, 160-164, 1987.
- [4] Y. J. Liu. *Fast Multipole Boundary Element Method - Theory and Applications in Engineering*. Cambridge University Press, Cambridge, 2009.

p-BEM and hp-BEM – efficient methods for achieving high accuracy

MATTHIAS MAISCHAK

It is well known, that we can achieve exponential fast convergence by approximating the solution of a pde using either the p-version bem or fem if the solution is smooth, or using the hp-version with geometrical refined mesh if the solution has singularities [2, 3]. Achieving exponential fast convergence asymptotically proves to be surprisingly difficult, due to requirements on memory, solution time and the necessary numerical precision.

In this presentation we investigate changes necessary to an existing fem/bem code, software tools for converting the code to a different data type using a multi-precision package [1] and discuss implementation issues which arise from considerable more time and memory consuming arithmetic operations.

We will compare standard double precision (hardware supported), quad precision (compiler supported) and higher precision (additional Software package [1]). We will present examples achieving errors with 1e-20 or less using p- and hp fem-bem methods in 1,2 and 3 dimensions.

Keywords: Integral equations, exponential fast convergence, extended precision

Mathematics Subject Classifications (2000): 65R20, 65Y20

Matthias Maischak

Brunel University, Uxbridge UB8 3PH, UK

matthias.maischak@brunel.ac.uk

REFERENCES

- [1] David H. Bailey, Yozo Hida, Xiaoye S. Li, and Brandon Thompson, *ARPREC: An Arbitrary Precision Computation Package*, Technical Report LBNL-53651, 2002
- [2] B. Guo, and I. Babuška, *The h-p version of the finite element method, part 1: The basic approximation results*, Computational Mechanics, 1 (1986), 21–41.
- [3] N. Heuer, M. Maischak, and E.P. Stephan, *Exponential convergence of the hp-version for the boundary element method on open surfaces*, Numerische Mathematik, 83 (1999), 641–666.

BEM Analysis of Quasistatic Delamination of Viscoelastic Bodies with Very Small Viscosity

VLADISLAV MANTIČ

(joint work with Christos G. Panagiotopoulos, Tomáš Roubíček)

Quasistatic delamination of viscoelastic solid bodies is examined. Whereas the so-called energetic solution may produce an unrealistically too early delamination, considered as energy-driven, when a certain small viscosity is assumed for approximately elastic bodies, stress-driven delamination may occur, which is in agreement with experiments. In the present work the Kelvin-Voigt rheology is assumed and delamination of a viscoelastic body of a very small viscosity glued by a thin adhesive layer to a rigid outer boundary is studied. This adhesive layer stores and dissipates a specific amount of energy during the delamination process. Damage of the layer is characterized by a scalar damage variable. A numerical procedure based on energy considerations is implemented in a collocation BEM code. The solution of a delamination problem for vanishing viscosity is presented and compared to the energetic solution.

1. INTRODUCTION

Quasistatic (neglecting inertia effects) inelastic processes on interfaces between solids referred to as *delamination* or *debonding* have intensively been studied in the last decades. The time scale of such processes is often much faster than the external loading time scale, and such processes are then modelled as rate independent [1, 2, 3, 4, 5, 6]. The above mentioned inelastic phenomena typically lead to sudden jumps during evolution, due to the nonconvexity of the governing stored energy and then it is not entirely clear which solution concept suits well for a specific application. The “physically” safe way to solve this problem is to reduce rate-independency on only such variables with respect to which the stored energy is convex, the resting ones being subjected to certain viscosity. Such viscosities can be very small and are usually completely neglected. However, although arbitrarily small, such viscosities are critically important to keep energetics valid. In the limit, we thus get some solutions of the underlying rate-independent system which, however, might be different from solutions arising when viscosity are directly zero and global energy minimization is applied. In the present work bulk viscosity and fully rate-independent inelastic delamination are considered.

We confine ourselves to viscoelastic bodies *at small strains* and we consider the viscosity in the *Kelvin-Voigt rheology* [7], which is the simplest rheology which makes the desired effect of natural prevention of the too-early delamination [8, 9]. We mainly focus on the case of very small values of viscosity as well as on the inviscid problem, where viscosity coefficient χ vanishes.

2. QUASISTATIC DELAMINATION PROBLEM OF A VISCOELASTIC BODY

We consider the standard model of a *unilateral frictionless Signorini contact*. The quasistatic boundary-value problem for the displacement u in a viscoelastic

domain Ω and the so-called delamination parameter z on the adhesive-contact part of boundary $\Gamma_C \subset \Gamma := \partial\Omega$ ($z \in [0, 1]$), representing Frémond's concept [10] of delamination, is defined as [8, 9]:

$$(1a) \quad \operatorname{div} \mathbb{C}\epsilon + f = 0 \quad \text{with} \quad \epsilon = \epsilon(u, \dot{u}) = \chi e(\dot{u}) + e(u) \quad \text{on } \Omega,$$

$$(1b) \quad u = w_D \quad \text{on } \Gamma_D,$$

$$(1c) \quad \mathbf{t}(\epsilon) = g \quad \text{on } \Gamma_N,$$

$$(1d) \quad \left. \begin{array}{l} \mathbf{t}_t(\epsilon) + z(\mathbb{K}u - ((\mathbb{K}u) \cdot \vec{n})\vec{n}) = 0, \\ u \cdot \vec{n} \geq 0, \quad \mathbf{t}_n(\epsilon) + z(\mathbb{K}u) \cdot \vec{n} \geq 0, \quad (\mathbf{t}_n(\epsilon) + z(\mathbb{K}u) \cdot \vec{n})(u \cdot \vec{n}) = 0, \\ \dot{z} \leq 0, \quad \mathfrak{d} \leq \alpha, \quad \dot{z}(\mathfrak{d} - \alpha) = 0, \\ \mathfrak{d} \in \frac{1}{2}\mathbb{K}u \cdot u + N_{[0,1]}(z) \end{array} \right\} \text{on } \Gamma_C,$$

where traction vector and its normal and tangential components, respectively, are defined on $\Gamma_C \cup \Gamma_N$ by the formulas

$$(1e) \quad \mathbf{t}(\epsilon) = (\mathbb{C}\epsilon)|_{\Gamma}\vec{n}, \quad \mathbf{t}_n(\epsilon) = \vec{n}(\mathbb{C}\epsilon)|_{\Gamma}\vec{n}, \quad \mathbf{t}_t(\epsilon) = (\mathbb{C}\epsilon)|_{\Gamma}\vec{n} - \mathbf{t}_n(\epsilon)\vec{n},$$

with $\vec{n} = \vec{n}(x)$ being the unit outward normal to Γ , \mathbb{C} is the 4th-order tensor of elastic moduli, $e(u) = \frac{1}{2}((\nabla u)^\top + \nabla u)$ is the small-strain tensor, χ a ‘‘Kelvin-Voigt’’ relaxation time, \mathbb{K} the matrix of elastic moduli of the adhesive and \mathfrak{d} driving energy for delamination. The loading f , g , and w_D in (1a-c) depend on time t . The parameter $\alpha > 0$ in (1d) is a given phenomenological scalar quantity (possibly a function of $x \in \Gamma_C$) with the meaning of a specific energy needed (and thus deposited in the newly created surface) to delaminate a unit surface under adhesion or, equally, the energy dissipated by this delamination process. In engineering, α is also called *fracture toughness* (or fracture energy). The initial-value problem for (1a-e) is further defined by prescribing the initial conditions

$$(1f) \quad u(0) = u_0 \quad \text{and} \quad z(0) = z_0.$$

The inviscid limit problem arising for $\chi \rightarrow 0$ is a quasistatic problem for purely elastic material which consists in replacing (1a) by

$$(2) \quad \operatorname{div} \mathbb{C}e(u) + f = 0 \quad \text{on } \Omega,$$

and in replacing $\mathbf{t}(\epsilon)$ by $\mathbf{t}(e(u))$ in (1c) and similarly $\mathbf{t}_n(\epsilon)$ and $\mathbf{t}_t(\epsilon)$ by $\mathbf{t}_n(e(u))$ and $\mathbf{t}_t(e(u))$ in (1d) with $\mathbf{t}(\cdot)$, $\mathbf{t}_n(\cdot)$, and $\mathbf{t}_t(\cdot)$ again from (1e). This limit *rate-independent problem* itself, however, does not record any trace of energy dissipated by viscosity in the bulk during rupture of the delaminating surface, but there are explicit examples [9], showing that this energy is not negligible no matter how the viscosity coefficient $\chi > 0$ is small. This leads to a notion of *Kelvin-Voigt approximable solution* (u, z, μ) [8, 9] to this limit rate-independent problem involving a certain so-called *defect measure* μ recording this dissipated energy, which somehow remains even if viscosity coefficient χ vanishes, $\chi \rightarrow 0$.

In the vanishing viscosity limit the energy equality has the form [8, 9]:

$$(3) \quad \mathcal{E}(t, u(t), z(t)) + \int_{\Gamma_C} \alpha(z_0 - z(t)) \, dS + \int_0^t \int_{\Omega} \mu(\mathbf{d}x \, dt) = \mathcal{E}(0, u_0, z_0) + \int_0^t \langle \dot{\mathbf{f}}, u \rangle \, dt,$$

where a suitable functional $\mathbf{f}(t)$ has been defined by

$$(4) \quad \langle \mathbf{f}(t), v \rangle := \int_{\Omega} f(t) \cdot v - \mathbb{C}e(\chi \dot{u}_D(t) + u_D(t)) : e(v) + \int_{\Gamma_N} g(t) \cdot v \, dS.$$

Here, the measure μ , invented in [8], reflects the possible additional dissipated energy of Kelvin-Voigt-approximable solutions when compared to the so-called energetic solutions. This fact produces an essentially stress driven rupture of Kelvin-Voigt approximable solutions, in opposite to the energy-driven rupture of energetic solutions, where the energy dissipated by delamination is compensated by the elastic energy got from the bulk and adhesive.

3. TIME DISCRETISATION

After *semi-implicit time discretisation* and using an equidistant partition of the time interval $[0, T]$ with a time step $\tau > 0$ such that $T/\tau \in \mathbb{N}$, the problem may be cast to two convex minimization problems: first, we

$$(5a) \quad \begin{cases} \text{minimize} & \mathcal{E}(k\tau, u, z_\tau^{k-1}) + \tau \mathcal{R}_\chi \left(\frac{u - u_\tau^{k-1}}{\tau}, 0 \right) \\ \text{subject to} & u \in H^1(\Omega; \mathbb{R}^d), \quad u|_{\Gamma_D} = 0, \quad u|_{\Gamma_C} \cdot \vec{n} \geq 0 \end{cases}$$

and then, denoting its unique solution by u_τ^k , we

$$(5b) \quad \begin{cases} \text{minimize} & \mathcal{E}(k\tau, u_\tau^k, z) + \mathcal{R}_\chi(0, z - z_\tau^{k-1}) \\ \text{subject to} & z \in L^\infty(\Gamma_C), \quad 0 \leq z \leq z_\tau^{k-1} \end{cases}$$

with the stored energy \mathcal{E} and the dissipation (pseudo)potential \mathcal{R}_χ defined by

$$(6a) \quad \mathcal{E}(t, u, z) = \int_{\Omega} \frac{1}{2} \mathbb{C}e(u) : e(u) \, dx + \int_{\Gamma_C} \frac{1}{2} z \mathbb{K} u \cdot u \, dS - \langle \mathbf{f}(t), u \rangle,$$

$$(6b) \quad \mathcal{R}_\chi(\dot{u}, \dot{z}) = \int_{\Omega} \frac{\chi}{2} \mathbb{C}e(\dot{u}) : e(\dot{u}) \, dx - \int_{\Gamma_C} \alpha \dot{z} \, dS.$$

The time discrete analog of the energy equality equation [5] degenerates to the (im)balance equation [8, 9]:

$$(7) \quad \int_0^t \left(\int_{\Omega} \chi \mathbb{C}e(\dot{u}_{\chi, \tau}) : e(\dot{u}_{\chi, \tau}) \, dx + \int_{\Gamma_C} \alpha(z_0 - z_{\chi, \tau}(t)) \, dS - \langle \dot{\mathbf{f}}_\tau, \underline{u}_{\chi, \tau} \rangle \right) dt + \mathcal{E}(t, u_{\chi, \tau}(t), z_{\chi, \tau}(t)) - \mathcal{E}(0, u_0, z_0) =: \mathfrak{E}_{\chi, \tau}(t) \leq 0,$$

for any $t = k\tau$, $k = 1, \dots, T/\tau$ and $\underline{u}_{\chi, \tau}$ the piecewise constant ‘‘forward’’ interpolant. The residuum $\mathfrak{E}_{\chi, \tau} \in L^\infty(I)$ in the discrete energy (im)balance (7) can be controlled by making the time step $\tau > 0$ sufficiently small [9].

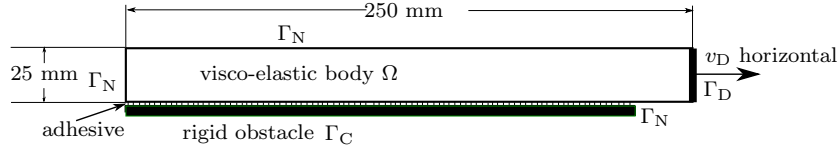
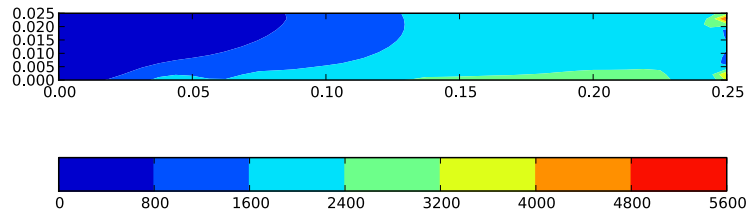


FIGURE 1. Geometry and boundary conditions of the problem.

FIGURE 2. Spatial distribution of the energy dissipated (J/m) by viscosity, $\int_0^t \chi \mathbb{C} e(\dot{u}_{\chi, \tau}) : e(\dot{u}_{\chi, \tau}) dt$, at the time of total rupture.

4. SPATIAL DISCRETISATION BY COLLOCATIONAL BEM

The BEM combined with linear-quadratic programming for variables defined on Γ_C provides an efficient numerical solution to the above problem as all nonlinear effects are exclusively located on Γ_C . BEM standardly uses a fundamental solution, which is quite simple in the static case of a homogeneous isotropic elastic material considered. Yet, we have to calculate the viscoelastic modification and here we benefit from choosing the ansatz of the tensor of viscous moduli as simply proportional to the elastic moduli, i.e. $\chi \mathbb{C}$. Therefore we can use the BEM with the same fundamental solution as in the static case for a new variable $v_\tau^k := u_\tau^k + \chi(u_\tau^k - u_\tau^{k-1})/\tau$. Then, in terms of this new variable, one obviously has the Kelvin-Voigt strain $\epsilon_\tau^k = e(v_\tau^k)$, the velocity $(u_\tau^k - u_\tau^{k-1})/\tau = (v_\tau^k - u_\tau^{k-1})/(\tau + \chi)$, and the displacement $u_\tau^k = (\tau v_\tau^k + \chi u_\tau^{k-1})/(\tau + \chi)$, which is to be used in the time discretized system of equation of motion. Then, like in (5), one constructs the corresponding minimization problems in terms of (v_τ^k, z_τ^k) . The evaluation of the energy balance (7) in terms of v is possible at least approximately.

5. NUMERICAL EXAMPLE

We demonstrate applicability of the current methodology to a nontrivial problem where the defect measure μ is unknown and non-uniformly distributed in space. The hard-device loading is given by $w_D(t) = v_D t$ with $|v_D| = 333.3 \mu\text{m/s}$, Fig. 1. The bulk's elasticity modulus is $E=70\text{GPa}$ and the Poisson ratio $\nu=0.35$, while we consider $\mathbb{K} = \text{diag}(K_n, K_t)$ with $K_n = 150 \text{ GPa/m}$ and $K_t = 75 \text{ GPa/m}$, and the fracture toughness $\alpha = 187.5 \text{ J/m}^2$. We use $\chi = 0.01\text{s}$ and a time step $\tau = 5 \times 10^{-3}\text{s}$, for the calculations.

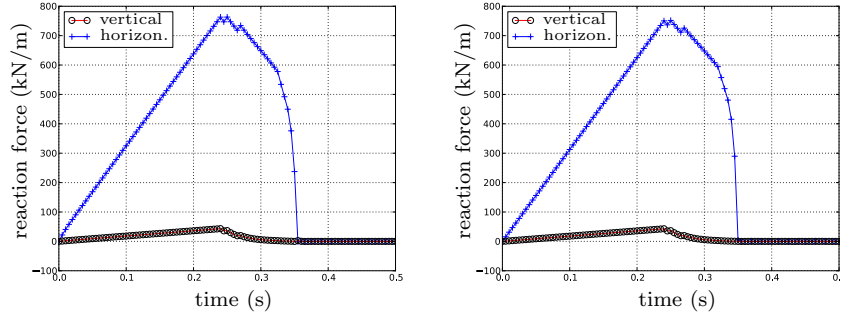


FIGURE 3. Vertical and horizontal components of the reaction force on the Dirichlet loading for small viscosity $\chi = 0.01s$ and energy well preserved (left) compared with the inviscid solution calculated by a semi-implicit method but with the energy balance completely violated (right).

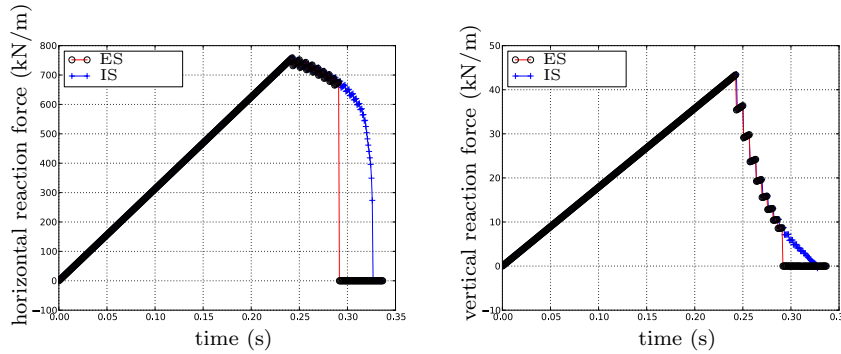


FIGURE 4. Horizontal and vertical components of reaction force with time for the energetic solution approximation (ES) and direct calculation of the inviscid solution approximation (IS).

Fig. 2 displays the overall dissipation, at the time of total rupture ($t = 0.36s$), which approximates the total variation of the defect measure $\int_0^t [\mu(\cdot, x)](dt)$ as a function of x . It is not surprising that the dissipated energy is bigger in the right-hand part of the specimen which is particularly stretched during the delamination. Noteworthy this energy is not localized along Γ_C .

Fig. 3(left) displays the force response $t \mapsto \int_{\Gamma_D} \mathbf{t}(\epsilon(u, \dot{u}))(t, x) \mathbf{d}S$. A comparison with the force response obtained by the simplified inviscid algorithm, using a semi-implicit method but energy balance completely violated, see Fig. 3(right), gives a surprisingly excellent match.

Now, the results obtained by the inviscid case of the above example are compared with those computed for the same configuration utilizing similar algorithms based on the concept of energetic solutions [6]. Here, for both calculations a finer time step $\tau = 8.33 \times 10^{-4}$ s is used. Fig. 4 shows that actually the simplified inviscid solution approximation (IS) avoids the early rupture presented in the energetic solution approximation (ES). In principle, our semi-implicit time discretisation works for $\chi = 0$, too. Actually, solving directly the inviscid problem is algorithmically much simpler. Yet, we cannot expect reasonable results if χ will converge to 0 too fast with respect to τ , and in particular if straight $\chi = 0$ would be used [9]. The stress-driven rupture seems to be much more natural than the energy-driven one (especially if a large bulk would lead to an extremely early delamination). From the numerical results for the computed reaction forces in time obtained by the respective approximations it may be observed that a too early rupture present in the energetic solution is avoided by using the simplified inviscid algorithm. Note that these two variants of approximations might also be seen as a discussion on global versus local minimization in mathematical literature [11, 12].

Christos G. Panagiotopoulos, Vladislav Mantič

Group of Elasticity and Strength of Materials, Department of Continuum Mechanics,
School of Engineering, University of Seville, Seville, ES-41092, Spain
cpanagiotopoulos@us.es, mantic@us.es

Tomáš Roubíček

Mathematical Institute, Charles University, Prague, CZ-18675, Czech Republic, and In-
stitute of Thermomechanics of the ASCR, Prague, CZ-18200, Czech Republic
tomas.roubicek@mff.cuni.cz

REFERENCES

- [1] M. Kočvara, A. Mielke, and T. Roubíček. A Rate-Independent Approach to the Delamination Problem. *Math. Mechanics Solids*, 11:423-447, 2006.
- [2] A. Mielke and T. Roubíček. Numerical Approaches to Rate-Independent Processes and Applications in Inelasticity. *Math. Model. Numer. Anal. (M2AN)*, 43:399-428, 2009.
- [3] T. Roubíček, L. Scardia, and C. Zanini. Quasistatic Delamination Problem. *Continuum Mechanics and Thermodynamics*, 21:223-235, 2009.
- [4] T. Roubíček, M. Kružík and J. Zeman. Delamination and Adhesive Contact Models and Their Mathematical Analysis and Numerical Treatment. In *Math. Methods & Models in Composites*, Chap. 9. (V. Mantič, ed.), Imperial College Press, London, 2013.
- [5] T. Roubíček, V. Mantič and C.G. Panagiotopoulos. A Quasistatic Mixed-Mode Delamination Model. *Discrete and Continuous Dynamical Systems Series S*, 6:591-610, 2013.
- [6] C.G. Panagiotopoulos, V. Mantič and T. Roubíček. BEM Solution of Delamination Problems Using an Interface Damage and Plasticity Model. *Comput. Mech.* (submitted).
- [7] A. Mielke, T. Roubíček, and J. Zeman. Complete Damage in Elastic and Viscoelastic Media and its Energetics. *Computer Methods Appl. Mech. Engr.*, 199:1242-1253, 2009.
- [8] T. Roubíček. Adhesive Contact of Visco-Elastic Bodies and Defect Measures Arising by Vanishing Viscosity. *SIAM J. Math. Anal.* (to appear).

-
- [9] T. Roubíček, C.G. Panagiotopoulos and V. Mantič. Quasistatic Adhesive Contact of Visco-Elastic Bodies and its Numerical Treatment for Very Small Viscosity. *ZAMM – Zeitschrift für Angewandte Mathematik und Mechanik* (submitted).
 - [10] M. Frémond. Dissipation dans l'adhérence des solides. *Comptes rendus de l'Académie des sciences. Série 2*, 300:709-714, 1985.
 - [11] M. Charlotte, G. Francfort, J.-J. Marigo and L. Truskinovsky. Revisiting Brittle Fracture as an Energy Minimization Problem: Comparison of Griffith and Barenblatt Surface Energy Models. In *Continuous Damage and Fracture* (A. Cachan, ed.), Elsevier, Paris, 2000.
 - [12] U. Stefanelli. A Variational Characterization of Rate-independent Evolution. *Math. Nach.*, 282:1492-1512, 2009.

Iso-geometric Boundary Element Methods for Tunneling

BENJAMIN MARUSSIG

(joint work with Christian Duenser, Gernot Beer)

Since the first book [1] published in 2009 iso-geometric methods have gained increasing popularity. The term iso-geometric is supposed to convey that the same (=iso) NURBS functions (-geometric) as they are used in CAD programs are used for the description of the geometry as well as for the variation of the unknown. This is expected to shortcut the way from the problem definition to the results of the simulation, basically eliminating the need for mesh generation. In this paper a variation of the iso-geometric concept will be presented where different functions are used for the description of the geometry and the variation of the unknowns. The motivation comes from tunneling, because the cross-section of a tunnel can be described exactly with a few NURBS curves.

1. NURBS (NON-UNIFORM RATIONAL B-SPLINES)

1.1. Basis function. NURBS are generalizations of B-splines and B-spline basis functions $N_{i,p}$ are defined by a *knot vector* Ξ , which is a non-decreasing sequence of coordinates in the parametric space u . The coordinates u_i themselves are called *knots* and the half-open interval $[u_i, u_{i+1})$ is called the *ith knot span*. The basis functions $N_{i,p}$ are defined recursively, starting with piecewise constant ($p = 0$) function, where the support of each $N_{i,0}$ is contained in the *ith knot span*.

$$(1) \quad N_{i,0}(u) = \begin{cases} 1 & \text{if } u_i \leq u < u_{i+1} \\ 0 & \text{otherwise} \end{cases}$$

Higher order basis functions ($p = 1, 2, 3, \dots$) are defined by

$$(2) \quad N_{i,p}(u) = \frac{u - u_i}{u_{i+p} - u_i} \cdot N_{i,p-1}(u) + \frac{u_{i+p+1} - u}{u_{i+p+1} - u_{i+1}} \cdot N_{i+1,p-1}(u)$$

which is basically a linear combination of basis functions of the previous order ($p - 1$). Therefore the support of each $N_{i,p}$ is no longer contained in only one, but all knot spans of its previous basis functions, $[u_i, u_{i+p+1})$. Basis functions usually have $p - 1$ continuous derivatives, but if a knot u_j is repeated k times within their interval, the number of continuous derivatives at u_j decreases by k . An example for basis functions and the influence of repeated knots is shown in Figure 1. Note that each basis function is non-negative and has local supports. The sum of all basis functions at a specific coordinate u is always 1. The knot vector is made of $N + p + 1$ components, where N is the total number of basis functions ($n + 1$).

B-spline *curves* are build by a linear combination of given basis functions,

$$(3) \quad C(u) = \sum_{i=0}^n N_{i,p}(u) \cdot B_i$$

where the corresponding coefficients B_i are called *control points*. They affect the shape of the curve in some way, depending on the corresponding basis function $N_{i,p}$, as illustrated in Figure 2. For instance, if $N_{i,p}$ is interpolatory the control

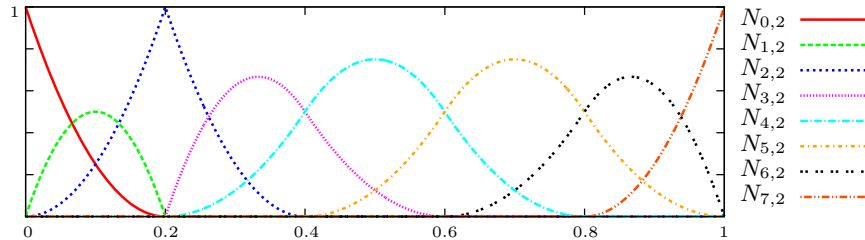


FIGURE 1. Basis functions for a non-uniform knot vector $\Xi = \{0, 0, 0, 0.2, 0.2, 0.4, 0.6, 0.8, 1, 1, 1\}$.

point is on the curve and determines the position of this knot in the physical space, just like nodal coordinates in conventional analysis. In all other cases the control points attract the curve, but do not lie on it. Hence there is no concrete physical interpretation of their values.

The definition of a NURBS curve is exactly the same as for a B-spline curve. But as the name implies, the NURBS basis functions are piecewise rational functions, based on B-splines and in general, the knot vectors of these B-splines can be non-uniform. NURBS basis functions are given by

$$(4) \quad R_{i,p}(u) = \frac{N_{i,p}(u) \cdot w_i}{\sum_{j=0}^n N_{j,p}(u) \cdot w_j} = \frac{N_{i,p}(u) \cdot w_i}{W(u)}$$

where w_i refers to the i th weight, which is associated to the control point B_i . The dominator is called *weighting function* $W(u)$. Basically $R_{i,p}$ is a modification of $N_{i,p}$ and both are identical if all weights are set equal to 1. But because of the weights w_i the influence of a specific $R_{i,p}$ can be modified. Thus, a multitude of very common objects in engineering design, like conic sections, can be described exactly.

1.2. Refinement. There are two mechanism to refine the basis of a NURBS curve, thereby the NURBS curve itself does not change neither geometrically nor parametrically. Both expand a given knot vector Ξ to an *extended knot vector* $\setminus\Xi$, such that $\Xi \subset \setminus\Xi$. Based on $\setminus\Xi$ new basis functions $\setminus R_{i,p}$ are defined.

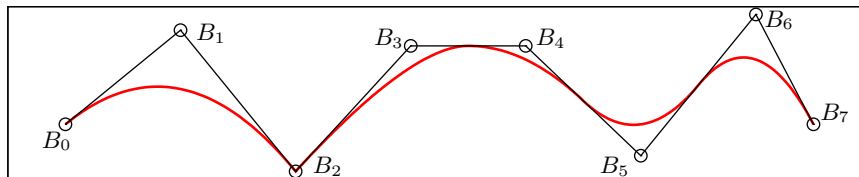


FIGURE 2. B-spline curve build by a set of control points B_i and the basis function $N_{i,2}$ of Figure 1.

The first mechanism is called *knot insertion*. Thus new knots are inserted into the knot vector. The new control points $\setminus B_i$ and weights $\setminus w_i$ are a linear combination of the original control points B_i and their weights w_i .

Order elevation is the other mechanism. To elevate the order by k the existing knots are replicated k times. For the computation of the new control points $\setminus B_i$ and weights $\setminus w_i$ it is proposed by Piegl and Tiller [4] to perform the order elevation in the following steps. First subdivide the NURBS curve into Bézier segments¹ by knot insertion, second order elevate these segments, third combine them afterwards again to get the NURBS curve again.

2. ISOGEOMETRIC BOUNDARY ELEMENT METHOD

This section focuses on two dimensional elasticity problems, but the explanations are equally valid for the three dimensional case. The boundary integral equation for an elastic continuum can be written as (Beer et al. [6])

$$(5) \quad \mathbf{c}(P) \cdot \mathbf{u}(P) = \int_S \mathbf{U}(P, Q) \cdot \mathbf{t}(Q) dS - \int_S \mathbf{T}(P, Q) \cdot \mathbf{u}(Q) dS$$

where P is the source point and Q is the field point on the boundary S . The coefficient $\mathbf{c}(P)$ is a free term related to the boundary geometry. $\mathbf{u}(Q)$ and $\mathbf{t}(Q)$ are the displacements and tractions on the boundary and $\mathbf{U}(P, Q)$ and $\mathbf{T}(P, Q)$ are matrices containing Kelvin's fundamental solutions (*Kernels*) for the displacements and tractions, respectively.

2.1. Discretisation. As mentioned before, unlike the conventional Boundary Element Method the isogeometric concept uses NURBS curves for the representation of the elements geometry $\mathbf{x}(u)$.

$$(6) \quad \mathbf{x}(u) = \sum_{i=0}^n R_{i,p}(u) \cdot B_i$$

Regarding to tunneling problems the geometry is usually described by arcs, which can exactly represented by simple NURBS curves. However these NURBS curves may not able to sufficiently describe the displacements and tractions. Because the geometry is already exactly defined we propose to only refine the basis of the variation of the unknowns. So the representation of the elements traction $\mathbf{t}^e(u)$ and displacement $\mathbf{u}^e(u)$ is

$$(7) \quad \mathbf{t}^e(u) = \sum_{i=0}^{\setminus n} \setminus R_{i,p}(u) \cdot \mathbf{q}_i^e, \quad \mathbf{u}^e(u) = \sum_{i=0}^{\setminus n} \setminus R_{i,p}(u) \cdot \mathbf{d}_i^e \quad n < \setminus n$$

The extended basis functions $\setminus R_{i,p}$ are the basis functions $R_{i,p}$ refined by knot insertion, order elevation or both. \mathbf{q}_i^e and \mathbf{d}_i^e are coefficients that arise from the refinement procedure. These coefficients have the same characteristics as the control points $\setminus B_i$ of a refined NURBS curve. Hence, they have to be considered as control points for the description of \mathbf{t}^e and \mathbf{u}^e , respectively, but do not correspond

¹The curve becomes interpolatory at every knot value u_i .

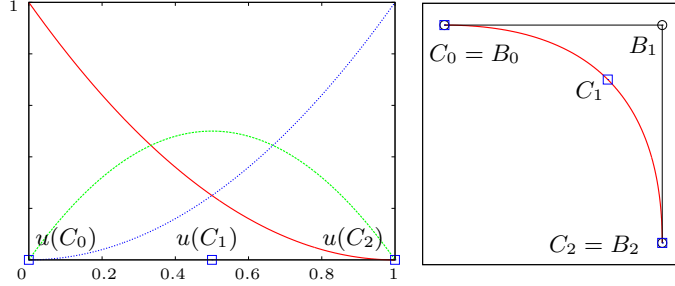


FIGURE 3. Collocation points C_i in the parametric and physical space for $\Xi = \{0, 0, 0, 1, 1, 1\}$.

to physical values, unless the basis function $\setminus R_{i,p}$ is interpolatory. The discretized integral equation (5) can now be written as

$$(8) \quad \mathbf{c}(P_a) \sum_{i=0}^{\setminus n} \setminus R_{i,p}(u(P_a)) \cdot \mathbf{d}_i^{ec} = \sum_{e=1}^E \sum_{i=0}^{\setminus n} \left(\int_{S_e} \mathbf{U}(P_a, Q) \cdot \setminus R_{i,p} dS \right) \cdot \mathbf{q}_i^e - \sum_{e=1}^E \sum_{i=0}^{\setminus n} \left(\int_{S_e} \mathbf{T}(P_a, Q) \cdot \setminus R_{i,p} dS \right) \cdot \mathbf{d}_i^e \quad \text{for } a = 0, 1, 2, \dots, \setminus n$$

where ec indicates the element where the collocation point resides and E is the number of elements. Note that the free term \mathbf{c} not only occurs in the diagonal of \mathbf{T} but, if the collocation point does not coincide with a control points, also occurs off the diagonal.

Due to the fact that the control points may not lie on the element or rather on the boundary, the collocation points C_i do not coincide with the control point, as shown in Figure 3. Thus, their coordinates have to be computed. According to Kang Li et al. [5], the best numerical accuracy and robustness is given by the Greville abscissae scheme, which defines the coordinates within the parametric space as

$$(9) \quad u(C_i) = \frac{u_{i+1} + u_{i+2} + \dots + u_{i+p}}{p} \quad i = 0, 1, \dots, n$$

2.2. Boundary Condition. Considering a pure Neumann problem the tractions over the boundary are known. For excavation problems they are computed directly related to the outward normal \mathbf{n}

$$(10) \quad \mathbf{t} = \sigma_0 \cdot \mathbf{n}$$

where σ_0 is the virgin stress tensor.

Or by computing the corresponding control parameters \mathbf{q}_i^e by

$$(11) \quad [\mathbf{R}]^{-1} \{\mathbf{t}^e\} = \{\mathbf{q}^e\}$$

3. TEST EXAMPLE

In a two-dimensional example, we present the isogeometric Boundary Element Method for an excavation of a NATM tunnel in an infinite domain, subjected to a vertical compressive virgin stress p of magnitude 1.0 MPa. The material properties are $E = 10\,000$ MPa and $\nu = 0,0$. The reference solution is calculated using a conventional iso-parametric analysis with 62 quadratic boundary elements.

The half of the tunnel is described by three arcs. Therefore we assume a description of the geometry with only one NURBS curve per arc as illustrated in Figure 4. Quadratic NURBS basis functions ($p=2$) are used and the associated knot vectors are $\Xi_i = \{0, 0, 0, 1, 1, 1\}$.

Knot insertion as well as order elevation was used to enrich the basis of the variation of the unknowns. Figure 5 shows the deformed shape of the tunnel after the excavation and the corresponding values for the displacements in y -direction after the first order elevation ($p=3$).

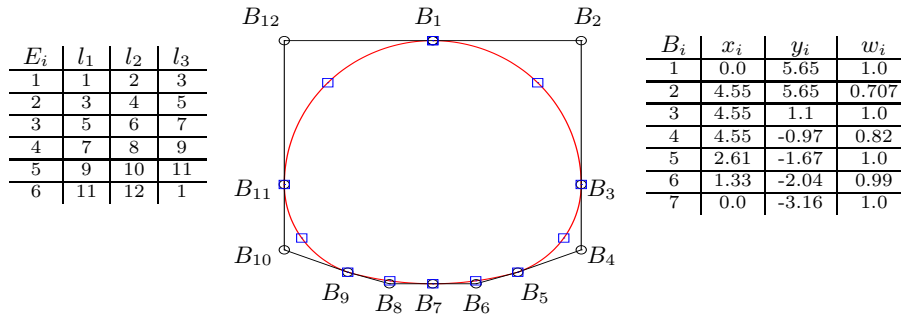


FIGURE 4. Element connectivity l and geometrical details.

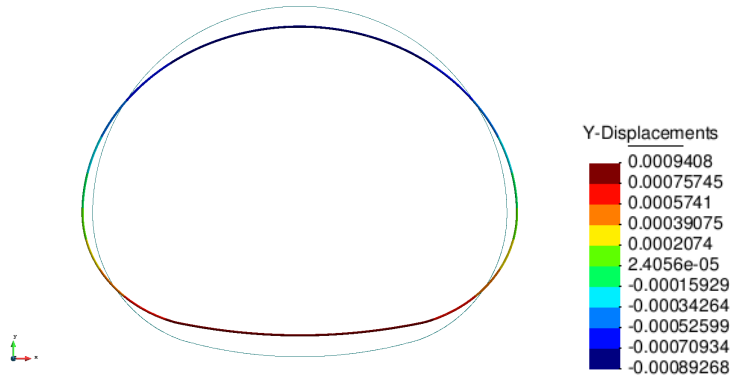


FIGURE 5. Displacements along the boundary using cubic NURBS basis functions.

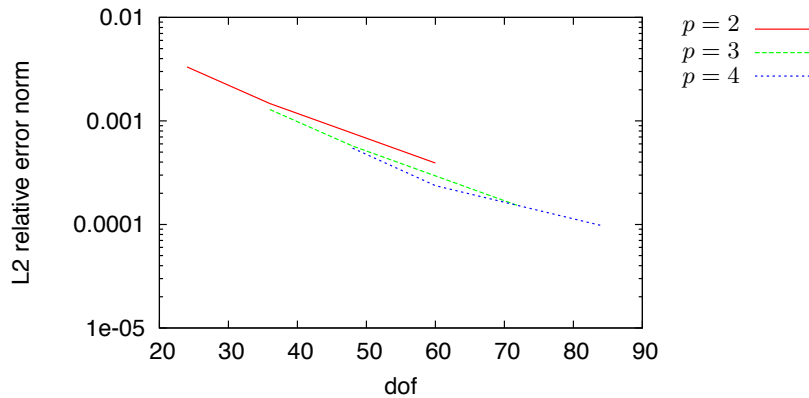


FIGURE 6. Error of the displacements measured in the L^2 -norm.

For a comparison with the reference solution the relative error of the displacements around the boundary measured in the L^2 -norm was taken. In Figure 6 all results related to the used order p are represented in a line.

4. ACKNOWLEDGMENTS

The work reported here is supported by the Austrian Science Fund FWF (Project no. 24974).

Benjamin Marussig

Institute for Structural Analysis, TU Graz
marussig@tugraz.at

Christian Duenser

Institute for Structural Analysis, TU Graz
duenser@tugraz.at

Gernot Beer

Institute for Structural Analysis, TU Graz and University of Newcastle, Australia
gernot.beer@tugraz.at

REFERENCES

- [1] J.A. COTTRELL, T.J.R. HUGES AND Y. BAZILEVS., *Isogeometric Analysis: Toward Integration of CAD and FEA*, Wiley, Chichester, UK, 2009.
- [2] R.N. SIMPSON, S.P.A. BORDAS, J. TREVELYAN , T. RABCZUK, *A two-dimensional isogeometric boundary element method for elastostatic analysis*, Computer Methods in Applied Mechanics and Engineering , 209 – 212: 87–100, 2012.
- [3] G. BEER, B. MARUSSIG, *Super-geometric Boundary Element Method, Part 1: Plane problems*, in preparation.
- [4] L. PIEGL, W. TILLER., *The NURBS Book (Monographs in Visual Communication)*, Second ed., Springer New York, 1997.

- [5] L. KANG, Q. XIAOPING, *Isogeometric analysis and shape optimization via boundary integral*, *Computer-Aided Design* 43, pages 1427–1437, 2011.
- [6] G. BEER, I. SMITH AND C. DUENSER, *The Boundary Element Method with programming*, Springer Wien New York, 2008.

Generalized Maxwell's Methodology for Evaluating the Effective Properties of Orthotropic Composites

SOFIA G. MOGILEVSKAYA

(joint work with Steven L. Crouch, Henryk K. Stolarski)

This talk describes an application of the generalized Maxwell's methodology to evaluation of the effective properties of fiber-reinforced composites that exhibit the overall orthotropic behavior. It is assumed that the effective properties of the materials can be deduced from the comparison of the far-field asymptotics of the elastic fields due to a representative cluster of fibers, or pores embedded in an infinite matrix and subjected to far-field loads with those due to a cylindrical orthotropic inhomogeneity with the effective properties to be found. Contrary to the classical Maxwell's approach, the interactions between all the constituents in the cluster that represent the material in question are precisely accounted for (using the BEM technique), which allows to capture the microstructure induced anisotropy. Comparison of the numerical results obtained by the proposed approach with those available in the literature for the materials with periodic structure exposes its accuracy and efficiency.

The work is an extension of the previous studies by the same authors related to isotropic and transversely isotropic composite materials. **Keywords:** Integral equations, composite materials

Sofia G. Mogilevskaya, Steven L. Crouch, Henryk K. Stolarski

College of Science and Engineering, University of Minnesota, 500 Pillsbury Drive S.E., Minneapolis 55455, USA

mogil003@umn.edu, crouch@umn.edu, stola001@umn.edu

REFERENCES

- [1] C. Maxwell. *Treatise on Electricity and Magnetism*, Clarendon Press, Oxford (1st edn. 1873), 3rd edn, 1892.
- [2] S.G. Mogilevskaya, and S.L. Crouch. Combining Maxwell's methodology with the BEM for evaluating the two-dimensional effective properties of composite and micro-cracked materials *Computational Mechanics*, DOI 10.1007/s00466-012-0735-5, 2012.
- [3] [S.G. Mogilevskaya, H.K. Stolarski, S.L. Crouch. On Maxwell's concept of equivalent inhomogeneity: when do the interactions matter? *Journal of the Mechanics and Physics of Solids*, 60:391-417, 2012.
- [4] [S.G. Mogilevskaya, V.I. Kushch, O. Koroteeva, and S.L. Crouch. Equivalent inhomogeneity method for evaluating the effective conductivities of isotropic particulate composites. *Journal of Mechanics of Materials and Structures*, 7:103-117, 2012.
- [5] [A.V. Pyatigorets, and S.G. Mogilevskaya. Evaluation of effective transverse mechanical properties of isotropic viscoelastic composite materials. *Journal of Composite Materials*, 45:2641-2658, 2011.
- [6] [O. Koroteeva, S.G. Mogilevskaya, S.L. Crouch, and E. Gordeliy. A computational technique for evaluating the effective thermal conductivity of isotropic porous materials. *Engineering Analysis with Boundary Elements*, 34:793-801, 2010.

Boundary Element Methods for Electrostatic Field Problems with Floating Potentials

GÜNTHER OF

(joint work with Dominic Amann, Andreas Blaszczyk, Olaf Steinbach)

For the solution of electrostatic field problems we discuss several boundary integral formulations. In particular, we present and compare two approaches on how to handle floating potentials, i.e., domains in which the potential has a constant but unknown value.

The first approach is to treat the floating potential as a dielectricum with a very high relative permittivity. Thus one achieves an approximation of the potential which is almost constant.

The second approach is a saddle point formulation which includes the unknown constant value of the potential in the floating domain as an Lagrangian multiplier into the formulation. As constraint the flux over the boundary of the floating potential has to vanish.

For both approaches an indirect formulation using the single layer potential and a Steklov–Poincaré interface formulation are considered. The strengths and weaknesses of the presented formulations are demonstrated for several numerical examples. Besides academic examples, real life problems like transformers are presented.

Keywords: boundary element method, electrostatic field problems, floating potential

Mathematics Subject Classifications (2000): 65N38

Dominic Amann, Günther Of, Olaf Steinbach

Institute of Computational Mathematics, Graz University of Technology, Steyrergasse 30, 8010 Graz, Austria

dominic.amann@student.tugraz.at, of@tugraz.at, o.steinbach@tugraz.at

Andreas Blaszczyk

Corporate Research, ABB Switzerland Ltd., CH 5405 Baden–Dättwil, Switzerland

andreas.blaszczyk@ch.abb.com

Fast boundary element analysis for 3D magneto-electro-elastic bimaterial

ERNIAN PAN

(joint work with Yanfei Zhao)

Magneto-electro-elastic (MEE) materials are widely used in smart structures and nano-electromechanical systems due to their extraordinary mechanical-electromagnetic coupling properties. Several numerical methods including FEM and BEM have been developed to investigate MEE. However, few studies can be found in the existing literature about the BEM analysis of 3D MEE bimaterial under general extended loading over a circular area.

On the other side, fast BEMs such as fast multipole method or adaptive cross-approximation (ACA) approach have been used to efficiently reduce the computing operations and memory requirements for solving various engineering problems using BEM. However, the existing fast BEMs have been mainly applied to elastic problems and its application to inhomogeneous MEE materials in 3D has not been achieved yet. Therefore, it is of significant and interesting research in developing the most efficient fast BEM for the 3D inhomogeneous MEE materials.

A 3D fast boundary element analysis of MEE bimaterial is presented in the study. First, the analytical solutions or fundamental solutions are derived in 3D anisotropic MEE bimaterial space subject to different extended dislocation or traction distributions within a horizontal circular area by virtue of the Stroh formalism and Fourier transformation. The final expressions are in elegant line integral and can be reduced to various simpler cases. Then, the obtained BIEs are calculated by fast multipole method or ACA approach. The results from the proposed fast BEMs are compared with the analytical ones to show the accuracy and efficiency of the new algorithm. The study will provide an important basis for further research in fast BEM with applications to MEE materials, and could be extended to the multi-layered and multi-domain inhomogeneous MEE materials or composites.

Keywords: BEM, Fast multipole method, ACA, Magneto-electro-elastic, 3D, Bimaterial, Dislocation, Traction, Circular area, BIE.

Ernian Pan, Yanfei Zhao

Department of Civil Engineering, University of Akron, Akron, OH, 44325-3905, USA
pan2@uakron.edu, yz50@zips.uakron.edu

REFERENCES

- [1] F. Maerten. Adaptive cross-approximation applied to the solution of system of equations and post-processing for 3D elastostatic problems using the boundary element method. *Engineering Analysis with Boundary Elements*, 34: 483-491, 2010.
- [2] M. S. Bapat and Y. J. Liu. A new adaptive algorithm for the fast multipole boundary element method. *CMES*, 58(2): 161-183, 2010.
- [3] X. Zhu, Z. Huang et al (2010): Fast multipole boundary element analysis for 3D 2D problems of magneto-electro-elastic media, *Eng. Anal. Bound. Elem.* **34**:927-933.[3] place1. Benedetti,

- M. H. Aliabadi and A. Milazzo. A fast BEM for the analysis of damaged structures with bonded piezoelectric sensors. *Comput. Meth. Appl. Mech. Engrg.* 199: 490-501, 2010.
- [4] I. Benedetti, A. Milazzo and M. H. Aliabadi. A fast dual boundary element method for 3D anisotropic crack problems. *Int. J. Numer. Meth. Engrng*, 80: 1356-1378, 2009.
- [5] Y. J. Liu. (2008): A fast multipole boundary element method for 2D multi-domain elastostatic problems based on a dual BIE formulation., *Comput. Mech.* 42: 761-773, 2008..
- [6] M. S. Bapat, Y. J. Liu (2010): A new adaptive algorithm for the fast multipole boundary element method, CMES, Vol. **58**, No. **2**: 161-183.
- [7] E. Pan and F. G. Yuan. Three-dimensional Green's functions in anisotropic piezoelectric bimetals. *International Journal of Engineering Science*, 38: 1939-1960, 2000.

**DPG method with optimal test functions for hypersingular operators
in two dimensions**

FELIPE PINOCHET

(joint work with Norbert Heuer)

The discontinuous Petrov-Galerkin (DPG) method with optimal test functions is known to deliver the best approximation in the energy norm, see [1] for standard elliptic boundary value problems. The method has several advantages, among them the possibility to calculate the error rather than estimating it (up to the approximation of the so-called trial-to-test operator). In this way, reliability and efficiency of error estimators is not an issue and adaptivity can be implemented in a natural way.

In this talk we present a first study of the DPG method with optimal test functions for the approximation of solutions to hypersingular boundary integral equations, governing the Laplacian in two dimensions. We present the underlying ultra-weak variational formulation (which gives rise to an approximation in L^2 rather than $H^{1/2}$) and show numerical results that confirm the expected performance of the method.

Support by FONDECYT project 1110324 and CONICYT project Anillo ACT1118 (ANANUM) is gratefully acknowledged.

Keywords: DPG method, boundary elements, hypersingular operator

Norbert Heuer

Facultad de Matemáticas, Pontificia Universidad Católica de Chile, Santiago, Chile
nheuer@mat.puc.cl

Felipe Pinochet

Facultad de Ingeniería, Pontificia Universidad Católica de Chile, Santiago, Chile
fipinoch@gmail.com

REFERENCES

- [1] L. Demkowicz, J. Gopalakrishnan. Analysis of the DPG method for the Poisson problem. *SIAM Journal on Numerical Analysis*, 49 (5), 1788–1809, 2011.

Black-Box Preconditioning of BEM matrices by \mathcal{H} -matrix techniques

DIRK PRAETORIUS

(joint work with Markus Faustmann, Jens Markus Melenk)

The matrices arising in BEM are dense. Various compression techniques such as \mathcal{H} -matrices have been developed in the past to store the BEM matrices and realize the matrix-vector-multiplication with log-linear (or even linear) complexity. One particular strength of \mathcal{H} -matrices is that the \mathcal{H} -format includes some arithmetics that provides the (approximate) inversion, (approximate) LU-decomposition etc. In particular, it thus allows for black-box preconditioning of the BEM systems in iterative solvers. Numerically it has been observed that such an approach works well in practice [2, 5]. In our talk, we give a mathematical underpinning to these observations: We establish that the \mathcal{H} -matrix format is rich enough to permit good approximations of BEM inverses.

As a model problem, we take the lowest-order Galerkin matrix \mathbf{V} for the simple-layer potential V of the 3D Laplacian on quasi-uniform meshes on polyhedral boundaries. The cluster tree is generated using the standard admissibility condition. For the resulting \mathcal{H} -matrix format, which is also used for the \mathcal{H} -approximation of \mathbf{V} , we show that \mathbf{V}^{-1} can be approximated at an exponential rate in the block rank.

The question of approximating the inverses of system matrices in the \mathcal{H} -format by approximate \mathcal{H} -inversion or \mathcal{H} -LU factorization has previously only been studied in the context of FEM [1, 3, 4]. The present analysis differs from these works in some of the techniques employed. The most important outcome of this shift in tools is that we are able to work in a fully discrete setting and can show exponential convergence in the block rank; the previous techniques relied on an approximation on the continuous level and involved a projection step, which entails errors related to the mesh size h .

Keywords: Boundary element method, hierarchical matrices, preconditioning

Mathematics Subject Classifications (2000): 65F05, 65N30, 65N38

Markus Faustmann, Jens Markus Melenk, Dirk Praetorius

Institute for Analysis and Scientific Computing, Vienna University of Technology

Markus.Faustmann@tuwien.ac.at, Melenk@tuwien.ac.at, Dirk.Praetorius@tuwien.ac.at

REFERENCES

- [1] M. Bebendorf and W. Hackbusch. Existence of \mathcal{H} -matrix approximants to the inverse FE-matrix of elliptic operators with L^∞ -coefficients. *Numerische Mathematik*, 95:1–28, 2003.
- [2] M. Bebendorf. Hierarchical LU decomposition based preconditioners for BEM. *Computing*, 74:225–247, 2005.
- [3] M. Bebendorf. Why finite element discretizations can be factored by triangular hierarchical matrices. *SIAM Journal on Numerical Analysis*, 45:1472–1494, 2007.
- [4] S. Börm. Approximation of solution operators of elliptic partial differential equations by \mathcal{H} - and \mathcal{H}^2 -matrices. *Numerische Mathematik*, 115:165–193, 2010.

- [5] L. Grasedyck. Adaptive Recompression of \mathcal{H} -matrices for BEM. *Computing*, 74:205–223, 2005.

**Multiple Traces Boundary Integral Formulation for Helmholtz
Transmission Problems with screens**

SERGIO ROJAS

(joint work with Carlos Jerez-Hanckes, Ralf Hiptmair)

The local Multiple Traces Method (MTF) was first presented in [1] for the Helmholtz transmission problem and relies on local traces on subdomains and weak enforcement of transmission conditions. The variational formulation is set in Cartesian products of standard Dirichlet and special Neumann traces for which restriction and extension by zero are well defined. We develop extend the MTF to account for the presence of screens at some of the interfaces of the penetrable object. We show uniqueness of solutions, continuity and coercivity of the formulation in *ad hoc* functional spaces and we develop numerical experiments to confirm the efficacy of the method.

Keywords: Helmholtz equation, boundary integral equations, transmission problems, multi-trace formulations

Sergio Rojas, Carlos Jerez-Hanckes

School of Engineering, Pontificia Universidad Católica de Chile, Santiago, Chile
sarojas@uc.cl, cjerez@ing.puc.cl

Ralf Hiptmair

SAM, ETH Zurich
ralf.hiptmair@sam.math.ethz.ch

REFERENCES

- [1] R. Hiptmair, and C. Jerez-Hanckes. Multiple traces boundary integral formulation for Helmholtz transmission problems. *Adv. Comput. Math.*, 37 (2012), no. 1, 3991.

Recent advances in modeling time dependent problems via boundary elements

A. SALVADORI

(joint work with A. Temponi, F. Valvona)

The present note aims at showing recent developments carried out at the Ce.Si.A., that may be of interest for the scientific international community. The work concerns hyperbolic problems involving 3D scalar fields (scalar wave problems) and 3D elastodynamics modeled by integral equations and numerically approximated via Boundary Element Methods.

Space-time collocation schemes as well as energetic weak forms are considered. Space discretization is made of trapezoidal (flat) tessellation of the boundary, adopting polynomial test and shape functions of arbitrary degree. Time marching schemes make use of polynomial test and shape functions of arbitrary degree in time. Analytical integrations in time and space, wave front approximation, implementation details are depicted.

In addition, we discuss some preliminary results concerning infinite elements, useful for the modeling of an half-space, and special elements for 3D fracture mechanics, necessary to obtain an accurate evaluation of SIFs and Tstress. Actual features and future developments of this topics, related to wave propagation, are presented.

Some numerical results pertaining to simple benchmark tests are also shown.

Keywords: Integral equations, time dependent problems, infinite elements, fracture mechanics.

Mathematics Subject Classifications (2000): 45E10 - Integral equations of the convolution type, 74H15 - Numerical approximation of solutions of Dynamical Problems, 74S15 - Boundary element methods.

Salvadori A., Temponi A.

Ce.Si.A. - University of Brescia, Italy

alberto.salvadori@ing.unibs.it, alessandro.temponi@ing.unibs.it

Valvona F.

Faculty of Architecture, University of Chieti-Pescara, Italy

f.valvona@unich.it

News from the Single Layer Potential for the Transient Stokes Problem

FRANCISCO-JAVIER SAYAS

(joint work with Constantin Bacuta, George C Hsiao)

The aim of this work is the development of a complete theory for the single layer potential (and the associated single layer operator) for the Stokes problem in transient regime, on general Lipschitz curves/surfaces in two/three dimensions. This includes a careful variational analysis of transmission problems for the Brinkman equation, which is the resolvent equation for the Stokes problem. We will also deal with semidiscretization in space with Galerkin methods and will analyze the resulting semidiscrete operator. Finally, we will give error estimates for the fully discrete method that uses Galerkin-BEM in space and Convolution Quadrature in time.

Keywords: Stokes problem, Convolution Quadrature, Galerkin method

Mathematics Subject Classifications (2000): 65R20, 65M38

Constantin Bacuta, George C Hsiao, Francisco-Javier Sayas

University of Delaware

bacuta@math.udel.edu, hsiao@math.udel.edu, fjsayas@math.udel.edu

REFERENCES

- [1] R. Bürger, K.H. Karlsen, and J.D. Towers. An Engquist-Osher-type scheme for conservation laws with discontinuous flux adapted to flux connections. *SIAM Journal on Numerical Analysis*, 47(3):1684-1712, 2009.
- [2] G.N. Gatica, A. Márquez, and S. Meddahi. A new dual-mixed finite element method for the plane linear elasticity problem with pure traction boundary conditions. *Computer Methods in Applied Mechanics and Engineering*, 197(9-12):1115-1130, 2008.
- [3] G.N. Gatica and G.C. Hsiao. *Boundary-Field Equation Methods for a Class of Nonlinear Problems*, volume 331 of *Pitman Research Notes in Mathematics Series*. Longman, 1995.
- [4] R. ADAMS, *Sobolev Spaces*, Pure and Applied Mathematics: A Series of Monographs and Textbooks, Academic Press, London, UK, 1975.
- [5] W. MCLEAN, *Strongly Elliptic Systems and Boundary Integral Equations*, Cambridge University Press, Cambridge, UK, 2000.
- [6] J.-C. NÉDÉLEC, *Acoustic and Electromagnetic Equations: Integral Representations for Harmonic Problems*, vol. 44 of Applied Mathematical Sciences, Springer-Verlag, Berlin, 2001.
- [7] S. SAUTER AND C. SCHWAB, *Randelementmethoden*, BG Teubner, Stuttgart, 2004.
- [8] O. STEINBACH, *Numerical approximation methods for elliptic boundary value problems*, Springer, New York, 2008.
- [9] T. VON PETERSDORFF, *Boundary integral equations for mixed Dirichlet, Neumann and transmission problems*, *Math. Meth. Appl. Sci.*, 11 (1989), pp. 185–213.

Time Domain BE Formulation for Partially Saturated Poroelasticity

MARTIN SCHANZ

(joint work with Peng Li)

A lot of applications, especially, in geomechanics require the computation of waves in porous media, e.g., earthquake waves in soil. Soil is a partial saturated poroelastic material which sometimes can be modelled by a saturated theory, however, sometimes a partial saturated theory is necessary. Having waves in semi-infinite domains in mind a boundary element formulation for such materials seems to be preferable.

A linear theory for partial saturated poroelasticity is formulated based on the mixture theory, resulting in a set of coupled partial differential equations for the solid displacements and the pore pressures of both fluids. For such a system fundamental solutions are derived in Laplace domain with the method of Hörmander. The integral equations can be deduced based on the weighted residual technique. A standard discretisation in the spatial variable and the convolution quadrature for time discretisation yield, finally, a time stepping procedure for dynamic processes in partial saturated poroelastic media.

The validation of this method is done with the help of a 1D semi-analytical solution for a column. Finally, waves in a poroelastic half space are studied.

1. GOVERNING EQUATIONS

For a partially saturated porous continuum, the following assumptions are made: i) the medium is a mixture of the solid phase (index s), wetting fluid phase (index w), and non-wetting phase (index a); ii) a state transformation of the three phases is not allowed; iii) all three phases have the same temperature and any temperature change is ignored; iv) all the three phases are compressible. The governing equations are stated following [4].

With an averaging process, the porosity n and the saturation degree S_f can be defined as

$$(1) \quad n = \frac{V_w + V_a}{V_s + V_w + V_a} \quad S_f = \frac{V_f}{V_s + V_w + V_a} \quad (f = w, a) \quad ,$$

where V_s , V_w and V_a represent the corresponding phase volumes. The bulk density $\rho = (1-n)\rho_s + nS_w\rho_w + nS_a\rho_a$ is the averaged density of the mixture, where ρ_s , ρ_w and ρ_a represent the density of the solid skeleton, wetting fluid and non-wetting fluid, respectively.

The capillary pressure $p^c = p^a - p^w = p^d S_e^{-1/\vartheta}$ is based on the suggestion of [3], where p^a and p^w are the pore pressure, p^d is the non-wetting fluid entry pressure, ϑ is the pore size distribution index, and S_e denotes the effective wetting fluid saturation degree. Neglecting the osmotic suction yields the total stress σ_{ij}

$$(2) \quad \sigma_{ij} = \sigma'_{ij} - \delta_{ij}\alpha(S_w p^w + S_a p^a) \quad ,$$

where $\alpha = 1 - K/K_s$ describes the compressibility of the solid skeleton with the drained bulk modulus of the mixture K , and K_s is the bulk modulus of the solid

grains. The introduction of the factor α is used to describe the compressibility of the solid grains, while $\alpha = 1$ fits to the incompressible case.

The balances of mass for the solid phase and both fluid phases are

$$(3a) \quad \partial_t[(1-n)\rho_s] + \operatorname{div}[(1-n)\rho_s \partial_t u_i] = 0$$

$$(3b) \quad \partial_t(nS_f \rho_f) + \operatorname{div}[nS_f \rho_f \partial_t(u_i + u_i^w)] = \rho_f I^f \quad (f = w, a) \quad ,$$

where u_i^f ($f = w, a$) is the relative displacement of the respective fluid to the solid. I^f ($f = w, a$) denote source terms.

The momentum balance equation for the mixture is the sum of the equations for each individual constituent, which is given by

$$(4) \quad G u_{i,jj} + \left(K + \frac{G}{3}\right) u_{j,ij} - \alpha(S_w p_{,i}^w + S_a p_{,i}^a) + F_i = \rho \partial_t^2 u_i + n S_w \rho_w \partial_t^2 u_i^w + n S_a \rho_a \partial_t^2 u_i^a \quad ,$$

where F_i denotes the bulk body force. The momentum balance equations for each fluid phase yield generalized Darcy's laws for each fluid phase

$$(5) \quad n S_f \partial_t u_i^f = -\kappa_f \left(p_{,i}^f + \rho_f \partial_t^2 u_i + \rho_f \partial_t^2 u_i^w \right) .$$

In (5), the coupling terms between the two fluids are neglected and the phase permeabilities ($f = w, a$) are given by $\kappa_f = \frac{K_{rf} k}{\eta_f}$. K_{rf} denotes the relative fluid phase permeability, k the intrinsic fluid permeability of a porous continuum, and η_f the viscosity of the fluid.

Equations (3), (4) and (5) are sufficient to solve the problem of partially saturated poroelasticity. The combination of the solid displacement u_i and the fluids pore pressure p^f ($f = w, a$) is sufficient to describe the system behavior and, hence, are selected as unknowns. In time domain, however, the elimination of the relative displacement is not possible because it appears in (3), (4) and (5) in different orders of time derivatives. Hence, the Laplace transformation is introduced to eliminate the time derivatives.

After the Laplace transformation, the relative displacements \hat{u}_i^f can be substituted, and the governing equations in the Laplace domain are obtained

$$(6) \quad \mathcal{B} [\hat{u}_i, \hat{p}^w, \hat{p}^a]^\top = [-\hat{F}_i, -\hat{I}^w, -\hat{I}^a]^\top \quad ,$$

where \mathcal{B} is the partial differential operator and its explicit expression can be found in [1].

2. FUNDAMENTAL SOLUTIONS

The fundamental solutions $\hat{\mathbf{U}} = \hat{\mathbf{U}}(\mathbf{x}, \mathbf{y})$ of a differential operator \mathcal{B} are a full space solution of the differential equations and are given by

$$(7) \quad \mathcal{B}^* \hat{\mathbf{U}} + \mathbf{I} \delta(\mathbf{x}, \mathbf{y}) = \mathbf{0} \quad ,$$

where \mathcal{B}^* is the adjoint operator of \mathcal{B} . The solution can be found following Hörmander's method. Assuming $\hat{\mathbf{U}} = \mathcal{B}^{*co} \varphi$, where \mathcal{B}^{*co} denotes the co-factors

of \mathcal{B}^* and φ is some scalar function. This leads to

$$\mathcal{B}^* \cdot \mathcal{B}^{*co} \varphi + \mathbf{I} \delta(\mathbf{x}, \mathbf{y}) = \mathbf{0} \quad \Longrightarrow \quad \det(\mathcal{B}^*) \varphi + \delta(\mathbf{x}, \mathbf{y}) = 0 \quad .$$

After the determination of the scalar function φ , by backward substitution, the fundamental solutions $\hat{\mathbf{U}}$ can be determined.

The fundamental solutions have a matrix structure of nine entries, and the singular behavior of each entry can be determined by a series expansion of the exponential function. The results show that only weak singularities exist in the diagonal entries of the fundamental solutions, e.g., \hat{U}_{ij}^{ss} , \hat{P}^{ww} , and \hat{P}^{aa} , respectively. The other entries are all regular.

3. BOUNDARY ELEMENT FORMULATION

Using in the weighted residuals method the fundamental solutions as weighting functions, the differential equations for partially saturated poroelasticity can be transformed to the integral equation. Two partial integrations with respect to the spatial variable result in the representation formula. Moving the load point \mathbf{y} to the boundary, the boundary integral equations are obtained

$$(8) \quad \mathcal{C}(\mathbf{y}) \hat{\mathbf{u}}(\mathbf{y}) = \int_{\Gamma} \hat{\mathbf{U}}^{\top}(\mathbf{y}, \mathbf{x}) \hat{\mathbf{t}}(\mathbf{x}) d\Gamma - \oint_{\Gamma} \hat{\mathbf{T}}^{\top}(\mathbf{y}, \mathbf{x}) \hat{\mathbf{u}}(\mathbf{x}) d\Gamma .$$

In (8), the vector of unknowns is collected in $\hat{\mathbf{u}}$ and $\hat{\mathbf{t}}$. The tensors $\hat{\mathbf{U}}$ and $\hat{\mathbf{T}}$ denote the fundamental solutions. $\mathcal{C}(\mathbf{y})$ is the integral free term and the strong singular integral over $\hat{\mathbf{T}}$ is defined in the sense of a Cauchy Principal Value. Following the work in [5] the strong singular integral is analytically transformed to a weakly singular integral through integration by parts, and can be numerically solved by Duffy transformation.

To approximate the geometry, the boundary is divided into E boundary elements Γ_e via a standard triangulation. The ansatz functions $N_e^f(\mathbf{x})$ are used with the time-dependent nodal values, e.g., for the solid displacement and the total stress vector

$$u_i(\mathbf{x}, t) = \sum_{e=1}^E \sum_{f=1}^F N_e^f(\mathbf{x}) u_i^{ef}(t) \quad t_i(\mathbf{x}, t) = \sum_{e=1}^E \sum_{f=1}^F N_e^f(\mathbf{x}) t_i^{ef}(t) .$$

The Dirichlet datum is approximated by continuous linear shape functions and the Neumann datum by discontinuous constant shape functions.

By dividing the time period t in N intervals of equal duration Δt , i.e., $t = N \Delta t$, the convolution integrals between the fundamental solutions and the nodal values are approximated by the Convolution Quadrature Method. This results in the following boundary element time stepping formulation for $n = 0, 1, 2, \dots, N$

$$(9) \quad \sum_{e=1}^E \sum_{f=1}^F \sum_{k=0}^n \left\{ \omega_{n-k}^{ef} (\hat{\mathbf{U}}, \mathbf{y}, \Delta t)^{\top} \mathbf{t}^{ef}(k \Delta t) - \omega_{n-k}^{ef} (\hat{\mathbf{T}}, \mathbf{y}, \Delta t)^{\top} \mathbf{u}^{ef}(k \Delta t) \right\} = \mathcal{C}(\mathbf{y}) \mathbf{u}(\mathbf{y}, n \Delta t)$$

with the integration weights $\omega_n^{ef}(\cdot, \mathbf{y}, \Delta t) = \frac{\mathcal{R}^{-n}}{L} \sum_{\ell=0}^{L-1} \int_{\Gamma} \left(\mathbf{x}, \mathbf{y}, \frac{\gamma(\mathcal{R}e^{i\ell \frac{2\pi}{L}})}{\Delta t} \right) N_e^f(\mathbf{x}) d\Gamma e^{-in\ell \frac{2\pi}{L}}$.

The numerical implementation is accomplished by using the open source C++ BEM library HyENA ¹.

4. NUMERICAL RESULTS

For all numerical examples, the surface is discretized with linear triangle elements and a BDF 2 in the CQM is used. For the material data, the Massilon Sandstone [1] is chosen. The initial water saturation is set to $S_w = 0.9$.

4.1. 3D Column. The column has a length of 3 m, a width and height of 1 m. In order to compare with the one dimensional solution [1], no flux at the bottom and around the column is allowed, and the normal displacement at the bottom and the four sides is also set to zero. The top of the column is excited by a stress jump according to a unit step function (Heaviside load). Furthermore, the Poisson's ratio artificially is set to zero. The displacement u_z at the top center of the column, the pore water pressure p^w and the pore air pressure p^a at the bottom center of the column are calculated (see figure 1).

In order to obtain good numerical results and to reduce as much as possible numerical damping, an optimal time step size Δt corresponding to every mesh should be chosen. This optimal choice depends basically on the wave velocities and the spatial discretization. Therefore, the dimensionless Courant–Friedrichs–Levy number $\beta_{CFL} = v_{p1} \Delta t / r_e$ is introduced, where v_{p1} is the fast compressional wave velocity and r_e is the characteristic element length.

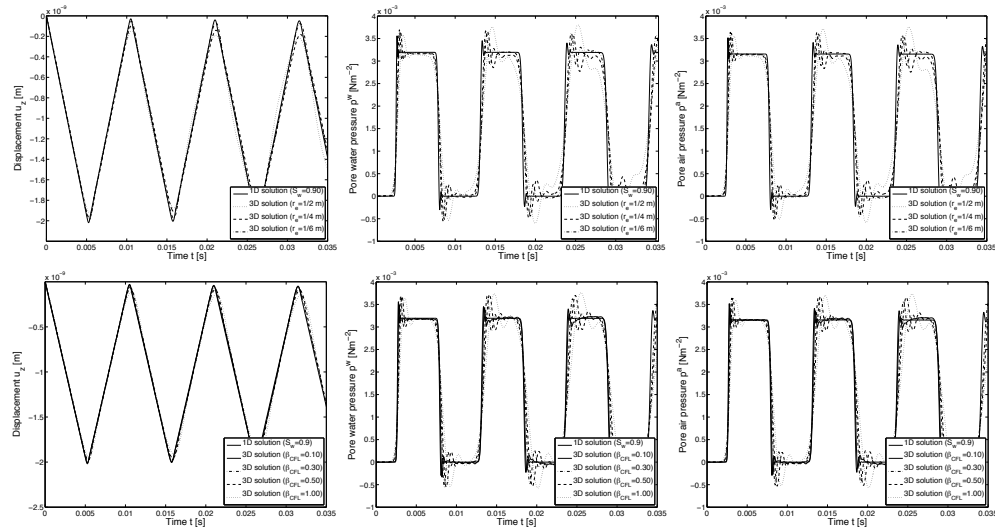


FIGURE 1. Displacement and pore pressure versus time

¹see <http://www.mech.tugraz.at/HyENA>

Three different surface meshes with 224, 896 and 2016 linear triangle elements are used to study the influence of the spatial discretization ($\beta_{CFL} = 0.3$). To study the influence of the time discretization, the mesh with 2016 elements is calculated with $\beta_{CFL} = 0.1, 0.3, 0.5$, and 1.0. The time domain numerical results are presented in figure 1 and are compared with the 1D results [1]. The displacement results of different mesh and time step size are acceptable. On the other hand, good pore pressure results require fine mesh and small time step size.

4.2. Open Trench. In this section, the vibration isolation of a partially saturated half space using an open trench will be studied with the proposed BEM code. A square surface ($10\text{ m} \times 10\text{ m}$) is discretized with $r_e = 0.25\text{ m}$ (see figure 2). At the

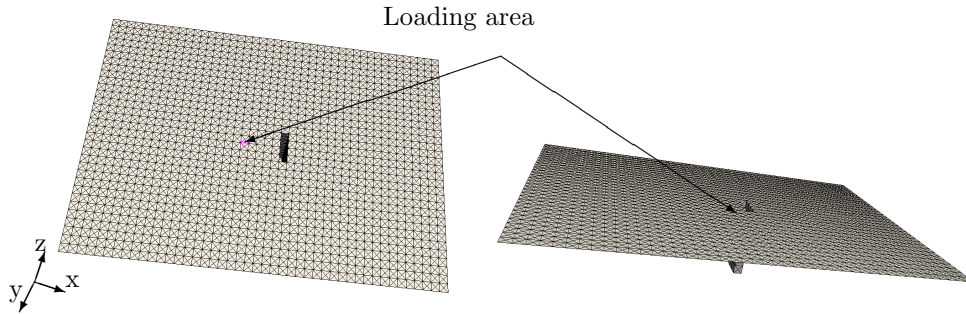


FIGURE 2. Surface meshes

loading area a vertical total stress $\sigma_z = 1\text{ Nm}^{-2}H(t)$ is applied and the remaining surface is traction free. Both, the pore water and the pore air pressure are assumed to be zero all over the surface. Three different cases are considered as case 1 (no trench), case 2 (trench depth 1 m), and case 3 (trench depth 3 m).

For a easy comparison, absolute values of the displacement amplitude A_a are defined and calculated for each node along the center line behind the open trench, where $A_a = \sqrt{(u_{z_{max}} - u_{z_{min}})^2 + (u_{x_{max}} - u_{x_{min}})^2}$, $u_{z_{max}}$ and $u_{z_{min}}$ denote the maximum and the minimum vertical displacement of the observation point, $u_{x_{max}}$ and $u_{x_{min}}$ represent the maximum and minimum radial displacement of the observation point. Since all the observation points locate in the center line of the trench according to the load, u_y is zero.

In Figure 3, the absolute values of the displacement amplitude A_a are calculated for each node along the center line behind the open trench. An amplitude reduction factor $A_{r,f}$ is also calculated by normalizing A_a to the corresponding absolute displacement without a trench. At a point 0.25 m behind the trench, the absolute value of the displacement amplitude A_a can drop from $3.5 \times 10^{-12}\text{ m}$ to $2.5 \times 10^{-12}\text{ m}$ with the deep open trench, and the amplitude reduction factors of the shallow and deep open trenches are about 1.30 and 1.42, respectively. At a point 4.25 m behind the trench, the absolute value of the displacement amplitude can drop from $1.75 \times 10^{-12}\text{ m}$ to $1.55 \times 10^{-12}\text{ m}$ with the deep open trench, and the

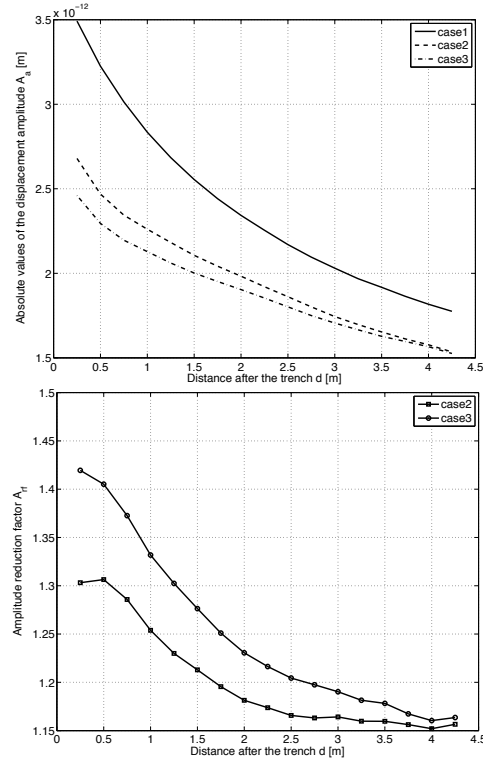


FIGURE 3. Displacement amplitude A_a and the corresponding amplitude reduction factor A_{rf}

amplitude reduction factors of the shallow and deep open trenches are about 1.155 and 1.16, respectively.

In order to obtain the best effect, the position of the open trench should be as close as possible to the object to be isolated. A deeper trench will produce a better isolation effect since the traveling distance of the wave will be longer. However, taking the soil as an example, a deeper trench means a more difficult maintaining work of the trench to keep the stability as well as to avoid later back filling. A shallow trench but close enough to the object may be a viable solution, or by using an array of shallow trenches.

Peng Li, Martin Schanz

Institute of Applied Mechanics, Graz University of Technology, Austria
 tunnelee@gmail.com, m.schanz@tugraz.at

REFERENCES

- [1] P. Li and M. Schanz. Wave propagation in a one dimensional partially saturated poroelastic column. *Geophysical Journal International*, 184(3):1341–1353, 2011.
- [2] P. Li and M. Schanz. Fundamental solutions for a partially saturated poroelastic continuum. *Proceedings in Applied Mathematics and Mechanics*, 11(1):243-244, 2011.
- [3] R. H. Brooks and A. T. Corey. Hydraulic Properties of Porous Media. *Hydraulic Papers*, 3–27, 1964.
- [4] R. W. Lewis and B. A. Schrefler. The Finite Element Method in the Static and Dynamic Deformation and Consolidation of Porous Media. *John Wiley and Sons*, 1998.
- [5] M. Messner and M. Schanz: A regularized collocation boundary element method for linear poroelasticity. *Computational Mechanics*, 47(6):669–680, 2011.

Second-kind Single Trace BEM for Acoustic Scattering

E. SPINDLER

(joint work with R. Hiptmair, X. Claeys)

We consider acoustic scattering at composite objects with Lipschitz boundary. The classical first kind approach leads to ill-conditioned linear systems and no preconditioner seems to be available for it. This has motivated us to devise a new second-kind boundary integral formulation that is intrinsically well conditioned. Moreover, it supports a variational formulation in L^2 , which makes it possible to use discontinuous boundary element spaces to approximate both, the unknown Dirichlet and Neumann boundary data.

Computational results in 2D and 3D confirm the excellent conditioning of the Galerkin matrices of our new second-kind approach which is directly reflected in the fast convergence of the iterative solver GMRES. Several numerical tests indicate the absence of spurious modes in our new formulation and convergence studies show competitive accuracy compared to the classical first kind approach. Additionally, we obtain superconvergence of the L^2 -error of the Dirichlet data after L^2 -projection onto piecewise linear continuous functions.

Keywords: second-kind boundary integral equation, boundary element methods, acoustic scattering, composite scatterer.

Mathematics Subject Classifications (2000): 65N38, 78M15, 78A45.

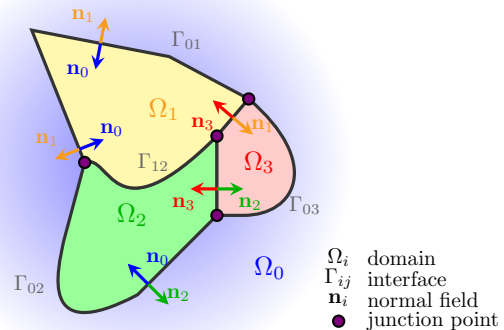
1. EXTENDED ABSTRACT

In this abstract we consider the geometric setting of a composite bounded scatterer $\Omega_* \subset \mathbb{R}^d$, $d \in \{2, 3\}$. It features a Lipschitz boundary and is composed of so-called sub-domains $\Omega_i \subset \mathbb{R}^d$, $i = 1, \dots, N$. We demand that they do not intersect ($\Omega_i \cap \Omega_j = \emptyset$) for $i \neq j$, and that they form a partition of Ω_* in the sense that $\overline{\Omega_*} = \bigcup_{i=1}^N \overline{\Omega_i}$.

The unbounded complement of $\overline{\Omega_*}$ should be connected and will provide another sub-domain Ω_0 , which means $\Omega_0 := \mathbb{R}^d \setminus \overline{\Omega_*}$.

The common interface of Ω_i and Ω_j is denoted by $\Gamma_{ij} := \partial\Omega_i \cap \partial\Omega_j$, $i \neq j$.

We render acoustic scattering with penetrable materials, modelled by a transmission problem for the Helmholtz equation [4, Ch. 2],



(ii) every solution of (1) can be written as

$$u = -\mathbb{D}_i[\kappa](\gamma_D^i u) + \mathbb{S}_i[\kappa](\gamma_N^i u), \quad \text{on } \Omega_i.$$

In a more compact way we can write

$$(4) \quad \begin{aligned} & u = \mathbb{G}_i[\kappa](\gamma_D^i u, \gamma_N^i u) \quad \text{on } \Omega_i, \\ & \text{with } \mathbb{G}_i[\kappa](\gamma_D^i u, \gamma_N^i u) := -\mathbb{D}_i[\kappa](\gamma_D^i u) + \mathbb{S}_i[\kappa](\gamma_N^i u). \end{aligned}$$

Inherent in the definition of potentials is that they generate a function defined both inside and outside of Ω_i . This enables us to take traces of potentials also from the exterior of $\partial\Omega_i$.

Boundary integral operators are obtained by letting the trace operators γ_D^i and γ_N^i act on the potentials \mathbb{S}_i and \mathbb{D}_i . Using the famous jump relations (cf. [5, Sect. 3.3.1] for proof and details), we obtain out of (4) the relation

$$\begin{aligned} & \begin{pmatrix} \gamma_D^i \\ \gamma_N^i \end{pmatrix} \mathbb{G}_i[\kappa] : H^{\frac{1}{2}}(\partial\Omega_i) \times H^{-\frac{1}{2}}(\partial\Omega_i) \rightarrow H^{\frac{1}{2}}(\partial\Omega_i) \times H^{-\frac{1}{2}}(\partial\Omega_i) \\ & \begin{pmatrix} \gamma_D^i \\ \gamma_N^i \end{pmatrix} \mathbb{G}_i[\kappa] = \frac{1}{2} \text{Id} + \mathcal{A}_i[\kappa], \quad \text{with } \mathcal{A}_i[\kappa] = \begin{pmatrix} \mathbb{K}_i[\kappa] & \mathbb{V}_i[\kappa] \\ \mathbb{W}_i[\kappa] & \mathbb{K}'_i[\kappa] \end{pmatrix}. \end{aligned}$$

The individual boundary integral operators are known as the single layer $\mathbb{V}_i[\kappa]$, double layer $\mathbb{K}_i[\kappa]$, adjoint double layer $\mathbb{K}'_i[\kappa]$, and hypersingular $\mathbb{W}_i[\kappa]$ boundary integral operators. Our notation follows [5, Ch. 3].

We are ready to start with the boundary integral formulation of (1). It is based on the skeleton multi-trace space

$$(5) \quad \begin{aligned} & \mathcal{MT}(\Sigma) := \mathcal{MT}_D(\Sigma) \times \mathcal{MT}_N(\Sigma), \\ & \text{with } \begin{aligned} \mathcal{MT}_D(\Sigma) &:= H^{\frac{1}{2}}(\partial\Omega_0) \times \cdots \times H^{\frac{1}{2}}(\partial\Omega_N), \\ \mathcal{MT}_N(\Sigma) &:= H^{-\frac{1}{2}}(\partial\Omega_0) \times \cdots \times H^{-\frac{1}{2}}(\partial\Omega_N). \end{aligned} \end{aligned}$$

It owes its name to the fact that on each interface Γ_{ij} a function $\mathbf{u} \in \mathcal{MT}(\Sigma)$ comprises two pairs of Dirichlet and Neumann data, one contributed by the sub-domain on either side.

To isolate the contribution of a single sub-domain we rely on trivial localization operators

$$\mathbb{R}_i : \mathcal{MT}(\Sigma) \rightarrow H^{\frac{1}{2}}(\partial\Omega_i), \quad \mathbb{R}_i \mathbf{u} := \begin{pmatrix} u_i \\ \nu_i \end{pmatrix}, \quad \begin{aligned} \mathbf{u} &= (u_0, \dots, u_N, \nu_0, \dots, \nu_N), \\ u_i &\in H^{\frac{1}{2}}(\partial\Omega_i), \nu_i \in H^{-\frac{1}{2}}(\partial\Omega_i). \end{aligned}$$

The multi-trace spaces inherit all properties of their local components.

$$(6) \quad \langle \langle \mathbf{u}, \mathbf{v} \rangle \rangle := \sum_{i=0}^N \langle \mathbb{R}_i \mathbf{u}, \mathbb{R}_i \mathbf{v} \rangle_{H^{\frac{1}{2}}(\partial\Omega_i) \times H^{-\frac{1}{2}}(\partial\Omega_i)}, \quad \mathbf{u}, \mathbf{v} \in \mathcal{MT}(\Sigma).$$

The *single-trace space* is the subset of $\mathcal{MT}(\Sigma)$ containing all boundary data that fulfill the transmission conditions arising on the interfaces $\Gamma_{i,j}$ of the domains

Ω_i, Ω_j in (1).

$$(7) \quad \begin{aligned} \mathcal{ST}(\Sigma) &:= \mathcal{ST}_D(\Sigma) \times \mathcal{ST}_N(\Sigma) \subset \mathcal{MT}(\Sigma), \\ \mathcal{ST}_D(\Sigma) &:= \{(u_0, \dots, u_N) \in \mathcal{MT}_D(\Sigma) : \exists u \in H^1(\mathbb{R}^d), u_i = \gamma_D u\}, \\ \mathcal{ST}_N(\Sigma) &:= \{(\nu_0, \dots, \nu_N) \in \mathcal{MT}_N(\Sigma) : \exists \phi \in H(\operatorname{div}, \mathbb{R}^d), \nu_i = \mathbf{n}_i \cdot \begin{pmatrix} \gamma_D^i \\ \gamma_D^i \end{pmatrix} \phi\}. \end{aligned}$$

In words, functions in $\mathcal{ST}_D(\Sigma)$ and $\mathcal{ST}_N(\Sigma)$ are skeleton traces of functions defined on \mathbb{R}^d .

A fundamental result is the ‘‘polar set’’ characterization of $\mathcal{ST}(\Sigma)$ as a subspace of $\mathcal{MT}(\Sigma)$ given in [2, Prop. 2.1].

Theorem 1.2.

$$\mathcal{ST}(\Sigma) = \{\mathbf{u} \in \mathcal{MT}(\Sigma) : \langle \langle \mathbf{u}, \mathbf{v} \rangle \rangle = 0 \forall \mathbf{v} \in \mathcal{MT}(\Sigma)\}.$$

From this identity we obtain closedness of $\mathcal{ST}(\Sigma)$ in $\mathcal{MT}(\Sigma)$.

We may now start with the derivation of our new second kind formulation for scattering at composite objects. We consider the geometry resp. domain decomposition of \mathbb{R}^d as described in the beginning of this extended abstract.

We introduce the globally defined multi-potential.

Definition 1.3 (multi-potential). The *multi-potential* is defined as the sum over all domain-wise potentials $\mathbb{G}_i[\kappa_i]$ defined in (4), $i = 0, \dots, N$:

$$\mathbb{M}_\Sigma : \mathcal{MT}(\Sigma) \rightarrow \prod_{i=1}^N H_{\text{loc}}(\Delta, \mathbb{R}^d \setminus \partial\Omega_i), \quad \mathbb{M}_\Sigma(\mathbf{u}) := \sum_{i=0}^N \mathbb{G}_i[\kappa_i](\mathbb{R}_i \mathbf{u}).$$

An immediate consequence of Theorem 1.1 is

Corollary 1.4 (global representation formula). *Let u solve the transmission problem (1). Then*

$$(8) \quad u = \mathbb{M}_\Sigma(\gamma_\Sigma u),$$

$$(9) \quad \gamma_\Sigma u = (\gamma_D^0 u, \gamma_D^1 u, \dots, \gamma_D^N u, \gamma_N^0 u, \dots, \gamma_N^N u) \in \mathcal{ST}(\Sigma).$$

An important Theorem for our new formulation is

Theorem 1.5.

$$(10) \quad \langle \langle \gamma_\Sigma \mathbb{M}_\Sigma \mathbf{u}, \mathbf{v} \rangle \rangle = \langle \langle \mathbf{u}, \mathbf{v} \rangle \rangle, \quad \forall \mathbf{u} \in \mathcal{MT}(\Sigma), \forall \mathbf{v} \in \mathcal{ST}(\Sigma).$$

For more details we refer to [2]. Combining Theorem 1.5 together with (8), we obtain the stability result for the second kind formulation (11).

Theorem 1.6. *Assuming that there is a unique solution u , the next formulation (11) is equivalent to (1). Search $u \in \mathcal{ST}(\Sigma)$:*

$$(11) \quad \langle \langle (\operatorname{Id} - \gamma_\Sigma \mathbb{M}_\Sigma) \mathbf{u}, \mathbf{v} \rangle \rangle = \langle \langle \mathbf{u}_{\text{inc}}, \mathbf{v} \rangle \rangle, \quad \forall \mathbf{v} \in \mathcal{ST}^c(\Sigma), \mathbf{u}_{\text{inc}} := \gamma_\Sigma u_{\text{inc}}.$$

$\mathcal{ST}^c(\Sigma)$ is a complement space of $\mathcal{ST}(\Sigma)$ in $\mathcal{MT}(\Sigma)$. We use the space which has “interchanged roles” of Dirichlet and Neumann datum compared to $\mathcal{ST}(\Sigma)$. This means that we change sign in the Dirichlet datum when taking the trace on an interface Γ_{ij} from the two adjacent sides and assume that there is no jump in the Neumann datum (cf. the figure on the right).

$$\begin{array}{cc} \gamma_N^j u = \gamma_N^i u & \gamma_D^j u = -\gamma_D^i u \\ \begin{array}{c} \text{---} \text{---} \text{---} \\ | \\ \Omega_j \quad \Omega_i \end{array} & \begin{array}{c} \text{---} \text{---} \text{---} \\ | \\ \Omega_j \quad \Omega_i \end{array} \end{array}$$

To obtain the final weak form, we need the next Lemma 1.7 which is going to help us in arriving at a regularized form:

Lemma 1.7. *Assume that $\kappa_0 = \kappa_1 = \dots = \kappa_N$. In this case,*

$$(12) \quad \mathbb{M}_\Sigma(u)(x) = 0 \quad \forall x \in \mathbb{R}^d, \quad \forall u \in \mathcal{ST}(\Gamma).$$

This means that we can modify Theorem 1.6 by the vanishing term $\gamma_\Sigma \mathbb{M}_\Sigma[\kappa_0](u)$, defined by setting $\kappa_i = \kappa_0$, $i \in \{1, \dots, N\}$:

Theorem 1.8. *Assuming that (11) has a unique solution $\mathbf{u} \in \mathcal{ST}(\Sigma)$, the next formulation (13) is equivalent to (1).*

Search $u \in \mathcal{ST}(\Sigma)$:

$$(13) \quad \langle\langle (\text{Id} - \gamma_\Sigma(\mathbb{M}_\Sigma - \mathbb{M}_\Sigma[\kappa_0])) \mathbf{u}, \mathbf{v} \rangle\rangle = \langle\langle \mathbf{u}_{inc}, \mathbf{v} \rangle\rangle, \quad \forall \mathbf{v} \in \mathcal{ST}^c(\Sigma).$$

The advantage of this form is the regularizing effect of adding $\gamma_\Sigma \mathbb{M}_\Sigma[\kappa_0](u)$. We even obtain the result of Theorem 1.8 in the L^2 setting:

Theorem 1.9. *Assuming that (11) has a unique solution $\mathbf{u} \in \mathcal{ST}(\Sigma)$, the next formulation (14) is equivalent to (1).*

Search $u \in \mathcal{ST}_{L^2}(\Sigma)$:

$$(14) \quad \langle\langle (\text{Id} - \gamma_\Sigma(\mathbb{M}_\Sigma - \mathbb{M}_\Sigma[\kappa_0])) \mathbf{u}, \mathbf{v} \rangle\rangle = \langle\langle \mathbf{u}_{inc}, \mathbf{v} \rangle\rangle, \quad \forall \mathbf{v} \in \mathcal{ST}_{L^2}^c(\Sigma).$$

The spaces $\mathcal{ST}_{L^2}(\Sigma)$ and $\mathcal{ST}_{L^2}^c(\Sigma)$ are defined by interchanging the boundary spaces $H^{\frac{1}{2}}(\partial\Omega_i)$, $H^{-\frac{1}{2}}(\partial\Omega_i)$ by $L^2(\partial\Omega_i)$ in the definitions of $\mathcal{ST}(\Sigma)$, $\mathcal{ST}^c(\Sigma)$ and $\mathcal{MT}(\Sigma)$.

A proof of Theorem 1.9 can be found in [1].

Working in the L^2 setting allows us to use arbitrary L^2 -stable basis functions for the discretization. In Figure 1 we present a numerical experiment in $2D$ for a composite scatterer consisting of two half discs (cf. left upper plot in Figure 1). We use piecewise constant ansatz and test functions for both Dirichlet and Neumann data. A comparison is made to the solution of a classical first kind approach (cf. von Petersdorff [6]).

We observe that our new second kind formulation is intrinsically well-conditioned with a condition number independent of the mesh size (lower right plot) while we have a quadratic growth for the classical approach. This is directly reflected in the convergence of the iterative solver GMRES (lower right plot). Moreover, the convergence plot in the upper right plot shows that our formulation has competitive accuracy compared to the classical first kind approach.

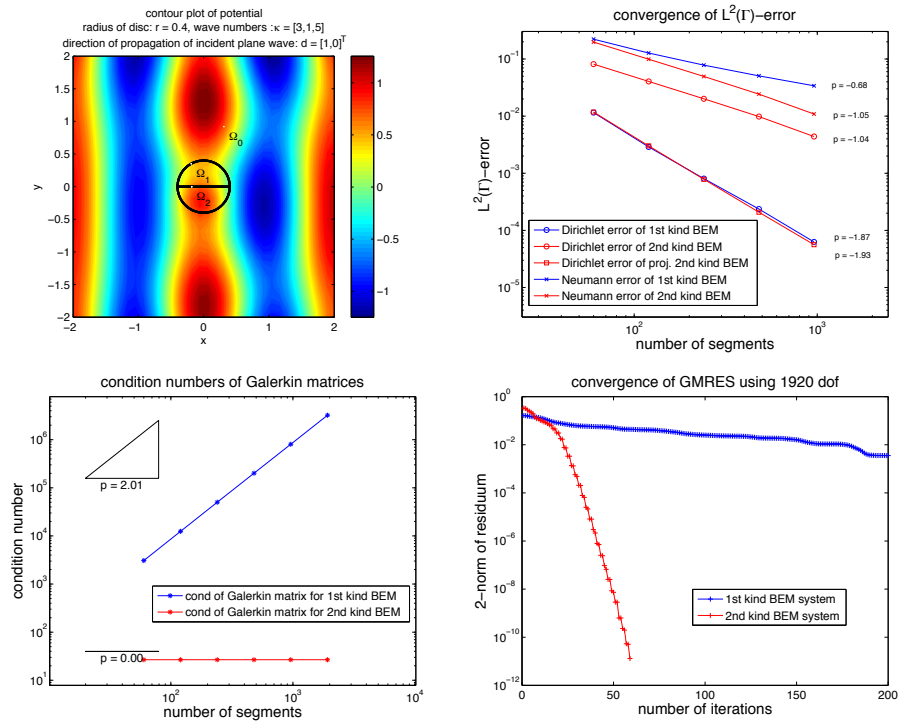


FIGURE 1. Numerical results

E. Spindler, R. Hiptmair

Seminar for Applied Mathematics, ETH Zürich

elke.spindler@sam.math.ethz.ch, hiptmair@sam.math.ethz.ch

X. Claeys

Laboratoire Jacques-Louis Lions, Paris IV

xavier.claeys@upmc.fr

REFERENCES

- [1] E. SPINDLER, *Second kind single trace boundary element methods*, Master Thesis, ETH Zürich, 2012.
<http://www.sam.math.ethz.ch/~hiptmair/StudentProjects/Spindler.Elke/thesis.pdf>
- [2] X. CLAEYS, *A single trace integral formulation of the second kind for acoustic scattering*. Technical Report No. 14, ETH Zürich, 2011.
- [3] X. CLAEYS, R. HIPTMAIR, AND C. JEREZ-HANCKES, *Multi-trace boundary integral equations*. Technical Report No. 20, ETH Zürich, 2012.
- [4] J.-C. NÉDÉLEC, *Acoustic and Electromagnetic Equations: Integral Representations for Harmonic Problems*, vol. 44 of Applied Mathematical Sciences, Springer-Verlag, Berlin, 2001.

- [5] S.A. SAUTER, C. SCHWAB, vol. 39 of Computational Mathematics, *Boundary element methods*, Springer-Verlag, Berlin, 2011.
- [6] T. VON PETERSDORFF, *Boundary integral equations for mixed Dirichlet, Neumann and transmission problems*, Math. Meth. Appl. Sci., 11 (1989), pp. 185–213.

Certified Reduced Basis Method for the Electric Field Integral Equation

BENJAMIN STAMM

(joint work with Jan S. Hesthaven, Shun Zhang)

This talk gives an overview of the certified Reduced Basis Method applied to parametrized PEC scattering problems. We give a mathematical background of the model reduction by the reduced basis method where an efficient input/output reduced order model is developed.

More precisely, we consider the Electric Field Integral Equation (EFIE) under variation of a set of parameters consisting the wave-number, wave-direction and the polarization of the incident plane wave. In the framework of the input/output procedure, for any in parameter value (input) we are interested in the radar cross section (RCS, output). In addition, the reduced order model is trustable as we develop *a posteriori* estimates to certify the error committed by the model order reduction for both the electric current and the RCS.

Keywords: Integral equations,

Mathematics Subject Classifications (2000): please, name your files after the lastname of the first author, that is `lastname.tex`, and send both the `.tex` and `.pdf` files.

Jan S. Hesthaven, Shun Zhang

Division of Applied Mathematics, Brown University, Providence, RI 02912
Jan.Hesthaven@Brown.edu, ShunZhang@Brown.edu

Benjamin Stamm

UPMC University Paris 06, UMR 7598, Laboratoire Jacques-Louis Lions, F-75005, Paris, France
stamm@ann.jussieu.fr

REFERENCES

- [1] J.Hesthaven, B.Stamm, S.Zhang, Certified Reduced Basis Method for the Electric Field Integral Equation, *SIAM J. Sci. Comput.*, Vol. 34, No. 3, pp. A1777-A1799, 2012

High order BEM for contact problems

E.P. STEPHAN

We consider exterior Signorini contact for the Laplacian in R^2 . We use the Poincaré-Steklov operator, which realizes the Dirichlet-to-Neumann map, and represent the negative of the unknown normal derivative on the contact boundary by a Lagrange multiplier. Herewith we derive a mixed formulation which is equivalent to a variational inequality on the contact boundary, where the non-penetration condition is incorporated in the convex set of admissible ansatz and test functions. Both formulations are uniquely solvable. We use Gauss-Lobatto-Lagrange basis functions on a regular mesh on the contact boundary for the primal variable and biorthogonal basis functions of the same degree on the same mesh for the Lagrange multiplier. We present a reliable a posteriori error estimate of residual type for the Galerkin solution of the mixed formulation. The discrete mixed system is solved by the semi-smooth Newton algorithm in combination with a penalized Fischer-Burmeister complementarity function taking care of the contact condition. Numerical experiments are given which support our theoretical results.

Keywords: Signorini problems, Poincaré-Steklov operator, biorthogonal basis functions.

Mathematics Subject Classifications (2000): 65N30, 65N38.

E.P. Stephan

Leibniz Universität Hannover, Institute for Applied Mathematics
stephan@ifam.uni – hannover.de

Application Of Boundary Element Method To The Modelling Of A Wave Powered Plant

WOJCIECH SULISZ

A theoretical approach is applied for the modeling of a wave-powered multitask maritime plant. The solution is achieved by applying three-dimensional boundary element method and is valid for a structure of arbitrary configuration. The derived model has been applied to analyze the effect of the plant geometry and its configuration on diffracted wave field and the efficiency of the plant wave-powered system. A high efficiency of the plant is achieved by specifically diffracted and amplified waves which enforce large-amplitude oscillations of a power system and, in consequence, result in a highly efficient and cost-effective plant. The derived 3-D theoretical model, which describes wave diffraction, shoaling and focusing effects, indicates that it is possible to achieve amplification of energy more than ten times. The concept provides an opportunity for many regions and nations to solve a problem of the shortages of energy or fresh water, or to secure protection of coastal and harbor areas by applying local resource and cost-effective environmentally-friendly technology. Laboratory experiments have been conducted in a wave flume to verify theoretical results. A high efficiency of the proposed concept is confirmed by data collected during laboratory experiments.

1. INTRODUCTION

The lack of energy is probably one of the greatest challenges for the contemporary and future generations. The shortages of energy affect developed and developing countries. The problem is of significant importance for societies because the lack of energy is a serious development constrain for many regions and nations. Nowadays, alternative energy sources are believed to be the most attractive sources of energy worldwide.

In this study a novel and attractive concept of a wave-powered multitask maritime plant is proposed. The plant is economically efficient and is based on an new original concept of using alternative energy sources to power the pneumatic breakwater. First, the main concept is described. Then, a boundary-value problem is formulated to describe diffracted water wave field which is applied to power the multitask plant. The boundary-value problem is solved numerically by applying a 3-D boundary element method and diffracted wave fields are derived. The results are discussed with the emphasis on the possibility to amplify waves and wave energy to make the plant more efficient. Finally, laboratory experiments are conducted to verify the efficiency of the proposed concept and then conclusions are specified.

2. THEORETICAL INVESTIGATION

2.1. Pneumatic breakwater concept. According to the present concept, a multitask maritime plant is powered by alternative energy sources as it is shown schematically in Figure 1. The main part of energy for the plant arises from

specifically diffracted and amplified waves achieved in a channel. The amplified waves enforce large-amplitude oscillations of a power system and, in consequence, result in a highly efficient and cost-effective plant.

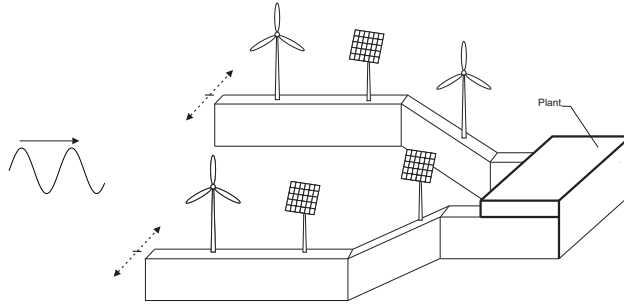


FIGURE 1. Multitask maritime plant powered by alternative energy sources.

The plant is applied to power a pneumatic breakwater. The concept provides an opportunity for many regions and nations to solve a problem of the shortages of energy or fresh water, or to secure protection of coastal and harbor areas by applying local resource and cost-effective environmentally-friendly technology. The coupling of energy sources is an attractive solution for water scarce regions and remote areas (Cruze 2008, Davies 2005). Moreover, the utilization of wind and wave energy to run a multitask maritime plant is an attractive idea of good perspectives for practical applications, because such energy and water are simultaneously available in abundance.

2.2. Theoretical Formulation and Solution. The situation considered for theoretical analysis is shown schematically in Figure 2. It is assumed that the channel bottom and side walls are impervious. Moreover, it is assumed that the fluid is inviscid and incompressible, and that the excitation is provided by plane waves of amplitude A and frequency ω . Additionally, it is assumed that the fluid motion is irrotational.

The boundary-value problem is formulated in terms of velocity potential, ϕ_1 , and the solution is achieved by applying the Green second identity. Accordingly, the following integral equation is applied to derive a solution

$$(1) \quad \int_{S_1} \left[\phi_1 \frac{\partial}{\partial n_1} \left(\frac{1}{r} \right) - \frac{\partial \phi_1}{\partial n_1} \frac{1}{r} \right] dS_1 = 0,$$

in which r is the distance between a field point and a point on the boundary.

Equation (1) is solved numerically by discretizing the boundary into triangular elements (Sulisz 1986, Sulisz 2005). In order to reduce computational efforts, a

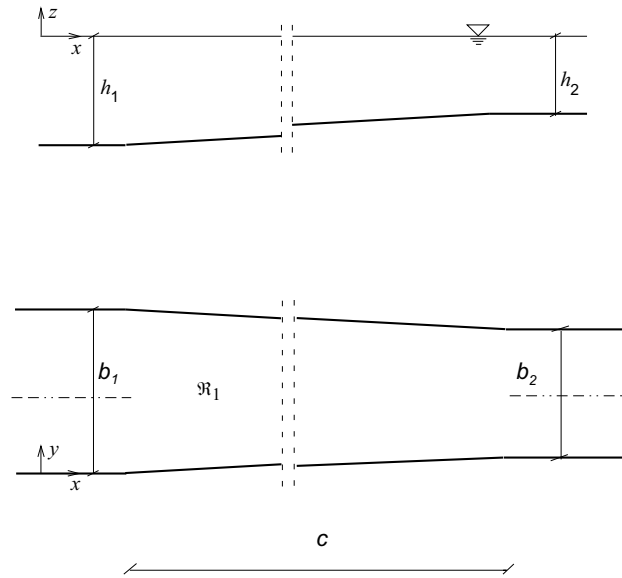


FIGURE 2. Definition sketch and coordinate systems.

symmetric problem is considered. An example of a mesh for a simple area, which represents half of the free-surface segment of length $20h_1$, is illustrated in Figure 3.

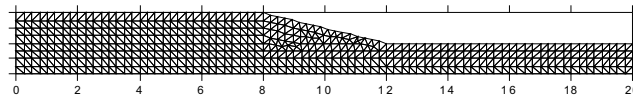


FIGURE 3. Example of boundary grid for a free-surface segment.

2.3. Theoretical Results. The numerical model derived to describe the diffracted wave field is applied to investigate the possibility to amplify water waves in a channel, especially an amplification at the position of a chamber to run a pneumatic breakwater. The main focus is on a symmetric problem which is sufficiently general for practical applications and enables us to reduce computational time. The calculations are conducted for several wave frequencies and main parameters of the model, including water depth, channel width, geometry of the convergent sector, etc.

Typical wave fields arising from wave diffraction, shoaling and focusing effects indicate that the incoming wave train is partially reflecting from the converging segment. Wave reflection is small as desired. In fact, a small wave reflection

from the convergent segment is important to provide more energy for a pneumatic breakwater system. The main part of the wave energy is transmitted down the channel where the free-surface oscillations enforces large amplitude water oscillations in a chamber, triggering the pneumatic breakwater system. The analysis of theoretical results shows that in the area affected by the converging segment, wave field is very complex due to the wave reflection, formation of cross modes, and cross mode attenuation. The complexity of free-surface oscillations indicates that the wave field in the area affected by a converging segment should be analyzed individually for each case.

The amplification of free-surface oscillations achieved in the channel is of significant practical importance. This is because the amplified free-surface oscillations are more efficient in increasing the pneumatic breakwater system output by providing more energy for a pneumatic breakwater. It is obvious that a large amplification of free-surface oscillations enforces a large amplitude motion in a chamber and, in consequence, increases the efficiency of the pneumatic breakwater system. It is worth noting that wave energy is proportional to the square of wave amplitude. The derived model, which describes wave diffraction, shoaling and focusing effects, indicates that it is possible to achieve amplification of energy more than ten times.

3. EXPERIMENTAL INVESTIGATIONS

The interaction of water waves with an air barrier is a very complex phenomenon and little is known on its physics. In order to get an insight into the physics of this phenomenon, the investigations on wave interactions with an air barrier were conducted by performing laboratory experiments. The experiments were conducted in the wave flume of hydraulic laboratory of the Institute of Hydroengineering, Polish Academy of Sciences, Gdask. The wave flume at the Institute of Hydro-Engineering is 64 m long, 0.6 m wide and 1.4 m deep. Water waves are generated in the flume by a programmable wave generator. The waves are absorbed at the end of the flume by an absorber made from porous material.

A pneumatic breakwater was constructed in the middle part of the flume. The width of the channel sector was 0.6 m. A system of perforated pipes was installed at the bottom of the flume. The pipes were connected to an air supply system.

The wave measurement system consisted of two groups of resistance-type wave gauges and a computer system. A group of three resistance-type wave gauges was located before the breakwater to measure the free-surface elevation in the inlet sector and a similar group of wave gauges was used to measure the free-surface oscillations in the outlet sector. Moreover, the velocity field was measured in the middle part of the flume. The measurements were conducted by applying a PIV system.

The program of laboratory work comprises experiments conducted for the water depths, $h = 0.2$ m, $h = 0.3$ m, and $h = 0.4$ m, five wave periods, and three wave heights for each wave period. For each case the wavemaker generated wave trains for about 60 s, and free-surface oscillations were recorded at the rate of 100 Hz.

The analysis of the free-surface elevation was conducted by applying the multi-gauge method (Sulisz and Hudspeth 1993). Application of this method enabled us to separate nonlinear wave effects from wave records and to determine incoming, reflected, and transmitted wave properties.

The analysis of experimental data shows that in the area affected by the pneumatic breakwater, the wave field is very complex due to the wave reflection, dissipation effects due to the interaction of waves with a barrier, and a formation of transmitted wave train. The analysis indicates a substantial dissipation of incoming wave energy. The amplitude of transmitted wave train is considerably reduced in comparisons with incoming wave amplitude. The reduction is significant and often exceeds 90% of the incoming wave energy.

4. SUMMARY

A theoretical approach was applied for the modeling of a wave-powered multi-task maritime plant. The main part of energy for the plant arises from specifically diffracted and amplified waves achieved in a channel. The plant is applied to power a pneumatic breakwater.

The results show that the proposed concept is economically efficient. A large amplification of free-surface oscillations achieved in the channel is of significant practical importance. This is because the amplified free-surface oscillations are more efficient in increasing the pneumatic breakwater system output by providing more energy for a pneumatic breakwater. It is obvious that a large amplification of free-surface oscillations enforces a large amplitude motion in a chamber and, in consequence, increases the efficiency of the pneumatic breakwater system. The derived model, which describes wave diffraction, shoaling and focusing effects, indicates that it is possible to achieve amplification of energy more than ten times.

The concept provides an opportunity for many regions and nations to solve a problem of the shortages of energy or fresh water, or to secure protection of coastal and harbor areas by applying local resource and cost-effective environmentally-friendly technology.

Laboratory experiments were conducted in a wave flume to verify theoretical results. A high efficiency of the proposed concept is confirmed by data collected during laboratory experiments.

4.1. Acknowledgements. The author would like to thank Dr M. Paprota and Prof. R. Staroszczyk from the Institute of Hydro-Engineering, Polish Academy of Sciences, for their comments on the first draft. The project is funded by the National Science Center - grant DEC-2011/01/B/ST8/07508.

Wojciech Sulisz

Institute of Hydro-Engineering, Polish Academy of Sciences, Kosciarska 7, 80-328 Gdansk, Poland

sulisz@ibwpan.gda.pl

REFERENCES

- [1] J. CRUZE, *Ocean Wave Energy*, Springer, Berlin Heidelberg, 2008.
- [2] P.A. DAVIESL, *Wave-powered desalination: resource assessment and review of technology*, *Desalination*, 186 (2005), pp. 97–109.
- [3] W. SULISZ, *Solving a baoundary problem for the Poisson differential equation by the bound-ary element method*, *Rozprawy Hydrotechniczne*, 48 (1986), pp.133–146.
- [4] W. SULISZ, *Solving a baoundary problem for the Poisson differential equation by the bound-ary element method*, *Rozprawy Hydrotechniczne*, 48 (1986), pp.133–146.
- [5] W. SULISZ, *Wave propagation in channel with side porous caves*, *Journal of Waterways, Port, Coastal and Ocean Engineering*, ASCE, 131 (2005), pp.162–170.
- [6] W. SULISZ AND R.T. HUDSPETH, *Complete second-order solution for water waves generated in wave flumes*, *Journal of Fluid in Structures*, 7 (1986), pp.253–268.

BEM for Parabolic Moving Boundary Problems

JOHANNES TAUSCH

Many phase change problems are governed by the heat equation in the liquid and solid domain and the Stefan condition

$$v_n = k_s \frac{\partial u_s}{\partial n} - k_l \frac{\partial u_l}{\partial n},$$

on the boundary between the two. Here, v_n is the normal velocity of the interface, u is the temperature, k is a non-dimensionalized diffusion constant, and subscripts indicate solid and liquid phase. The goal is to determine the evolution of the unknown interface. We consider a boundary integral formulation based on the Green's representation formula of the heat equation. Unlike the more standard approaches to this type of problem there are only unknowns on the boundary. However, every time step involves a convolution over the entire history of the problem.

The time-dependent integral equation is discretized with the Nyström method of [1]. Here, special attention must be given to extra terms due to the moving interfaces. We obtain a simple time-stepping method and illustrate the stability and convergence on a number of example problems.

Keywords: Parabolic boundary integral equation, moving boundary problem, Stefan problem

Mathematics Subject Classifications (2000): 35K05, 65R20, 80A22

Johannes Tausch

Southern Methodist University, Dallas, Texas, USA

tauschk@smu.edu

REFERENCES

- [1] J. Tausch. Nystrom discretization of parabolic boundary integral equations. *Appl. Numer. Math.*, 59(11):2843–2856, 2009.

Unsteady mixed convection in a porous lid-driven enclosure under a magnetic field

M. TEZER-SEZGIN

(joint work with B. Pekmen)

Time-dependent mixed convection flow in a lid-driven square cavity filled with a porous medium under the effect of a magnetic field is studied numerically using the dual reciprocity boundary element method (DRBEM) with Houbolt time integration scheme. The moving hot top wall, the cold bottom wall and adiabatic vertical walls are assumed for the cavity which also contains internal heat generation. Effects of the variations of Darcy (Da), Reynolds (Re), Grashof (Gr), Prandtl (Pr) and Hartmann (Ha) numbers on the flow and heat transfer in the cavity are investigated. The average Nusselt number is obtained for several problem parameters and depicted graphically. It is found that the decrease in Darcy number or the increase in Hartmann number cause the fluid to flow slowly. The isotherms cover almost all parts of the cavity showing the increase in the temperature when the internal heat generation is increased. The significant parameter Richardson number ($Ri = Gr/Re^2$) in mixed convection determines either the dominance of buoyancy effect or the effect of mechanically lid-driven wall. The combination of DRBEM with the Houbolt scheme has the advantage of using considerably small number of boundary elements and large time increment which results in very small computational cost for solving the unsteady mixed convection flow in a porous cavity.

1. PROBLEM DEFINITION

The governing non-dimensional, unsteady partial differential equations in a fluid-saturated porous medium under the effect of a horizontally applied magnetic field are

$$\begin{aligned}
 \nabla^2 \psi &= -w \\
 (1) \quad \frac{1}{Re} \nabla^2 w &= \frac{\partial w}{\partial t} + u \frac{\partial w}{\partial x} + v \frac{\partial w}{\partial y} - \frac{Gr}{Re^2} \frac{\partial T}{\partial x} + \frac{w}{DaRe} + \frac{Ha^2}{Re} \frac{\partial v}{\partial x} \\
 \frac{1}{PrRe} \nabla^2 T &= \frac{\partial T}{\partial t} + u \frac{\partial T}{\partial x} + v \frac{\partial T}{\partial y} - \frac{Ra_I}{Ra_E} \frac{1}{PrRe}
 \end{aligned}$$

where $u = \frac{\partial \psi}{\partial y}$, $v = -\frac{\partial \psi}{\partial x}$ are velocity components, ψ, w and T are the stream function, vorticity and temperature, respectively. The dimensionless parameters Re , Gr , Da , Ha , Pr , Ra_I , Ra_E are Reynolds, Grashof, Darcy, Hartmann, Prandtl, internal Rayleigh and external Rayleigh numbers, respectively.

Initial and boundary conditions are

$$\begin{aligned}
 (2) \quad & w = T = 0, \text{ at } t = 0 \\
 & v = \psi = 0, \text{ on } x = 0, 1 \text{ and } y = 0, 1 \\
 & u = 0 \text{ on } x = 0, 1 \text{ and } y = 0; \quad u = 1 \text{ on } y = 1 \\
 & T = 1 \text{ on } y = 1; \quad T = 0 \text{ on } y = 0; \quad \frac{\partial T}{\partial x} = 0 \quad \text{on } x = 0, 1.
 \end{aligned}$$

2. DRBEM APPLICATION

Eqs.(1) are rewritten as coupled Poisson equations

$$\begin{aligned}
 (3) \quad & \nabla^2 \psi = b_1(x, y, t, w) \\
 & \nabla^2 w = b_2(x, y, t, u, v, w, w_x, w_y, w_t, v_x, T_x) \\
 & \nabla^2 T = b_3(x, y, t, u, v, T_x, T_y, T_t).
 \end{aligned}$$

In DRBEM, for a right hand side function b (here b_1, b_2 or b_3) the following approximation is proposed [1]

$$b \approx \sum_{j=1}^{N+L} \alpha_j f_j$$

where α_j 's are sets of initially unknown coefficients, the f_j 's are approximating functions, N is the number of boundary nodes and L is the number of interior points. The radial basis functions f_j 's are usually chosen as polynomials of radial distance r_{ij} as $f_{ij} = 1 + r_{ij} + r_{ij}^2 + \dots + r_{ij}^n$ where i and j correspond to the source(fixed) and the field(variable) points, respectively.

Furthermore, the f_j 's are related to particular solutions \hat{u}_j 's with the Poisson equation $\nabla^2 \hat{u}_j = f_j$ and

$$(4) \quad b = \sum_{j=1}^{N+L} \alpha_j (\nabla^2 \hat{u}_j) \Rightarrow \nabla^2 \varphi = \sum_{j=1}^{N+L} \alpha_j (\nabla^2 \hat{u}_j)$$

where φ denotes either ψ, T or w .

Multiplying both sides by the fundamental solution of Laplace equation $u^* = \frac{1}{2\pi} \ln\left(\frac{1}{r}\right)$ and integrating over the domain, we have

$$(5) \quad \int_{\Omega} (\nabla^2 \varphi) u^* d\Omega = \sum_{j=1}^{N+L} \alpha_j \int_{\Omega} (\nabla^2 \hat{u}_j) u^* d\Omega$$

Once the Green's second identity is used, all the domain integrals will be transformed to the integrals on the boundary.

The discretization of these boundary integrals using linear boundary elements, corresponding to stream function, vorticity and temperature equations, results in

matrix-vector equations as

$$(6) \quad \begin{aligned} H\psi - G\psi_q &= (H\hat{U} - G\hat{Q})\alpha_1 \\ Hw - Gw_q &= (H\hat{U} - G\hat{Q})\alpha_2 \\ HT - GT_q &= (H\hat{U} - G\hat{Q})\alpha_3 \end{aligned}$$

where the vectors ψ_q, w_q and T_q contain the known and unknown information at the nodes about normal derivatives of ψ, w and T . \hat{U} and \hat{Q} are constructed from \hat{u}_j and then $\hat{q}_j = \frac{\partial \hat{u}_j}{\partial n}$ columnwise, and are matrices of size $(N + L) \times (N + L)$. The vectors α_1, α_2 and α_3 are employed as

$$\alpha_1 = F^{-1}b_1, \quad \alpha_2 = F^{-1}b_2, \quad \alpha_3 = F^{-1}b_3,$$

where F is the $(N+L) \times (N+L)$ coordinate matrix containing radial basis functions f_j 's as columns evaluated at $N + L$ points. H and G are BEM matrices containing the boundary integrals of u^* and $q^* = \partial u^* / \partial n$ evaluated at the nodes, respectively.

DRBEM coordinate matrix F is used for evaluating the derivatives in b_2 and b_3 , i.e.

$$\frac{\partial T}{\partial x} = \frac{\partial F}{\partial x} F^{-1} T, \quad u = \frac{\partial F}{\partial y} F^{-1} \psi, \quad v = -\frac{\partial F}{\partial x} F^{-1} \psi, \quad \frac{\partial v}{\partial x} = \frac{\partial F}{\partial x} F^{-1} v.$$

By means of coordinate matrix and the third order backward difference formula which is called Houbolt method, the iteration with respect to time is carried between the system of equations for ψ, w and T as

$$(7) \quad H\psi^{m+1} - G\psi_q^{m+1} = -S w^m$$

$$(8) \quad u^{m+1} = \frac{\partial F}{\partial y} F^{-1} \psi^{m+1}, \quad v^{m+1} = -\frac{\partial F}{\partial x} F^{-1} \psi^{m+1}$$

$$(9) \quad Hw^{m+1} - Gw_q^{m+1} = ReS \left[\left. \frac{\partial w}{\partial t} \right|^{m+1} + Mw^{m+1} \right] \\ - \frac{Gr}{Re} S \frac{\partial F}{\partial x} F^{-1} T^{m+1} + S \frac{w^{m+1}}{Da} + Ha^2 S \frac{\partial F}{\partial x} F^{-1} v^{m+1}$$

$$(10) \quad HT^{m+1} - GT_q^{m+1} = PrReS \left[\left. \frac{\partial T}{\partial t} \right|^{m+1} + MT^{m+1} \right] - S \frac{Ra_I}{Ra_E}$$

where $S = (H\hat{U} - G\hat{Q})F^{-1}$, $M = \left(u^{m+1} \frac{\partial F}{\partial x} F^{-1} + v^{m+1} \frac{\partial F}{\partial y} F^{-1} \right)$, m shows the time iteration, the vectors u^{m+1} and v^{m+1} enter into the system as diagonal matrices of size $(N + L) \times (N + L)$. Ra_I/Ra_E is a constant vector of size $N + L$. The Houbolt time integration scheme is

$$(11) \quad \left. \frac{\partial \varphi}{\partial t} \right|^{m+1} = \frac{11\varphi^{m+1} - 18\varphi^m + 9\varphi^{m-1} - 2\varphi^{m-2}}{6\Delta t},$$

in which φ is either w or T .

The system of equations (7)-(10), after the replacement of time derivatives with Eq.(11), is solved by direct Gaussian elimination.

The solution procedure requires the iteration steps :

- ψ^{m+1} is solved in (7) using the values of w from m -th iteration. Then, the velocities u^{m+1}, v^{m+1} are computed using ψ^{m+1} in Eq.(8).
- Boundary conditions for u, v are inserted in equations (8).
- The energy equation is solved for T^{m+1} from Eq.(10).
- Vorticity boundary conditions are employed by using the definition of vorticity and coordinate matrix F

$$(12) \quad w = \frac{\partial v}{\partial x} - \frac{\partial u}{\partial y} = \frac{\partial F}{\partial x} F^{-1} v^{m+1} - \frac{\partial F}{\partial y} F^{-1} u^{m+1}.$$

- Vorticity w^{m+1} is obtained from Eq.(9).
- Iterations continues until the criterion [4]

$$(13) \quad \frac{\|\psi^{m+1} - \psi^m\|_\infty}{\|\psi^{m+1}\|_\infty} + \frac{\|T^{m+1} - T^m\|_\infty}{\|T^{m+1}\|_\infty} + \frac{\|w^{m+1} - w^m\|_\infty}{\|w^{m+1}\|_\infty} < \epsilon$$

is satisfied, where $\epsilon = 1e - 05$.

3. NUMERICAL RESULTS

The results are performed using $f = 1 + r$ radial basis functions in F matrix. Further, 8-point Gaussian quadrature is used for the integrals in H and G matrices. In general, 120 linear boundary elements and 841 interior points are taken in all computations. $Pr = 0.71$ is taken.

Steady-state flow pattern and temperature distribution are visualized in terms of streamlines and isotherms showing the effects of Da, Re and Ha .

The decrease in Da (fixing $Gr = 10^2$, $Re = 400$, $Ha = Ra_I = 0$) causes the fluid to flow slowly due to the decrease in permeability, and the convective heat transfer is reduced which points to the conductive heat transfer (Figure 1).

As Re increases (fixing $Da = 0.1$, $Ri = 10$, $Ha = Ra_I = 0$), a second counter-rotating cell emerges in streamlines while the effect of the moving lid increases on the top cell forming strong boundary layer from left to right on the top wall (Figure 2). Isotherms alter a little bit on the top right corner due to the motion of the upper lid.

As Ha increases (fixing $Da = 0.1$, $Gr = Re = 100$, $Ra_I = 0$), the effect of moving lid diminishes both in streamlines and isotherms (Figure 3). This is due to the horizontally applied magnetic field. Furthermore, a new counter rotating cell emerges as Ha is increased. The flow is still concentrated near the top lid with the well known characteristic boundary layer formation near the walls when Ha gets larger. Isotherms become nearly horizontal due to the effect of Lorentz force overwhelming the effect of moving lid.

When the average Nusselt number is taken into consideration (Figures 4-5),

$$\overline{Nu} = - \int_0^1 \frac{\partial T}{\partial y} dx \text{ on the top lid is almost the same for all values of } Da \text{ when}$$

$Ri > 1$ ($Re \leq 10$) fixing $Gr = 10^2$, $Ra_I = 0$, $Ha = 0$. On the other hand, \overline{Nu} increases as Da increases for $Ri \leq 1$ due to the increase in inertial forces as Re ($Re > 10$) increases (Figure 4) which demonstrates the increase in convective heat transfer. When $Gr = 10^2$, $Re = 10^2$, $Ra_I = 0$ are fixed, \overline{Nu} decreases and becomes almost the same for all Da values as Ha increases (Figure 5). As Ha decreases, the increase in \overline{Nu} is well observed, and the values of \overline{Nu} is larger for large values of Da which points to the increase in convection.

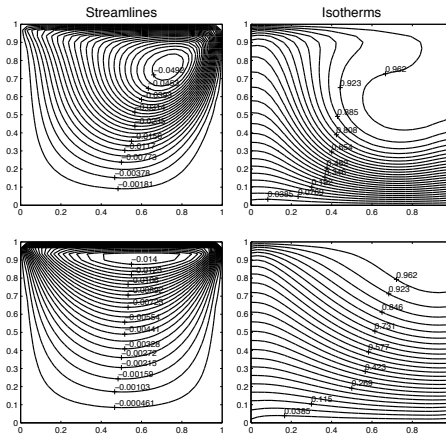


FIGURE 1. $Da = 0.01$ and $Da = 0.001$

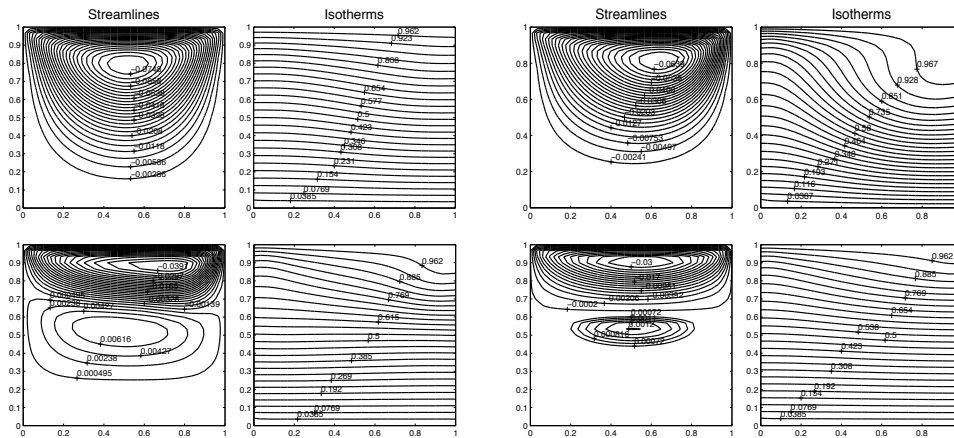


FIGURE 2. $Re=10$ and $Re=100$.

FIGURE 3. $Ha=10$ and $Ha=50$.

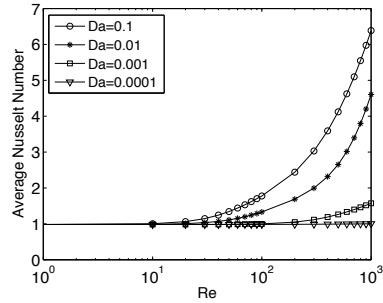


FIGURE 4. Variation of \overline{Nu} with Re .

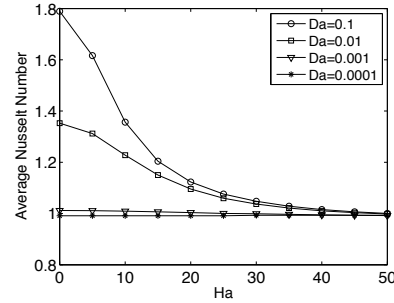


FIGURE 5. Variation of \overline{Nu} with Ha .

Department of Mathematics, Middle East Technical University, Ankara, Turkey
 munt@metu.edu.tr

B. Pekmen

Department of Mathematics, Atılım University; Institute of Applied Mathematics, Middle East Technical University, Ankara, Turkey
 e146303@metu.edu.tr

REFERENCES

- [1] P.W. PARTRIDGE, C.A. BREBBIA, L.C. WROBEL, *The Dual Reciprocity Boundary Element Method*, Southampton, U.K.; Boston: Computational Mechanics Publications; London ; New York : Elsevier Applied Science, 1992.
- [2] R. IWATSU, J.M. HYUN, K. KUWAHARA, *Mixed Convection in a driven cavity with a stable vertical temperature gradient*, Int J. Heat Mass Transfer, 36 (1993) 1601-1608.
- [3] K. M. KHANAFER, A. J. CHAMKHA, *Mixed convection flow in a lid-driven enclosure filled with a fluid-saturated porous medium*, Int J Heat Mass Transfer 42 (1999) 2465-2481.
- [4] K. M. KHANAFER, A. J. CHAMKHA, *Hydromagnetic natural convection from an inclined porous square enclosure with heat generation*, Num Heat Trans, Part A, 33 (1998) 891-910.
- [5] B. PEKMEK, M. TEZER-SEZGIN, *DRBEM solution of free convection in porous enclosures under the effect of a magnetic field*, Int. J. Heat Mass Transfer, 56 (2013) 454-468.

A Directional Fast Multipole Method for Elastodynamics

THOMAS TRAUB

(joint work with Martin Schanz)

The boundary element method is very well suited for the the study of wave propagation phenomena in semi-infinite or infinite linear elastic media. However, the system matrices are densely populated and when dealing with time domain integral equations a block Töplitz system arises. To alleviate these drawbacks, we use the convolution quadrature method (CQM) as proposed in [1] where the convolution breaks up into a system of decoupled problems in Laplace domain. To further decrease memory consumption and to speed up the solution time we extend a directional Fast Multipole Method (DFMM) described in [3] to the Lamé kernel.

1. LAMÉ-NAVIER EQUATIONS AND THE FUNDAMENTAL SOLUTION

We are considering the dynamics of linear elastic media, therefore we need to solve the Lamé-Navier equations which read as

$$(1) \quad (c_1^2 - c_2^2) \nabla (\nabla \cdot \mathbf{u}(\tilde{\mathbf{x}})) + c_2^2 \Delta \mathbf{u}(\tilde{\mathbf{x}}) + \frac{\mathbf{f}(\tilde{\mathbf{x}})}{\rho} - \frac{\partial^2 \mathbf{u}(\tilde{\mathbf{x}})}{\partial t^2} = 0,$$

where c_1^2 and c_2^2 represent the velocity of the compression and shear wave, respectively, ρ is the density, \mathbf{u} the displacement and \mathbf{f} describes the body forces. We solve this equations for $\tilde{\mathbf{x}} \in \Omega$ with a boundary $\Gamma = \partial\Omega$ and $t \in (0, T)$. For simplicity we assume vanishing body forces, i.e., $\mathbf{f}(\tilde{\mathbf{x}}) = 0$ and vanishing initial conditions

$$\mathbf{u}(\tilde{\mathbf{x}}, 0) = \partial_t \mathbf{u}(\tilde{\mathbf{x}}, 0) = 0.$$

We are considering a Dirichlet problem with given boundary data $\mathbf{u}(\mathbf{x}, t) = \mathbf{g}(\mathbf{x}, t)$ for $\mathbf{x} \in \Gamma$ and $t \in (0, T)$. By introducing the single layer potential (SLP) we can write

$$\mathbf{u}(\tilde{\mathbf{x}}, t) := (\tilde{\mathbf{V}} \star \mathbf{w})(\tilde{\mathbf{x}}, t) = \int_{\Gamma} \mathbf{U}^*(\tilde{\mathbf{x}}, \mathbf{y}, t) \star \mathbf{w}(\mathbf{y}, t) d\Gamma \quad \text{with } \tilde{\mathbf{x}} \in \Omega,$$

where $\mathbf{U}^*(\tilde{\mathbf{x}}, \mathbf{y}, t)$ denotes the fundamental solution of the homogeneous partial differential equation (1). The symbol \star is an abbreviation for the temporal convolution involved in this calculation and $\mathbf{w}(\mathbf{y}, t)$ represents a density. Applying the limiting process to the boundary yields the indirect approach using the SLP in time domain which is given by

$$(\mathbf{V} \star \mathbf{w})(\mathbf{x}, t) = \mathbf{g}(\mathbf{x}, t) \quad \text{with } \mathbf{x} \in \Gamma.$$

To perform the convolution directly in time domain is often unpractical, since the kernel is distributional and sometimes, e.g., in the case of viscoelastodynamics and poroelastodynamics, not even known. Hence, we use the CQM described in Sec.

2, where the fundamental solution is needed in Laplace domain. Indeed, the kernel function takes a quite simple form and can be written as

$$(2) \quad \hat{U}_{ij}(r, s_l) = \sum_{m=1}^2 A_{ij}^m(r, s_l) e^{ik_m r} \quad , \text{ with } r = |\mathbf{x} - \mathbf{y}|$$

and the coefficients

$$(3) \quad A_{ij}^m(r, s) = \frac{e^{-d_m r}}{4\pi\rho s^2} \left(\frac{3r_{,i}r_{,j} - \delta_{ij}}{r^3} \left(\frac{s_l}{c_m} r + 1 \right) + \left(\frac{s_l}{c_m} \right)^2 \frac{r_{,i}r_{,j}}{r} \right).$$

Here s_l is the Laplace parameter and c_m the wave velocity. We also define $d_m = \text{Re}(s_l/c_m)$ and $k_m = \text{Im}(s_l/c_m)$. Furthermore, we use the Kronecker delta δ_{ij} and introduce the indicial notation $r_{,i} = \frac{x_i - y_i}{r}$ for the directional derivative.

2. CONVOLUTION QUADRATURE METHOD

We use the CQM method as proposed by Banjai and Sauter [1], which leads to a decoupled system of equations of the form

$$(4) \quad \hat{\mathbf{V}}(s_l) \hat{\mathbf{w}}_l = \hat{\mathbf{g}}_l.$$

This has the main advantage that the storage requirement is reduced to one problem in Laplace domain. The drawbacks are that the complete time history of the given boundary data needs to be known in advance and that for N_t time steps $N_t/2$ problems need to be solved. Hence, to further decrease memory requirements and to speed up solution the time fast methods have to be applied.

The Laplace parameter s_l can be calculated using

$$s_l = \gamma(\lambda \zeta_{N+1}^{-l}) / \Delta t$$

where $\zeta_{N+1} = e^{\frac{2\pi i}{N+1}}$, λ is a numerical parameter and γ is the generating polynomial of the underlying time stepping method, e.g.,

$$\gamma(\zeta) = \frac{1}{2}(\zeta^2 - 4\zeta + 3) \quad \text{for BDF2.}$$

The transformation of the given Dirichlet data and the calculated density is given by

$$\hat{\mathbf{g}}_l = \sum_{n=0}^N \lambda^n \mathbf{g}_n(x) \zeta_{N+1}^{-ln} \quad \text{and} \quad \mathbf{w}_n = \frac{\lambda^{-n}}{N+1} \sum_{l=0}^N \lambda^n \hat{\mathbf{w}}_l(x) \zeta_{N+1}^{ln}.$$

3. DIRECTION FAST MULTIPOLE METHOD FOR ACOUSTICS

Discretizing (4) leads to a linear system of equations, which we want to solve iteratively. Hence, we need to compute matrix vector products of the form

$$f_i = \sum_{j=1}^N K(\mathbf{x}_i, \mathbf{y}_j) \sigma_j, \quad i = 1, \dots, N,$$

with N the number of unknowns and K the kernel function. Evaluating this sum directly has computational effort of order $\mathcal{O}(N^2)$ and thus is very inefficient. If,

however, we find a low rank approximation of the kernel, we can construct a fast summation scheme. This can be achieved by using Chebyshev interpolation. As a starting point we note that any function $f(x)$ within the interval $x \in [-1, 1]$ can be approximated by

$$f(x) = \sum_{m=1}^{\ell} S_{\ell}(x, \{x_m\}) f(\{x_m\}) + \epsilon(\ell),$$

where $\{x_m\}$ represent the Chebyshev nodes. The symbol $\epsilon(\ell)$ denotes the truncation error and the interpolation operator reads as

$$S_{\ell}(x, \{x_m\}) = \frac{1}{\ell} + \frac{2}{\ell} \sum_{n=1}^{\ell-1} T_n(x) T_n(\{x_m\}).$$

The error can be bounded by

$$\left| f(x) - \sum_{n=0}^{\ell} a_n T_n(x) \right| \leq \frac{M}{\rho^{\ell}(\rho - 1)}$$

if $f(z)$ is analytic on the ellipse E_{ρ} and

$$|f(z)| \leq M, \quad \text{for all } z \in E_{\rho}, \quad \text{with } E_{\rho} = \left\{ z \in \mathbb{C} \mid z = \frac{\rho e^{i\theta} + \rho^{-1} e^{-i\theta}}{2} \right\}$$

holds. Consequently, we can construct a fast summation scheme for $\mathbf{x} \in \mathbb{R}^3$ of the form

$$f_i \sim \underbrace{\sum_{m=1}^{\ell} S_m(\bar{\mathbf{x}}_m, \mathbf{x}_i)}_{\text{L2L}} \underbrace{\sum_{n=1}^{\ell} K(\bar{\mathbf{x}}_m, \bar{\mathbf{y}}_n)}_{\text{M2L}} \underbrace{\sum_{j=1}^N S_n(\bar{\mathbf{y}}_n, \mathbf{y}_j)}_{\text{M2M}} \sigma_j.$$

However, we have to control the error of this approximation. Unfortunately we can not apply this approach directly to our problem at hand, which can be seen by extending the kernel of the Helmholtz problem

$$(5) \quad K_k(r) = \frac{e^{ikr}}{4\pi r} \quad \text{with } r = |\mathbf{x} - \mathbf{y}|$$

to the complex plane. If we choose $z = z(\rho, -\pi/2)$ we note that

$$K_k(z) = \frac{e^{k(\rho - \rho^{-1})/2}}{4\pi z}$$

holds. Hence, we can not find an upper bound for the error of our approximation independently of k . This problem can be solved by introducing a modified kernel function of the form

$$\begin{aligned} K_k(\mathbf{x}, \mathbf{y}) &= \frac{1}{4\pi|\mathbf{x}-\mathbf{y}|} e^{ik|\mathbf{x}-\mathbf{y}|} \\ &= \frac{1}{4\pi|\mathbf{x}-\mathbf{y}|} \underbrace{e^{ik(|\mathbf{x}-\mathbf{y}| - \mathbf{u} \cdot (\mathbf{x}-\mathbf{y}))}}_{K^{\mathbf{u}}(\mathbf{x}, \mathbf{y})} e^{ik \mathbf{u} \cdot (\mathbf{x}-\mathbf{y})}, \end{aligned}$$

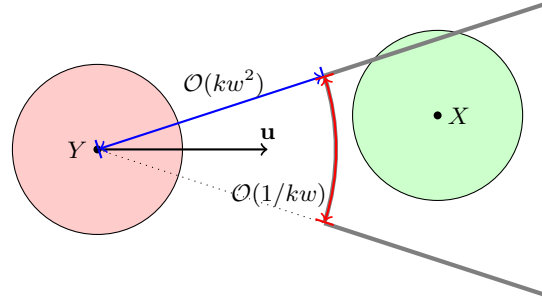


FIGURE 1. Illustration of the admissibility criterion for a cluster pair

where \mathbf{u} is some unit vector. Using this representation we can derive two admissibility conditions for clusters

$$kw \left| \frac{\mathbf{c}}{|\mathbf{c}|} - \mathbf{u} \right| \leq A \quad \text{and} \quad \frac{kw^2}{|\mathbf{c}|} \leq A.$$

Here \mathbf{c} is the vector connecting cluster Y and X and w is the cluster width. The first condition represents a cone aperture and the latter a cluster separation criterion which is illustrated in Fig. 1. Two clusters are admissible if the center of Cluster X lies within the cone around \mathbf{u} with the origin at the center of cluster Y . Using this modified kernel function we can construct a directional summation scheme for the Helmholtz kernel which looks like

$$f_i \sim \underbrace{e^{ik \mathbf{u} \cdot \mathbf{x}_i} \sum_{m=1}^{\ell} S_m(\mathbf{x}_i) e^{-ik \mathbf{u} \cdot \bar{\mathbf{x}}_m}}_{\text{directional L2L}} \underbrace{\sum_{n=1}^{\ell} K(\bar{\mathbf{x}}_m, \bar{\mathbf{y}}_n)}_{\text{M2L}} \underbrace{e^{ik \mathbf{u} \cdot \bar{\mathbf{y}}_n} \sum_{j=1}^N S_n(\mathbf{y}_j) e^{-ik \mathbf{u} \cdot \mathbf{y}_j}}_{\text{directional M2M}} \sigma_j.$$

4. MODIFICATION FOR ELASTODYNAMICS

Modification of this method to elastodynamics can be done in a straight forward way. Since two oscillatory functions with two distinct frequencies are present in the elastodynamic fundamental solution

$$U_{ij}^* = A_{ij}^1 e^{ik_1 r} + A_{ij}^2 e^{ik_2 r},$$

we split the operator accordingly, to calculate the far field contributions separately

$$(\mathbf{V}\mathbf{w})(\mathbf{x}) = \underbrace{\int_{\Gamma} A_{ij}^1 e^{ik_1 r} w_j(\mathbf{y}) d\Gamma}_{V^1} + \underbrace{\int_{\Gamma} A_{ij}^2 e^{ik_2 r} w_j(\mathbf{y}) d\Gamma}_{V^2}.$$

Furthermore, it is convenient to separate the vector valued problem into scalar operators for each degree of freedom

$$\left(\left(\begin{pmatrix} V_{11}^1 & V_{12}^1 & V_{13}^1 \\ V_{21}^1 & V_{22}^1 & V_{23}^1 \\ V_{31}^1 & V_{32}^1 & V_{33}^1 \end{pmatrix} + \begin{pmatrix} V_{11}^2 & V_{12}^2 & V_{13}^2 \\ V_{21}^2 & V_{22}^2 & V_{23}^2 \\ V_{31}^2 & V_{32}^2 & V_{33}^2 \end{pmatrix} \right) \begin{pmatrix} w_1 \\ w_2 \\ w_3 \end{pmatrix} \right) = \begin{pmatrix} g_1 \\ g_2 \\ g_3 \end{pmatrix}.$$

We thus can directly apply the techniques derived in the previous chapter to our problem.

5. NUMERICAL EXAMPLES

As a model example for a first validation of our code we use a unit cube centered at its origin. The Dirichlet boundary data are calculated using the fundamental solution with the source point at $(2, 2, 2)$ and direction $(1, 0, 0)$. We use a set of model material parameters: $c_1 = 1$ m/s, $c_2 = \sqrt{0.5}$ m/s and $\rho = 1$. To solve our system of equations we use a GMRES-solver without preconditioning. The error is calculated using an inner point evaluation on a coarse mesh inscribed into the unit cube.

In Tab. 4 we show the convergence rate of the method using a non directional approximation. Here 'dof' is the total number of degrees of freedoms, L denotes the number of multipole levels used, ℓ the expansion coefficient and 'it' the number of iterations. Finally 'error' is the pointwise error of the inner point evaluation and 'eoc' the convergence rate. Tab. 5 shows the timings to assemble the necessary data structures for the FMM matrix $t_{assembly}$ and one matrix vector product $t_{product}$. Tab. 6 presents a convergence study for a directional approximation of the operator with $s_l = 4i$. Finally, in Tab. 7 we present timing results with increasing frequency as we refine the mesh.

dof	L	ℓ	it	error	eoc
4152	1	5	44	9,99E-6	
16608	2	5	55	1,79E-6	2,48
66432	3	5	69	2,21E-7	3,02
265728	4	7	86	6,95E-8	1,67
1062912	5	7	117	1,82E-8	1,93

TABLE 4. Convergence study: $s_l = i$

dof	L	$t_{assembly}$	$t_{product}$		
9216	2	83,51	8,03		
36864	3	273,10	3,27	48,22	6,01
147456	4	946,18	3,46	267,25	5,54
589824	5	3493,18	3,69	325,10	1,22
2359296	6	14075,00	4,03	1200,11	3,69

TABLE 5. Timings for $\ell = 5$, $s_l = i$

dof	L	ℓ	$t_{assembly}$	$t_{product}$			it	error	eoc
9216	3	4	4,58	2,25			81	2,92E-05	
36864	4	5	21,09	4,61	47,73	21,26	96	5,80E-06	2,33
147456	5	6	101,10	4,79	846,38	17,73	134	6,83E-007	3,09

TABLE 6. Convergence study: $s_l = 4i$

dof	L	s_l	$t_{assembly}$	$t_{product}$		
9216	3	$4i$	3,72	0,24		
36864	4	$8i$	14,82	3,98	1,06	4,45
147456	5	$16i$	62,87	4,24	7,04	6,67
589824	6	$32i$	249,81	3,97	21,56	3,06

TABLE 7. Timings for $\ell = 3$

Martin Schanz, Thomas Traub

Institute of Applied Mechanics, Graz University of Technology, Technikerstr. 4 8010
Graz, Austria

m.schanz@tugraz.at, thomas.traub@tugraz.at

REFERENCES

- [1] L. Banjai and S. Sauter. Rapid solution of the wave equation in unbounded domains. *SIAM Journal on Numerical Analysis*, 47(1):227–249, 2008.
- [2] B. Engquist and L. Ying. Fast directional multilevel algorithms for oscillatory kernels. *SIAM Journal on Scientific Computing*, 29(4):1710–1737, 2007.
- [3] M. Messner, M. Schanz and E. Darve. Fast directional multilevel summation for oscillatory kernels based on chebyshev interpolation. *Journal of Computational Physics*, 231(4): 1175–1196, 2012.

Operator preconditioning for two-dimensional screen and fracture problems using boundary elements

CAROLINA A. URZÚA

(joint work with Carlos Jerez-Hanckes)

Operator preconditioning [1, 2] based on Calderón identities breaks down when considering open boundaries as when modeling screens or cracks. On the one hand, the double layer operator and its adjoint disappear. On the other hand, the associated weakly singular and hypersingular operators no longer map fractional Sobolev spaces in a dual fashion but degenerate into different subspaces depending on their extensibility by zero. Based on Calderón-type identities deduced from Jerez-Hanckes and Nédélec [3, 4] for an open interval, novel preconditioners can be established for associated integral operators. In this presentation, we show the numerical implementation of these preconditioners for the Laplacian, as well as an extension to the Helmholtz operators and other interesting formulations. Furthermore we discuss two solution methods obtained by these Calderón-type identities and some future extensions.

1. PRELIMINARIES

Set $\Omega := \mathbb{R}^2 \setminus \Gamma$, where $\Gamma := I \times \{0\}$, $I := (-1, 1)$. Let $\mathcal{O} \subseteq \mathbb{R}^2$, with $d = 1, 2$, be open. For $s \in \mathbb{R}$, $H^s(\mathcal{O})$ denote standard Sobolev spaces [5, Chapter 3]. If $s > 0$ and \mathcal{O} Lipschitz, $\tilde{H}^s(\mathcal{O})$ denotes the space of functions whose extension by zero over a closed domain $\tilde{\mathcal{O}}$ belongs to $H^s(\tilde{\mathcal{O}})$. We identify

$$\tilde{H}^{-1/2}(\mathcal{O}) \equiv (H^{1/2}(\mathcal{O}))' \quad \text{and} \quad H^{-1/2}(\mathcal{O}) \equiv (\tilde{H}^{1/2}(\mathcal{O}))'.$$

If $w = \sqrt{1 - x^2}$, let us introduce the subspaces:

$$(1) \quad \tilde{H}_{(0)}^{-1/2}(\Gamma) := \left\{ \varphi \in \tilde{H}^{-1/2}(\Gamma) : \langle \varphi, 1 \rangle_{H^{1/2}(\Gamma)} = 0 \right\},$$

$$(2) \quad \tilde{H}_*^{1/2}(\Gamma) := \left\{ g \in \tilde{H}^{1/2}(\Gamma) : \langle g, w^{-1} \rangle_{\Gamma} = 0 \right\}.$$

We recall the Calderón-type identities shown by Jerez-Hanckes and Nédélec [3, 4]

Proposition 1.1. The following identities hold:

$$(3a) \quad -\mathcal{L}_2 \circ D^* \circ \mathcal{L}_1 \circ D = \text{Id}_{\tilde{H}^{1/2}(\Gamma)}, \quad -\mathcal{L}_1 \circ D \circ \mathcal{L}_2 \circ D^* = \text{Id}_{\tilde{H}_*^{1/2}(\Gamma)},$$

$$(3b) \quad -D \circ \mathcal{L}_2 \circ D^* \circ \mathcal{L}_1 = \text{Id}_{\tilde{H}_{(0)}^{-1/2}(\Gamma)}, \quad -D^* \circ \mathcal{L}_1 \circ D \circ \mathcal{L}_2 = \text{Id}_{H^{-1/2}(\Gamma)}.$$

wherein, for $x \in I$,

$$\mathcal{L}_1 \varphi(y) := \int_I \log \frac{1}{|x - y|} \varphi(x) dx,$$

$$\mathcal{L}_2 \varphi(y) := \int_I \log \frac{M(x, y)}{|x - y|} \varphi(x) dx,$$

and

$$M(x, y) := \frac{1}{2} \left((y - x)^2 + (w(x) + w(y))^2 \right).$$

Observe that \mathcal{L}_1 and $D^* \circ \mathcal{L}_1 \circ D$ are the standard weakly and hyper-singular operators. As shown on [3, 4], there are symmetric and coercive variational formulations of the integral equation for both operators. In addition, each one of these has an associated inverse operator, which is a bijection and also admits a symmetric and coercive variational formulation.

In the following, we are interested in building numerical preconditioners for these operators and compare it to previous attempts as described by Steinbach and McLean [2]. For this, we rely on the abstract theory given by Hiptmair [1]:

Proposition 1.2. Let $V_h := \text{span}\{\varphi_i\} \subset V$ and $W_h := \text{span}\{\phi_j\} \subset W$ be as shown on [1]. Let $a \in L(V \times V, C)$ and $b \in L(W \times W, C)$ be continuous sesquilinear forms satisfying their inf-sup conditions. Consider a continuous sesquilinear form $t \in L(V \times W, C)$ also satisfying an inf-sup condition.

Then, their associated Galerkin-matrices:

$$\mathbf{A}[i, j] := (a(\varphi_i, \varphi_j))_{i, j=1}^N, \mathbf{B}[i, j] := (b(\phi_i, \phi_j))_{i, j=1}^M, \mathbf{T}[i, j] := \langle t(\phi_i, \varphi_j) \rangle_{i, j=1}^{N, M},$$

satisfy

$$(5) \quad \kappa(\mathbf{T}^{-1} \mathbf{B} \mathbf{T}^{-T} \mathbf{A}) \leq \frac{\|a\| \|b\| \|t\|}{c_A c_B c_T^2}$$

where c_A , c_B and c_T are associated inf-sup condition constants with $N := \dim V_h = M := \dim W_h$.

Now, we can build a preconditioner for each one of our integral operators by finding a sesquilinear form such as (5) is minimal. Since we already have explicit inverses, we will use them as corresponding sesquilinear forms b .

2. DISCRETIZATION SCHEME

Define a mesh Γ_h of Γ and introduce the following bases:

$$\mathcal{S}^{-1,0}(\Gamma_h) := \text{span}\{q_k\}_{k=1}^N \subseteq H^{-1/2}(\Gamma),$$

$$\mathcal{S}^{0,1}(\Gamma_h) := \text{span}\{b_k\}_{k=1}^M \subseteq H^{1/2}(\Gamma),$$

where q_i and b_j are p.w. constant and p.w. linear functions, respectively. A relevant hypothesis in Proposition 1.2 is the equality $N = M$. Thus, the dual mesh $\hat{\Gamma}_h$ and spaces thereon defined are chosen to fulfill this condition (see Figure 1).

2.1. Weakly Singular. Given

$$a := \mathcal{L}_1 : \tilde{H}_{(0)}^{-1/2}(\Gamma) \rightarrow H_*^{1/2}(\Gamma),$$

we use the identity (3b) to identify

$$b := -\mathcal{D} \circ \mathcal{L}_2 \circ \mathcal{D}^* : H_*^{1/2}(\Gamma) \rightarrow \tilde{H}_{(0)}^{-1/2}(\Gamma)$$

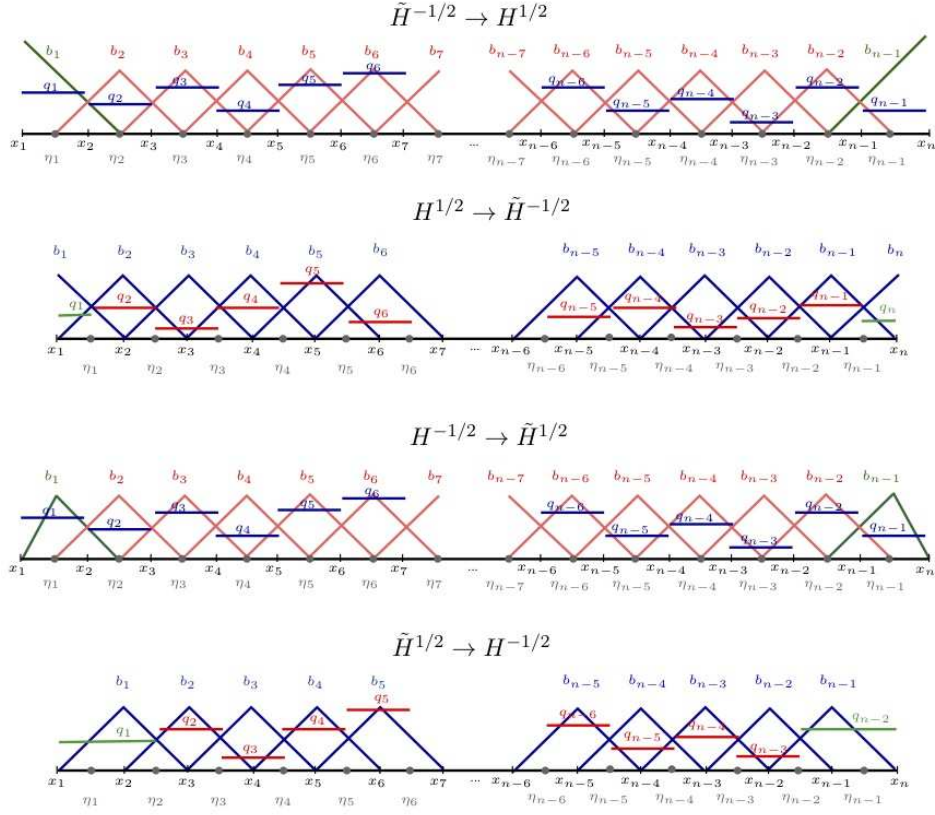


FIGURE 1. Trial Spaces Basis for Original and Dual Meshes

as a preconditioner. In order to avoid restricting the discrete space to account for restrictions (1), (2), we extend these operators to define the following sesquilinear forms:

$$\tilde{a} : \tilde{H}^{-1/2}(\Gamma) \rightarrow H^{1/2}(\Gamma) \quad \text{and} \quad \tilde{b} : H^{1/2}(\Gamma) \rightarrow \tilde{H}^{-1/2}(\Gamma).$$

where their respective Galerkin matrices are constructed as

$$\mathbf{A}[i, j] := \mathbf{V}_0[i, j] = \langle \mathcal{L}_1 q_i, q_j \rangle + \langle q_i, 1 \rangle \langle q_j, 1 \rangle \Big|_{i, j=1}^N$$

and

$$\mathbf{B}[i, j] := \left(\langle \mathcal{L}_2 b'_i, b'_j \rangle + \langle b_i, \frac{1}{w} \rangle \langle b_j, \frac{1}{w} \rangle \right) \Big|_{i, j=1}^M.$$

The corresponding operator $t : \tilde{H}^{-1/2}(\Gamma) \times H^{1/2}(\Gamma) \rightarrow \mathbb{C}$ is taken as the duality product with Galerkin matrix:

$$\mathbb{T}[i, j] := \langle b_i, q_j \rangle_{i,j=1}^{N,M}$$

2.2. Hypersingular. In this case,

$$a := -\mathcal{D} \circ \mathcal{L}_1 \circ \mathcal{D}^* : \tilde{H}^{1/2}(\Gamma) \rightarrow H^{-1/2}(\Gamma),$$

for which we deduced from (3a) the following operator as its preconditioner

$$b := \mathcal{L}_2 : H^{-1/2}(\Gamma) \rightarrow \tilde{H}^{1/2}(\Gamma).$$

The related matrices are

$$\mathbb{A}[i, j] := \mathbb{W}_0[i, j] = \langle -\mathcal{D} \circ \mathcal{L}_1 \circ \mathcal{D}^* b_i, b_j \rangle_{i,j=1}^N = \langle \mathcal{L}_1 b'_i, b'_j \rangle_{i,j=1}^N$$

and

$$\mathbb{B}[i, j] := \langle \mathcal{L}_2 q_i, q_j \rangle_{i,j=1}^M.$$

Lastly, we consider the corresponding operator $t : \tilde{H}^{1/2}(\Gamma) \times H^{-1/2}(\Gamma) \rightarrow \mathbb{C}$ as the dual product between these trial spaces. We introduce its Galerkin matrix \mathbb{T} with entries

$$\mathbb{T}[i, j] := \langle q_i, b_j \rangle_{i,j=1}^{N,M}.$$

3. NUMERICAL RESULTS

Figures 2 and 3 reveal relative error convergence results for GMRES implementations for the original and preconditioned weakly singular operator over an uniform mesh. The inf-sup conditions for the t operators are satisfied on a uniform mesh scheme, and Proposition 1.2 holds, so the preconditioned operator converges almost in the same iteration for any N . This is not the case for a non-uniform mesh. Nevertheless, Tables ?? and ?? show conditioning numbers for both uniform and non-uniform meshes, the last one given by the roots Tchebyshev polynomial.

N	GMRES Number of Iterations			
	Uniform mesh		Non-uniform mesh	
	No precon	Precon	No precon	Precon
16	8	10	8	9
64	26	11	40	10
256	44	11	171	8
1024	70	10	672	7

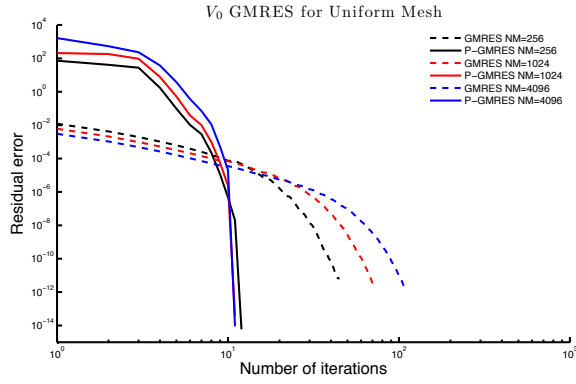


FIGURE 2. GMRES residual error convergence for the weakly singular operator

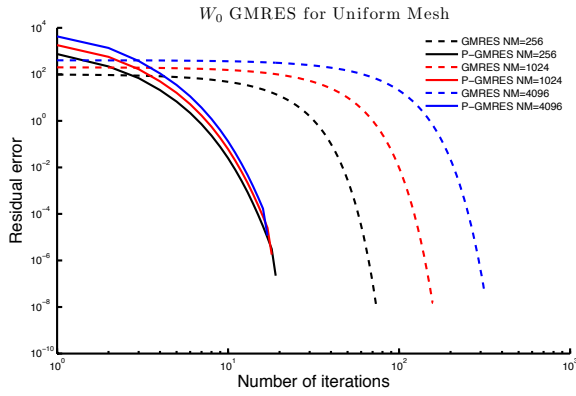


FIGURE 3. GMRES residual error convergence for the hypersingular operator

N	GMRES Number of Iterations			
	Uniform mesh		Non-Uniform mesh	
	No precon	Precon	No precon	Precon
16	7	7	7	14
64	30	19	30	20
256	74	18	73	19
1024	157	17	155	18

Figures 4 and 5 the preconditioning results obtained for the Helmholtz equation on the interval when considering $k=4$ and a uniform mesh.

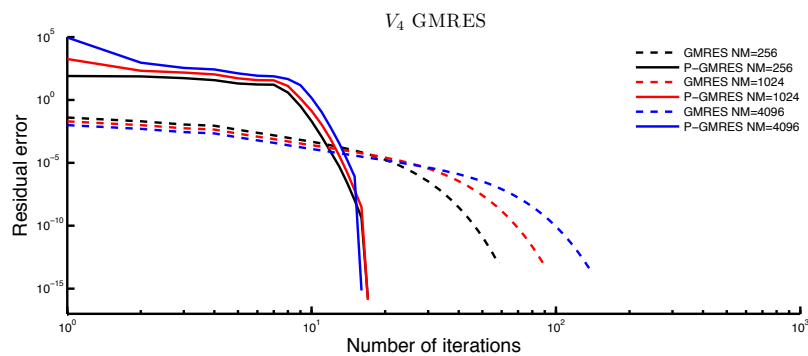


FIGURE 4. GMRES residual error convergence for the Helmholtz weakly singular operator

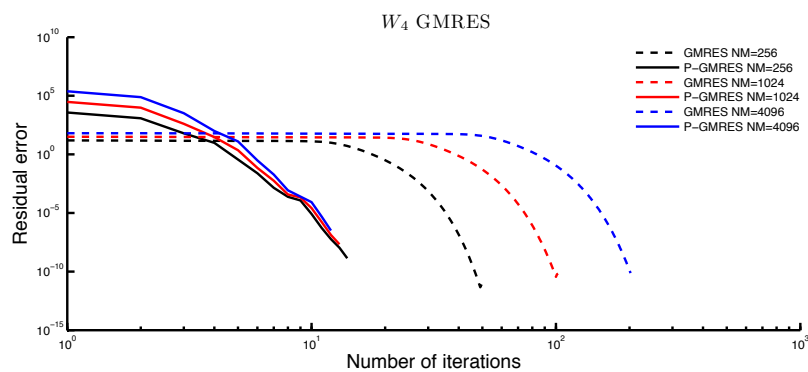


FIGURE 5. GMRES residual error convergence for the Helmholtz hypersingular operator

Carolina A. Urzúa Torres, Carlos Jerez-Hanckes

Escuela de Ingeniería, Pontificia Universidad Católica de Chile, Santiago Chile
 curzuat@uc.cl, cjerez@ing.puc.cl

REFERENCES

- [1] Hiptmair, R. Operator Preconditioning. *Computers and Mathematics with Applications*. (52), pp. 699-706, 2006.
- [2] McLean, W., Steinbach, O. Boundary element preconditioners for a hypersingular integral equation on an interval. *Advances in Computational Mathematics*. (11), pp. 271-286, 1999.
- [3] Jerez-Hanckes, C. and Nédélec, J.-C. Variational forms for the inverses of integral logarithmic operators over an interval. *Comptes Rendus Mathématique*.(349), pp. 547-552, 2011.

- [4] Jerez-Hanckes, C. and Nédélec, J.-C. Explicit Variational Forms For The Inverses Of Integral Logarithmic Operators Over An Interval. *SIAM Journal on Mathematical Analysis*. 44(4), pp 26662694 , 2012.
- [5] W. MCLEAN, *Strongly Elliptic Systems and Boundary Integral Equations*, Cambridge University Press, New York, USA, 2000.

On the relationship between the frequency-domain BEM and the convolution quadrature BEM

W. YE

(joint work with J. Xiao)

Transient analysis is encountered in almost every engineering field. For large-scale problems with complex domains, the boundary element method (BEM) offers a viable approach for obtaining accurate and efficient solutions. Typically transient problems can be solved either by direct computation of the time-domain boundary integral formulation or by utilizing inverse transformation and solving the integral formulation in the frequency or Laplace domain. The inverse-transformation approaches have the advantages in stability and simplicity since only the frequency-domain or Laplace-domain BEM formulation needs to be solved. Recently Convolution Quadrature Method (CQM) proposed by Lubich [1, 2] has received much attention and has been applied to various problems including acoustics and elastodynamics [3, 4]. Impressive results have been demonstrated. In the meantime, the frequency-domain BEM approach has also been actively developed [5] and from the results, it is clear that this approach is as accurate as the convolution quadrature BEM if not better. A question naturally arises: which method is better in terms of accuracy and efficiency? In fact, the two methods should share some common features since the frequency transform can be regarded as a special type of the Laplace transform. In this paper, the relationship between the two methods is examined both theoretically and numerically. We first show that the frequency-domain BEM approach is equivalent to the convolution quadrature BEM approach with a multistep scheme of infinite-order of accuracy. We then present several numerical examples to further justify the theoretical finding.

Keywords: Transient analysis; Frequency-domain BEM; Convolution quadrature BEM

W. Ye

Department of Mechanical Engineering, Hong Kong University of Science and Technology
mewye@ust.hk

J. Xiao

College of Astronautics, Northwestern Polytechnical University
xiaojy@nwpu.edu.cn

REFERENCES

- [1] Lubich C. Convolution quadrature and discretized operational calculus. I. *Numer. Math.*, 52:129-145, 1988.
- [2] Lubich C. Convolution quadrature and discretized operational calculus. II. *Numer. Math.*, 52:413-425, 1988.
- [3] Abreu, A.I., Carrer, J.A.M., Mansur, M.J. Scalar wave propagation in 2D: a BEM formulation based on the operational quadrature method. *Engrg. Anal. Bound. Elem.*, 27:101-106, 2003.

- [4] Schanz, M., *Wave propagation in viscoelastic and poroelastic continua: a boundary element approach*, vol. 2 of Lecture Notes in Applied Mechanics, Springer-Verlag, Berlin, Heidelberg, New York, 2001.
- [5] Xiao, J., Ye, W., Cai, Y. and J. Zhang. Precorrected-FFT Accelerated BEM for Large-Scale Transient Elastodynamic Analysis using Frequency-Domain Approach. *International Journal for Numerical Methods in Engineering*, 90(1):116-134, 2012.

Hybrid Extended Displacement Discontinuity-Fundamental Solution Method For Two- And Three-Dimensional Smart Media

MINGHAO ZHAO

(joint work with Ernian Pan, Cuiying Fan, Guoning Liu)

Combining the Extended Displacement Discontinuity Method (EDDM) and the Fundamental Solution Method (FSM), the hybrid extended displacement discontinuity-fundamental solution (HEDD-FS) method was proposed by Fan et al. [6] to study the linear and nonlinear fracture of piezoelectric media [7, 3] and MEE media [5, 4]. In this paper, we summarize and present the application of HEDD-FS method in linear and nonlinear fracture mechanics of two- and three-dimensional smart media.

Keywords: MEE medium, PEMPS model, PEMB model, extended displacement discontinuity, boundary integral equation, extended stress intensity factor

CuiYing Fan, MingHao Zhao, Ernian Pan, GuoNing Liu

The School of Mechanical Engineering, Zhengzhou University, Zhengzhou, 450001, China
fancy@zzu.edu.cn, memhzhao@zzu.edu.cn

panernian@zzu.edu.cn, l11egn@yahoo.com

REFERENCES

- [1] Crouch SL. Solution of plane elasticity problems by the displacement discontinuity method. *Int. J. Meth. Eng.*, 10: 301-343, 1976.
- [2] Kupradze VD, Aleksidze MA. The method of functional equations for the approximate solution of certain boundary value problems. *Comput Math Math Phys*, 4: 82-126, 1964.
- [3] Fan CY, Zhao MH, Wang JP, Pan E.. Analysis of an arbitrarily oriented crack in a finite piezoelectric plane via the hybrid extended displacement discontinuity-fundamental solution method *Comput Mech*, 2012.
- [4] Fan Cui Ying, Zhao Ming Hao. Nonlinear fracture of 2D magneto-electroelastic media: Analytical and numerical solutions. *International Journal of Solids and Structures*, 48(16-17): 2373-2382, 2011.
- [5] Zhao MH, Xu GT, Fan CY Numerical Method of Crack Analysis in 2D Finite Magneto-electroelastic Media. *Comput Mech*, 45: 401-413, 2010.
- [6] Fan CY, Zhao MH, Zhou YH. Numerical solution of polarization saturation/dielectric breakdown model in 2D finite piezoelectric media. *J Mech Phys Solids*, 57: 1527-1544, 2009.
- [7] Zhao MH, Xu GT, Fan CY Hybrid extended displacement discontinuity-charge simulation method for analysis of cracks in 2D piezoelectric media. *Eng Anal Bound Elem*, 33: 592-600, 2009.